Plasma membrane organization during EGFR signaling: a FRET-based analysis

Organisatie van de plasma membraan gedurende EGFR signalering: een FRET-gebaseerde analyse

(met een samenvatting in het Nederlands)

Proefschrift

ter verkrijging van de graad van doctor aan de Universiteit Utrecht op gezag van de rector magnificus, prof. dr. J.C. Stoof, ingevolge het besluit van het college voor promoties in het openbaar te verdedigen op woensdag 24 september 2008 des middags te 4.15 uur

door

Erik Gerben Hofman

geboren op 25 juni 1977 te Joure

Promotor: Prof. A.J. Verkleij

Co-promotor: Dr. P.M.P. van Bergen en Henegouwen

Voor mijn moeder

The research described in this thesis was performed at the division of Cellular Architecture and Dynamics, Institute of Biomembranes, University Utrecht, the Netherlands.

Printing of this thesis was financially supported by Fermentas Life Sciences and Corning Life Sciences.

ISBN: 978-90-393-4905-2

Print: Gildeprint, Enschede

Table of contents

Abbreviations

A488	Alexa Fluor 488
A594	Alexa Fluor 594
Cav	caveolin
CTB	cholera toxin B-subunit
CTRFAIM	confocal time-resolved fluorescence anisotropy imaging microscopy
DAG	diacylglycerol
DOPC	dioleoylphosphatidylcholine
DRM	detergent-resistant membrane fraction
EGF	epidermal growth factor
EGFR	epidermal growth factor receptor
Eps15	epidermal growth factor receptor pathway substrate 15
FACS	fluorescence activated cell sorter
FKBP	FK506-binding protein
FLIM	fluorescence lifetime imaging microscopy
FRAP	fluorescence recovery after photobleaching
FRET	Förster resonance energy transfer
GFP	green fluorescent protein
GPCR	G-protein coupled receptor
GPI	glycosylphosphatidylinositol
Grb2	growth factor receptor-bound protein 2
IP3	inositol-1,3,5-triphosphate
LiMo	lifetime module
MAPK	mitogen-activated protein kinase
mGFP	monomeric green fluorescent protein
NA	numerical aperture
OPE	one-photon excitation
PC	phosphatidylcholine
PE	phosphatidylethanolamine
PI	phosphatidylinositol
$PtdInsP_2$	phosphatidylinositoldiphosphate
$PtdInsP_3$	phosphoinositide-3,4,5-triphosphate
PKC	protein kinase C
PLC	phospholipase C
PTB	phosphotyrosine-binding
PTP	protein-tyrosine phosphatases
PS	phosphatidylserine
RoI	region of interest
SH2	Src homology 2
SH3	Src homology 3
Sos	Son of sevenless
TCSPC	time-correlated single photon counting
TCZ	transient confinement zone
TfR	transferrin receptor
TGF-α	transforming growth factor- α
TPE	two-photon excitation

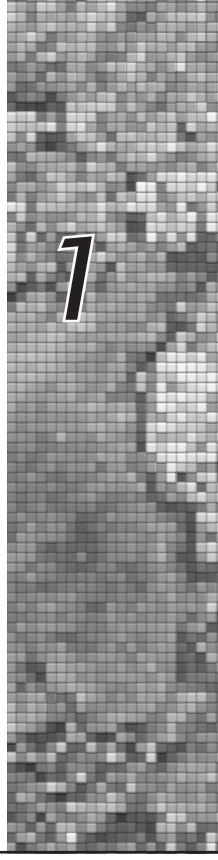

Chapter 1

General introduction

General introduction

Cell proliferation is a fundamental process to maintain or regulate the number of cells in an organism. In adult multicellular organisms, maintainance of the total body volume is the result of a delicate balance between multiplication and breakdown of cells. Growth factors and their receptors provide the basis for the regulation of cell proliferation, by initiating a process of signal transduction. The signaling process essentially starts at the plasma membrane. Receptors for growth factors such as the epidermal growth factor receptor (EGFR) contain a transmembrane region and belong to the type I integral membrane proteins. Upon activation of the receptor, signaling molecules are recruited to the receptor resulting in the activation of diverse signaling pathways including the Ras-MAPkinase pathways. Members of these pathways are membrane associated via their diverse lipid anchors such as the fatty acids myristoyl or palmitoyl, which are connected to Ras and Src, respectively. Membrane anchoring is essential for efficient signaling. It is suggested that the membrane has an important function in the orchestration of signaling process by organizing and concentrating the individual signaling components. In addition, all types of regulation of EGFR signaling, such as Ras activation, involve processes at the plasma membrane.

This thesis focusses on the function of the plasma membrane organization in the regulation of the signaling process. As a model system for growth factor signalling the EGFR is used. This introduction comprises a biological (I) and a methodological part (II). In part I, the activation mechanism of EGFR and factors involved in its functioning will be discussed. After that, the organizing principles of the membrane components will be described. Finally, in part II the principles of the technical approaches are explained. The plasma membrane of the mammalian cell is investigated with several novel spectroscopical techniques that allow the investigation of membrane organization at the nanometer scale.

Part I. Plasma membrane organization and signaling

EGFR

One of the best characterized growth factor receptors is the epidermal growth factor receptor, commonly named as EGFR but also indicated with ErbB1 or Her1. The EGF receptor is a member of the ErbB family of tyrosine kinase receptors, consisting of four homologous transmembrane proteins indicated as ErbB1, 2, 3 and 4. Receptors from this family are capable of forming receptor dimers with their own receptor type, indicated as homodimers (Yarden and Sliwkowski, 2001). Tight regulation of EGFR signaling is crucial for proper control of cell proliferation. A number of mutations in EGFR have been found in malignant tumors, of which the vIII variant is the most prevalent. This mutant lacks exons 2-7 coding for residues 6-273 of the ectodomain, resulting in a constitutively active receptor (Moscatello et al., 1995; Yamazaki

et al., 1988). EGF is the main ligand for EGFR, but the receptor can also be activated by a range of different proteins. Until now, seven ligands for EGFR have been described: EGF, TGF-α, HB-EGF, amphiregulin (AR), betacellulin (BTC), epiregulin and epigen.

EGFR Structure

All four homologues of the ErbB family have similar architectures. The proteins consist of three functional regions: a) a ligand-binding extracellular region, b) a single transmembrane domain, and c) an intracellular region containing a tyrosine kinase domain (fig.1A). The EGFR is synthesized as a 1210-residue precursor protein, which becomes an 1186-residue long transmembrane protein after cleavage of the N-terminal signal peptide. The 621 residues of the EGFR extracellular region or ectodomain are divided into four functional and structural domains. Domains I and III (or L1 and L2) are involved in ligand binding, and consist of 6 turns of a β–helix capped at each end by an α-helix and a disulfide bond, and a large β-sheet. Domains II and IV (CR1 and CR2) are cysteine-rich modules and consists of 7-8 small modules,

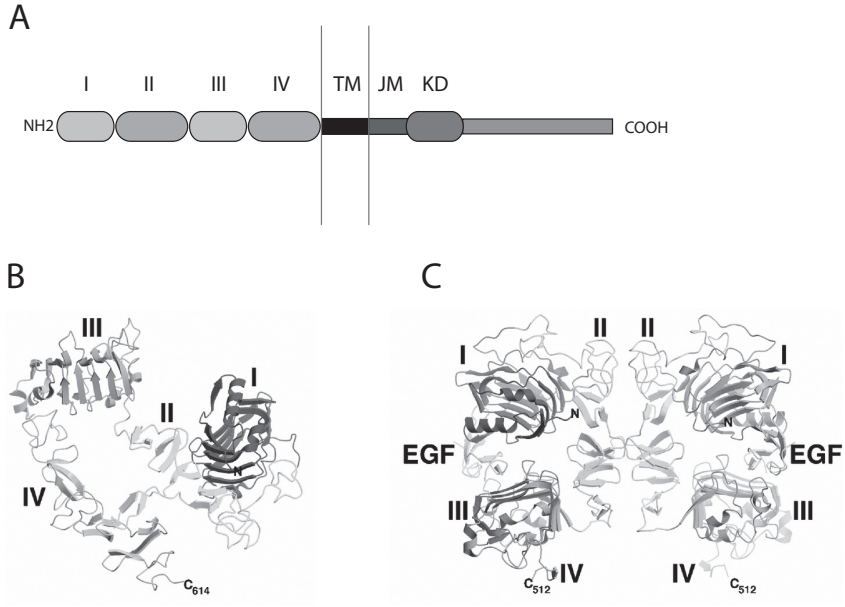

Fig 1. Modular structure of EGFR. (A) Schematic representation of EGFR structure. The ectodomain comprises domain I-IV, followed by a transmembrane domain (TM). The intracellular part is composed of a juxtamembrane domain (JM) connected to the kinase domain (KD) followed by a C-terminal part containing the tyrosine residues. (B) The closed or tethered configuration of the EGFR ectodomain. In the absence of ligand, a loop protruding from domain II forms a tight interaction with domain IV. (C) Ligand-bound EGFR dimer. Upon binding of EGF, domains I and II make a rotational translation over a hinge region at the domain II-III interface. The exposed loop from domain II interacts with the identical region of a second EGFR molecule. Figure B and C were adapted from (Ferguson, 2004)

respectively, that are individually structured by one or two disulfide bonds. Domain II contains an extending loop that is involved in dimerization with other ErbB members (Garrett et al., 2002; Ogiso et al., 2002). Crystalization studies have revealed the existence of two possible conformations of the EGFR ectodomain (fig 1B, C). In the closed or tethered conformation, domains II and IV interact by means of hydrogen bonds, burying the dimerization arm of domain II against domain IV. In this conformation, the two ligand binding domain I and III are too far apart to simultaneously bind a ligand protein. In the open conformation, domain I and II are hinged 130 degrees over the domain II/III interface. This reorganisation exposes domain II, allowing interlocking with a second domain II and resulting in the formation of a back-to-back dimer (Ogiso et al., 2002). The function of domain II is threefold: primarily it creates a scaffold for the ligand binding pocket by orienting domains I and III in the right position. These domains form the ligand binding pocket, as EGF simultaneously binds both domains in a single receptor. In addition, domain II is responsible for the auto-inhibited tethered conformation, affecting ligand binding. It also forms a crucial factor for receptor dimerization, as illustrated by the fact that deletion of domain II prevents the receptor to dimerize in response to stimulation with EGF (Garrett et al., 2002).

The EGFR extracellular domains are extensively glycosylated, as 20% of the 170 kDa molecular mass is due to N-linked glycosylation (Lax et al., 1990). So far, 11 potential N-glycosylation sites have been identified. Deregulation of the glycosylation affects trafficking, ligand binding, internalization and ligand-induced phosphorylation (Fernandes et al., 2001; Miljan et al., 2002; Sato et al., 2001; Slieker et al., 1986; Soderquist and Carpenter, 1984; Wang et al., 2001). Interestingly, the site-specific glycosylation-defective N420Q or N579Q mutants increase the ligand-independent dimerization of EGFR, suggesting that glycosylation of these sites auto-inhibits the predimerization of EGFR (Tsuda et al., 2000; Whitson et al., 2005).

The single transmembrane domain stretches from residues 622 to 644. The crystal structure of the transmembrane and intracellular domains are mostly incomplete, but the structure of the kinase domain has been resolved (Stamos et al., 2002). It is composed of a small N-terminal and a large C-terminal lobe, where ATP is oriented between the two lobes. Based on crystallographic data, an allosteric mechanism of kinase activation has been suggested (Zhang et al., 2006). In the autoinhibited monomeric form, the kinase has a conformation that closely resembles that of Src-family kinases or cyclin-dependent kinases (CDKs). Increasing the concentration results in the formation of an asymmetric dimer, adopting a conformation that resembles the interaction between CDK2 and cyclin A. Ligand-binding results in EGF receptor dimerization, thereby increasing the local concentration of the kinase domain, resulting in activation of the kinase activity. In addition, ligand binding to EGFR is also inducing a rotation of transmembrane domains, causing a reorientation of the kinase domains, which may be required for the allosteric activation (Moriki et al., 2001).

Ligand-dependent and -independent dimerization

In contrast to bivalent growth factors such as human growth hormone (hGH), ErbB ligands do not bind two receptor molecules. Association of ligand with the EGFR occurs in a 1:1 stoichiometry (Lemmon et al., 1997). In the classical model of EGFR activation, the EGFR exists on the non-stimulated cell surface as monomers. Binding of a ligand to the EGFR induces the formation of a signaling dimer, in which the kinase domains mutually phosphorylate tyrosine residues on the C-terminal tail, known as trans- or crossphosphorylation. The dimerization is entirely receptor-mediated, and stabilized by ligand-binding. The EGFR becomes phosphorylated on multiple tyrosine residues, including Y992, Y1068, Y1086, Y1148 and Y1173 (Jorissen et al., 2003). In addition, other tyrosine residues may be phosphorylated indirectly through the action of tyrosine kinases such as Src or JAK-2. Phosphorylation of the EGFR tyrosine residues generates docking sites for SH2 or PTB domain containing-proteins such as Grb2. The binding of adaptor proteins to the activated EGFR eventually leads to the recruitment of several signaling proteins. A number of signaling pathways are initiated by the activation of EGFR (for a review see (Jorissen et al., 2003)).

Several studies have reported that the EGFR exists on the surface of the non-stimulated cell as monomers, and partially as dimers or even oligomers. This has first been demonstrated with electron microscopical studies using freeze fracture labeling (van Belzen et al., 1988). In this paper, non-stimulated A431 cells were demonstrated to have ~ 40% of the receptor population as predimers, and 10% oligomerized. Upon activation, this ratio shifted to 30% monomers, 40 % dimers and 30% oligomers (van Belzen et al., 1988). Later, chemical crosslinking studies and co-immunoprecipitation studies using differentially tagged proteins have confirmed the existance of EGFR in the predimerized state. Based on these data, the EGFR predimer has been defined as the inactive but dimerized EGFR. More recently, different light microscopical methods have been used to detect the dimerized state of the receptor. These studies include image correlation microscopy, fluorescence intensity distribution analysis, single molecule analysis and steady-state anisotropy (Clayton et al., 2007; Lidke et al., 2003; Saffarian et al., 2007; van Belzen et al., 1988; Yu et al., 2002). However, the degree of dimerization or oligomerization varies greatly between the different studies and methods, indicating the need for better imaging methods to determine the oligomerized state of the EGFR before and after stimulation.

Affinity

Binding of ligand to a receptor can be analyzed both under equilibrium and non-equilibrium condition. The method of Scatchard is performed under equilibrium conditions (Scatchard, 1949). Binding studies with radiolabeled EGF on EGFR expressing cells revealed a concave-up (biphasic) Scatchard plot, which is usually interpreted as the existance of two receptor populations: a high affinity (K_d=10-100 pM) and a low-affinity (K_d=1-2 nM) population. Evidence for this hypothesis has come from observations that in cells treated with phorbol esters such

as PMA high affinity receptor have been converted into low affinity receptors. Furthermore, pre-incubation of the cells with the monoclonal antibody 2E9 selectively prevents low-affinity binding, suggesting that the different affinity populations of the EGFR are pre-existing (Defize et al., 1988; Lax et al., 1989). Similar concave-up Scatchard plots have been observed in cell types of diverse origins, suggesting that this phenomenon is an inherent characteristic of EGFR (Berkers et al., 1991; Defize et al., 1988; Mattoon et al., 2004). However, also exceptions to this observation have been found: cells from different colon carcinomas were shown to possess only high affinity receptor (Francoual et al., 2006).

Structural and biochemical data have provided structural evidence for high- and low-affinity binding. In the closed conformation, interaction of EGF with the ectodomain is restricted to either domain I or III. In contrast, the dimerized open conformation forms a binding pocket for EGF, in which the ligand can interact with two domains. Therefore, the high- and low-affinity receptor binding may reflect a balance between low-affinity tethered monomers and pre-assembled dimers in open conformations.

In favour of this model is the finding that both EGFR monomers and predimers can be found in unstimulated cells such as A431. Scatchard analysis of both forms showed that the affinity of the dimers was 10-fold higher than the monomer, suggesting that the presence of both affinity forms on the cell membrane results from an equilibrium between monomeric and predimerized EGFR (Boni-Schnetzler and Pilch, 1987). A cysteine mutant of EGFR, used to predimerise EGFR in the absence of EGF, was found to have an increased fraction of high-affinity receptors (Sorokin et al., 1994). Mutants in domain II that perturb the dimerization of EGFR, were found to result in low-affinity receptors, or increased the dissociation rates of EGF (Mattoon et al., 2004; Walker et al., 2004). Complete removal of domain II also resulted in a loss of the high-affinity EGFR, suggesting that the extended conformation of EGFR is stabilized by the formation of predimers (Garrett et al., 2002). Mutations in domain IV that break the intramolecular tether were indeed found to increase the receptor's affinity for EGF by almost 3-fold (Ferguson et al., 2003). Conversely, locking this tether by introducing a cysteine bridge between domains II and IV was found to result in the loss of high-affinity EGFRs (Walker et al., 2004).

Interestingly, mathematical modeling revealed that the two affinity states can not be explained solely by a population of receptors alternating between open and closed conformations (Klein et al., 2004; Mattoon et al., 2004). Modeling EGF-binding data with the presence of two conformations requires the introduction of "external" sites, enabling stabilization of the EGFR pre-dimers (Klein et al., 2004). These external factors may be components of the clathrin machinery, or factors involved in receptor endocytosis. The cytosolic domain is likely to interact with such factors, which is in line with earlier findings. Several deletion mutants of the EGFR cytosolic domain have been reported to display exclusively low-affinity binding (Livneh et al., 1986; Prywes et al., 1986; Van der Heyden et al., 1997). A mutant lacking a peptide stretch of 19 aminoacids in the tyrosine kinase domain only displays low affinity receptors (Van der

Heyden et al., 1997). This suggests that intracellular factors are involved in maintaining the balance between low and high affinity receptors.

Also alternative models have been described to explain the binding characteristics of EGF. Instead of pre-dimers, heterogeneities in receptor density were proposed to account for the concave-up shape of the Scatchard plots (Mayawala et al., 2005). Regions with high EGFR densities would result in the steep part of the plot, whereas low-density regions represent the shallow, low-affinity part. From these data it was concluded that in A431 cells, 14% of the receptors are found in 0.2% of the cell surface, which correlates with the percentage of high-affinity receptors. In addition, the presence of two affinity classes has been explained by suggesting negative cooperativity mechanisms. The structural model of high- and low-affinty receptors predicts that EGF binding contributes positively to binding of other EGF molecules, resulting in a concave-down Scatchard plot. Negative cooperativity on the other hand can theoretically result in a concave-up plot. In a recent paper, binding data were fitted with a model that allows different kinetics between the binding of the first and second ligand to the dimer (Macdonald and Pike, 2008). EGFR binding data correspond with a model in which the first ligand binds with kinetics that correspond to the high affinity receptor (~200 pM). This event lowers the dimer's affinity for the second ligand to values that correspond to the low affinity receptor (2.9 nM). However, the authors fail to incorporate the presence of higher-order oligomers into their model.

The functionality of the presence of two affinity forms of one receptor on each cell has not been unraveled yet. Low-affinity receptors appear not to be involved in early signaling in response to EGF. Although lower in number, the high-affinity receptors appear to be sufficient for signaling. Blocking the low-affinity receptors with monoclonal antibody 2E9 specifically blocked binding of EGF to the low-affinity EGFR, without decreasing the ligand induced phosphorylation of EGFR (Defize et al., 1989). Conversely, blocking high affinity binding with Moab108 blocked EGFR signaling. Single-molecule analysis of fluorescent EGF binding to cell surfaces has been applied to study the kinetics of EGF binding. Interestingly, EGF predominantly binds to a dimerized EGFR complex, followed by the direct arrest of the second EGF (Sako et al., 2000). Moreover, EGF binding occurs two orders of magnitude faster to EGFR dimers than to monomers (Teramura et al., 2006). Based on these data a kinetic model for EGFR activation was suggested which predicts that the signaling through predimers would occur two orders of magnitude faster then via the monomeric receptors.

Negative feedback control

Affinity regulation

The activation of EGFR can be inhibited by a process called receptor desensitization or

receptor transmodulation: the reduction of the affinity for its ligand. This can be achieved by the EGFR itself, or by other transmembrane receptors. These latter receptors involve other tyrosine kinase receptors such as the PDGF receptor but also receptors from the class of G-protein coupled receptors (GPCR)(Countaway et al., 1989; Santiskulvong and Rozengurt, 2007a). Interestingly, activation of GPCRs by their ligands has also been shown to increase the activity of EGFR, mediated by release of precursor EGFR ligands via metalloproteases (Gschwind et al., 2003; Sunnarborg et al., 2002). Activation of the GPCRs induces the activation of coupled heterotrimeric G-proteins, leading to the $G\alpha_q$ induced activation of phospholipase C β (PLCβ). Consequently, diacylglycerol (DAG) is produced by hydrolysis of $PtdInsP_2$, which leads to the activation of several PKC isoforms, which is probably responsible for the transmodulation (Newton and Johnson, 1998). Proof for this PKC dependent transmodulation has come from observation that treating cells with phorbol esters or DAGs leads to inhibition the tyrosine kinase activity of EGFR, and a decrease in the affinity for its ligands (Friedman et al., 1984; Hunter et al., 1984). This inhibition has been attributed to the phosporylation of Thr-654 by PKC in several studies (Cochet et al., 1984; Lund et al., 1990; Santiskulvong and Rozengurt, 2007b).

Internalization

The strength and duration of the EGFR signaling is strongly regulated by removal of the receptor from the cell membrane and targetting for lysosomal degradation. Two processes are responsible for the reduction in cell surface located EGFR: a) an increase in the rate of internalization, and b) a decrease in the fraction of receptors that recycle. Directly after EGFR activation, the endocytosis rate constant k_e of the active receptor is increased 5-10 fold as compared to the endocytosis of non-stimulated EGFR. Interestingly, internalization rates of the other members of the ErbB family are identical in both activated and resting states, which is probably due to the absence of regulatory internalization sequences in their intracellular domains (Sorkin et al., 1993; Waterman et al., 1999). Initial steps in the endocytosis of EGFR are the recruitment of adaptor proteins for the internalization machinery. Following autophosphorylation of the tyrosine residues on EGFR, Eps15 is recruited to the plasma membrane where it undergoes phosphorylation by EGFR (Fazioli et al., 1993; van Delft et al., 1997). Subsequently, adaptor protein-2 (AP-2) complex is recruited to the EGFR-Eps15 complex. In turn, AP-2 forms a docking site for clathrin, eventually leading to the formation of a clathrin coat around the activated receptor. The curvature induced by the assembly of the clathrin coat initiates the formation of a clathrin coated vesicle. The GTPase dynamin is involved in the final steps during vesicle fission. Although deletion of cytosolic parts of EGFR often leads to impaired internalization, complete inhibition has not been accomplished. Moreover, kinase-deficient mutants of EGFR are also internalized, albeit at a slower rate. Thus, multiple redundant mechanisms of EGFR internalization may exist. Knocking down different components of the endocytosis machinery such as clathrin with siRNa results in a reduced

EGFR internalization speed, suggesting the existance of different parallel pathways: clathrin dependent and clathrin-independent (Sigismund et al., 2005). The local EGF concentration may be an important determinant for the internalization pathways, and may regulate EGFR internalization via parallel pathways. After stimulation with low EGF concentrations, the receptor is mainly endocytosed via clathrin-coated vesicles, whereas at higher EGF doses the receptor was equally partitioned between clathrin-coated pits and caveolae (Sigismund et al., 2005). Internalization via the non-clathrin route can be effectively inhibited with farmacological tools such as filipin and nystatin.

Interestingly, EGF receptor ubiquitination appears to correlate to the internalization pathway. EGFR ubiquitination is mediated by the ubiquitin ligase Cbl, which binds either directly to pY^{1045} via its PTB domain, and is in addition recruited to that site by the adaptor protein Grb2 (Levkowitz et al., 1999; Levkowitz et al., 1998). Although first thought to be polyubiquitinated, later studies found that the EGFR is monoubiquitinated on multiple residues, referred to as multiubiquitination (Haglund et al., 2003b). However, more recent mass spectroscopic analysis has shown that the EGF receptor is polyubiquitinated, as more than half of the total EGFR-bound ubiquitin is present in K63 or K48 polyubiquitin (Huang et al., 2006). By fusion of EGFR with an ubiquitin moiety, it was found that a single ubiquitin is sufficient for receptor internalization and degradation. (Haglund et al., 2003a; Huang et al., 2006; Mosesson et al., 2003). The clathrin-dependent internalization of EGFR is reported to be independent of ubiquitination, but the alternative route correlates with the appearance of detectable ubiquitinated EGFR (Sigismund et al., 2005). Nevertheless, a 15KR mutant of EGFR, lacking 15 lysine residues, is negligibly ubiquitinated, but has internalization rates similar as the wildtype receptor (Huang et al., 2007). However, these studies were performed at low EGF concentrations, allowing exclusive internalization through the clathrin-mediated pathway. In addition, recent findings have shown that a dileucine motif at positions 1010/1011 is essential in EGFR endocytosis. Mutation of these residues resulted in an impaired EGFR internalization in response to EGF-binding, independent of kinase activity (Wang et al., 2007a). The EGF-induced dimerization may be sufficient for internalization mediated by the dileucine motif. In certain cell types, internalization may be even more complex, as migratory epithelial or mesenchymal cells have revealed a novel pathway for EGFR internalization, dorsal waves or ruffles. This pathway requires EGFR phosphorylation, dynamin-2 and active PI-3-K, but is independent of clathrin or caveolae (Orth et al., 2006).

Plasma membrane organization

Lipid environment

Numerous reports suggest that the activity of EGFR can direcly be modulated by its lipid environment. Reconstitution of the receptor in liposomes has shown that cholesterol and

phosphatidylinositides positively regulate EGFR affinity (den Hartigh et al., 1993). Likewise, the affinity of the insulin receptor for insulin increases by using liposomes of saturated lipids (Gould et al., 1982). The EGF receptor is also modulated by gangliosides, sphingolipids with an oligosaccharide headgroup including one or more sialic acids. Direct interactions have been reported between EGFR and a number of gangliosides (Miljan et al., 2002; Murozuka et al., 2007). Inhibitory alterations in the ligand-induced phosphorylation of EGFR, or proliferation rate were found after treatment with ganglioside GM3 (Bremer et al., 1984; Miljan and Bremer, 2002; Mirkin et al., 2002; Murozuka et al., 2007). Also endogenous GM3 is suggested to be involved in PKC- induced suppression of EGFR activity and signaling (Wang et al., 2007b). On the other hand, gangliosides such as GD1a or GM1 have been reported to have a stimulatory effect on EGFR activity (Liu et al., 2004; Miljan and Bremer, 2002). Further characterization of the effect of GD1a learned that the number of high-affinity EGFR was increased, as well as the number of predimerized receptors (Liu et al., 2004). These data indicate that also the lipid bilayer of the cell membrane that forms the direct environment of the EGF receptor, can contribute to the regulation of EGFR signaling

Lipid heterogeneity

Heterogeneity in lipid distribution is a very general phenomenon throughout the cell. First of all, differences in lipid composition can be seen between different organelles. The cellular lipidome comprises over 1000 lipids. A number of bulk lipids can be found in a large number of locations, but less abundant lipids are found only in certain structures.Although technical limitations prevent a detailed analysis of the organelle composition, a number of organelle-specific differences have been found. The ER and Golgi contain almost exclusively the glycerophospholipids PC, PE, PS and PI. In the TGN and endosomes, besides the glycerophospholipids also sphingomyelin and cholesterol can be found (for a review see (van Meer, 1989)). Also between apical and basolateral parts of the plasmamembrane significant differences in lipid composition can be found. This was demonstrated by analysing the lipid composition of viruses budding off from either basolateral or apical membranes of MDCK cells (van Meer and Simons, 1982).

A second layer of asymmetry is caused by different lipid compositions of the two bilayer leaflets (Gordesky and Marinetti, 1973; Verkleij et al., 1973); reviewed in (Verkleij and Post, 2000)). The bilayer asymmetry in principle reflects the biosynthetic pathways of the lipids. In addition, this asymmetry is maintained by a very slow spontaneous flip-flop rate of lipids, retentive factors that trap lipids in one leaflet, or proteins involved in lipid transport (van Meer et al., 2008). Glycerophospholipids are synthesized on the cytosolic side of the ER membrane (Henneberry et al., 2002). Only PC is then transported to the luminal side. Vesicles originating from the ER are transported via the Golgi to the plasma membrane, resulting in an enrichment of PS, PE and PI on the cytosolic leaflet on the plasma membrane. Sphingomyelin is produced on the lumenal side of the Golgi vesicle, and consequently ends

up on the extracellular side of the plasma membrane. Although lipids can flip-flop between the two leaflets, this process is rather slow. Additionally, the lipid asymmetry is actively maintained by the activity of flippases, which transport the PS and PE against the electrochemical gradient in a ATP-dependent manner. The importance of the bilayer asymmetry is best illustrated by the role of PS in removal of apoptotic cells by macrophages. During apoptosis, a PS-specific flippase is activated, leading to the exposure of PS on the apoptotic cell surface. The inner leaflet PS is then recognized by macrophages, phagocytosing the apoptotic cells (Fadok et al., 1992).

The lipid raft

A third and most recently discovered level of heterogeneity can be found in the plane of the membrane. In the Singer and Nicholson model of the membrane, lipids serve mainly as passive components of the cellular borders. Irrespective of their very diverse nature, the movement and distribution of the population of lipids was considered to be random. Novel insights into the behaviour of lipids in solution drastically changed the view of lipid distribution in the cell membrane. Certain species of proteins were found to be difficult to solubilize in non-ionic detergents such as Triton X-100. Although this was initially attibuted to the attachment of these proteins to the cytoskeleton, later observation demonstrated that this could not hold true for proteins with an outer leaflet GPI-anchor (Hooper and Turner, 1988). Instead, the idea that lipids were responsible for the DRM localization of these proteins, and could guide the membrane organization led to the lipid raft hypothesis (Simons and Ikonen, 1997; Simons and van Meer, 1988).

Model membrane studies provided clear evidence that mixtures of phospholipids and sphingolipids could easily organize into distinct domains, based on the phase separation of the lipids (Baumgart et al., 2003; Brown and London, 1998; Dietrich et al., 2001; Hammond et al., 2005; Kahya et al., 2004). The most important determinant of phase behavior is the phase transition temperature (T_m). Simple phospholipid bilayers below their T_m form a solidified gel phase, which melts to a fluid liquid disordered (L_D) phase above the T_m. Different lipids have different T_ms, which is a result of the length and saturation of their fatty acids, and the composition of the headgroup. Typical glycerophospholipids have a saturated acyl chain at the glycerol sn-1 position, and unsaturated acyl chains connected to sn-2, for example 16:0/18:1. In contrast, sphingolipids are comprised of a 18:0 sphingoid base with a saturated fatty acid with various lenghths (18:0-24:0) (Brown, 1998). As a result, glycerophospholipids have a lower T_m than sphingolipids. Most glycerophospholipids undergo the phase transition at temperatures around 0°C (Koynova and Caffrey, 1995). This is partially due to the saturation level of the fatty acid tails, which contain less cis double bonds in most sphingolipids. Sphingolipids are still in a solid gel phase at 37°C, but can be fluidized by the addition of cholesterol. Besides the temperature-dependent phase transition of lipids, another form of phase-separation can occur

in a lipid bilayer. Hydrogen bonding between the double saturated fatty acids and cholesterol allows tight packing into a liquid ordered (L_O) domain. Mixtures of sphingomyelin, PC and cholesterol do not form homogeneous lipid bilayer, but instead organize into phase-separated domains. The L_O domains are mainly composed of sphingomyelin and cholesterol, surrounded by the L_D phospholipid phase. The driving force for the formation of domains probably involves two major factors. First, hydrogen bonding between sphingolipids and cholesterol allows tight packing of the lipids (Brown, 1998; Rietveld and Simons, 1998). The flatness of the rigid sterol ring structure is assumed to preferentially interact with saturated acyl chains. Secondly, by coalescing into larger domains, the unfavored line tension between the two phases is minimalized.

As the composition of the cell membrane resembles a non-ideal liquid mixture, phase separation may drive the formation of raft in cells. Using model membranes, the lipids from the lipid-ordered phase were found to be resistant to treatment with non-ionic detergents such as Triton X-100, whereas lipids from the liquid-disordered phase were readily solubilized (Brown and London, 2000; London and Brown, 2000; Schroeder et al., 1998). As a result, detergent-resistance was soon introduced as powerful discriminator between liquid-order “raft” domains, and liquid-disordered “bulk” membrane.

Transient confinement zones

Molecules embedded in the plasma membrane can diffuse in the two-dimensional space of the bilayer. However, free movement is restricted to certain areas, and diffusional speed can vary between these areas. Lipids such as GM1, or GPI-anchored proteins, were found to reside preferentially in areas in which they have a relatively low diffusional speed. Furthermore, movement to other areas involves a fast and stepwise hop-diffusion. Consequently, the existence of transient confinement zones was proposed as an organizing characteristic of plasma membranes (Simson et al., 1995). Single particle tracking has shown that these “transient confinement zones” (TCZ) display properties of lipid rafts, as the abundance and size of the zones was diminished by cholesterol extraction or sphingolipid depletion (Dietrich et al., 2002; Sheets et al., 1997; Simson et al., 1995). However, also cytoskeletal factors are assumed to be involved in the behavior of TCZs.

Pickets and fences

Kusumi and coworkers have proposed a model in which the plasma membrane is organized by “fences” and “pickets” (Kusumi and Suzuki, 2005). The actin fiber network, lining the cytosolic side of the membrane, forms the fence that restricts the movement of transmembrane proteins in two ways. First, due to the cytosolic part of the protein, it has to cross a energetic barrier to pass the fences imposed by the actin network (Sako and Kusumi, 1994; Sako et al., 1998; Tomishige et al., 1998). Thus, the membrane component resides within the actin-lined compartment for certain period, before it hops to a neighboring compartment. Secondly, most

transmembrane proteins are capable of binding the actin network either directly or through the action of adaptor proteins. This results in the formation of pickets, lining the actin network. However, this can not explain the restricted movement of lipids and GPI-anchored proteins so additional mechanisms complicate the model. The pickets are thought to result in a higher viscosity of the local membrane, rendering the surrounding lipids less mobile. Furthermore, arranging the pickets on the cytoskeleton mesh would result in a linear zone that would suppress the mobility of enclosed membrane components. Consequently, dependent of the density of the pickets, the movement of single-leaflet membrane components is restricted.

Caveolae

Besides the classical raft domain, other domain-like structures have been characterized. Caveolae ("little cavities") are flask-shaped invaginations of the plasma membrane, morphologically distinct from clathrin coated pits. Caveolae are identified by the presence of the protein caveolin. This protein is a found to form the inner membrane coat of caveolae (Rothberg et al., 1992). It is characterized by cytosolic N- and C-termini and a hairpin loop that is inserted into the membrane. Caveolin-1 is a lipid-binding protein, capable of binding cholesterol and fatty acids (Murata et al., 1995; Trigatti et al., 1999). The protein is palmitoylated on three cysteine residues, modifications that are involved in cholesterol binding and oligomerization of the protein (Monier et al., 1996; Uittenbogaard and Smart, 2000). In fractionation studies, caveolin-1 comigrates with the DRM fractions, suggesting that caveolin-1 is a raft resident protein (Chang et al., 1994; Sargiacomo et al., 1993; Yamabhai and Anderson, 2002). However, the presence of caveolin-1 is not essential for the formation of lipid domains. Cells lacking detectable levels of caveolin have comparable DRM compositions, suggesting that rafts do not depend on the formation of caveolae (Wu et al., 1997).

Strikingly, bilayers made of cholesterol and lipids characteristic of the inner leaflet, PS and PE with unsaturated acyl chains, do not form L_O domains (Wang and Silvius, 2001). This suggests that the inner leaflet must be organized by other factors such as proteins. Thus, caveolin may be important for the coupling between the outer and inner leaflet by forming domains in the latter while sensing cholesterol in the former.

Raft targeting

How a resident molecule is targeted to lipid rafts, is far from clear. The molar partitioning coefficient K_p only describes how a membrane-associated protein distrubutes over coexisting phases in membrane, but does not explain why. Dual acylation of Src family members may promote targeting to L_O domains, as also shown for GPI-anchored proteins. These mechanisms however do not account for the raft localization of transmembrane proteins, suggesting that other mechanisms apply to this class of molecules. In its simplest form, raft targeting of transmembrane proteins is a problem of solubility in the L_D domain, driving the partitioning equilibrium towards the L_O side. Another factor implicated in raft partitioning is

the length of the transmembrane domain, since the saturated and packed L_O phase is thicker than a L_D membrane. Hydrophobic mismatching between a long transmembrane domain and hydrocarbon thickness of L_D lipids may therefore be a driving force for raft partitioning. However, no evidence for this mechanism has been found so far (van Duyl et al., 2002; Vidal and McIntosh, 2005).

Alternatively, oligomerization is a good candidate for targeting proteins to raft domains. If oligomerization does not alter the K_p of each monomers in the oligomer, the partition coefficient is the product of the partition coefficients of the monomers that constitute it (Simons and Vaz, 2004). Thus, a K_p weakly in favor of the L_O phase, is drastically increased towards raft partitioning after oligomerization. Moreover, a number of proteins have caveolin-binding motifs which interacts with the 'scaffolding domain' consensus of caveolin-1, which may explain their presence in caveolae and, consequently, DRMs (Smart et al., 1999).

Transmembrane rafts

A major disadvantage of model membrane systems is that they differ from biological membranes in two important aspects: biological membranes are not in equilibrium but instead highly dynamic, and secondly, biological membranes are highly asymmetric. The lipid composition of cells is very complex, and membrane lipids are constantly added, removed or converted. Secondly, due to the lipid asymmetry, the composition of the plasma membrane's inner leaflet is atypical for lipid raft formation. The low abundance of glycosphingolipids in the inner leaflet does not allow formation of typical glycolipid-enriched rafts as found in the outer leaflet. Phosphoinositide lipids such as $PtdInsP_2$ have been suggested to be involved in inner leaflet rafts, and have actually been found in DRMs (Pike et al., 2005). Interestingly, $PtdInsP_2$ is intimately involved in the regulation of the actin cytoskeleton, and a number of proteins can directly bind to $PtdInsP_2$ by means of their PH or FYVE domains.

Patching of GPI-anchored proteins on the extracellular side induces changes in the distribution of lipid-anchored components of the signaling machinery on the cytosolic leaflet of the same membrane. For instance, clustering of GPI-coupled HA proteins induced clusters of raft-resident H-Ras on the inner leaflet, but not of the non-raft isoform K-Ras (Eisenberg et al., 2006). In addition, immunoprecipitates of GPI-linked proteins co-immunoprecipitate the Src family kinase Lck (Stefanova et al., 1991). These observations suggest that rafts or membrane domains are not only present in the outer leaftlet, but are somehow connected to the inner leaflet through an unknown mechanism. Interdigitation of the long acyl chains found in L_O domains may generate a domain in the bilayer. Alternatively, transmembrane proteins are possible candidates by their ability to contact and thereby organize both leaflets.

Different scales

Although the concept of lipid domains has gained more and more acceptance, no consensus on the size of raft has been found so far. Attempts to visualize rafts directly by immunofluorescence

have so far been unsuccesful. However, indirect methods such as FRET provided clear evidence for phase separation in cells, driven by the saturation of the acyl chains (Sengupta et al., 2007). Single particle tracking studies on non-raft lipids has provided domain sizes of 30-230 nm (Murase et al., 2004). Lack of consensus in the field broadened the definition of a raft to a structure which involves more than two molecules, so as not to exclude any possibilities (Kusumi and Suzuki, 2005; Prior et al., 2003). Nevertheless, even at these dimensions the structures may be functional as signaling platforms (Harder and Engelhardt, 2004).

Ken Jacobson recently proposed an extended model for membrane domains, in which they are classified into three types (Jacobson et al., 2007). In its smallest form, including shells, complexes and nanodomains, the domains are very transient and dynamic. In the shell model, proteins form the nucleation sites for raft formation, by assembling a lipid shell around the proteins GPI-anchor or transmembrane domain. This shell is conceptually analogous to a solvent shell, for instance hydration shells that surround proteins or ions in solution. Functionally, these shells mediate the transition from the solute to the bulk solution. Rafts are transient and unstable structures, that can be stabilized by association with proteins (Kusumi et al., 2004). By association with stabilizing components such as caveolin, larger nanodomains up to 100 nm including caveolae can be formed. The more stable microdomains comprise the third class of domains, can be more than 1 μm in size and are the result of signaling processes (Jacobson et al., 2007).

Function of rafts and caveolae

Lipid raft have been proposed to be an internalization pathway, in particular caveolae. Caveolin can be associated with tubular structures that can protrude into the cell for several micrometers and even form tubular transcellular structures (Carozzi et al., 2000; Dvorak and Feng, 2001). Numerous reports have shown that caveolae may be involved in a clathrin-independent internalization pathway (Anderson, 1998; Pelkmans et al., 2001)(reviewed in (Lajoie and Nabi, 2007)). The GTPase dynamin, involved in pinching off invaginations of the membrane to form endosomes, is found at the neck of caveolae (Henley et al., 1998; Oh et al., 1998) For instance, the SV40 virus enters the cells via a clathrin-independent, dynamin-dependent pathway (Pelkmans et al., 2001). Caveolae have also been identified as endocytosis site for the B-subunit of cholera toxin (CTB) (Nichols, 2002; Parton et al., 1994). In contrast, others have suggested that caveolae are more likely to inhibit the internalization (Kirkham et al., 2005; Le et al., 2002). The raft-mediated endocytosis of CTB is inhibited by overexpression of caveolin-1, whereas reduction of caveolin-1 expression was associated with an increased plasma membrane mobility and internalization speed (Kirkham et al., 2005).

In addition, lipid rafts have often been mentioned to be involved in signal transduction processes. In particular immune signaling significantly involves rafts, as an increasing number of receptors on B-cells, T-cells and mast cells are found to be raft resident in resting or activated cells (Holowka et al., 2005; Kabouridis, 2006; Pierce, 2002). Also the insulin receptor

is dynamically associated with DRM fractions during insulin signaling (Vainio et al., 2002). As a result of the preferential association of certain proteins with the L_o domain, rafts may serve as signaling platforms that facilitate signaling by clustering these components. In particular GPI-anchored proteins, double acylated proteins of the Src family and certain transmembrane receptors are found preferentially in DRMs (Puri et al., 2005). Interestingly, many of these proteins are involved in signal transduction processes. Thus, lipid rafts may enhance the signal transduction by sequestering components of the signaling machinery.

On the contrary, the assumed heterogeneity in the lipid raft population may reflect a way to prevent signal transduction. By separating components of the signal transduction machinery between distinct domains, preliminary signal transduction is prevented. Signal transduction may require fusion or rearrangement of the smaller domains into larger platforms (Jacobson et al., 2007; Larson et al., 2005; Wang et al., 2002; Wilson et al., 2004). Additionally, signaling and endocytosis may converge in rafts or caveolae. In fact, inhibition of tyrosine kinase activity decreased the caveolae-mediated internalization rate, whereas treatment with phosphatase inhibitors okadaic enhances the internalization speed (Kirkham et al., 2005; Parton et al., 1994; Pelkmans et al., 2002). Moreover, caveolin-1 is phosphorylated at position 14 by Src, although the role of this modification in endocytosis is unclear (Glenney, 1989).

EGFR and rafts

Biochemical approaches have shown that EGFR is a raft-resident protein, and is also found in caveolae (Puri et al., 2005). Moreover, direct binding between the caveolin-1 scaffolding domain and the EGFR kinase domain has been shown previously (Couet et al., 1997). So far, most studies on the association between EGFR and caveolae indicate that caveolin-1 suppresses EGFR activity (Matveev and Smart, 2002). Depletion of caveolin-1 greatly increases the proloferating activity of tumor cells, whereas re-introduction of caveolin-1 in oncogenically transformed cells inhibits cell growth (Engelman et al., 1997; Lee et al., 1998; Razani et al., 2001). The association between EGFR and caveolin-1 was studied in human glioblastoma cells, and found to be related to the phosphorylation state of the receptor. In these cells, EGFR dissociated from caveolin after ligand-induced tyrosine phosphorylation (Abulrob et al., 2004). Conversely, association of EGFR with caveolae inhibits its kinase activity (Wang et al., 2007b). Nevertheless, the majority of EGFR is found to reside in non-caveolar regions on the cell membrane (Puri et al., 2005).

Plasma membrane organization is thought to be essential for proper functioning of its constituents. One of these organizing principles, lipid rafts, is hypothesized to form a signaling platform (Simons and Toomre, 2000). The EGF receptor has been reported as a raft-resident membrane protein, and the function for this raft localization is of particular interest in raft studies. The dependence on particular outer leaflet lipids for proper signaling, and the involvement of various membrane bound signal transduction components, suggest an important role for the plasma membrane. Consequently, proper organization of the membrane

is thought to be essential for adequate receptor functioning. Knowledge of this organization may therefore lead to a better understanding how the EGF receptor and the organization of the plasma membrane mutually influence each other.

Detergent-resistance is, due to its relatively simple procedure, popular in studies on lipid rafts and membrane domains. Although widely used as a method to study raft localization of molecules of interest, preparation of detergent-resistant membrane fractions has a number of major disadvantages. First, the organization of the membrane structure is highly disturbed, possibly leading to induced protein interactions or clustering (Heerklotz, 2002; van Rheenen et al., 2005). Secondly, conclusion of spatial organization can not be drawn from DRM analysis. Different domains may run together at similar densities in the gradient, leading to overinterpretation of colocalization in the cell membrane. To understand the behavior and interaction of membrane components, alternative approaches under non-invasive and possibly live-cell conditions are therefore highly preferable.

Knowledge about the organization of the plasma membrane requires spatial information about the molecules of interest. Acquiring this information in a non-invasive and preferably live-cell fashion can be obtained by microscopy. A major limitation of classical light microscopy is the spatial resolution of the system. This maximal resolution, or the minimal distance at which two objects can be seen as spatially separate, is known as the Abbe resolution limit. This resolution is proportional to the wavelength λ and numerical aperture of the objectives, and is described as $0.61 \times \lambda$ /NA, resulting in maximal 200 nm for visible light under optimal conditions. Consequently, different objects within this 200 nm cannot be observed as separate entities. Electronmicroscopy has made it possible to improve the resolution thousand-fold, but is limited by the requirement for fixed specimens. Moreover, due to the specimen preparation it is very time-consuming. Nevertheless, information on molecular interactions and dynamics can be obtained in an indirect manner, by applying the changes in spectroscopic properties of fluorescent markers dependent on local circumstances. This method, called Forster resonance energy transfer (FRET) can be used to determine molecular proximities in the nanometer range. In this thesis, the organization of the plasma membrane surrounding the EGFR is studied with FRET based assays to gain more insight in the organization of the EGFR and other plasma membrane constituents, and how they mutually interact.

Part II: methodology

A. Spectroscopy

Fluorescence

Fluorescence light microscopy is an important tool for modern cell biology research. Using fluorescent markers, specific cellular structures or molecules can be specifically visualized, or even tracked when using live cells. One of the basic principles of fluorescent molecules is the excitablity of a fluorochrome by specific wavelengths of (near-)visible light. The photons excite singlets to a higher vibrational level. By absorbance of the excitation light, electrons make a transition from a ground state S_0 to an excited state S_1' or S_2' (Fig 2). The energy of this transition equals the energy of the absorbed photon, which is described in

$$E = h \times c / \lambda \qquad [1]$$

where h is Planks constant, and c and λ are the velocity and wavelength of light in vacuum, respectively . Within picoseconds, the singlet falls back to the lowest excitated vibrational state S_1 due to non-radiative energy losses .

From the S_1 level, the electron can return to the S_0 state with the emission of a photon (Fig.2). The energy of the emitted light equals the energy of the photon that was used to excite the electron, minus the energy lost in secondary processes such as internal conversion. Consequently, the emission wavelength is red-shifted, i.e. has increased wavelength. This difference between excitation and emission is known as the Stokes shift, named after Sir George C. Stokes who first described this phenomenon. The Stokes shift is essential to the application of fluorescence, since it allows separation of the excitation from the emission light. As described above, processes other than photon emission can result in a transition back to the S_0 state. This is described in the quantum yield, which is the ratio of the number of photons emitted to the number of photons absorbed.

Using fluorescent labels, a number of tools have been developed that opened new areas of investigation. By using live cell imaging, fluorescent recovery after photobleaching (FRAP) provides data on the diffusion and immobility of protein populations, whereas single molecule tracking can be used to follow and track the paths of individual cellular components.

FRET

The excitated state of a particular fluorophore is not infinite, but lasts for a certain time, usually in the range of 1-10 ns, before its returns to the ground state under the emission of light. During this period, the singlet can also return to its S_0 state under the influence of a number of environmental factors in a non-radiative manner. This process, known as quenching, can

be a result of collision with molecules that will function as acceptors for the excitated state energy. One particular form of quenching is Fluorescence Resonance Energy Transfer (FRET) which occurs in the presence of a particular acceptor molecule. The excited donor probe can transfer the energy of the S_1 state to this acceptor, usually a fluorescent molecule, without the emission of light (Fig. 2). A first requirement for this process is a close proximity of the donor and acceptor probe, as the efficiency of FRET is inversely proportional to the sixth power of the distance between donor and acceptor. The relationship between the intermolecular distance R and FRET efficiency E are given in the equation

$$E = \frac{{R_0}^6}{{R_0}^6 + R^6} \qquad [2]$$

The Förster distance R_0, which is the intermolecular distance at which the FRET-efficiency is 50%, is for most fluorophores in the range of 10 to 100 Å. Furthermore, the donor's emission spectrum and the acceptor's excitation spectrum need to have sufficient overlap. The Förster radius is described as

$$R_0 = \left[8.8 \times 10^{23} \bullet \kappa^2 \bullet n^{-4} \bullet QY_D \bullet J(\lambda)\right]^{1/6} \qquad [3]$$

where κ^2 is the orientation factor of the donor and acceptor dipole moments, n is the refractive index, QY_D is the quantum yield of the donor in the absence of acceptor, and $J(\lambda)$ is the integral of the spectral overlap.
The orientation factor κ^2 is described as

$$\kappa^2 = \left(\cos\theta_T - 3\cos\theta_D \cos\theta_A\right)^2 \qquad [4]$$

where θ_T is the angle between the donor emission transition moment and the acceptor absorption transition moment, θ_D and θ_A are the angles between the donor-acceptor connecting line and the donor emission transition moment and acceptors absorption transition moment, respectively. In case of random orientation of the donor and acceptor probes, κ^2 equals 2/3.
The spectral overlap integral is described as

$$J(\lambda) = \int_0^\infty \varepsilon_A(\lambda) \bullet F_D(\lambda) \bullet \lambda^4 d\lambda \qquad [5]$$

where ε_A is the excitation coefficient of the acceptor, F_D is the fluorescent emission intensity of the donor as a fraction of the total integrated intensity.

FLIM

One way to observe FRET is to measure the sensitized emission of the acceptor, and consequently the reduction of donor emission. These ratiometric methods are relatively easy to perform and have become generally integrated in software supplied with confocal laser scanning microscopes. However, the relative contribution of donor and acceptor emission to this ratio is highly dependent on the concentrations of both probes, which is often difficult to control or determine. To avoid unwanted effects of local probe concentrations, FRET can also be determined by measuring the excited state time of the donor probe. As a result of the depopulation of the S_1 state of the donor due to FRET, the average time that a singlet will be in the S_1 state is reduced. Consequently, the loss of fluorescence of the donor is accelerated. This is described in the equation

$$E = 1 - \frac{\tau_{DA}}{\tau_D} \qquad [6]$$

where the lifetime of the donor in the presence (τ_{DA}) and absence of acceptor (τ_D) is given as

$$\tau_{DA} = \frac{1}{K_T + K_D + K_i} \qquad [7]$$

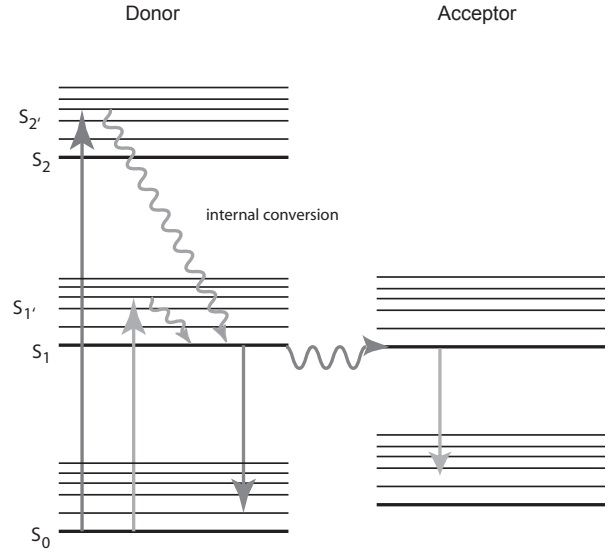

Fig 2. Jablonski diagram of fluorescent excitation, emission and FRET. From the S_0 ground state, absorbance of a photon can excite a singlet to S_1' or S_2' state . Non-radiative processes (diagonal sinus) return the singlet to the S_1 state, from where it can return to the S_0 state by emitting a photon. In proximity of an acceptor probe, the S_1 state can be depopulated by FRET, transferring the excitation energy to the acceptor (horizontal sinus). This acceptor in its turn can return to the S_0 state by emitting a photon.

$$\tau_D = \frac{1}{K_D + K_i} \quad [8]$$

in which K_T is the FRET rate, K_D is the radiative rate and K_i is the rate constant of non-radiative processes.

In order to measure the lifetime decay, the excitation mode of the donor probe differs from the steady-state excitation in ratiometric assays. First, a short pulse of light, generated by a picosecond or femtosecond laser source, is used to excite the donor probe. Subsequently, the decay in donor fluorescence is measured by a detector coupled to a recording device with a high temporal resolution, allowing a very precise determination of the decay time. The pattern of the donor emission behaves like a (mono-)exponential decay curve, and can be fitted in the equation

$$I(t) = I_0 e^{-t/\tau} \quad [9]$$

in which I_0 is the intensity of the donor at *t*=0 after excitation. Consequently, the lifetime of the donor can be derived from this equation.
A reliable fit of the time-resolved data requires a minimal number of counts througout the decay curve, which can be achieved by prolonged acquisition times. These requirements however limit a fast acquisition of the data, preventing the application of FRET-FLIM in live-cell measurements. By limiting the number of data points along the time-scale, the processes can be simplified and data collection can be reduced to seconds (Gerritsen et al., 2002). For this purpose, time-gated lifetime measurements have been developed, in which the decay of emitted light is recorded in consecutive time gates of a few nanoseconds. Data collection in four time gates enables a fast data acquisition without significant loss of sensitivity.

Homo-FRET

In addition to FRET between a donor-acceptor pair of different fluorophores, a similar process can also occur between identical fluorophores. Dependent on the particular Stokes shift, the red end of the emission spectrum partially overlaps the blue end of the excitation spectrum, allowing energy transfer between a pair of identical fluorophores. This approach has a number of advantages over hetero-FRET. In particular when studying the interaction between identical molecules, homo-FRET has a higher sensitivity and accuracy. Co-expression of donor and acceptor probes such as CFP and YFP-tagged proteins can lead to proper hetero-FRET pairs. However, also homo-interactions between YFP-YFP and CFP-CFP will be induced, which will not contribute to a hetero-FRET signal. The presence of only one fluorophore in the homo-FRET approach will circumvent this problem, increasing the sensitivity of the system.

In homo-FRET, the lack of spectral differences between donor and acceptor does not allow the use of ratiometric approaches, or the use of lifetime imaging. Although the lifetime of the donor probe is reduced, this is practically compensated by an increase in fluorescence from the acceptor in the same spectral range. Therefore, homo-FRET makes use of differences in the three-dimensional orientation of donor and acceptor. The excitablity of fluorophores is dependent on the orientation of the absorption dipole moment and the polarization direction of the light. When applying a polarized light source on a population of randomly oriented fluorophores, excitation of properly oriented molecules is favored. In a situation where the fluorophores are static, the orientation of the light will be retained during emission. However, the proximity of other fluorophores allows homo-FRET to take place. On average, this acceptor probe will have an orientation which is different from the donor probe, i.e. less polarized. Indirect excitation of the acceptor by FRET and subsequent emission will therefore result in the loss of polarization.

When the FRET efficiency is sufficiently high and FRET is fast and reversible, donor and acceptor probes will have identical chance of emission, and therefore the excitation energy will be distributed over the molecules within reach for FRET. Consequently, the orientation of the emission light will be proportional to the contribution of donor and acceptor probes. Since this is dependent on the number of molecules in the proximity, the final polarization will be a resultant of the number of FRET steps. Thus, the loss of polarization is a measure of clustersize of identical probes.

The fluorescent anisotropy r is defined as

$$r = \frac{I_{par} - I_{per}}{I_{par} + 2I_{per}} \qquad [10]$$

where I_{par} and I_{per} are the fluorescent intensities in the parallel and perpendicular channels with respect to the polarization direction of the excitation light, respectively.
In a non-static situation, the initial anisotropy will decay due to rotational translation of the fluorophore, as described in

$$r(t) = r_0 e^{-t/\phi} \qquad [11]$$

where ϕ is the rotational correlation factor of the fluorophore. In the additional presence of homo-FRET processes, the anisotropy decay is more complicated, but can be simplified by using a static system, e.g. in viscous solutions such as glycerol. Then, the anisotropy decays according to the following equation:

$$r(t) = (r_0 - r_{\inf})e^{-2\omega t} + r_{\inf} \qquad [12]$$

where r_{inf} is the limiting anisotropy at infinite time and ω is the homo-FRET rate.
The correlation between ω and homo-FRET efficiency E and fluorescent lifetime τ is defined as

$$E = \omega / \tau^{-1} + \omega \quad [13]$$

Now assume a cluster of fluorophores of size N, localized within FRET range. The initial anisotropy of the donor equals 0.4. If random orientation is assumed for the the acceptor molecules, which results in anisotropy values of 0.016 for these molecules, and FRET efficiency is sufficiently high, r_{inf} is only dependent on the number of FRET steps. This is described as

$$r_{\text{inf}} = r_0 / N \quad [14]$$

where N describes the number of fluorophores in the cluster. This demonstrates a direct correlation between the clustersize and r_{inf}, allowing determination of the clustersize by obtaining the r_{inf} value.

B. Probes

Fluorescent labeling is a powerful way to determine the localization of cellular components like proteins and glycans in cells. Fluorescent ligands or substrates can be applied to study receptors or enzymes, whereas a large number of specific antibodies are available for investigation of proteins, modifications or other epitopes. In addition, recombinant technologies have facilitated the imaging and tracking of proteins in live cells, by tagging the proteins of interest with fluorescent proteins such as GFP or DsRed. Simply applying these technologies, however, to resolve scientific questions has to be taken with great care, as they have certain technological limitations. Antibodies, mostly of the IgG isotype, are bivalent by nature. This feature increases the avidity to their epitopes, but may also lead to dimerization of their target proteins. In the light of clustering-induced signaling, this property of antibodies might lead to artifacts and mistinterpretations. Fusion of the protein of interest with fluorescent proteins may solve these problems, since these components don't need any additional labeling after expressing the recombinant proteins in cells. However, the fluorescent tag may, due to its relatively high mass (30 kDa for GFP) restrict the protein in its functioning and may prevent interaction with other components. Moreover, since the fusion protein is fluorescent already in early stages in the biosynthesis, it is nearly impossible to label specific cellular structures such as the cell membrane.

The suggested raft localization of EGFR was thought to increase the local

concentration of the receptor, but the sequence of events leading to this relationship is very speculative. Whereas raft localization might be the driving force for the clustering of EGFR on the membrane, others suggested that EGFR clustering by itself induced the formation of rafts or lipid shells around it. This characteristic imposes difficulties on the use of conventional antibodies in fluorescence studies, so the development of novel probes was a prerequisite for studying the interaction between EGFR and lipid environments. The development of small, monovalent, non-stimulatory and highly specific probes against the EGFR was a first step to unravel the membrane localization of EGFR in a non-invasive manner.

A number of animal species including cameloids contain a unique class of antibodies, comprised of only heavy chains (Hamers-Casterman et al., 1993). In contrast to conventional antibodies such as IgG, the absence of a light chain results in an antigen binding domain consisting of only a V_H domain (fig 3). The full immune repertoire of these V_H domains can therefore be cloned relatively easy into phage expression libraries. These nanobodies or VHHs (V_H fragments from Cameloid heavy-chain-only antibodies) can be selected from a library (immune or native), and can be produced in high amounts after selection. Due to their small size (15-17 kDa) nanobodies combine all the characteristics required for these FRET-FLIM studies. In theory, the epitopes recognized by the phages in a library are diverse, resulting in a group of nanobodies with differential antagonism or agonism. By applying the proper selection criteria, nanobodies with the desired characteristics can be retrieved from this library.

The visualization of lipids requires other approaches. Fluorescent lipid analogs have been used in lipid raft research, in particular in combination with FRET-based approaches (Sengupta et al., 2007). The fluorophore may be incorporated either in the acyl chain, or be part of the headgroup. Furthermore, lipid probes such as Laurdan can be used as a reporter of lipid order, by differing the fluorescent properties between L_O and L_D domains (Bagatolli et al., 2003), and has been used to demonstrate the presence of L_O domains in living cells (Gaus et al., 2003). However, the addition of lipid to the cells may disturb the metabolism and organisation of other lipids and proteins. Preferentially, probes are applied that report the localization of native lipids.

Antibodies against lipids are more difficult to generate. Due to the ubiquitous nature of lipids, phospholipid headgroups form aspecific epitopes. However, proteins with PH domains can interact with inner leaflet lipids such as $PtdInsP_2$, making them highly specific probes for these lipids. Glycosphingolipids have more complicated headgroups, comprising multiple glycans. Although their epitope-specificity is often demonstrated by binding to lipids on TLC plates, the specificity in intact cells, including a large collection of glycoproteins, is difficult to verify (reviewed in (Hoetzl et al., 2007)). Moreover, binding of antibodies directed against GM3 was found to depend on its clustering in domains, suggesting that the antibody's affinity is relatively low (Nores et al., 1987).

Cholera toxin is a hexameric protein complex of one A and five B subunits that specifically binds to ganglioside GM1. The intact complex is secreted by the bacteria Vibrio

cholerae and binds to the cell surface of the intestine, where subunit A enters the cell to disturb adenylate cyclase activity. The remaining circular and pentameric B subunit binds to the cell surface through interaction with the terminal sugar groups of GM1 (Merritt et al., 1994). Since it was recognized as a specific probe for a typical ganglioside, the cholera toxin B subunit (CTB) found many applications in microscopy. When conjugated to fluorescent probes, it is commonly used as a lipid raft marker.

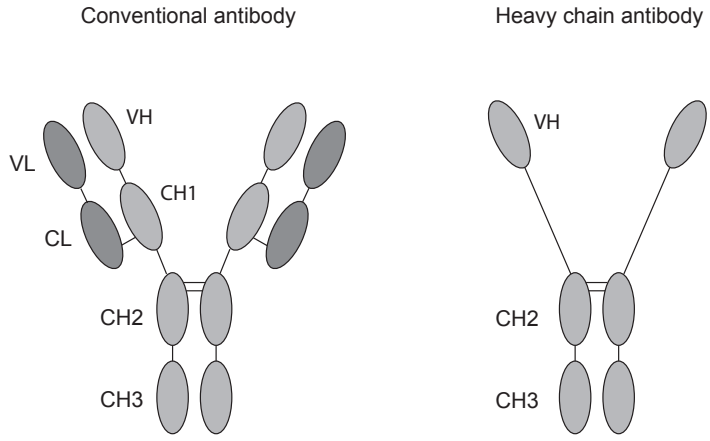

Fig 3. Composition of conventional antibodies versus heavy chain antibodies. Conventional antibodies consist of two heavy chains (light gray) and two light chains (dark gray). The heavy chains each comprise three constant domains (CH1-3) and a variable region (VH). The light chain consist of one constant (CL) and one variable domain (VL). The antigen binding region in composed of both VH and VL domains. In contrast, heavy chain antibodies are composed solely of heavy chains. Furthermore, they lack the CH1 domain. The antigen binding region in comprised entirely of the VH domain. In isolation, this domain is referred to as VHH or nanobody.

Outline of this thesis

Questions concerning the interaction between EGFR and membrane lipids have until now been limited to either biochemical approaches, or model systems like liposomes. Although these studies have generated valuable data, concern has rised whether the data from these studies can be extrapolated to the situation in vivo. In chapter 2, the raft localization of EGFR is studied in intact cells using a FRET-FLIM based study. To circumvent the possibility of receptor agonism by EGFR-specific fluorescent probes, we developed different highly specific, non-stimulating and non-antagonistic nanobodies against EGFR, and labeled these with fluorescent dyes. By applying these nanobodies on FRET-FLIM measurements, the EGFR appeared to localize to

membrane regions rich in the raft lipid ganglioside GM1. Surprisingly, the lipid environment of EGFR was found to change upon stimulation with EGF. In the resting state, EGFR interacts with GM1 in a cholesterol-independent manner. Interestingly, the colocalization of EGFR and another raft marker, GPI-GFP, was found to be non-existing in the resting state, but arised after EGF-induced receptor stimulation. According to these data, EGFR activation induces rearrangements of lipids in the outer leaflet of the plasma membrane, eventually leading to fusion of smaller lipid clusters (shells) into a larger signaling platform.

Fusion of the different rafts may play a role in the oligomerization of the EGFR, a process essential for EGFR signaling. The second aim of this study was to monitor the oligomerization state of the EGFR using homo-FRET. In chapter 3, a novel method indicated as confocal time-resolved fluorescence anisotropy imaging microscopy (CTR-FAIM) was developed to determine the clustersize of membrane proteins in a non-invasive manner. Although fluorescence anisotropy had been used in previous reports to study the clustering of GPI-GFP (Sharma et al., 2004), these studies were based on a different mode of data collection. In contrast to steady-state anisotropy, time-gated data collection was used, which results in a more sensitive determination of the oligomers. As an example, the clustersize of GPI-GFP, expressed in fibroblasts, was measured and was dependent on the subcellular localization, ranging from 1.2 in the Golgi, to 1.6 in membrane ruffles. In chapter 4, the homo-FRET approach was further evaluated and improved. To validate the system and the values obtained from the measurements, an inducible GFP dimerization system was developed. The rapamycin derived FKBP system is suitable for induced dimerization by the compound AP20187. By fusion of GFP to one or two FKBP dimerization domains, dimers or oligomers can be formed, respectively. Biochemical analysis in blue-native PAGE was performed to confirm the induced crosslinking by AP20187. Significant differences were observed between monomeric, dimeric and oligomeric GFP. This method was subsequnetly used to demonstrate unequivocally the presence of EGFR predimers in the resting cell.

In chapter 5, CTR-FAIM was used to study the effect of EGF on the oligomerization state of the receptor. After stimulation of the cells expressing EGFR-GFP with EGF, within 5 minutes a strong decrease in anisotropy was observed, suggesting that EGFR forms oligomers after stimulation with EGF. By applying the same approach to the kinase dead mutant of EGFR, or a mutant lacking 9 C-terminal autophosphorylation tyrosine residues, we found that EGFR tyrosine phosphorylation is necessary for its EGF-induced oligomerization. This oligomerization is probably involved in receptor internalization, as shown by the increase endocytosis of an artificially dimerized kinase dead mutant. These data provide evidence for a model in which oligomerization or dimerizations are the result of kinase-dependent assembly by other proteins, Finally, in chapter 6 the result are summarized and discussed from a broader perspective.

References

Abulrob, A., Giuseppin, S., Andrade, M. F., McDermid, A., Moreno, M. and Stanimirovic, D. (2004). Interactions of EGFR and caveolin-1 in human glioblastoma cells: evidence that tyrosine phosphorylation regulates EGFR association with caveolae. *Oncogene* **23**, 6967-79.
Anderson, R. G. (1998). The caveolae membrane system. *Annu Rev Biochem* **67**, 199-225.
Bagatolli, L. A., Sanchez, S. A., Hazlett, T. and Gratton, E. (2003). Giant vesicles, Laurdan, and two-photon fluorescence microscopy: evidence of lipid lateral separation in bilayers. *Methods Enzymol* **360**, 481-500.
Baumgart, T., Hess, S. T. and Webb, W. W. (2003). Imaging coexisting fluid domains in biomembrane models coupling curvature and line tension. *Nature* **425**, 821-4.
Berkers, J. A., van Bergen en Henegouwen, P. M. and Boonstra, J. (1991). Three classes of epidermal growth factor receptors on HeLa cells. *J Biol Chem* **266**, 922-7.
Boni-Schnetzler, M. and Pilch, P. F. (1987). Mechanism of epidermal growth factor receptor autophosphorylation and high-affinity binding. *Proc Natl Acad Sci U S A* **84**, 7832-6.
Bremer, E. G., Hakomori, S., Bowen-Pope, D. F., Raines, E. and Ross, R. (1984). Ganglioside-mediated modulation of cell growth, growth factor binding, and receptor phosphorylation. *J Biol Chem* **259**, 6818-25.
Brown, D. A. and London, E. (1998). Structure and origin of ordered lipid domains in biological membranes. *J Membr Biol* **164**, 103-14.
Brown, D. A. and London, E. (2000). Structure and function of sphingolipid- and cholesterol-rich membrane rafts. *J Biol Chem* **275**, 17221-4.
Brown, R. E. (1998). Sphingolipid organization in biomembranes: what physical studies of model membranes reveal. *J Cell Sci* **111 (Pt 1)**, 1-9.
Carozzi, A. J., Ikonen, E., Lindsay, M. R. and Parton, R. G. (2000). Role of cholesterol in developing T-tubules: analogous mechanisms for T-tubule and caveolae biogenesis. *Traffic* **1**, 326-41.
Chang, W. J., Ying, Y. S., Rothberg, K. G., Hooper, N. M., Turner, A. J., Gambliel, H. A., De Gunzburg, J., Mumby, S. M., Gilman, A. G. and Anderson, R. G. (1994). Purification and characterization of smooth muscle cell caveolae. *J Cell Biol* **126**, 127-38.
Clayton, A. H., Tavarnesi, M. L. and Johns, T. G. (2007). Unligated epidermal growth factor receptor forms higher order oligomers within microclusters on A431 cells that are sensitive to tyrosine kinase inhibitor binding. *Biochemistry* **46**, 4589-97.
Cochet, C., Gill, G. N., Meisenhelder, J., Cooper, J. A. and Hunter, T. (1984). C-kinase phosphorylates the epidermal growth factor receptor and reduces its epidermal growth factor-stimulated tyrosine protein kinase activity. *J Biol Chem* **259**, 2553-8.
Couet, J., Sargiacomo, M. and Lisanti, M. P. (1997). Interaction of a receptor tyrosine kinase, EGF-R, with caveolins. Caveolin binding negatively regulates tyrosine and serine/threonine kinase activities. *J Biol Chem* **272**, 30429-38.
Countaway, J. L., Girones, N. and Davis, R. J. (1989). Reconstitution of epidermal growth factor receptor transmodulation by platelet-derived growth factor in Chinese hamster ovary cells. *J. Biol. Chem.* **264**, 13642-13647.
Defize, L. H., Arndt-Jovin, D. J., Jovin, T. M., Boonstra, J., Meisenhelder, J., Hunter, T., de Hey, H. T. and de Laat, S. W. (1988). A431 cell variants lacking the blood group A antigen display increased high affinity epidermal growth factor-receptor number, protein-tyrosine kinase activity, and receptor turnover. *J Cell Biol* **107**, 939-49.
Defize, L. H., Boonstra, J., Meisenhelder, J., Kruijer, W., Tertoolen, L. G., Tilly, B. C., Hunter, T., van Bergen en Henegouwen, P. M., Moolenaar, W. H. and de Laat, S. W. (1989). Signal transduction by epidermal growth factor occurs through the subclass of high affinity receptors. *J Cell Biol* **109**, 2495-507.
den Hartigh, J. C., van Bergen en Henegouwen, P. M., Boonstra, J. and Verkleij, A. J.

(1993). Cholesterol and phosphoinositides increase affinity of the epidermal growth factor receptor. *Biochim Biophys Acta* **1148**, 249-56.
Dietrich, C., Bagatolli, L. A., Volovyk, Z. N., Thompson, N. L., Levi, M., Jacobson, K. and Gratton, E. (2001). Lipid rafts reconstituted in model membranes. *Biophys J* **80**, 1417-28.
Dietrich, C., Yang, B., Fujiwara, T., Kusumi, A. and Jacobson, K. (2002). Relationship of lipid rafts to transient confinement zones detected by single particle tracking. *Biophys J* **82**, 274-84.
Dvorak, A. M. and Feng, D. (2001). The vesiculo-vacuolar organelle (VVO). A new endothelial cell permeability organelle. *J Histochem Cytochem* **49**, 419-32.
Eisenberg, S., Shvartsman, D. E., Ehrlich, M. and Henis, Y. I. (2006). Clustering of raft-associated proteins in the external membrane leaflet modulates internal leaflet H-ras diffusion and signaling. *Mol Cell Biol* **26**, 7190-200.
Engelman, J. A., Wykoff, C. C., Yasuhara, S., Song, K. S., Okamoto, T. and Lisanti, M. P. (1997). Recombinant Expression of Caveolin-1 in Oncogenically Transformed Cells Abrogates Anchorage-independent Growth. *J. Biol. Chem.* **272**, 16374-16381.
Fadok, V. A., Voelker, D. R., Campbell, P. A., Cohen, J. J., Bratton, D. L. and Henson, P. M. (1992). Exposure of phosphatidylserine on the surface of apoptotic lymphocytes triggers specific recognition and removal by macrophages. *J Immunol* **148**, 2207-16.
Fazioli, F., Minichiello, L., Matoskova, B., Wong, W. T. and Di Fiore, P. P. (1993). eps15, a novel tyrosine kinase substrate, exhibits transforming activity. *Mol Cell Biol* **13**, 5814-28.
Ferguson, K. M. (2004). Active and inactive conformations of the epidermal growth factor receptor. *Biochem Soc Trans* **32**, 742-5.
Ferguson, K. M., Berger, M. B., Mendrola, J. M., Cho, H. S., Leahy, D. J. and Lemmon, M. A. (2003). EGF activates its receptor by removing interactions that autoinhibit ectodomain dimerization. *Mol Cell* **11**, 507-17.
Fernandes, H., Cohen, S. and Bishayee, S. (2001). Glycosylation-induced conformational modification positively regulates receptor-receptor association: a study with an aberrant epidermal growth factor receptor (EGFRvIII/DeltaEGFR) expressed in cancer cells. *J Biol Chem* **276**, 5375-83.
Francoual, M., Etienne-Grimaldi, M. C., Formento, J. L., Benchimol, D., Bourgeon, A., Chazal, M., Letoublon, C., Andre, T., Gilly, N., Delpero, J. R. et al. (2006). EGFR in colorectal cancer: more than a simple receptor. *Ann Oncol* **17**, 962-967.
Friedman, B., Frackelton, A. R., Jr., Ross, A. H., Connors, J. M., Fujiki, H., Sugimura, T. and Rosner, M. R. (1984). Tumor promoters block tyrosine-specific phosphorylation of the epidermal growth factor receptor. *Proc Natl Acad Sci U S A* **81**, 3034-8.
Garrett, T. P., McKern, N. M., Lou, M., Elleman, T. C., Adams, T. E., Lovrecz, G. O., Zhu, H. J., Walker, F., Frenkel, M. J., Hoyne, P. A. et al. (2002). Crystal structure of a truncated epidermal growth factor receptor extracellular domain bound to transforming growth factor alpha. *Cell* **110**, 763-73.
Gaus, K., Gratton, E., Kable, E. P., Jones, A. S., Gelissen, I., Kritharides, L. and Jessup, W. (2003). Visualizing lipid structure and raft domains in living cells with two-photon microscopy. *Proc Natl Acad Sci U S A* **100**, 15554-9.
Gerritsen, H. C., Asselbergs, M. A., Agronskaia, A. V. and Van Sark, W. G. (2002). Fluorescence lifetime imaging in scanning microscopes: acquisition speed, photon economy and lifetime resolution. *J Microsc* **206**, 218-24.
Glenney, J. R., Jr. (1989). Tyrosine phosphorylation of a 22-kDa protein is correlated with transformation by Rous sarcoma virus. *J Biol Chem* **264**, 20163-6.
Gordesky, S. E. and Marinetti, G. V. (1973). The asymetric arrangement of phospholipids in the human erythrocyte membrane. *Biochem Biophys Res Commun* **50**, 1027-31.
Gould, R. J., Ginsberg, B. H. and Spector, A. A. (1982). Lipid effects on the binding properties of a reconstituted insulin receptor. *J Biol Chem* **257**, 477-84.

Gschwind, A., Hart, S., Fischer, O. M. and Ullrich, A. (2003). TACE cleavage of proamphiregulin regulates GPCR-induced proliferation and motility of cancer cells. *Embo J* **22**, 2411-21.
Haglund, K., Sigismund, S., Polo, S., Szymkiewicz, I., Di Fiore, P. P. and Dikic, I. (2003a). Multiple monoubiquitination of RTKs is sufficient for their endocytosis and degradation. *Nat Cell Biol* **5**, 461.
Haglund, K., Sigismund, S., Polo, S., Szymkiewicz, I., Di Fiore, P. P. and Dikic, I. (2003b). Multiple monoubiquitination of RTKs is sufficient for their endocytosis and degradation. *Nat Cell Biol* **5**, 461-6.
Hamers-Casterman, C., Atarhouch, T., Muyldermans, S., Robinson, G., Hamers, C., Songa, E. B., Bendahman, N. and Hamers, R. (1993). Naturally occurring antibodies devoid of light chains. *Nature* **363**, 446-8.
Hammond, A. T., Heberle, F. A., Baumgart, T., Holowka, D., Baird, B. and Feigenson, G. W. (2005). Crosslinking a lipid raft component triggers liquid ordered-liquid disordered phase separation in model plasma membranes. *Proc Natl Acad Sci U S A* **102**, 6320-5.
Harder, T. and Engelhardt, K. R. (2004). Membrane domains in lymphocytes - from lipid rafts to protein scaffolds. *Traffic* **5**, 265-75.
Heerklotz, H. (2002). Triton promotes domain formation in lipid raft mixtures. *Biophys J* **83**, 2693-701.
Henley, J. R., Krueger, E. W., Oswald, B. J. and McNiven, M. A. (1998). Dynamin-mediated internalization of caveolae. *J Cell Biol* **141**, 85-99.
Henneberry, A. L., Wright, M. M. and McMaster, C. R. (2002). The major sites of cellular phospholipid synthesis and molecular determinants of Fatty Acid and lipid head group specificity. *Mol Biol Cell* **13**, 3148-61.
Hoetzl, S., Sprong, H. and van Meer, G. (2007). The way we view cellular (glyco)sphingolipids. *J Neurochem* **103 Suppl 1**, 3-13.
Holowka, D., Gosse, J. A., Hammond, A. T., Han, X., Sengupta, P., Smith, N. L., Wagenknecht-Wiesner, A., Wu, M., Young, R. M. and Baird, B. (2005). Lipid segregation and IgE receptor signaling: a decade of progress. *Biochim Biophys Acta* **1746**, 252-9.
Hooper, N. M. and Turner, A. J. (1988). Ectoenzymes of the kidney microvillar membrane. Differential solubilization by detergents can predict a glycosyl-phosphatidylinositol membrane anchor. *Biochem J* **250**, 865-9.
Huang, F., Goh, L. K. and Sorkin, A. (2007). EGF receptor ubiquitination is not necessary for its internalization. *Proc Natl Acad Sci U S A* **104**, 16904-9.
Huang, F., Kirkpatrick, D., Jiang, X., Gygi, S. and Sorkin, A. (2006). Differential regulation of EGF receptor internalization and degradation by multiubiquitination within the kinase domain. *Mol Cell* **21**, 737-48.
Hunter, T., Ling, N. and Cooper, J. A. (1984). Protein kinase C phosphorylation of the EGF receptor at a threonine residue close to the cytoplasmic face of the plasma membrane. *Nature* **311**, 480-3.
Jacobson, K., Mouritsen, O. G. and Anderson, R. G. (2007). Lipid rafts: at a crossroad between cell biology and physics. *Nat Cell Biol* **9**, 7-14.
Jorissen, R. N., Walker, F., Pouliot, N., Garrett, T. P., Ward, C. W. and Burgess, A. W. (2003). Epidermal growth factor receptor: mechanisms of activation and signalling. *Exp Cell Res* **284**, 31-53.
Kabouridis, P. S. (2006). Lipid rafts in T cell receptor signalling. *Mol Membr Biol* **23**, 49-57.
Kahya, N., Scherfeld, D., Bacia, K. and Schwille, P. (2004). Lipid domain formation and dynamics in giant unilamellar vesicles explored by fluorescence correlation spectroscopy. *J Struct Biol* **147**, 77-89.
Kirkham, M., Fujita, A., Chadda, R., Nixon, S. J., Kurzchalia, T. V., Sharma, D. K., Pagano, R. E., Hancock, J. F., Mayor, S. and Parton, R. G. (2005). Ultrastructural identification of uncoated caveolin-independent early endocytic vehicles. *J Cell Biol* **168**, 465-76.

Klein, P., Mattoon, D., Lemmon, M. A. and Schlessinger, J. (2004). A structure-based model for ligand binding and dimerization of EGF receptors. *Proc Natl Acad Sci U S A* **101**, 929-34.
Koynova, R. and Caffrey, M. (1995). Phases and phase transitions of the sphingolipids. *Biochim Biophys Acta* **1255**, 213-36.
Kusumi, A., Koyama-Honda, I. and Suzuki, K. (2004). Molecular dynamics and interactions for creation of stimulation-induced stabilized rafts from small unstable steady-state rafts. *Traffic* **5**, 213-30.
Kusumi, A. and Suzuki, K. (2005). Toward understanding the dynamics of membrane-raft-based molecular interactions. *Biochim Biophys Acta* **1746**, 234-51.
Lajoie, P. and Nabi, I. R. (2007). Regulation of raft-dependent endocytosis. *J Cell Mol Med* **11**, 644-53.
Larson, D. R., Gosse, J. A., Holowka, D. A., Baird, B. A. and Webb, W. W. (2005). Temporally resolved interactions between antigen-stimulated IgE receptors and Lyn kinase on living cells. *J Cell Biol* **171**, 527-36.
Lax, I., Bellot, F., Honegger, A. M., Schmidt, A., Ullrich, A., Givol, D. and Schlessinger, J. (1990). Domain deletion in the extracellular portion of the EGF-receptor reduces ligand binding and impairs cell surface expression. *Cell Regul* **1**, 173-88.
Lax, I., Bellot, F., Howk, R., Ullrich, A., Givol, D. and Schlessinger, J. (1989). Functional analysis of the ligand binding site of EGF-receptor utilizing chimeric chicken/human receptor molecules. *Embo J* **8**, 421-7.
Le, P. U., Guay, G., Altschuler, Y. and Nabi, I. R. (2002). Caveolin-1 is a negative regulator of caveolae-mediated endocytosis to the endoplasmic reticulum. *J Biol Chem* **277**, 3371-9.
Lee, S. W., Reimer, C. L., Oh, P., Campbell, D. B. and Schnitzer, J. E. (1998). Tumor cell growth inhibition by caveolin re-expression in human breast cancer cells. *Oncogene* **16**, 1391-7.
Lemmon, M. A., Bu, Z., Ladbury, J. E., Zhou, M., Pinchasi, D., Lax, I., Engelman, D. M. and Schlessinger, J. (1997). Two EGF molecules contribute additively to stabilization of the EGFR dimer. *Embo J* **16**, 281-94.
Levkowitz, G., Waterman, H., Ettenberg, S. A., Katz, M., Tsygankov, A. Y., Alroy, I., Lavi, S., Iwai, K., Reiss, Y., Ciechanover, A. et al. (1999). Ubiquitin Ligase Activity and Tyrosine Phosphorylation Underlie Suppression of Growth Factor Signaling by c-Cbl/Sli-1. *Molecular Cell* **4**, 1029.
Levkowitz, G., Waterman, H., Zamir, E., Kam, Z., Oved, S., Langdon, W. Y., Beguinot, L., Geiger, B. and Yarden, Y. (1998). c-Cbl/Sli-1 regulates endocytic sorting and ubiquitination of the epidermal growth factor receptor. *Genes Dev.* **12**, 3663-3674.
Lidke, D. S., Nagy, P., Barisas, B. G., Heintzmann, R., Post, J. N., Lidke, K. A., Clayton, A. H., Arndt-Jovin, D. J. and Jovin, T. M. (2003). Imaging molecular interactions in cells by dynamic and static fluorescence anisotropy (rFLIM and emFRET). *Biochem Soc Trans* **31**, 1020-7.
Liu, Y., Li, R. and Ladisch, S. (2004). Exogenous Ganglioside GD1a Enhances Epidermal Growth Factor Receptor Binding and Dimerization. *J. Biol. Chem.* **279**, 36481-36489.
Livneh, E., Prywes, R., Kashles, O., Reiss, N., Sasson, I., Mory, Y., Ullrich, A. and Schlessinger, J. (1986). Reconstitution of human epidermal growth factor receptors and its deletion mutants in cultured hamster cells. *J Biol Chem* **261**, 12490-7.
London, E. and Brown, D. A. (2000). Insolubility of lipids in triton X-100: physical origin and relationship to sphingolipid/cholesterol membrane domains (rafts). *Biochim Biophys Acta* **1508**, 182-95.
Lund, K. A., Lazar, C. S., Chen, W. S., Walsh, B. J., Welsh, J. B., Herbst, J. J., Walton, G. M., Rosenfeld, M. G., Gill, G. N. and Wiley, H. S. (1990). Phosphorylation of the epidermal growth factor receptor at threonine 654 inhibits ligand-induced internalization and down-regulation. *J Biol Chem* **265**, 20517-23.

Macdonald, J. L. and Pike, L. J. (2008). Heterogeneity in EGF-binding affinities arises from negative cooperativity in an aggregating system. *Proc Natl Acad Sci U S A* **105**, 112-7.
Mattoon, D., Klein, P., Lemmon, M. A., Lax, I. and Schlessinger, J. (2004). The tethered configuration of the EGF receptor extracellular domain exerts only a limited control of receptor function. *Proc Natl Acad Sci U S A* **101**, 923-8.
Matveev, S. V. and Smart, E. J. (2002). Heterologous desensitization of EGF receptors and PDGF receptors by sequestration in caveolae. *Am J Physiol Cell Physiol* **282**, C935-46.
Mayawala, K., Vlachos, D. G. and Edwards, J. S. (2005). Heterogeneities in EGF receptor density at the cell surface can lead to concave up scatchard plot of EGF binding. *FEBS Lett* **579**, 3043-7.
Merritt, E. A., Sarfaty, S., van den Akker, F., L'Hoir, C., Martial, J. A. and Hol, W. G. (1994). Crystal structure of cholera toxin B-pentamer bound to receptor GM1 pentasaccharide. *Protein Sci* **3**, 166-75.
Miljan, E. A. and Bremer, E. G. (2002). Regulation of growth factor receptors by gangliosides. *Sci STKE* **2002**, RE15.
Miljan, E. A., Meuillet, E. J., Mania-Farnell, B., George, D., Yamamoto, H., Simon, H. G. and Bremer, E. G. (2002). Interaction of the extracellular domain of the epidermal growth factor receptor with gangliosides. *J Biol Chem* **277**, 10108-13.
Mirkin, B. L., Clark, S. H. and Zhang, C. (2002). Inhibition of human neuroblastoma cell proliferation and EGF receptor phosphorylation by gangliosides GM1, GM3, GD1A and GT1B. *Cell Prolif* **35**, 105-15.
Monier, S., Dietzen, D. J., Hastings, W. R., Lublin, D. M. and Kurzchalia, T. V. (1996). Oligomerization of VIP21-caveolin in vitro is stabilized by long chain fatty acylation or cholesterol. *FEBS Lett* **388**, 143-9.
Moriki, T., Maruyama, H. and Maruyama, I. N. (2001). Activation of preformed EGF receptor dimers by ligand-induced rotation of the transmembrane domain. *J Mol Biol* **311**, 1011-26.
Moscatello, D. K., Holgado-Madruga, M., Godwin, A. K., Ramirez, G., Gunn, G., Zoltick, P. W., Biegel, J. A., Hayes, R. L. and Wong, A. J. (1995). Frequent expression of a mutant epidermal growth factor receptor in multiple human tumors. *Cancer Res* **55**, 5536-9.
Mosesson, Y., Shtiegman, K., Katz, M., Zwang, Y., Vereb, G., Szollosi, J. and Yarden, Y. (2003). Endocytosis of Receptor Tyrosine Kinases Is Driven by Monoubiquitylation, Not Polyubiquitylation. *J. Biol. Chem.* **278**, 21323-21326.
Murase, K., Fujiwara, T., Umemura, Y., Suzuki, K., Iino, R., Yamashita, H., Saito, M., Murakoshi, H., Ritchie, K. and Kusumi, A. (2004). Ultrafine Membrane Compartments for Molecular Diffusion as Revealed by Single Molecule Techniques. *Biophys. J.* **86**, 4075-4093.
Murata, M., Peranen, J., Schreiner, R., Wieland, F., Kurzchalia, T. V. and Simons, K. (1995). VIP21/Caveolin is a Cholesterol-Binding Protein. *Proceedings of the National Academy of Sciences* **92**, 10339-10343.
Murozuka, Y., Watanabe, N., Hatanaka, K. and Hakomori, S. I. (2007). Lyso-GM3, its dimer, and multimer: their synthesis, and their effect on epidermal growth factor-induced receptor tyrosine kinase. *Glycoconj J* **24**, 551-63.
Newton, A. C. and Johnson, J. E. (1998). Protein kinase C: a paradigm for regulation of protein function by two membrane-targeting modules. *Biochim Biophys Acta* **1376**, 155-72.
Nichols, B. J. (2002). A distinct class of endosome mediates clathrin-independent endocytosis to the Golgi complex. *Nat Cell Biol* **4**, 374-8.
Nores, G. A., Dohi, T., Taniguchi, M. and Hakomori, S. (1987). Density-dependent recognition of cell surface GM3 by a certain anti-melanoma antibody, and GM3 lactone as a possible immunogen: requirements for tumor-associated antigen and immunogen. *J Immunol* **139**, 3171-6.
Ogiso, H., Ishitani, R., Nureki, O., Fukai, S., Yamanaka, M., Kim, J. H., Saito, K., Sakamoto, A., Inoue, M., Shirouzu, M. et al. (2002). Crystal structure of the complex of human epidermal

growth factor and receptor extracellular domains. *Cell* **110**, 775-87.
Oh, P., McIntosh, D. P. and Schnitzer, J. E. (1998). Dynamin at the neck of caveolae mediates their budding to form transport vesicles by GTP-driven fission from the plasma membrane of endothelium. *J Cell Biol* **141**, 101-14.
Orth, J. D., Krueger, E. W., Weller, S. G. and McNiven, M. A. (2006). A novel endocytic mechanism of epidermal growth factor receptor sequestration and internalization. *Cancer Res* **66**, 3603-10.
Parton, R. G., Joggerst, B. and Simons, K. (1994). Regulated internalization of caveolae. *J Cell Biol* **127**, 1199-215.
Pelkmans, L., Kartenbeck, J. and Helenius, A. (2001). Caveolar endocytosis of simian virus 40 reveals a new two-step vesicular-transport pathway to the ER. *Nat Cell Biol* **3**, 473-83.
Pelkmans, L., Puntener, D. and Helenius, A. (2002). Local actin polymerization and dynamin recruitment in SV40-induced internalization of caveolae. *Science* **296**, 535-9.
Pierce, S. K. (2002). Lipid rafts and B-cell activation. *Nat Rev Immunol* **2**, 96-105.
Pike, L. J., Han, X. and Gross, R. W. (2005). Epidermal growth factor receptors are localized to lipid rafts that contain a balance of inner and outer leaflet lipids: a shotgun lipidomics study. *J Biol Chem* **280**, 26796-804.
Prior, I. A., Muncke, C., Parton, R. G. and Hancock, J. F. (2003). Direct visualization of Ras proteins in spatially distinct cell surface microdomains. *J Cell Biol* **160**, 165-70.
Prywes, R., Livneh, E., Ullrich, A. and Schlessinger, J. (1986). Mutations in the cytoplasmic domain of EGF receptor affect EGF binding and receptor internalization. *Embo J* **5**, 2179-90.
Puri, C., Tosoni, D., Comai, R., Rabellino, A., Segat, D., Caneva, F., Luzzi, P., Di Fiore, P. P. and Tacchetti, C. (2005). Relationships between EGFR signaling-competent and endocytosis-competent membrane microdomains. *Mol Biol Cell* **16**, 2704-18.
Razani, B., Schlegel, A., Liu, J. and Lisanti, M. P. (2001). Caveolin-1, a putative tumour suppressor gene. *Biochem Soc Trans* **29**, 494-9.
Rietveld, A. and Simons, K. (1998). The differential miscibility of lipids as the basis for the formation of functional membrane rafts. *Biochim Biophys Acta* **1376**, 467-79.
Rothberg, K. G., Heuser, J. E., Donzell, W. C., Ying, Y. S., Glenney, J. R. and Anderson, R. G. (1992). Caveolin, a protein component of caveolae membrane coats. *Cell* **68**, 673-82.
Saffarian, S., Li, Y., Elson, E. L. and Pike, L. J. (2007). Oligomerization of the EGF receptor investigated by live cell fluorescence intensity distribution analysis. *Biophys J* **93**, 1021-31.
Sako, Y. and Kusumi, A. (1994). Compartmentalized structure of the plasma membrane for receptor movements as revealed by a nanometer-level motion analysis. *J Cell Biol* **125**, 1251-64.
Sako, Y., Minoghchi, S. and Yanagida, T. (2000). Single-molecule imaging of EGFR signalling on the surface of living cells. *Nat Cell Biol* **2**, 168-72.
Sako, Y., Nagafuchi, A., Tsukita, S., Takeichi, M. and Kusumi, A. (1998). Cytoplasmic regulation of the movement of E-cadherin on the free cell surface as studied by optical tweezers and single particle tracking: corralling and tethering by the membrane skeleton. *J Cell Biol* **140**, 1227-40.
Santiskulvong, C. and Rozengurt, E. (2007a). Protein kinase C[alpha] mediates feedback inhibition of EGF receptor transactivation induced by Gq-coupled receptor agonists. *Cellular Signalling* **19**, 1348.
Santiskulvong, C. and Rozengurt, E. (2007b). Protein kinase Calpha mediates feedback inhibition of EGF receptor transactivation induced by Gq-coupled receptor agonists. *Cell Signal* **19**, 1348-57.
Sargiacomo, M., Sudol, M., Tang, Z. and Lisanti, M. P. (1993). Signal transducing molecules and glycosyl-phosphatidylinositol-linked proteins form a caveolin-rich insoluble complex in MDCK cells. *J Cell Biol* **122**, 789-807.
Sato, Y., Takahashi, M., Shibukawa, Y., Jain, S. K., Hamaoka, R., Miyagawa, J., Yaginuma,

Y., Honke, K., Ishikawa, M. and Taniguchi, N. (2001). Overexpression of N-acetylglucosam inyltransferase III enhances the epidermal growth factor-induced phosphorylation of ERK in HeLaS3 cells by up-regulation of the internalization rate of the receptors. *J Biol Chem* **276**, 11956-62.

Scatchard, G. (1949). The attractions of proteins for small molecules and ions. *Annals of the New York Academy of Sciences* **51**, 660-672.

Schroeder, R. J., Ahmed, S. N., Zhu, Y., London, E. and Brown, D. A. (1998). Cholesterol and sphingolipid enhance the Triton X-100 insolubility of glycosylphosphatidylinositol-anchored proteins by promoting the formation of detergent-insoluble ordered membrane domains. *J Biol Chem* **273**, 1150-7.

Sengupta, P., Holowka, D. and Baird, B. (2007). Fluorescence resonance energy transfer between lipid probes detects nanoscopic heterogeneity in the plasma membrane of live cells. *Biophys J* **92**, 3564-74.

Sharma, P., Varma, R., Sarasij, R. C., Ira, Gousset, K., Krishnamoorthy, G., Rao, M. and Mayor, S. (2004). Nanoscale organization of multiple GPI-anchored proteins in living cell membranes. *Cell* **116**, 577-89.

Sheets, E. D., Lee, G. M., Simson, R. and Jacobson, K. (1997). Transient confinement of a glycosylphosphatidylinositol-anchored protein in the plasma membrane. *Biochemistry* **36**, 12449-58.

Sigismund, S., Woelk, T., Puri, C., Maspero, E., Tacchetti, C., Transidico, P., Di Fiore, P. P. and Polo, S. (2005). Clathrin-independent endocytosis of ubiquitinated cargos. *Proc Natl Acad Sci U S A* **102**, 2760-5.

Simons, K. and Ikonen, E. (1997). Functional rafts in cell membranes. *Nature* **387**, 569-72.

Simons, K. and Toomre, D. (2000). Lipid rafts and signal transduction. *Nat Rev Mol Cell Biol* **1**, 31-9.

Simons, K. and van Meer, G. (1988). Lipid sorting in epithelial cells. *Biochemistry* **27**, 6197-202.

Simons, K. and Vaz, W. L. (2004). Model systems, lipid rafts, and cell membranes. *Annu Rev Biophys Biomol Struct* **33**, 269-95.

Simson, R., Sheets, E. D. and Jacobson, K. (1995). Detection of temporary lateral confinement of membrane proteins using single-particle tracking analysis. *Biophys J* **69**, 989-93.

Slieker, L. J., Martensen, T. M. and Lane, M. D. (1986). Synthesis of epidermal growth factor receptor in human A431 cells. Glycosylation-dependent acquisition of ligand binding activity occurs post-translationally in the endoplasmic reticulum. *J Biol Chem* **261**, 15233-41.

Smart, E. J., Graf, G. A., McNiven, M. A., Sessa, W. C., Engelman, J. A., Scherer, P. E., Okamoto, T. and Lisanti, M. P. (1999). Caveolins, liquid-ordered domains, and signal transduction. *Mol Cell Biol* **19**, 7289-304.

Soderquist, A. M. and Carpenter, G. (1984). Glycosylation of the epidermal growth factor receptor in A-431 cells. The contribution of carbohydrate to receptor function. *J Biol Chem* **259**, 12586-94.

Sorkin, A., Di Fiore, P. P. and Carpenter, G. (1993). The carboxyl terminus of epidermal growth factor receptor/erbB-2 chimerae is internalization impaired. *Oncogene* **8**, 3021-8.

Sorokin, A., Lemmon, M. A., Ullrich, A. and Schlessinger, J. (1994). Stabilization of an active dimeric form of the epidermal growth factor receptor by introduction of an inter-receptor disulfide bond. *J Biol Chem* **269**, 9752-9.

Stamos, J., Sliwkowski, M. X. and Eigenbrot, C. (2002). Structure of the epidermal growth factor receptor kinase domain alone and in complex with a 4-anilinoquinazoline inhibitor. *J Biol Chem* **277**, 46265-72.

Stefanova, I., Horejsi, V., Ansotegui, I. J., Knapp, W. and Stockinger, H. (1991). GPI-anchored cell-surface molecules complexed to protein tyrosine kinases. *Science* **254**, 1016-9.

Sunnarborg, S. W., Hinkle, C. L., Stevenson, M., Russell, W. E., Raska, C. S., Peschon, J. J., Castner, B. J., Gerhart, M. J., Paxton, R. J., Black, R. A. et al. (2002). Tumor necrosis factor-alpha converting enzyme (TACE) regulates epidermal growth factor receptor ligand availability. *J Biol Chem* **277**, 12838-45.

Teramura, Y., Ichinose, J., Takagi, H., Nishida, K., Yanagida, T. and Sako, Y. (2006). Single-molecule analysis of epidermal growth factor binding on the surface of living cells. *Embo J* **25**, 4215-22.

Tomishige, M., Sako, Y. and Kusumi, A. (1998). Regulation mechanism of the lateral diffusion of band 3 in erythrocyte membranes by the membrane skeleton. *J Cell Biol* **142**, 989-1000.

Trigatti, B. L., Anderson, R. G. and Gerber, G. E. (1999). Identification of caveolin-1 as a fatty acid binding protein. *Biochem Biophys Res Commun* **255**, 34-9.

Tsuda, T., Ikeda, Y. and Taniguchi, N. (2000). The Asn-420-linked sugar chain in human epidermal growth factor receptor suppresses ligand-independent spontaneous oligomerization. Possible role of a specific sugar chain in controllable receptor activation. *J Biol Chem* **275**, 21988-94.

Uittenbogaard, A. and Smart, E. J. (2000). Palmitoylation of caveolin-1 is required for cholesterol binding, chaperone complex formation, and rapid transport of cholesterol to caveolae. *J Biol Chem* **275**, 25595-9.

Vainio, S., Heino, S., Mansson, J. E., Fredman, P., Kuismanen, E., Vaarala, O. and Ikonen, E. (2002). Dynamic association of human insulin receptor with lipid rafts in cells lacking caveolae. *EMBO Rep* **3**, 95-100.

van Belzen, N., Rijken, P. J., Hage, W. J., de Laat, S. W., Verkleij, A. J. and Boonstra, J. (1988). Direct visualization and quantitative analysis of epidermal growth factor-induced receptor clustering. *J Cell Physiol* **134**, 413-20.

van Delft, S., Govers, R., Strous, G. J., Verkleij, A. J. and van Bergen en Henegouwen, P. M. (1997). Epidermal growth factor induces ubiquitination of Eps15. *J Biol Chem* **272**, 14013-6.

Van der Heyden, M. A., Nievers, M., Verkleij, A. J., Boonstra, J. and Van Bergen en Henegouwen, P. M. (1997). Identification of an intracellular domain of the EGF receptor required for high-affinity binding of EGF. *FEBS Lett* **410**, 265-8.

van Duyl, B. Y., Rijkers, D. T. S., de Kruijff, B. and Killian, J. A. (2002). Influence of hydrophobic mismatch and palmitoylation on the association of transmembrane Î±-helical peptides with detergent-resistant membranes. *FEBS letters* **523**, 79.

van Meer, G. (1989). Lipid traffic in animal cells. *Annu Rev Cell Biol* **5**, 247-75.

van Meer, G. and Simons, K. (1982). Viruses budding from either the apical or the basolateral plasma membrane domain of MDCK cells have unique phospholipid compositions. *Embo J* **1**, 847-52.

van Meer, G., Voelker, D. R. and Feigenson, G. W. (2008). Membrane lipids: where they are and how they behave. *Nat Rev Mol Cell Biol* **9**, 112-24.

van Rheenen, J., Achame, E. M., Janssen, H., Calafat, J. and Jalink, K. (2005). PIP2 signaling in lipid domains: a critical re-evaluation. *Embo J* **24**, 1664-73.

Verkleij, A. J. and Post, J. A. (2000). Membrane phospholipid asymmetry and signal transduction. *J Membr Biol* **178**, 1-10.

Verkleij, A. J., Zwaal, R. F. A. and Roelofsen, B. (1973). The asymmetric distribution of phospholipids in the human red cell membrane. A combined study using phospholipases and freeze etch electron microscopy. *Biochimica et Biophysica Acta* **323**, 178.

Vidal, A. and McIntosh, T. J. (2005). Transbilayer peptide sorting between raft and nonraft bilayers: comparisons of detergent extraction and confocal microscopy. *Biophys J* **89**, 1102-8.

Walker, F., Orchard, S. G., Jorissen, R. N., Hall, N. E., Zhang, H.-H., Hoyne, P. A., Adams, T. E., Johns, T. G., Ward, C., Garrett, T. P. J. et al. (2004). CR1/CR2 Interactions Modulate the Functions of the Cell Surface Epidermal Growth Factor Receptor *J. Biol. Chem.* **279**, 22387-

22398.
Wang, J., Gunning, W., Kelley, K. M. and Ratnam, M. (2002). Evidence for segregation of heterologous GPI-anchored proteins into separate lipid rafts within the plasma membrane. *J Membr Biol* **189**, 35-43.
Wang, Q., Zhu, F. and Wang, Z. (2007a). Identification of EGF receptor C-terminal sequences 1005-1017 and di-leucine motif 1010LL1011 as essential in EGF receptor endocytosis. *Exp Cell Res* **313**, 3349-63.
Wang, T. Y. and Silvius, J. R. (2001). Cholesterol does not induce segregation of liquid-ordered domains in bilayers modeling the inner leaflet of the plasma membrane. *Biophys J* **81**, 2762-73.
Wang, X. Q., Sun, P., O'Gorman, M., Tai, T. and Paller, A. S. (2001). Epidermal growth factor receptor glycosylation is required for ganglioside GM3 binding and GM3-mediated suppression [correction of suppresion] of activation. *Glycobiology* **11**, 515-22.
Wang, X. Q., Yan, Q., Sun, P., Liu, J. W., Go, L., McDaniel, S. M. and Paller, A. S. (2007b). Suppression of epidermal growth factor receptor signaling by protein kinase C-alpha activation requires CD82, caveolin-1, and ganglioside. *Cancer Res* **67**, 9986-95.
Waterman, H., Alroy, I., Strano, S., Seger, R. and Yarden, Y. (1999). The C-terminus of the kinase-defective neuregulin receptor ErbB-3 confers mitogenic superiority and dictates endocytic routing. *Embo J* **18**, 3348-58.
Whitson, K. B., Whitson, S. R., Red-Brewer, M. L., McCoy, A. J., Vitali, A. A., Walker, F., Johns, T. G., Beth, A. H. and Staros, J. V. (2005). Functional effects of glycosylation at Asn-579 of the epidermal growth factor receptor. *Biochemistry* **44**, 14920-31.
Wilson, B. S., Steinberg, S. L., Liederman, K., Pfeiffer, J. R., Surviladze, Z., Zhang, J., Samelson, L. E., Yang, L. H., Kotula, P. G. and Oliver, J. M. (2004). Markers for detergent-resistant lipid rafts occupy distinct and dynamic domains in native membranes. *Mol Biol Cell* **15**, 2580-92.
Wu, C., Butz, S., Ying, Y. and Anderson, R. G. (1997). Tyrosine kinase receptors concentrated in caveolae-like domains from neuronal plasma membrane. *J Biol Chem* **272**, 3554-9.
Yamabhai, M. and Anderson, R. G. (2002). Second cysteine-rich region of epidermal growth factor receptor contains targeting information for caveolae/rafts. *J Biol Chem* **277**, 24843-6.
Yamazaki, H., Fukui, Y., Ueyama, Y., Tamaoki, N., Kawamoto, T., Taniguchi, S. and Shibuya, M. (1988). Amplification of the structurally and functionally altered epidermal growth factor receptor gene (c-erbB) in human brain tumors. *Mol Cell Biol* **8**, 1816-20.
Yarden, Y. and Sliwkowski, M. X. (2001). Untangling the ErbB signalling network. *Nat Rev Mol Cell Biol* **2**, 127-37.
Yu, X., Sharma, K. D., Takahashi, T., Iwamoto, R. and Mekada, E. (2002). Ligand-independent Dimer Formation of Epidermal Growth Factor Receptor (EGFR) Is a Step Separable from Ligand-induced EGFR Signaling. *Mol. Biol. Cell* **13**, 2547-2557.
Zhang, X., Gureasko, J., Shen, K., Cole, P. A. and Kuriyan, J. (2006). An Allosteric Mechanism for Activation of the Kinase Domain of Epidermal Growth Factor Receptor. *Cell* **125**, 1137.

Chapter 2

EGF induces coalescence of different lipid rafts

Erik G. Hofman[1], Mika O. Ruonala[2], Arjen N. Bader[3], Dave van den Heuvel[3], Jarno Voortman[1], Rob C. Roovers[1], Arie J. Verkleij[1], Hans C. Gerritsen[3], and Paul M.P. van Bergen en Henegouwen[1]

[1]Department of Cellular Architecture and Dynamics, Institute of Biomembranes, Utrecht University, Utrecht, the Netherlands

[2] Center for Membrane Proteomics, University of Frankfurt, Biocenter, Frankfurt am Main, Germany

[3] Department of Molecular Biophysics, Utrecht University, Utrecht, the Netherlands

Based on : J Cell Sci (2008) 121(15): 2519-28

Abstract

The suggestion that microdomains might function as signaling platforms owes to the presence of growth factor receptors, such as the EGFR, in biochemically isolated lipid raft fractions. To investigate the role of EGFR activation in the organization of lipid rafts we have performed FLIM analyses using putative lipid raft markers such as ganglioside GM1 and glycosylphos phatidylinositol-anchored GFP. The EGFR was labeled using single domain antibodies from Llama glama that specifically bind the EGFR without stimulating its kinase activity. Our FLIM analyses demonstrate a cholesterol-independent colocalization of GM1 with EGFR, which was not observed for the transferrin receptor. In contrast, a cholesterol-dependent colocalization was observed for GM1 with GPI-anchored GFP. In the resting state no colocalization was observed between EGFR and GPI-GFP, but stimulation of the cell with EGF resulted in the colocalization at the nanoscale level of EGFR and GPI-GFP. Moreover, EGF induced the enrichment of GPI-GFP in a detergent-free lipid raft fraction. Our results suggest that EGF induces the coalescence of the two types of GM1 containing microdomains, which may lead to the formation of signaling platforms.

Introduction

Lateral membrane heterogeneity has been generally accepted as a requirement for proper functioning of biological membranes (for reviews see (Jacobson et al., 2007; Mayor and Rao, 2004; Pike, 2004). Within this concept, lipid rafts have been proposed to represent microdomains enriched in cholesterol and sphingolipids such as gangliosides. In response to signaling, lipid rafts may fuse into larger and more stable structures resulting in the formation of efficient signaling platforms (Simons and Toomre, 2000). Three different microdomain concepts have recently been suggested, which differ in both size and composition (Jacobson et al., 2007). Small scale domains or shells composed of a transmembrane protein surrounded by a shell of cholesterol and glycosphingolipids; nanodomains or lipid rafts that represent larger structures composed of cholesterol, glycosphingolipids and additional proteins such as caveolin; and, finally, larger microdomains identified by light microscopy and single molecule imaging containing both proteins and lipids which are limited in their free mobility by the membrane skeleton (Kusumi et al., 2004).

The EGF receptor (EGFR) was one of the first examples for a lipid raft localized growth factor receptor (Mineo et al., 1996; Pike, 2005). EGFR is a member of the ErbB family of receptor tyrosine kinases, consisting of an ectodomain composed of two ligand binding domains and two cysteine-rich domains, a transmembrane stretch, and an intracellular tyrosine kinase domain connected to a tyrosine-rich substrate region (Jorissen et al., 2003). Binding of EGF to the ligand binding sites induces a conformational change in the ectodomain that enables receptor dimerization which in turn leads to cross-phosphorylation of intracellular tyrosine residues and docking of SH2 or PTB containing adaptor/effector proteins (Dawson et al., 2007). Mutational analysis has revealed sequences in the second cysteine-rich domain of the EGFR ectodomain that are required for their cofractionation with detergent-free lipid raft fractions (Yamabhai and Anderson, 2002). Immunogold electron microscopy showed that a substantial amount of the EGFR is located in rafts but not in caveolae, supporting the hypothesis for the coexistence of different kinds of micro-domains (Ringerike et al., 2002). Stimulation of EGFR signaling induces the internalization via GM1 enriched vesicles that endocytose via both clathrin-dependent and clathrin-independent mechanisms (Puri et al., 2005; Sigismund et al., 2005). Indications for the presence of the EGFR in microdomains have been obtained using single molecule imaging of the EGFR (Orr et al., 2005). The mobility of the EGFR in those microdomains was shown to be dependent upon cholesterol and the cytoskeleton.

Localization of the EGFR in lipid rafts is suggested to have an effect on the two principal functions of the EGFR: ligand binding and tyrosine kinase activity. Interestingly, opposing effects have been obtained for the typical raft lipids on receptor functioning. Enhanced EGF-binding to EGFR was observed when cholesterol and phosphatidylinositol (PI) were added to dioleoylphosphatidylcholine (DOPC) liposomes in which the EGFR was reconstituted (den Hartigh et al., 1993). Conversely, extraction of cholesterol from cells was

shown to increase EGF-binding and to stimulate ligand-independent EGFR tyrosine kinase activity and subsequent signaling to ERK (Furuchi and Anderson, 1998; Pike and Casey, 2002; Roepstorff et al., 2002). Also, gangliosides were shown to alter the phosphorylation state of the EGFR (Miljan and Bremer, 2002). While some gangliosides, like GM3, were published to inhibit EGF-induced phosphorylation of the receptor (Bremer et al., 1984; Miljan and Bremer, 2002), other gangliosides, like GM1 or GD1a were reported to enhance EGFR phosphorylation in response to EGF (Li et al., 2001; Liu et al., 2004; Miljan et al., 2002). Moreover, cells with excess GD3 gangliosides were found to have decreased EGFR phosphorylation levels while overexpression of enzymes required for GM1 synthesis resulted in enhanced cell proliferation in response to EGF (Nishio et al., 2005; Zurita et al., 2001). Although the lipid composition of the membrane wherein the EGFR is embedded appear as an important regulator of the EGFR (Miljan and Bremer, 2002), the molecular mechanisms as to how these lipids regulate the EGFR functionality are far from clear.

A popular method to study the functionality of lipid rafts has been their biochemical isolation. Cofractionation of the EGFR with the detergent resistant membrane (DRM) fraction strongly depends on the applied purification method (Pike, 2004). EGFR is absent from the DRM fraction when the standard non-ionic detergent Triton X-100 was used, but detergent resistant fractions prepared with Brij 98 or Lubrol or the detergent-free floating fractions usually contain EGFR (Pike, 2004). Also, in the DRM fraction obtained from carbonate treated cells, the EGFR is detectable (Mineo et al., 1996). Thus, cofractionation of proteins with the DRM fraction does not necessarily imply that such components are present in lipid rafts in the cell membrane (Lichtenberg et al., 2005).

To study the presence and functioning of EGFR in lipid rafts in the context of the plasma membrane, non-invasive techniques, such as fluorescence microscopy, are required (Lagerholm et al., 2005; Rao and Mayor, 2005). Unfortunately, the resolution power of standard fluorescence microscopy (~200 nm) does not permit a direct visualization of lipid rafts with an estimated size of 1 to 100 nm. Logically, direct verification for the presence of the EGFR in lipid rafts is equally excluded. Förster Resonance Energy Transfer (FRET) imaging (Jares-Erijman and Jovin, 2006) reports for the intramolecular distance between two fluorescent molecules on a nanometer scale level (1 to 10 nm). Thus, FRET can be used to determine the close proximity and colocalization of two molecules. In the present work, the colocalization of the EGFR with molecules that are typically present in DRM fractions such as the ganglioside GM1 and glycosylphosphatidylinositol-anchored GFP (GPI-GFP) is studied by making use of FRET imaging (Jares-Erijman and Jovin, 2006). In this study, two levels of colocalization are considered, (1) microscopic scale colocalization on a pixel level and (2) nanoscale colocalization as determined using FRET. To label the EGFR without changing its activity state we have used monovalent, non-agonistic fragments from heavy-chain only antibodies from Llama glama (nanobodies[1]), which were directed against the ectodomain of the EGFR. Ganglioside GM1 was labeled using subunit B from cholera toxin (CTB). To circumvent effects

from probe concentrations on energy transfer, we investigated the occurrence of FRET by time-gated Fluorescent Lifetime Imaging Microscopy (FLIM). We report here the cholesterol-independent colocalization of GM1 with EGFR, while the colocalization of GM1 with GPI-GFP was cholesterol-dependent. No colocalization of GM1 was observed with the receptor for transferrin, demonstrating the selectivity of the assay. Stimulation of the cells with EGF induced EGFR colocalization with GPI-GFP. Our results suggest that the EGFR is surrounded by gangliosides and that EGF stimulation leads to coalescence of different types of lipid rafts into larger EGFR containing lipid nanodomains.

Materials and methods

Materials

Mouse Anti-EGFR and rabbit anti-EGFR was purchased from Santa-Cruz (Santa Cruz, CA) and Cell Signaling (Beverly, MA) respectively. Mouse anti-actin was from MP Biomedicals (Aurora, OH) and mouse anti-GM130 and anti-phospho-tyrosine (clone PY20) were from BD Biosciences (Alphen aan de Rijn, the Netherlands). Mouse anti-GFP was from Roche Diagnostics (Almere, the Netherlands), while anti-transferrin receptor (TfR) was obtained from Invitrogen (Breda, Netherlands). Human EGF was purchased from Oxford Biotechnologies (Oxfordshire, UK). Protein G-Sepharose 4B beads, BSA (Fraction V), Sepharose G25 medium beads, nystatin, filipin and mowiol were from Sigma-Aldrich (Zwijndrecht, the Netherlands). Microcon YM-3 spin-columns were from Millipore (Billerica, MA). Molecular biology products and IPTG were from Fermentas GmbH (St. Leon-Rot, Germany). Lipofectamine 2000, Zeocin and the fluorescent products EGF-Alexa Fluor 488 (EGF-A488), EGF-tetramethylrhodamine, Transferrin-Alexa Fluor 488, Cholera toxin subunit B conjugated to Alexa Fluor 594 (CTB-A594), biotin (CTB-biotin) or Horseradish Peroxidase (CTB-HRP), the Alexa Fluor 488-TFP and Alexa Fluor 594-NHS protein labeling kits were all from Invitrogen. Talon was purchased from BD Biosciences (Palo Alto, CA), and imidazole was obtained from Merck (Darmstadt, Germany). The GPI-GFP plasmid was kindly provided by Dr. P. Keller, Dresden, and the plasmid expressing the transferrin receptor was a gift from Dr. P. van der Sluijs, Utrecht.

Cell culture and transfection

A431 (ATCC CRL-1555) and HER14 (mouse NIH 3T3 fibroblasts expressing human EGFR) cells were cultured in Dulbecco's modified Eagle's medium (DMEM) (Invitrogen) supplemented with 7.5% foetal bovine serum (v/v), 100 U/ml Penicillin, 100 µg/ml streptomycin and 2 mM L-glutamine at 37°C in the presence of 5% CO_2 under a humidified atmosphere. For the immunoprecipitation and cell activation experiments, cells were seeded in a 35 mm culture dish, and grown to subconfluency. Prior to stimulation, cells were maintained 12 hours under low serum (0.1% FCS) conditions. For transfection, cells were grown to 50% confluency and transfected with the indicated expression vectors using Lipofectamine 2000 according to manufacturer's instructions (Invitrogen). Plasmid DNA was prepared using an endotoxin-free plasmid preparation kit (Machery-Nagel, Dueren, Germany). For FLIM experiments, the cells were used 48 hours post-transfection. To enrich cells expressing GPI-GFP, cells were sorted using a Fluorescence Activated Cell Sorter. Cells pretreated with nystatin or filipin were incubated for 30 minutes at 37°C with DMEM supplemented with 5 µg/ml nystatin or 2.5 µg/ml filipin.

Nanobody selection, production and labeling

Synthesis of an immune phage antibody library was performed essentially as previously

described (Roovers et al., 2007). In short, vesicles purified from the EGFR expressing A431 cell were injected into Llama glama. Four days after the last antigen injection, 150 ml of blood was collected and peripheral blood lymphocytes were collected by density gradient centrifugation using Ficoll-Paque PLUS gradients (Amersham Biosciences, UK). Total RNA was extracted and transcribed into cDNA using an oligo-dT primer and the SuperScript III First-Strand Synthesis System for RT-PCR (Invitrogen). The cDNA was subsequently treated with RNAse H to deplete residual RNA and then purified using the QIAquick PCR Purification Kit (Qiagen, Hilden, Germany). This cDNA was used as template to amplify the repertoire of gene segments encoding heavy chains of Ig with the use of a framework 1 (FR1) specific- primer and an oligo-dT primer. The resulting PCR fragments of 1.3kb (heavy chain IgGs lacking CH1 domain) and 1.6kb (conventional IgGs) were size separated on agarose gel and the genes encoding the heavy-chain only IgGs were purified. The full repertoire of PCR amplified genes was cut with appropriate restriction enzymes and the resulting 400-500bp fragments were ligated into a phagemid vector for display on filamentous phage. This resulted in repertoires of 10^7 – 10^8 transformants each. Nanobodies specific for the EGFR were subsequently selected by phage display. A431-derived membrane vesicles were coated onto a Maxisorp 96-well plate (Nunc, Denmark) during an overnight incubation at 4ºC. Non-specific binding was prevented by blocking with 4% skimmed milk (Marvell) in PBS (MPBS) at room temperature (RT) for 30 minutes. Phage (approximately 10^{10} colony forming units), prepared from the immune library were panned for binding to immobilized EGFR in 2% MPBS, 1% BSA containing suspended NIH 3T3 clone 2.2 cells (that do not express EGFR) for 90 minutes at RT. After extensive washing and elution with 100 mM triethylamine (TEA) for 10 minutes at RT, phages were neutralized and multiplied according to standard procedures. After selection, PCR products of single bacterial clones were analyzed by HinfI restriction pattern analysis. The cDNAs of specific Nanobody clones were re-cloned into pUR5850 allowing the expression of a triple tagged protein (Myc, biotinylation and His6) in the periplasmic space of E. coli . Four hours after induction of nanobody production with IPTG, the bacteria were lysed in 8 M Urea followed by purification of the nanobody with Talon beads according to the manufacturers instructions. Purified protein was dialyzed extensively against PBS, and checked for purity on a Coomassie blue stained SDS-PAGE gel. Micropore spin columns were used to concentrate the pure protein to a final concentration of 2-5 mg/ml. Labeling of nanobodies with Alexa Fluor-488 or -594 was performed as recommended by the manufacturer. In short, 15 µg of nanobody was incubated with 3-30 µg of DMSO-dissolved mono-reactive Alexa Fluor dye for 1 hr at room temperature in the dark. Labeled nanobody was separated from non-reacting dye using a 1 ml Sephadex G25 column and dialyzed against PBS. Labeling efficiency was determined with a Nanodrop spectrophotometer (Nanodrop Technologies, Wilmington, Delaware), and was on average 1.5 Alexa Fluor label per nanobody. Final concentration of the fluorescent nanobodies which was used for cell labeling varied between 50 and 100 nM.

An ELISA assay was performed to determine the competition between EGF and

nanobodies for binding to the EGFR as previously described (Roovers et al., 2007). In short, A431-derived membrane vesicles were immobilized overnight at 4°C in 96 wells plates (Maxisorp, Costar, Corning, U.S.A.) at 5 µg/ml of protein. Next day, plates were washed twice with PBS containing 0.05% (v/v) Tween-20 and subsequently blocked with PBS containing 1% (w/v) casein for 1 hr at room temperature. Serial dilutions of nanobodies (200nM to 10pM) were made in PBS/1% (w/v) casein, biotinylated EGF (Peprotech, New York, USA) was added to 8 ng/ml (1.3 nM) and the mixes were incubated in vesicle coated wells for 1 hr at room temperature with shaking. Maximal binding was determined by addition of a non-relevant (anti-GST) nanobody and background staining by the omission of biotinylated EGF. Wells were washed three times with PBS/0.05% (v/v) Tween-20 and receptor-bound biotinylated EGF was detected with a streptavidin-peroxydase conjugate (Sigma-Aldrich, Zwijndrecht, the Netherlands; 1:5000 in PBS/1% (w/v) casein). After washing, wells were stained using O-phenylenediamine (OPD, MP biomedicals, Illkirch, France) and the reaction was stopped by the addition of 1 M H_2SO_4. OD was read at 490nm in a 96-wells ELISA reader.

Immunoprecipitation

Immunoprecipitation experiments were principally performed as described previously (Klapisz et al., 2002). Her14 cells were grown in 35 mm dishes until 70% confluency and lysed in ice-cold 300 µl lysis buffer (1% Triton X-100, 150 mM NaCl, 20 mM Tris-HCl pH 7.4) supplemented with Complete protease inhibitor cocktail (Roche), 10 mM NaF, and 1 mM $NaVO_4$. The lysate was passed through a 23G needle for 3 times and centrifuged at 13,000 rpm for 5 minutes. Talon beads (20 µl), preloaded with 10 µg of the indicated nanobodies for 1 h were incubated with the lysates for 1 hr at 4°C. The beads were washed extensively with lysis buffer and resuspended in 40 µl sample buffer. Precipitated proteins were size-separated on 8% (w/v) SDS-PAGE and transferred onto PVDF membrane. EGFR was detected with anti-EGFR (Santa Cruz Biotechnology) and horseradish peroxidase-conjugated anti-rabbit IgG (Jackson ImmunoResearch Laboratories, USA), followed by signal detection using ECL (Du Pont NEN, USA).

Immunofluorescent labeling.

Cells (~$6x10^4$) were seeded on 18 mm glass coverslips and grown until 20% confluency. Medium was replaced by ice-cold binding medium (DMEM/Hepes (pH 7.8) supplemented with 1% BSA), and the cells were placed on ice. Cells were subsequently incubated with fluorescent EGF (8 nM), CTB (1 µg/ml), transferrin (20 µg/ml) or different nanobodies (50-100 nM) in binding medium for 1 h on ice. Cells preincubated with nystatin/filipin were maintained in binding medium supplemented with the labeling reagents. Cells were washed with binding medium, fixed with initially ice-cold 4% formaldehyde, and quenched with 50 mM glycine. Coverslips were finally embedded in mowiol and stored at -20° C until further use. Wide field microscopy was performed on an Olympus AX70 microscope equipped with a Nikon

CCD camera (DXM1200) using a 60x oil immersion objective (NA 1.25/ PlanFl). Confocal microscopy for figure 2C was done on a Zeiss LSM 510 microscope equipped with a 63x water immersion objective (NA 1.2/C-apochromat).

Fluorescence lifetime imaging measurements.

A Nikon PCM 2000 confocal scanning laser microscope (CSLM) was equipped with a fluorescence lifetime imaging module (LiMO, Nikon Instruments, Badhoevedorp, The Netherlands (de Grauw and Gerritsen, 2001)), which captures four images representing the total fluorescent intensity in four consecutive time gates of approximately 2 ns each. The excitation light was provided by a frequency doubled picosecond pulsed Ti:Sa laser (Tsunami, Spectra Physics); a pulse picker was used to reduce the repetition rate to 8.2 MHz. 460 nm pulses were transferred to the confocal microscope using a single-mode optical fiber. For imaging, a NA=1.20 / 40x water immersion objective (Plan Apo, Nikon) and the medium sized pinhole were used. The fluorescence emission was filtered (515/30 emission filter) and collected with a fiber-coupled PMT (Hamamatsu H7422P-40) that was connected to a pre-amplifier and the LiMo unit. To set the time offset of opening of the first gate of the LiMo with respect to the excitation pulse, a solution of Rose Bengal (lifetime 70 ps) was used in such a way that the first gate opened after 90% of the fluorescence was emitted. The widths of the time gates were calibrated using a continuous wave white light source; correction factors were introduced to ensure in all gates the intensity was equal. The four gate intensity decays recorded for each pixel were fitted with a monoexponential decay using the LiMo's software, meaning that also for probes with multiexponential decays, one single average lifetime is observed. Lifetimes described in this study should therefore be considered as average lifetimes.

Analysis of FRET/FLIM data.

Confocal FRET/FLIM microscopy is used to make lifetime images in an equatorial plane through the cell (Fig. 1A,B). Subsequently, intensity thresholding is performed to remove background- (glass) and auto-fluorescence (Fig. 1C,D). The fluorescence lifetimes of pixels above threshold (at least 1000 per cell) were plotted in a histogram that was fitted with a Gaussian function (using Origin, Origin Corporation, Northampton, MA, USA) to determine the average lifetime (Fig. 1E). To rule out the effects of cell-to-cell variation in FRET efficiency, the lifetimes of at least five cells were determined and a Students T-test was performed to determine the statistical significances (Fig. 1F). Fluorescent lifetimes were normalized against the lifetime for donor-only situation. For one cell, normalized fluorescence lifetime values are presented in a false color image; histograms show the normalized average donor lifetime $\tau/\tau_{donor} \pm$ SEM for $N \geq 5$ cells per measurement.

Purification of detergent-free lipid raft fractions.

The procedure for detergent-free cell fractionation and flotation was modified from MacDonald

and Pike (Macdonald and Pike, 2005). Briefly, two 100 mm dishes with Her14 cells expressing GPI-GFP were grown to 80% confluency. Cells were grown under serum-free conditions for 16 h. prior to the fractionation. Medium was replaced by ice-cold serum-free DMEM with Hepes buffer at pH7.2, and cells were either stimulated at 4°C with 8 nM EGF for 10 minutes or left untreated. After washing two times with ice-cold PBS, cells were scraped in base buffer (20 mM Tris-HCl, 250 mM sucrose, pH 7.8) supplemented with 1 mM $MgCl_2$ and 1 mM $CaCl_2$. After pelleting the cells by centrifugation at 250xg, they were resuspended in base buffer supplemented with Complete protease inhibitor cocktail, 1 mM $MgCl_2$ and 1 mM $CaCl_2$. The cells were lysed by passing through a 23G needle for 20 times. After centrifugation at 1000xg for 10 minutes, the post-nuclear supernatant was harvested. The remaining pellet was resuspended in base buffer with Complete protease inhibitor cocktail and cations, passed through the needle 20 times again, followed by centrifugation. The second supernatant was combined with the first. Optiprep was added to a final concentration of 25%. Subsequently, a 0-20% Optiprep step gradient with 5% intervals was layered on top of this lysate, and centrifuged at 52.000xg for 90 minutes in a Beckmann SW41Ti rotor. Fractions (12) of 1 ml each were collected from top to bottom of the gradient. To concentrate proteins, fractions were concentrated on Microcon columns (MWCO 3 kDa) until a final volume of 40 µl was reached. Proteins in the different fractions were size-separated on a 8% SDS-PAGE, and analyzed by Western blotting. Detection of GM1 was performed using a dot spot assay as described by Puri et al., using CTB conjugated to horse radish peroxidase (HRP) as ligand (Puri et al., 2005).

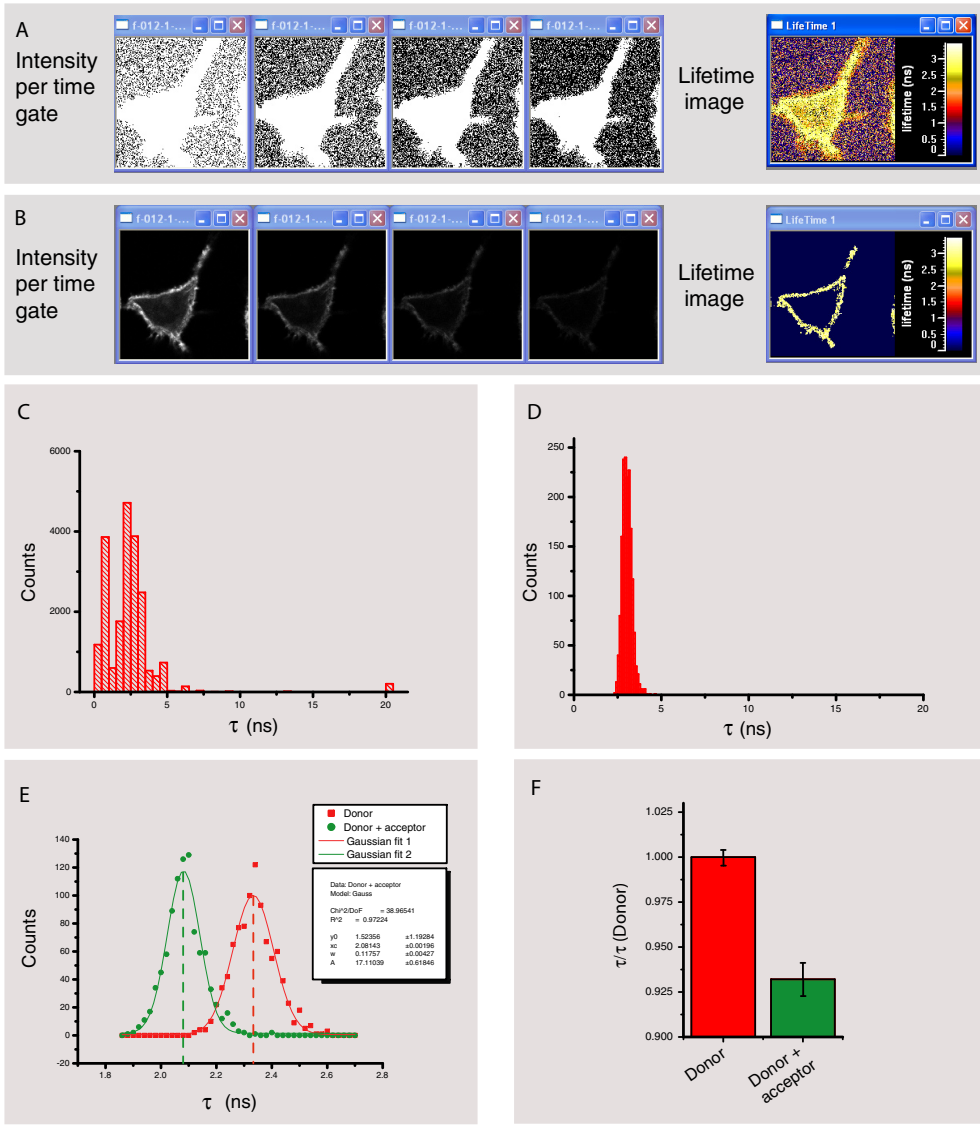

Figure 1. Analysis of FRET/FLIM data.

(A) Intensity images from the four time gates and lifetime image of GPI-GFP expressed in a NIH 3T3 cell. (B) Intensity images and lifetime image of the same cell after thresholding. (C) Histograms of lifetime distributions of one cell from non-thresholded pixels. (D) Similar histograms from thresholded pixels. Note the absence of the autofluorescence peak. (E) Determination of the average τ_{donor} value per cell by Gaussian fitting of the thresholded data as described in the Materials and methods section. (F) Plotting the normalized average donor lifetime τ/τ_{donor} ± SEM for N>5 cells per measurement.

Results

Development of nanobodies against EGFR.

To investigate the localization of the EGF receptor in the plasma membrane, monovalent, small, highly specific probes that do not induce EGFR activation or internalization are required. To this end, we decided to use antibodies from Llama glama that are devoid of light chains and as such only consists of heavy chains (Conrath et al., 2003). The Variable part of the Heavy chain of these Heavy-chain only antibodies (termed VHH) fulfils all the above described criteria. Because of their small size (~15 kDa) we refer to this antibody format as nanobody.

A VHH immune library directed against EGFR was produced as previously described (Roovers et al., 2007). From this library, three different nanobodies were selected and further characterized for EGFR binding specificity and biological activity. Binding to EGFR was analyzed by immunoprecipitation, and all three selected nanobodies were found to bind EGFR, as demonstrated by the immunoprecipitation of EGFR from the cell lysate (Fig. 2A). As a control, Talon beads were preloaded with nanobodies directed against glutathione-S-transferase (anti-GST), which did not precipitate EGFR. Biological activity of the nanobodies was checked by analysing EGFR activation with antibodies against the phosphorylated C-terminal domain of EGFR. Her14 cells stably expressing human EGFR were incubated for 10 minutes with 1 μM nanobody or 8 nM EGF, and immuno-precipitates of EGFR from the cell lysate were analyzed by Western blotting with anti-phosphotyrosine1068-EGFR or anti-EGFR as loading control. A clear EGF-mediated activation of EGFR was found, but no EGFR activation could be detected after incubation with the different nanobodies, although their concentration exceeded EGF concentration 125 times (Fig. 2B). To check the specificity of the nanobodies for EGFR, we incubated 3T3 2.2 cells, lacking any detectable levels of EGFR, and Her14 cells on ice with 100 nM anti-EGFR nanobody directly conjugated to Alexa Fluor 594 (EGb4-A594), in the presence of 8 nM EGF-A488. Nuclear staining with DAPI was used as counter stain. The 3T3 2.2 cells lacking EGFR expression displayed no cell surface labeling of anti-EGFR nanobodies while Her14 cells were heavily labeled with both probes (Fig. 2C). Moreover, the two probes colocalized exactly, indicating that the nanobody is specific for EGFR. Similar results were obtained with the nanobody EGbc5 (data not shown).

To examine the effect of the nanobodies on EGF binding, we performed a competition assay with biotinylated EGF as previously described (Roovers et al., 2007). Nanobody EGa1 at 1 nM or higher was clearly competitive with EGF while EGb4 had no effect on the binding of EGF within the tested concentration range. Only nanobody EGc5 has a minor antagonistic effect above 50 nM (Fig. 2D). In conclusion, we have selected different anti-EGFR nanobodies without detectable agonistic effects on the receptor. One of the nanobodies is able to block binding of EGF to EGFR, whereas the other nanobodies hardly display any blocking capacity, suggesting differential epitope specificity. In addition, conjugation of the nanobodies to Alexa Fluor probes did not interfere with their binding properties, making these molecules ideal

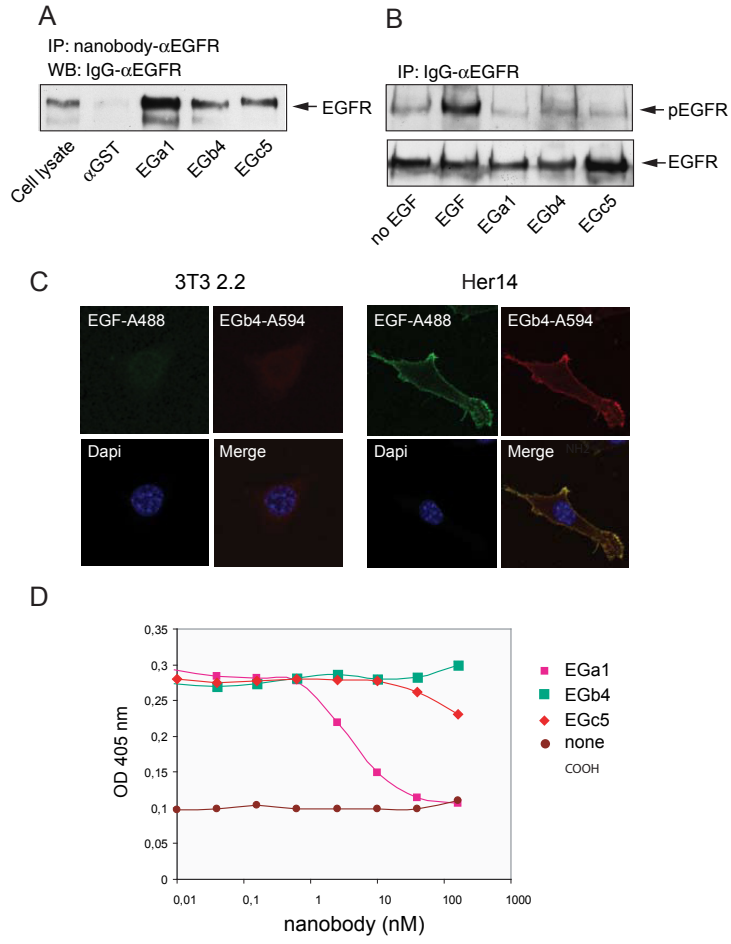

Figure 2. Characterization of anti-EGFR nanobodies.
(A) Immunoprecipitation of EGFR with nanobodies. Her14 cell lysates were prepared as described in Material & methods and incubated for 1 hr at 4°C with Talon beads preloaded with the indicated anti-EGFR nanobodies, or with an non-specific nanobody (anti-GST). Bound proteins were separated by SDS-PAGE, analyzed by Western blotting. Control lane (Cell lysate) is loaded with 10% of the lysate. (B) Selected nanobodies are non-agonistic. Equal number of serum-depleted Her14 cells were treated with either 8 nM EGF or 1 μM of the indicated nanobodies for 10 minutes, or mock-treated (no EGF), and immunoprecipitated EGFR was analyzed by Western blotting. Activation of EGFR was determined with an antibody against phosphotyrosine at position 1068 (pEGFR). Loading control was performed with anti-EGFR (EGFR). (C) Selected nanobodies bind specifically to EGFR. NIH 3T3 cells clone 2.2, lacking detectable expression of EGFR, or Her14 cells were labeled at 4°C for 60 minutes with 100 nM EGb4-A594. In parallel, the cells were labeled with 8 nM EGF-A488 and nuclei were visualized with 4'-6-diamidino-2-phenylindole (DAPI)(blue). (D) Different antagonistic activities of anti-EGFR nanobodies. Her14 cells grown in 96-wells plates, were pre-incubated with biotinylated EGF, followed by increasing concentrations of indicated nanobodies or EGF. Binding of EGF-biotin on the cell surface was quantitated with peroxidase-conjugated streptavidin, followed by addition of the substrate OPD.

probes for the localization of EGFR in the plasma membrane.

Colocalization of EGFR with GM1 but not with GPI-GFP.

The labeled, EGFR specific nanobodies were used to investigate the colocalization of EGFR with GM1. Her14 cells were labeled with EGa1 conjugated to A488 (EGa1-A488) and the B-subunit of cholera toxin conjugated to A594 (CTB-A594). On the light microscopy level, clear colocalization of the probes over the cell membrane is observed, in particular at membrane ruffles (Fig. 3A). The average lifetime of donor EGa1-A488 was determined in the absence and presence of acceptor CTB-A594 (Fig. 3B). The lifetime of EGa1-A488 was significantly reduced in the presence of CTB-A594, indicating that EGFR and GM1 are present in the plasma membrane within the range of FRET to occur. To exclude a possible nanobody specific effect, we also used other anti-EGFR nanobodies such as EGb4, with similar results (Fig. 3C). To exclude a possible crosslinking effect of the formaldehyde fixation, the colocalization of EGFR with GM1 was also studied using live cell frequency-domain FLIM setup, with similar results (M.O. Ruonala and Philippe Bastiaens, unpublished observations). As a negative control, we conducted a colocalization experiment with the receptor for transferrin (TfR), which has been found in cell fractionation studies in the detergent-soluble fraction (Harder et al., 1998; Puri et al., 2005). This control is particularly important since CTB may, as a result of its pentavalency, induce clustering of GM1 resulting in the recruitment of plasma membrane receptors into these GM1 clusters (Zhang et al., 1995). Her14 cells transiently expressing human TfR were fluorescently labeled with transferrin-A488 (Tf-A488). TfR labeling resulted in a heterogenous staining of the cell membrane with a clear microscale colocalization with CTB (Fig. 3D). The lifetime of Tf-A488 remained unaffected when measured in combination with CTB-A594 (Fig. 3E), excluding a colocalization on the nanoscale level of TfR with GM1.

We subsequently investigated whether the GPI-GFP colocalizes with EGFR. The GPI-GFP was ectopically expressed in Her14 cells and was found in the plasma membrane, as well as in subcellular compartments (Fig. 4A). Co-staining with the Golgi-resident protein GM130 identified this compartment as the Golgi complex (Fig. 4B). Confocal images showed a clear colocalization of EGFR with GPI-GFP (Fig. 4A). However, this colocalization was not confirmed at the nanoscale level by FLIM-analysis. Although a slight lifetime reduction was observed in the presence of EGb4-A594, this difference appeared not to be significant (Fig. 4C). These results demonstrate that EGFR and GPI-GFP do not colocalize in nonstimulated Her14 cells.

In summary, our results demonstrate that the EGFR colocalizes at a nanoscale level with the ganglioside GM1 in the plasma membrane of HER14 cells, while for the control receptor TrfR no colocalization was observed. Similarly, colocalization at the nanoscale level for EGFR with GPI-GFP, another frequently used lipid raft marker, was also absent. In addition, the microscopic colocalization of TfR with GM1 and EGFR with GPI-GFP is not detected on a nanoscale with FLIM, demonstrating the power of FRET/FLIM analysis for reliable conclusions

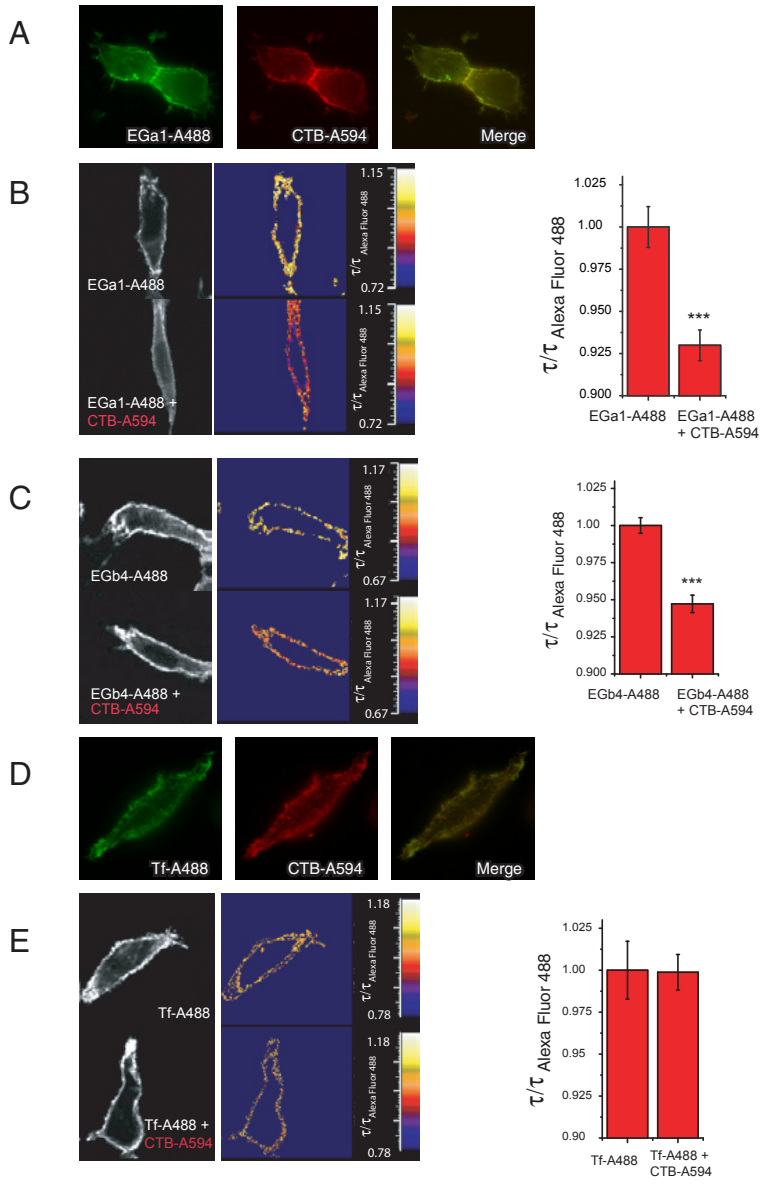

Figure 3. Nanoscale colocalization of EGFR with GM1 gangliosides. Her14 cells grown on coverslips were incubated on ice with 100 nM of the donor probes anti-EGFR nanobody EGa1 (A, B) or EGb4 (C) directly conjugated to Alexa Fluor 488, or with 20 µg/ml transferrin-A488 (Tf-A488) (D, E) in the absence or presence of 1 µg/ml of the acceptor probe CTB-A594. After labeling, the cells were fixed with 4% formaldehyde, embedded in mowiol and examined by wide-field fluorescence microscopy (A, D) or analysed with FLIM (B,C,E). The average lifetime values of GFP were determined as described in Materials and methods. Left panels in B, C and E represent the distributions of the donor probes with or without acceptor probe. The lifetimes are shown in the middle panels in false colors. Mean fluorescent lifetime values ± SEM (*** p< 0.0001) are presented in histograms on the right.

on colocalization experiments.

Nanoscale colocalization of GM1 with EGFR is cholesterol independent.

We next investigated the role of cholesterol in the colocalization of EGFR with the different markers. For these experiments we used the polyene antibiotic nystatin, which sequesters free cholesterol without considerable extraction of this sterol (Foster et al., 2003). Since another

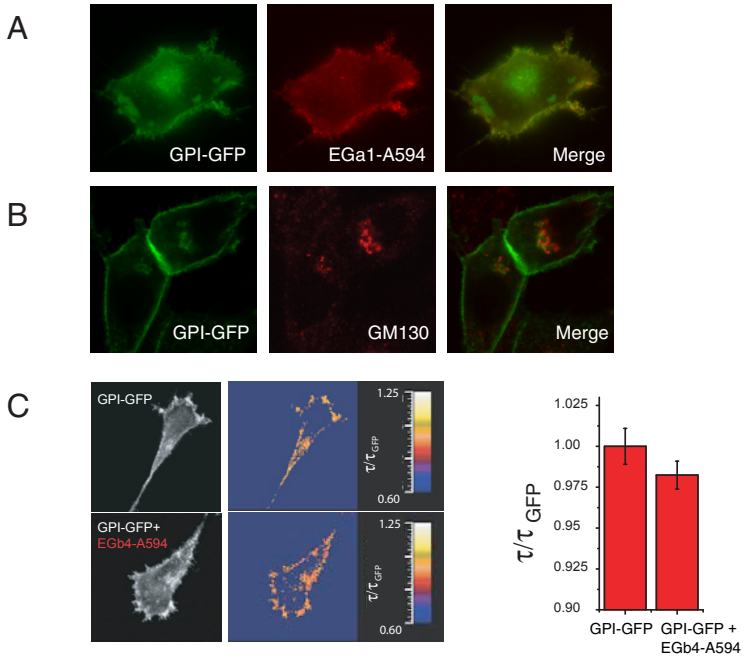

Figure 4. No nanoscale colocalization of EGFR with GPI-GFP

(A, B) Her14 cells expressing GPI-GFP were grown on coverslips, and incubated for 1 h on ice with 100 nM EGb4-A594 or, after fixation with 4% formaldehyde, permeabilized and incubated with antibody against GM130. After embedding, the cells were imaged by wide-field fluorescence microscopy. (C) Her14 cells expressing GPI-GFP were when indicated incubated for 1 h on ice with 100 nM EGb4-A594 (acceptor). After fixation with 4% formaldehyde, average lifetime values of GFP were determined as described in Materials and methods. Left panels represent the distributions of the donor probes with or without acceptor probe. The lifetimes are shown in the middle panels in false colors. Mean fluorescent lifetime values ± SEM (*** p< 0.0001) are presented in histograms on the right.

cholesterol extracting agent, methyl-β-cyclodextrin, was previously found to stimulate EGFR activity, we checked the effect of nystatin on several cellular functions (Lambert et al., 2006; Ringerike et al., 2002). These control experiments showed that nystatin treatment did not affect EGFR activity, cell shape or the distribution of GM1, GPI-GFP or EGFR (Fig. 5A-C).

We next analyzed the effect of nystatin on the distribution of the two raft markers GPI-GFP and GM1. GPI-GFP was found at the plasma membrane and in the Golgi complex (Fig. 5D).

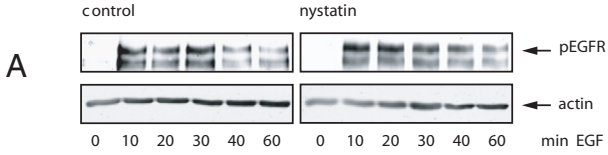
A
control
nystatin
pEGFR
actin
0 10 20 30 40 60 0 10 20 30 40 60 min EGF

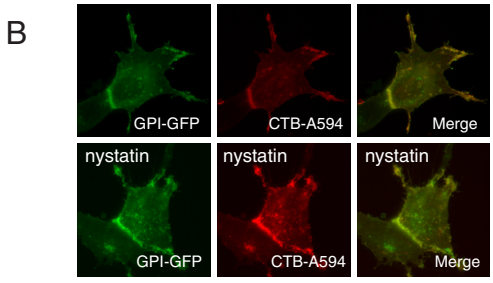
B
GPI-GFP
CTB-A594
Merge
nystatin
GPI-GFP
CTB-A594
Merge

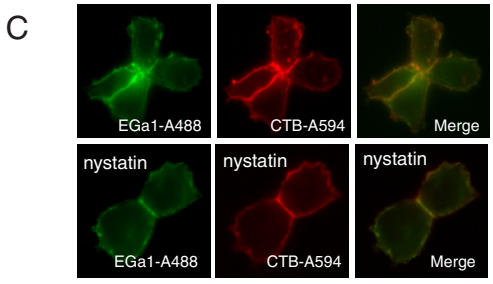
C
EGa1-A488
CTB-A594
Merge
nystatin
EGa1-A488
CTB-A594
Merge

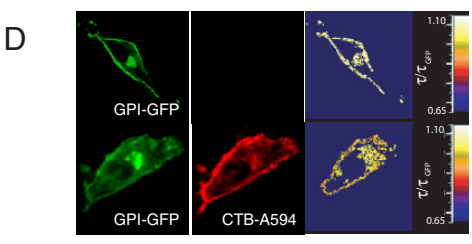
D
GPI-GFP
GPI-GFP
CTB-A594
1.10
0.65
τ/τ GFP

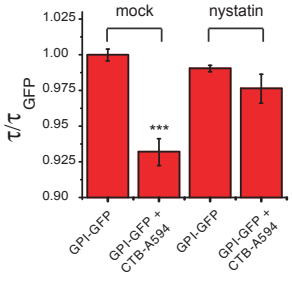
mock
nystatin
1.025
1.00
0.975
0.95
0.925
0.90
τ/τ GFP
***
GPI-GFP
GPI-GFP + CTB-A594
GPI-GFP
GPI-GFP + CTB-A594

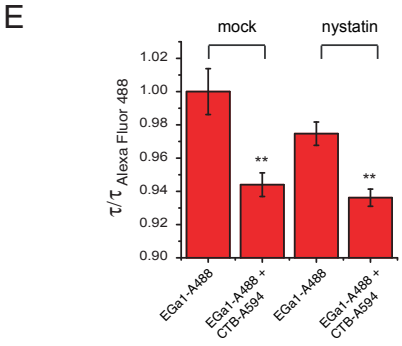
E
mock
nystatin
1.02
1.00
0.98
0.96
0.94
0.92
0.90
τ/τ Alexa Fluor 488
**
**
EGa1-A488
EGa1-A488 + CTB-A594
EGa1-A488
EGa1-A488 + CTB-A594

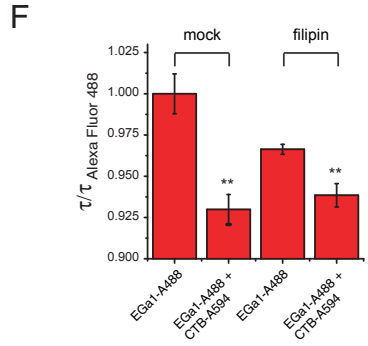
F
mock
filipin
1.025
1.000
0.975
0.950
0.925
0.900
τ/τ Alexa Fluor 488
**
**
EGa1-A488
EGa1-A488 + CTB-A594
EGa1-A488
EGa1-A488 + CTB-A594

Figure 5 (last page). Cholesterol-dependence of the colocalization of GPI-GFP and EGFR with GM1. (A) Her14 cells were when indicated treated with 5 µg/ml nystatin for 30 min at 37°C, and stimulated for the indicated times with 8 nM EGF. Cells were lysed and analyzed for the presence of of phosphotyrosine at position 1068 (pEGFR) by Western blotting. Anti-actin was used as loading control. (B) Her14 cells expressing GPI-GFP were when indicated preincubated with 5 µg/ml nystatin for 30 min at 37°C. The cells were labeled with 1 µg/ml CTB-A594, fixed with 4% formaldehyde and examined by wide field fluorescence microscopy. (C) Her14 cells were grown on glass coverslips and when indicated treated with 5 µg/ml nystatin for 30 min at 37°C. Cells were labeled with 100 nM anti-EGFR nanobody EGa1-A488 and with 1 µg/ml CTB-A594, fixed with 4% formaldehyde and examined by wide field fluorescence microscopy. (D) Cholesterol-dependent colocalization of GPI-GFP with GM1. Her14 cells expressing GPI-GFP (donor) were when indicated incubated with 5 µg/ml nystatin for 30 minutes at 37°C and whether or not labeled with CTB-A594 (donor probe). The fluorescent intensity of GPI-GFP or CTB-A594 is shown in the left or middle panel, respectively. Fluorescent lifetime of GPI-GFP was analyzed as described in Materials and methods and presented as false colored images in the right panel. Histograms represent the mean lifetime values ± SEM (*** $p<0.0001$) of GPI-GFP determined under the indicated conditions. (E + F) Cholesterol-independent colocalization EGFR with GM1 gangliosides. Her14 cells were treated with 5 µg/ml nystatin (E) or 2.5 µg/ml filipin (F) for 30 minutes at 37°C. Cells were labeled with anti-EGFR nanobody EGa1-A488 and whether or not with the acceptor probe CTB-A594. Lifetime values were determined as indicated in Materials and methods, and mean lifetime values of ± SEM (** $p<0.001$) are presented in histograms.

A clear lifetime reduction of GPI-GFP was observed when the cells were colabeled with CTB-A594 (Fig. 5D). As expected, the false color images reveal that this lifetime reduction is only found at the plasma membrane, while it remained unchanged in intracellular compartments (Golgi) (Fig. 5D). In parallel, GPI-GFP expressing cells were preincubated with nystatin for 30 minutes, followed by staining with CTB-A594. However, while in control cells the lifetime of GPI-GFP was clearly reduced after addition of CTB-A594, the lifetime of GPI-GFP was not reduced by CTB-A594 in the presence of nystatin (Fig. 5D). This result demonstrates that the two raft markers GM1 and GPI-GFP colocalize in a cholesterol-dependent fashion, which is in agreement with current models of lipid rafts (Kenworthy et al., 2000).

We subsequently studied the effect of nystatin on the colocalization of GM1 with EGFR. HER14 cells were preincubated with nystatin under similar experimental conditions as described above and labeled with EGa1-A488 and CTB-A595. Again, on a microscale level no clear differences in the distribution of either of the probes in the presence or absence of nystatin was observed (Fig. 5C). FRET/FLIM analysis showed that nystatin did not affect the observed FRET between the donor/acceptor pair indicating that the nanoscale colocalization of EGFR and GM1 is cholesterol-independent (Fig. 5E). A slight reduction was observed in the life time of the EGa1-probe alone, possibly resulting from EGFR clustering as a result of the cholesterol sequestration. Similar results were obtained when the cells were pretreated with another cholesterol sequestering agent, filipin (Fig. 5F). In conclusion, our results demonstrate that GM1 and GPI-GFP colocalize in the cell membrane of Her14 cells in a cholesterol-dependent manner. Conversily, the colocalization of GM1 with the EGFR was not affected by the sequestration of cholesterol demonstrating that the EGFR/GM1 colocalization is cholesterol-independent.

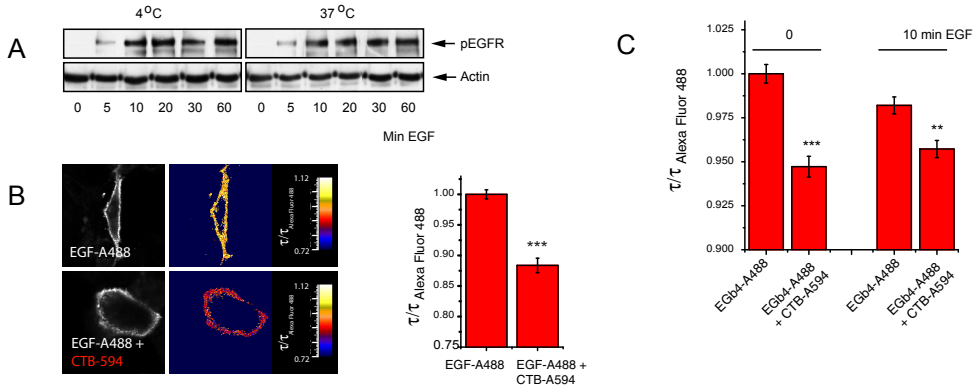

Figure 6. No effect of EGF on colocalization EGFR with GM1 gangliosides.
(A) EGFR is activated at 4°C. Her14 cells were stimulated with 8 nM EGF for indicated times and temperatures. Cell lysates were prepared and analyzed by Western blotting for the presence of phosphotyrosine at position 1068 (pEGFR). Actin staining was used as loading control. (B) Colocalization of activated EGFR with GM1. Her14 cells were incubated on ice with 8 nM EGF-488 (donor) in the absence or presence of 1 µg/ml acceptor probe CTB-A594. Confocal images representing the distribution of EGF-A488 are shown in the left panel. Lifetime of EGF-A488 was determined as described in Materials and methods and presented in false colors in the middle panel. Mean lifetime values ± SEM (*** p<0.0001) were determined and presented in the histogram in the right panel. (C) EGF does not alter colocalization EGFR/GM1. Her14 cells were incubated with 100 nM EGb4-A488 and 1 µg/ml CTB-A594 for 1 hour on ice. Cells were either treated with 8 nM EGF for 10 minutes or left untreated. After fixation and embedding, lifetime values of EGb4-A488 were analyzed as described in Materials and methods and presented as mean lifetime values ± SEM (** p<0.001, *** p<0.0001) in the histogram in the right panel.

EGF induces nanoscale colocalization of EGFR with GPI-GFP.

We next analyzed the effect of EGFR signaling on the nanoscale colocalization of the EGFR with the two lipid raft markers. To prevent internalization of the receptor after activation, these experiments were performed in ice-cold conditions. Stimulation with EGF at this temperature was found to result in phosphorylation of the receptor to an extent and with kinetics that was similar to the phosphorylation induced at 37°C (Fig. 6A). These results are in agreement with previous data showing that EGFR signaling was still able to proceed at 4°C (McCune and Earp, 1989). The effect of EGF-stimulation on the colocalization between EGFR and GM1 was first studied using EGF-A488 as donor probe and CTB-A594 as acceptor probe. In this way, EGF-A488 serves both as a donor-probe and as a ligand for EGFR. The presence of the acceptor probe reduced the lifetime of EGF-A488 significantly, indicating that the colocalization of EGFR with GM1 at the nanoscale level still exists after activation of EGFR (Fig. 6B). In an alternative approach, we used the non EGF-competing nanobody EGb4 conjugated to A488 as donor probe. Labeling of Her14 cells with EGb4-A488 was followed by activation of the cells with 8 nM EGF for 10 minutes. In the absence of EGF, a significant lifetime reduction was observed

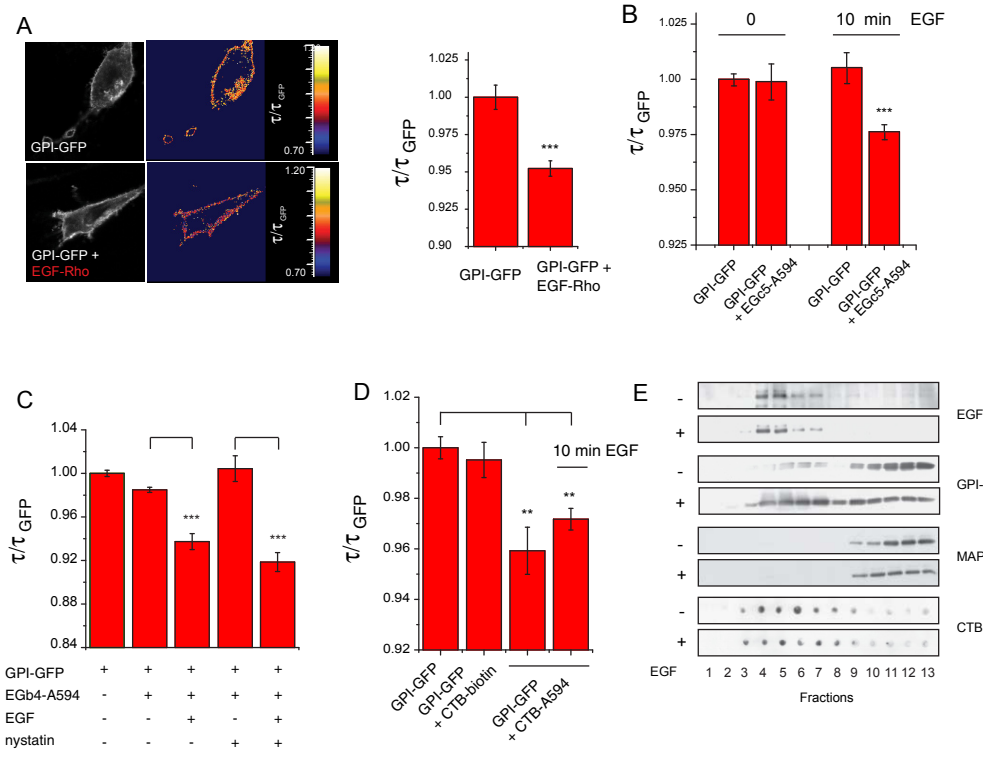

Figure 7. EGF-induced colocalization of EGFR with GPI-GFP.

(A) Colocalization active EGFR with GPI-GFP. Her14 cells expressing GPI-GFP were incubated for 1 h on ice with 8 nM EGF-Rhodamine (EGF-Rho) for 60 minutes, or mock-medium (without EGF-Rho). After fixation and embedding, the average lifetime values ± SEM (***p<0.0001) of GPI-GFP were determined as described in Materials and methods and presented in the histogram in the right panel. (B) Her14 cells expressing GPI-GFP were incubated for 1 hr on ice with 100 nM EGc5-A594. Activation with 8 nM EGF was performed on ice for 10 minutes. After fixation and embedding, mean lifetime values ± SEM (***p<0.0001) of GPI-GFP were determined as described in Materials and methods and presented in the histogram. (C) Her14 cells expressing GPI-GFP were when indicated preincubated with 5 µg/ml nystatin for 30 minutes at 37°C, for 1 hr on ice in the absence or presence of 100 nM EGb4-A594, and when idicated stimulated for 10 minutes with 8 nM EGF. After fixation and embedding, average lifetime values ± SEM (***p<0.0001) of GPI-GFP were determined as described in Materials and methods and presented in the histogram. (D) Her14 cells expressing GPI-GFP were incubated for 1 hr on ice in the absence or presence of 100 nM CTB-A594 or CTB-biotin as control. Activation with 8 nM EGF was performed on ice for 10 minutes. After fixation and embedding, mean lifetime values ± SEM (**p<0.001) of GPI-GFP were determined as described in Materials and methods and presented in the histogram. (E) EGF-induced recruitment of GPI-GFP into detergent-free lipid raft fraction. Her14 cells expressing GPI-GFP were whether or not stimulated with 8 nM EGF for 10 minutes and detergent-free lipid raft fractions were isolated as described in Materials and methods. Presence of EGFR, GPI-GFP and MAP kinase was analyzed by Western blotting, presence of GM1 was determined using a dot spot assay with CTB-HRP.

in the presence of CTB-A594, which remained unaltered after treatment of the cell with EGF (Fig. 6C). The results demonstrate that EGFR activation does not affect colocalization between EGFR and GM1. In addition, EGF was found to induce a slight reduction in the lifetime of the EGb4-A594 probe, which may be the result of the EGF-induced receptor oligomerization.

To measure the effect of EGF on the colocalization of the EGFR with GPI-GFP, Her14 cells stably expressing GPI-GFP were labeled for 1 h with EGF-Rhodamine, and the lifetime of the donor probe (GPI-GFP) was determined. Interestingly, the lifetime of GPI-GFP was clearly decreased in the presence of EGF-Rhodamine, suggesting that activation of the EGF receptor induces the colocalization of EGFR and GPI-GFP (Fig. 7A). EGF alone did not show an effect on the lifetime of GPI-GFP, indicating that the acceptor probe is required for this effect (Fig. 7B). In an alternative approach, we first labeled EGFR with EGc5-A594, a non-competing anti-EGFR nanobody conjugated to A594. After washing, the cells were stimulated with EGF and analyzed by FLIM. In the non-stimulated cells, no lifetime reduction of GPI-GFP was observed, while after 10 minutes of EGF-stimulation, a significant lifetime reduction became apparent (Fig. 7B). In parallel, nanobody EGb4 was used in a similar way as acceptor probe in combination with GPI-GFP yielding similar results (data not shown). We finally investigated the role of cholesterol in the EGF-induced colocalization of EGFR and GPI-GFP. Lifetime analysis of EGF-stimulated and nystatin treated GPI-GFP expressing cells demonstrated that the nanoscale colocalization of EGFR with GPI-GFP is cholesterol independent (Fig 7C).

Next, we were interested in the effect of EGF on the colocalization of GPI-GFP with CTB. A clear colocalization at the nanoscale level was observed in resting cells (Fig. 5D and 7D). This was not significantly altered by a stimulation of the cell for 10 minutes with 8 nM EGF (Fig. 7D). To exclude a possible effect of the binding of CTB alone on the lifetime of GFP, we performed a lifetime analysis using CTB conjugated to biotin instead of the acceptor probe Alexa594. No significant reduction in lifetime was observed, demonstrating the requirement for the fluorescent acceptor probe for this change in lifetime of the donor probe to occur (Fig. 7D). In summary, these data demonstrate that EGFR activation results in the induction of a cholesterol-independent colocalization at the nanoscale level of EGFR with the lipid raft marker GPI-GFP.

We finally investigated whether the EGF induced colocalization of GPI-GFP with the EGFR could be supported also by fractionations studies. Detergent free lipid raft fractions were purified and examined for the presence of EGFR, GPI-GFP and MAP kinase by Western blotting and GM1 by a dot-blot assay using CTB-HRP. EGF receptors, GPI-GFP and GM1 are all present in the lipid raft fraction, while MAP kinase is clearly absent. A clear enrichment in GPI-GFP was observed in the lipid raft fractions isolated from EGF-stimulated cells, while the distribution of EGFR, MAP kinase and GM1 remained unaffected (Fig. 7E). These data confirm the results that activation of the EGFR signaling pathway results in the coalescence of GM1/GPI-GFP and GM1/EGFR containing lipid rafts.

Discussion

In this study we have applied a microspectroscopic approach to investigate the role of EGF signaling in the organization of lipid rafts. Nanometer scale colocalization of the EGFR with putative lipid raft protein and glycolipid, GPI-GFP and GM1, was investigated by Förster resonance energy transfer as analyzed by fluorescence lifetime imaging microscopy. For a reliable interpretation of the FLIM results, the specific, non-agonistic and mono-valent labeling of the EGFR is a prerequisite. This was achieved using nanobodies obtained from Llama glama. Labeling of GM1 was done with the pentavalent CTB. To exclude possible recruitment effects of this multimeric molecule, we have performed several control experiments. The absence of colocalization of CTB with TfR indicates that CTB does not colocalize with all plasma membrane receptors. In addition, the fact that the colocalization of GM1 with GPI-GFP was dependent upon cholesterol, makes it very unlikely that this colocalization is induced by the recruitment of GPI-GFP by the pentavalent CTB. To prevent the internalization of EGF/EGFR complexes without the use of inhibitors we have used the cold-induced internalization block. Under these conditions the EGFR was found to be stimulated by EGF in a similar way as at 37°C, which is in agreement with previous studies (McCune and Earp, 1989). In model membranes, however, effects of low temperature have been shown to stabilize lipid rafts (Baumgart et al., 2003). FRAP studies have previously shown that the lateral diffusion coefficient of the EGFR was reduced from 8.5 x 10^{-10} cm^2/s at 37°C to 2.8 x 10^{-10} cm^2/s at 5°C without any indication for a phase transition. This suggest that on the plasma membrane the low temperature conditions do not induce seggregation of distinctive domains (Hillman and Schlessinger, 1982). Moreover, although the low temperature condition completely inhibits the clathrin-coated vesicle formation, the EGFR is still recruited to clathrin-coated pits (Puri et al., 2005). In conclusion, our control experiments seem to exclude side effects by the pentavalency of CTB and effects of the low temperature on the results.

Although we have obtained significant information about the occurrence of energy transfer between the EGFR and the GM1 specific probe, the transfer efficiency appeared low. This could be explained by the relatively large distance between the EGFR specific probes, i.e. the nanobodies and the GM1-probe. The crystal structure of the EGFR ectodomain suggests that, depending on the exact epitope recognized by the nanobody, the distance between the anti-EGFR nanobody and CTB can be more than 7 nm, which is larger than the Förster distance of the applied probes (Burgess et al., 2003; Ferguson et al., 2003). Although minor, the lifetime reduction due to FRET is highly significant. To exclude the possibility that the labeling of the EGFR or a conformational change of the receptor after activation does not influence the possibility of FRET, three different nanobodies which, according to their characteristics, bind to different sites of the EGFR ectodomain were used. In addition, we have also used fluorescent EGF to exclude any possible involvement of the nanobodies on the FRET analysis.

On a microscopic level, colocalization of the receptors for EGF and transferrin with GM1 and GPI-GFP was observed. At the nanometer scale level, our FRET analyses confirm the colocalization of GM1 with the EGFR but not with the transferrin receptor. The observed colocalization of EGFR with GM1 is in agreement with previous studies where

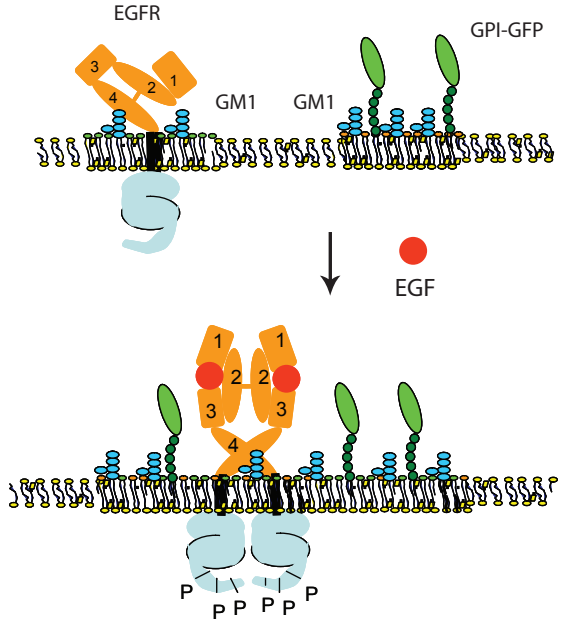

Figure 8. A model showing the coalescence of different lipid rafts.
In resting cells, GM1 forms a lipid shell surrounding the EGFR by binding to the ectodomain, and colocalizes in a cholesterol-dependent manner with GPI-GFP. Stimulation of the cell with EGF results in the coalescence of these two different microdomains possibly leading to the formation signaling platforms and initiation of EGFR internalization (see text for details).

electron microscopy was used (Puri et al., 2005; Ringerike et al., 2002). Similar results were obtained for HER2, another member of the EGFR family (Nagy et al., 2002). Sequestration of cholesterol did not affect the nanoscale colocalization of GM1 with the EGFR, suggesting that the colocalization of EGFR with GM1 is based upon a direct interaction between this ganglioside and the receptor. The gangliosides GM1 and GM3 were indeed shown to bind to the recombinant EGFR ectodomain purified from insect cells (Miljan et al., 2002). The interaction site appeared to be distinct from the ligand binding site, implying that the cysteine-rich domain may be responsible for this interaction. Interestingly, a mutational analysis demonstrated that the second cysteine-rich domain of the EGFR ectodomain is required for fractionation in the lipid raft fraction (Yamabhai and Anderson, 2002). NeuAc-lactose is essential for the direct interaction of gangliosides with the EGFR-ECD (Miljan et al., 2002). Whether sugar moieties on the EGFR-ECD are also involved in this interaction is currently unknown.

A consequence of the direct interaction between EGFR and gangliosides might be the formation of a lipid shell surrounding the transmembrane domain of the EGFR, which could explain their fractionation into the lipid raft fraction (Fig. 7D). Furthermore, in this model, the molecular organization of GM1 as well as cholesterol may affect the conformation of the ectodomain of the receptor, and consequently, ligand binding. It may also have an influence on receptor dimerization or even predimer formation. A possible role for cholesterol on receptor clustering including predimer formation has recently been demonstrated by Fluorescence Correlation Spectrocopy in combination with fluorescent brightness analysis (Saffarian et al., 2007). Positive effects of GM1 levels on EGFR signaling were obtained by overexpression of GM1 generating enzymes, which resulted in improved EGF-dependent cell proliferation (Nishio et al., 2005). Similarly, addition of GD1a ganglioside was shown to increase both the number of high affinity receptors as well as to stimulate EGF-induced cell proliferation (Liu et al., 2004). On the other hand, inhibitory effects of gangliosides on EGFR signaling have been described for GM3. This suggests that different gangliosides in the EGFR containing shell may have different effects on EGFR functioning. In conclusion, our data suggest the existence of a lipid shell around EGFR, composed of at least gangliosides, which have either a stimulative or inhibitory effect on EGFR functioning, depending on the type of prevailing ganglioside Development of novel probes to detect the specific gangliosides is required to further substantiate this hypothesis.

The cholesterol-dependent colocalization of the two lipid raft markers GM1 and GPI-GFP is in agreement with previous studies (Kenworthy et al., 2000). We and others have previously shown that GPI-GFP exists in small cholesterol-dependent nanoclusters (Bader et al., 2007; Sharma et al., 2004). These anisotropy experiments suggest the existence of small clusters of 3-4 GPI-GFP molecules per microdomain. Our data suggest that gangliosides like GM1 may also be present in these clusters as depicted in figure 6. The fact that the colocalization of GM1 with the EGFR was cholesterol-independent indicates the presence of two types of GM1 containing microdomains in the plasma membrane: a cholesterol-independent (GM1/EGFR) and a cholesterol-dependent microdomain (GM1/GPI-GFP).

The cholesterol independent colocalization of the EGFR with GM1 seems to exclude an effect of cholesterol on EGFR functioning. However, sequestration of cholesterol in the plasma membrane by nystatin or β-Cyclodextrin was found to increase EGF-binding and ligand-independent activation of EGFR kinase activity. Moreover, addition of cholesterol was found to inhibit EGFR signaling (Chen and Resh, 2002; Furuchi and Anderson, 1998; Ringerike et al., 2002). It is very well possible that the effect of cholesterol sequestration on EGFR functioning is indirect. Sequestration of cholesterol may lead to a disruption of the cholesterol-dependent lipid nanoclusters that contain GM1 and GPI-anchored proteins. Liberation of gangliosides from these type of raft may result in an increase in the direct interaction with the EGFR, and consequently in more dramatic effects of GM1 on EGFR functioning. Addition of cholesterol to the cell, on the other hand, may have the adverse effect and induce the formation of larger

cholesterol dependent GM1/GPI-GFP rafts leading to a decrease in the availability of GM1 to bind the EGFR, and consequently to an inhibition of EGF signaling.

Upon activation of the EGFR, also GPI-GFP was found to colocalize at the nanometer scale with the EGFR. Similar results have previously been obtained with another GPI-linked protein CD59 (Blagoev et al., 2003). This EGF-induced colocalization suggests the coalescence of the GM1/EGFR shells and the GM1/GPI-GFP nanoclusters into larger domains or rafts, a process schematically depicted in figure 8. Further proof for this interpretation was obtained by the isolation of detergent-free lipid raft fractions, which revealed an accumulation of GPI/GFP in the EGFR containing lipid raft fraction after activation of the receptor. No change was observed in the already existing colocalization of GPI-GFP with GM1. The GPI-linked proteins do not have a direct interaction with the EGFR, indicating that EGFR-induced colocalization of GPI-linked proteins with the EGFR is probably the result of the fusion of the different lipid rafts in which these molecules are present (Fig. 8). The induced colocalization of EGFR with GPI/GFP was independent of cholesterol, suggesting that these novel structures are relatively stable. The coalescence can be regulated intracellularly by EGF-induced protein: protein interactions and/or by alterations in the membrane skeleton, which would explain the cholesterol independency. This mechanism would require a coupling between inner and outer leaflet domains, which was recently described for the clustering of H-ras by patching of GPI-anchored proteins (Eisenberg et al., 2006). Interestingly, EGF was also found to recruit other signaling proteins as Shc and Grb2 into the lipid raft fraction (Puri et al., 2005). The coalescence of the different types of nanoclusters and the recruitment of other signaling molecules may therefore result in the formation of the so-called signaling platforms (Chen et al., 2006; Murakoshi et al., 2004; Simons and Toomre, 2000). Support for the signaling platform hypothesis was recently described for GPI-anchored receptor clusters to which the signaling proteins phospholipase $C_{\gamma 2}$, G_{α} and the non-receptor tyrosine kinase Lyn were recruited after initiation of signaling (Suzuki et al., 2007a; Suzuki et al., 2007b). These latter studies were performed using single molecule imaging emphasizing the need for different non-invasive biophysical methods for further analysis of membrane-bound signaling events.

An important negative feedback control mechanism for the EGFR is the EGF-induced internalization of active EGFRs and subsequent routing to the lysosomes where activated receptors become degraded (Wiley, 2003). Clathrin-coated vesicles are generally accepted as the main entry portal for the EGFR. However, accumulating evidence suggests that also non-coated vesicles are involved in EGFR endocytosis, such as GM1 enriched vesicles (Puri et al., 2005), caveolae (Sigismund et al., 2005) and other pinocytotic vesicles (Orth et al., 2006). As such, the clustering of different shells and nanoclusters, which may lead to the formation of larger nanodomains as observed in our study, may represent an initial step for internalization. The local lipid composition in the clustered rafts may induce membrane curvature which is essential for the internalization process (Hanzal-Bayer and Hancock, 2007). The question how this raft-mediated internalization of active EGFRs is regulated is the subject of our present

research.

Acknowledgements

We thank Dr. E. Dolk, Dr. H. Sprong and prof. Dr. G. Van Meer for helpful discussions and reading of the manuscript, and Dr. G.J.A. Arkestein for his help with the FACS sorting. This research was supported in part by the dutch organization for scientific research (NWO-ALW, Molecule to Cell (MtC) program)(E.G. Hofman and A.N. Bader). Dr. M. O. Ruonala was supported by a personal stipend from the Finnish Cultural Foundation.

References

Bader, A. N., Hofman, E. G., van Bergen en Henegouwen, P. M. P. and Gerritsen, H. C. (2007). Imaging of protein cluster size by means of confocal time-gated fluorescence anisotropy microscopy. *Optics express* **15**, 6934-45.

Baumgart, T., Hess, S. T. and Webb, W. W. (2003). Imaging coexisting fluid domains in biomembrane models coupling curvature and line tension. *Nature* **425**, 821-4.

Blagoev, B., Kratchmarova, I., Ong, S. E., Nielsen, M., Foster, L. J. and Mann, M. (2003). A proteomics strategy to elucidate functional protein-protein interactions applied to EGF signaling. *Nat Biotechnol* **21**, 315-8.

Bremer, E. G., Hakomori, S., Bowen-Pope, D. F., Raines, E. and Ross, R. (1984). Ganglioside-mediated modulation of cell growth, growth factor binding, and receptor phosphorylation. *J Biol Chem* **259**, 6818-25.

Burgess, A. W., Cho, H. S., Eigenbrot, C., Ferguson, K. M., Garrett, T. P., Leahy, D. J., Lemmon, M. A., Sliwkowski, M. X., Ward, C. W. and Yokoyama, S. (2003). An open-and-shut case? Recent insights into the activation of EGF/ErbB receptors. *Mol Cell* **12**, 541-52.

Chen, X. and Resh, M. D. (2002). Cholesterol depletion from the plasma membrane triggers ligand-independent activation of the epidermal growth factor receptor. *J Biol Chem* **277**, 49631-7.

Chen, Y., Thelin, W. R., Yang, B., Milgram, S. L. and Jacobson, K. (2006). Transient anchorage of cross-linked glycosyl-phosphatidylinositol-anchored proteins depends on cholesterol, Src family kinases, caveolin, and phosphoinositides. *J Cell Biol* **175**, 169-78.

Conrath, K. E., Wernery, U., Muyldermans, S. and Nguyen, V. K. (2003). Emergence and evolution of functional heavy-chain antibodies in Camelidae. *Dev Comp Immunol* **27**, 87-103.

Dawson, J. P., Bu, Z. and Lemmon, M. A. (2007). Ligand-induced structural transitions in ErbB receptor extracellular domains. *Structure* **15**, 942-54.

de Grauw, C. J. and Gerritsen, H. C. (2001). Multiple time-gate module for fluorescence lifetime imaging. *Applied Spectroscopy* **55**, 670-678.

den Hartigh, J. C., van Bergen en Henegouwen, P. M., Boonstra, J. and Verkleij, A. J. (1993). Cholesterol and phosphoinositides increase affinity of the epidermal growth factor receptor. *Biochim Biophys Acta* **1148**, 249-56.

Eisenberg, S., Shvartsman, D. E., Ehrlich, M. and Henis, Y. I. (2006). Clustering of Raft-Associated Proteins in the External Membrane Leaflet Modulates Internal Leaflet H-Ras Diffusion and Signaling. *Mol. Cell. Biol.* **26**, 7190-7200.

Ferguson, K. M., Berger, M. B., Mendrola, J. M., Cho, H. S., Leahy, D. J. and Lemmon, M. A. (2003). EGF activates its receptor by removing interactions that autoinhibit ectodomain dimerization. *Mol Cell* **11**, 507-17.

Foster, L. J., De Hoog, C. L. and Mann, M. (2003). Unbiased quantitative proteomics of lipid rafts reveals high specificity for signaling factors. *Proc Natl Acad Sci U S A* **100**, 5813-8.

Furuchi, T. and Anderson, R. G. (1998). Cholesterol depletion of caveolae causes hyperactivation of extracellular signal-related kinase (ERK). *J Biol Chem* **273**, 21099-104.

Hanzal-Bayer, M. F. and Hancock, J. F. (2007). Lipid rafts and membrane traffic. *FEBS Lett.*

Harder, T., Scheiffele, P., Verkade, P. and Simons, K. (1998). Lipid domain structure of the plasma membrane revealed by patching of membrane components. *J Cell Biol* **141**, 929-42.

Hillman, G. M. and Schlessinger, J. (1982). Lateral diffusion of epidermal growth factor complexed to its surface receptors does not account for the thermal sensitivity of patch formation and endocytosis. *Biochemistry* **21**, 1667-72.

Jacobson, K., Mouritsen, O. G. and Anderson, R. G. (2007). Lipid rafts: at a crossroad between cell biology and physics. *Nat Cell Biol* **9**, 7-14.

Jares-Erijman, E. A. and Jovin, T. M. (2006). Imaging molecular interactions in living cells by FRET microscopy. *Curr Opin Chem Biol* **10**, 409-16.

Jorissen, R. N., Walker, F., Pouliot, N., Garrett, T. P., Ward, C. W. and Burgess, A. W. (2003). Epidermal growth factor receptor: mechanisms of activation and signalling. *Exp Cell Res* **284**, 31-53.

Kenworthy, A. K., Petranova, N. and Edidin, M. (2000). High-resolution FRET microscopy of cholera toxin B-subunit and GPI-anchored proteins in cell plasma membranes. *Mol Biol Cell* **11**, 1645-55.

Klapisz, E., Sorokina, I., Lemeer, S., Pijnenburg, M., Verkleij, A. J. and van Bergen en Henegouwen, P. M. (2002). A ubiquitin-interacting motif (UIM) is essential for Eps15 and Eps15R ubiquitination. *J Biol Chem* **277**, 30746-53.

Kusumi, A., Koyama-Honda, I. and Suzuki, K. (2004). Molecular dynamics and interactions for creation of stimulation-induced stabilized rafts from small unstable steady-state rafts. *Traffic* **5**, 213-30.

Lagerholm, B. C., Weinreb, G. E., Jacobson, K. and Thompson, N. L. (2005). Detecting microdomains in intact cell membranes. *Annu Rev Phys Chem* **56**, 309-36.

Lambert, S., Vind-Kezunovic, D., Karvinen, S. and Gniadecki, R. (2006). Ligand-independent activation of the EGFR by lipid raft disruption. *J Invest Dermatol* **126**, 954-62.

Li, R., Liu, Y. and Ladisch, S. (2001). Enhancement of epidermal growth factor signaling and activation of SRC kinase by gangliosides. *J Biol Chem* **276**, 42782-92.

Lichtenberg, D., Goni, F. M. and Heerklotz, H. (2005). Detergent-resistant membranes should not be identified with membrane rafts. *Trends Biochem Sci* **30**, 430-6.

Liu, Y., Li, R. and Ladisch, S. (2004). Exogenous Ganglioside GD1a Enhances Epidermal Growth Factor Receptor Binding and Dimerization. *J. Biol. Chem.* **279**, 36481-36489.

Macdonald, J. L. and Pike, L. J. (2005). A simplified method for the preparation of detergent-free lipid rafts. *J Lipid Res* **46**, 1061-7.

Mayor, S. and Rao, M. (2004). Rafts: scale-dependent, active lipid organization at the cell surface. *Traffic* **5**, 231-40.

McCune, B. K. and Earp, H. S. (1989). The epidermal growth factor receptor tyrosine kinase in liver epithelial cells. The effect of ligand-dependent changes in cellular location. *J Biol Chem* **264**, 15501-7.

Miljan, E. A. and Bremer, E. G. (2002). Regulation of growth factor receptors by gangliosides. *Sci STKE* **2002**, RE15.

Miljan, E. A., Meuillet, E. J., Mania-Farnell, B., George, D., Yamamoto, H., Simon, H. G. and Bremer, E. G. (2002). Interaction of the extracellular domain of the epidermal growth factor receptor with gangliosides. *J Biol Chem* **277**, 10108-13.

Mineo, C., James, G. L., Smart, E. J. and Anderson, R. G. (1996). Localization of epidermal growth factor-stimulated Ras/Raf-1 interaction to caveolae membrane. *J Biol Chem* **271**, 11930-5.

Murakoshi, H., Iino, R., Kobayashi, T., Fujiwara, T., Ohshima, C., Yoshimura, A. and Kusumi, A. (2004). Single-molecule imaging analysis of Ras activation in living cells. *Proc Natl Acad Sci U S A* **101**, 7317-22.

Nagy, P., Vereb, G., Sebestyen, Z., Horvath, G., Lockett, S. J., Damjanovich, S., Park, J. W., Jovin, T. M. and Szollosi, J. (2002). Lipid rafts and the local density of ErbB proteins influence the biological role of homo- and heteroassociations of ErbB2. *J Cell Sci* **115**, 4251-62.

Nishio, M., Tajima, O., Furukawa, K. and Urano, T. (2005). Over-expression of GM1 enhances cell proliferation with epidermal growth factor without affecting the receptor localization in the microdomain in PC12 cells. *Int J Oncol* **26**, 191-9.

Orr, G., Hu, D., Ozcelik, S., Opresko, L. K., Wiley, H. S. and Colson, S. D. (2005). Cholesterol dictates the freedom of EGF receptors and HER2 in the plane of the membrane. *Biophys J* **89**, 1362-73.

Orth, J. D., Krueger, E. W., Weller, S. G. and McNiven, M. A. (2006). A novel endocytic mechanism of epidermal growth factor receptor sequestration and internalization. *Cancer Res*

66, 3603-10.
Pike, L. J. (2004). Lipid rafts: heterogeneity on the high seas. *Biochem J* **378**, 281-92.
Pike, L. J. (2005). Growth factor receptors, lipid rafts and caveolae: an evolving story. *Biochim Biophys Acta* **1746**, 260-73.
Pike, L. J. and Casey, L. (2002). Cholesterol levels modulate EGF receptor-mediated signaling by altering receptor function and trafficking. *Biochemistry* **41**, 10315-22.
Puri, C., Tosoni, D., Comai, R., Rabellino, A., Segat, D., Caneva, F., Luzzi, P., Di Fiore, P. P. and Tacchetti, C. (2005). Relationships between EGFR signaling-competent and endocytosis-competent membrane microdomains. *Mol Biol Cell* **16**, 2704-18.
Rao, M. and Mayor, S. (2005). Use of Forster's resonance energy transfer microscopy to study lipid rafts. *Biochim Biophys Acta* **1746**, 221-33.
Ringerike, T., Blystad, F. D., Levy, F. O., Madshus, I. H. and Stang, E. (2002). Cholesterol is important in control of EGF receptor kinase activity but EGF receptors are not concentrated in caveolae. *J Cell Sci* **115**, 1331-40.
Roepstorff, K., Thomsen, P., Sandvig, K. and van Deurs, B. (2002). Sequestration of epidermal growth factor receptors in non-caveolar lipid rafts inhibits ligand binding. *J Biol Chem* **277**, 18954-60.
Roovers, R. C., Laeremans, T., Huang, L., De Taeye, S., Verkleij, A. J., Revets, H., de Haard, H. J. and van Bergen en Henegouwen, P. M. (2007). Efficient inhibition of EGFR signaling and of tumour growth by antagonistic anti-EFGR Nanobodies. *Cancer Immunol Immunother* **56**, 303-317.
Saffarian, S., Li, Y., Elson, E. L. and Pike, L. J. (2007). Oligomerization of the EGF receptor investigated by live cell fluorescence intensity distribution analysis. *Biophys J* **93**, 1021-31.
Sharma, P., Varma, R., Sarasij, R. C., Ira, Gousset, K., Krishnamoorthy, G., Rao, M. and Mayor, S. (2004). Nanoscale organization of multiple GPI-anchored proteins in living cell membranes. *Cell* **116**, 577-89.
Sigismund, S., Woelk, T., Puri, C., Maspero, E., Tacchetti, C., Transidico, P., Di Fiore, P. P. and Polo, S. (2005). Clathrin-independent endocytosis of ubiquitinated cargos. *Proc Natl Acad Sci U S A* **102**, 2760-5.
Simons, K. and Toomre, D. (2000). Lipid rafts and signal transduction. *Nat Rev Mol Cell Biol* **1**, 31-9.
Suzuki, K. G., Fujiwara, T. K., Edidin, M. and Kusumi, A. (2007a). Dynamic recruitment of phospholipase C gamma at transiently immobilized GPI-anchored receptor clusters induces IP3-Ca2+ signaling: single-molecule tracking study 2. *J Cell Biol* **177**, 731-42.
Suzuki, K. G., Fujiwara, T. K., Sanematsu, F., Iino, R., Edidin, M. and Kusumi, A. (2007b). GPI-anchored receptor clusters transiently recruit Lyn and G alpha for temporary cluster immobilization and Lyn activation: single-molecule tracking study 1. *J Cell Biol* **177**, 717-30.
Wiley, H. S. (2003). Trafficking of the ErbB receptors and its influence on signaling. *Exp Cell Res* **284**, 78-88.
Yamabhai, M. and Anderson, R. G. (2002). Second cysteine-rich region of epidermal growth factor receptor contains targeting information for caveolae/rafts. *J Biol Chem* **277**, 24843-6.
Zhang, R. G., Westbrook, M. L., Westbrook, E. M., Scott, D. L., Otwinowski, Z., Maulik, P. R., Reed, R. A. and Shipley, G. G. (1995). The 2.4 A crystal structure of cholera toxin B subunit pentamer: choleragenoid. *J Mol Biol* **251**, 550-62.
Zurita, A. R., Maccioni, H. J. and Daniotti, J. L. (2001). Modulation of epidermal growth factor receptor phosphorylation by endogenously expressed gangliosides. *Biochem J* **355**, 465-72.

Chapter 3

Imaging of protein cluster sizes by means of confocal time gated fluorescence anisotropy microscopy

Arjen N. Bader [1], Erik G. Hofman [2], Paul M.P. van Bergen en Henegouwen [2], Hans C. Gerritsen [1]

[1] Molecular Biophysics, Institute of Biomembranes, Utrecht University, Utrecht, The Netherlands

[2] Cellular Architecture and Dynamics, Utrecht University, Utrecht, The Netherlands

Optics Express (2006) 15 (11):6934-6945

Abstract

A time-resolved fluorescence anisotropy imaging method for studying nanoscale clustering of proteins or lipids was developed and evaluated. It is based on FRET between the identical fluorophores (homo-FRET), which results in a rapid depolarization of the fluorescence. The method employs the time-resolved fluorescence anisotropy decays recorded in a confocal microscope equipped with pulsed excitation and time-gated detection. From the decay the limiting anisotropy r_{inf} was derived, which is a direct measure for the number of fluorophores per cluster. The method was evaluated by imaging GPI-GFP, a lipid raft marker. Small clusters were observed in the plasma membrane while the cytoplasm and the Golgi contained predominantly monomers.

Introduction

Hetero and homo-FRET

Advanced fluorescence microscopy based methods are indispensable tools in molecular cell biology (Periasamy, 2001; Valeur, 2002). For example, molecular scale colocalisation of proteins or lipids can be imaged by means of Förster resonance energy transfer (FRET) (Centonze et al., 2003; Periasamy, 2001; Valeur, 2002) (Jares-Erijman and Jovin, 2003). Here, the excited-state energy of a fluorescent probe (donor) is transferred to another probe (acceptor), provided that (1) the donor-acceptor distance is less than ~10 nm, (2) there is spectral overlap between the donor's emission and the acceptors absorption band and (3) the donor's emission and the acceptors absorption transition dipole moments are not perpendicularly oriented. FRET results in quenching of the donor emission and sensitized emission of the acceptor. The FRET efficiency can be quantified using the donor/acceptor intensity ratio, or using spectral imaging. Furthermore, donor quenching results in a reduction of its fluorescence lifetime. Fluorescence lifetime imaging (FLIM) is a straightforward way to quantify the FRET efficiency in a reliable way (Esposito et al., 2005; Sytsma et al., 1998). It is often regarded as the method of choice for FRET imaging.

The conditions for FRET to occur can be also met for a pair of identical fluorophores. Significant spectral overlap between the emission and absorption spectra of a fluorophore is often observed (Gautier et al., 2001; Jares-Erijman and Jovin, 2003; Sharma et al., 2004; Valeur, 2002). As a result, energy transfer may take place between two or more identical fluorophores (homo-FRET). Hetero-FRET can also be used for studying homoclustering. However, it is much less 'sensitive' than homo-FRET. In the case of hetero-FRET a dimer can consist of D+A, A+D, D+D and A+A, only half of the combinations result in hetero-FRET. Furthermore, hetero-FRET requires approximately equal amounts of donor and acceptor labeled molecules and its interpretation can be complicated when larger clusters are being formed. As a result of the complications related to hetero-FRET based imaging of clusters, homo-FRET imaging methods have recently gained interest (Gautier et al., 2001; Jares-Erijman and Jovin, 2003; Lidke et al., 2003; Sharma et al., 2004; Varma and Mayor, 1998); Squire, 2004 #416}.

Homo-FRET can not be imaged using standard hetero-FRET methodologies (Jares-Erijman and Jovin, 2003). Methods based on the difference in spectral properties between donor and acceptor (i.e., intensity ratio imaging or spectral imaging) are obviously not suitable. Moreover, homo-FRET does not change the donor's lifetime; the reduction in the lifetime of the directly excited donor is fully compensated by the additional emission of the indirectly excited 'donor'. Therefore, also FLIM can not be used. Since homo-FRET predominantly takes place between differently oriented fluorophores, it results in depolarization of the emission. This depolarization can be conveniently quantified using the fluorescence anisotropy (r) and homo-FRET can be imaged using fluorescence anisotropy imaging methods. Several approaches for imaging homo-FRET have been described in the literature (Gautier et al., 2001; Jares-

Erijman and Jovin, 2003; Lidke et al., 2003; Sharma et al., 2004; Squire et al., 2004; Varma and Mayor, 1998). In these studies, steady-state anisotropy images and time-resolved decays were recorded separately to derive homo-FRET efficiencies and inter fluorophore distances (Gautier et al., 2001; Sharma et al., 2004).

Cluster size imaging

An important feature of homo-FRET is that it can provide information about the number of fluorophores (N) per cluster. Clustering of proteins is often observed in cells and cluster size quantification is of great biological interest. For example, in cell signaling the binding of a ligand is often accompanied by receptor dimerization (Krauss, 2001). Also the clustering of certain lipids in membrane domains or lipid rafts has been suggested to play an important role in signaling (Anderson and Jacobson, 2002; Sharma et al., 2004). To study cellular processes that involve clustering, cluster size imaging methods are essential. So far, however, methods to directly image molecular scale clustering (in vivo) are not available.

In the present work it is shown that the average cluster size per pixel can be imaged using time-resolved fluorescence anisotropy imaging. The limiting value of the anisotropy r_{inf} in the time-resolved fluorescence anisotropy decay can be directly related to the cluster size N. Interestingly, only a limited number of time points and modest time resolution are required to determine the limiting anisotropy. In this work a confocal time-gated fluorescence anisotropy imaging microscope is used (Bader et al., 2007). The setup utilizes two detection modules that were originally developed for time-gating based FLIM (de Grauw and Gerritsen, 2001), one for each polarization direction. The detection modules (LiMo) collect the emission in four 2 nanosecond wide consecutive time gates. This affords the recording of course time-resolved anisotropy decay images.

Several other time-resolved fluorescence anisotropy imaging microscopes have been described in literature. These microscopes are all based on wide-field frequency-domain (Clayton et al., 2002; Lidke et al., 2003) and wide-field time-domain (Siegel et al., 2003; Suhling et al., 2004) imaging. In the current work a confocal time-resolved fluorescence anisotropy imaging system is used. The optical sectioning yields higher contrast and more details in the anisotropy and cluster size images. Furthermore, it allows the recording of 3D cluster size images.

The potential of imaging protein cluster sizes using confocal time-gated anisotropy imaging is demonstrated using cells expressing GFP linked to glycosylphosphatidylinositol (GPI-GFP). GPI-anchored proteins include different receptors for Thy-1, folate and the cellular prion protein. Clustering or crosslinking of these receptors trigger transmembrane signal transduction and internalization. GPI-anchored proteins are found in the detergent resistant membrane fraction and are frequently used as so-called lipid raft markers (Brown and London, 1998). Chemical crosslinking using short crosslinkers and FRET experiments suggest that the GPI-anchored proteins exist as small clusters in the plasma membrane (Sharma et al.,

2004). In the present work, it is shown that GPI-GFP expressing cells exhibit subcellular heterogeneities in GPI-GFP cluster sizes. Furthermore, controlled photobleaching yielded more details about the cluster size distribution of *N*-mers. GPI-GFP appears to be present in small clusters in the plasma membrane while cytoplasmic GPI-GFP appears monomeric.

Theoretical background

Fluorescence anisotropy and homo-FRET

Homo-FRET can be observed by exploiting changes in the fluorescence anisotropy r, defined as (Gautier et al., 2001; Jares-Erijman and Jovin, 2003; Sharma et al., 2004; Squire et al., 2004; Valeur, 2002):

$$r = \frac{I_{\text{par}} - I_{\text{per}}}{I_{\text{par}} + 2I_{\text{per}}} \quad [1]$$

with I_{par} and I_{per} the emission parallel and perpendicular respectively to the excitation polarization direction. Since the orientations of two identical dye molecules will in general be different, energy transfer between the fluorophores will decrease the anisotropy of the emission (Valeur, 2002). The anisotropy can, however, also decrease due to other effects than homo-FRET; the most common source of depolarization is rotation of the fluorophore. Directly after exciting the fluorescent molecules, the maximum initial anisotropy r_0 is 0.4. The exact value of r_0 depends on the relative orientation of the absorption and emission transition dipole moments of the fluorophore; a value of r_0=0.4 is found when the two dipole moments are parallel. Depending on the size of the molecule and the viscosity of the surrounding medium, rotation of molecules can occur on a sub-nanosecond to nanosecond timescale.This time scale may very well be similar to the time scale at which homo-FRET takes place. To discriminate between the rotation and homo-FRET, time-resolved fluorescence anisotropy decay curves can be recorded. For a free (spherical) rotor in solution in the absence of homo-FRET, this decay is described by:

$$r(t) = r_0 e^{-t/\Phi} \quad [2]$$

with Φ the rotation correlation time of the rotor. In the presence of homo-FRET both rotational depolarization and homo-FRET depolarization take place and the anisotropy decay has a multi-exponential character. Reliable analysis of the decay may be complicated. To measure homo-FRET it is advantageous to employ slowly rotating dye molecules such as GFPs (rotational correlation time $\Phi >> \tau$). Now, rotations can be ignored and the analysis of the anisotropy decay is comparatively simple. The time-resolved anisotropy decay can be written as (Tanaka and Mataga, 1979):

$$r(t) = (r_0 - r_{\text{inf}})e^{-2\omega t} + r_{\text{inf}} \quad [3[$$

Here, ω denotes the homo energy transfer rate and r_{inf} the limiting anisotropy at time infinity. ω and the homo-FRET efficiency E are defined as:

$$\omega = \left({}^{R_0}\!/_{R} \right)^6 \tau^{-1} \qquad [4]$$

$$E = {}^{\omega}\!/_{(\tau^{-1}+\omega)}$$

where R_0 is the Förster distance, R the inter fluorophore distance and τ the fluorescence lifetime.

Fluorescence anisotropy and cluster size

The number of fluorophores per cluster is directly related to the anisotropy (Runnels and Scarlata, 1995). For a monomer, in the absence of rotation the average anisotropy amounts to $r_{mono} = r_0 = 0.4$. For a dimer, however, the initial anisotropy of the excited donor equals r = 0.4 whereas the anisotropy of the donor that is indirectly excited after homo-FRET amounts to $r_{et} = 0.016$ (see Fig. 1(top))(Arganovich and Galanin, 1982; Runnels and Scarlata, 1995). When energy transfer is very fast ($E \approx 1$) and reversible, both donors have equal probabilities of emitting the photon and the average anisotropy of the dimer amounts to $r_{dimer} = 0.2$. For clusters of size N the observed average anisotropy equals:

$$r_N = r_{mono} / N \qquad [5]$$

When the energy transfer is less efficient, i.e. $E < 1$, most emission will come from the directly excited donor and there will be less depolarization by homo-FRET. The dependency of the steady-state anisotropy on the transfer rate in oligomers of size N is described by (Runnels and Scarlata, 1995):

$$r_N = r_{mono} \frac{1+\omega.\tau}{1+N.\omega.\tau} + r_{et} \frac{(N-1).\omega.\tau}{1+N.\omega.\tau} \qquad [6]$$

Fig. 1(bottom) shows graphs of the relation between the cluster size N and the steady-state anisotropy r for various values of the transfer efficiency. Dimers (N = 2) have a steady-state anisotropy r = 0.2 when $E \approx 1$, whereas this same anisotropy value corresponds to trimers (N = 3) when E = 0.5.

Different cluster sizes can be discriminated by employing Equation 6. This requires knowledge of the homo-FRET efficiency. Unfortunately, experimental determination of ω is difficult in time-resolved imaging experiments because high signal levels are required to obtain sufficient photon statistics (Lidke et al., 2003; Lidke et al., 2005). It should be realized, however, that in time-resolved anisotropy decays (as described by Eq. 3) only the increase in homo-FRET transfer rate ω is responsible for increased values of the steady-state anisotropy for e.g. dimers (see Fig. 2). When $r(t) = r_{inf}$, the probability of emitting a photon is equal for all

fluorescent molecules in the cluster. This condition is already met after ~2 ns for homo-FRET efficiencies higher than 0.5 (see Fig. 2(b)). The value of the limiting anisotropy r_{inf} in the time-resolved anisotropy decay therefore equals the steady state anisotropy in the case of E = 1, and:

$$r_{N,E=1} = r_{\inf} = r_{\text{mono}} / N \qquad [7]$$

Images of r_{inf} can be directly converted to images of the protein cluster size, without any prior knowledge of the homo-FRET transfer rate.

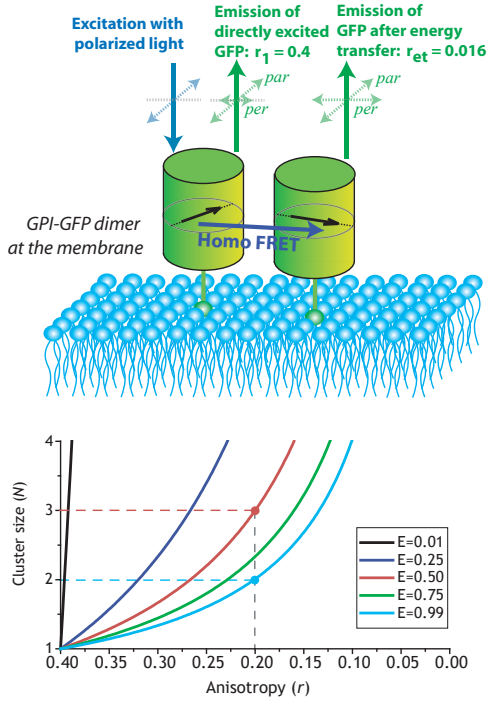

Fig. 1. (top) Schematic diagram of energy transfer in a dimer. (bottom) Graphs of the cluster size N as a function of the measured anisotropy for various values of efficiency E (based on Equation 6, with $\omega\tau = E/(1\text{-}E)$).

Experimental

NIH 3T3 fibroblasts expressing GPI-GFP

NIH 3T3 cells were cultured in Dulbecco's modified Eagle's medium (Invitrogen) supplemented with 7.5% foetal bovine serum (v/v) and 2 mM L-glutamine at 37°C in the presence of 5% CO_2 under a humidified atmosphere. For the generation of a cell-line stably expressing GPI-GFP, NIH 3T3 cells were transfected with plasmid DNA encoding this construct (kindly provided by dr. P. Keller, Dresden) using Lipofectamin 2000 (Invitrogen; Breda, The Netherlands). Stable expression was achieved by prolonged culturing in medium containing selective amounts of Zeocin (Invitrogen). For imaging, cells were seeded on 18 mm coverslips and grown for 2 days until 30% confluence. Cells were fixed with freshly prepared 4% formaldehyde at 37°C for 20 minutes, and quenched by 100 mM glycine. Coverslips were mounted with Mowiol and stored at -20°C until further use. These preparations are not expected to influence the observed cluster sizes (Bancroft and Stevens, 1982).

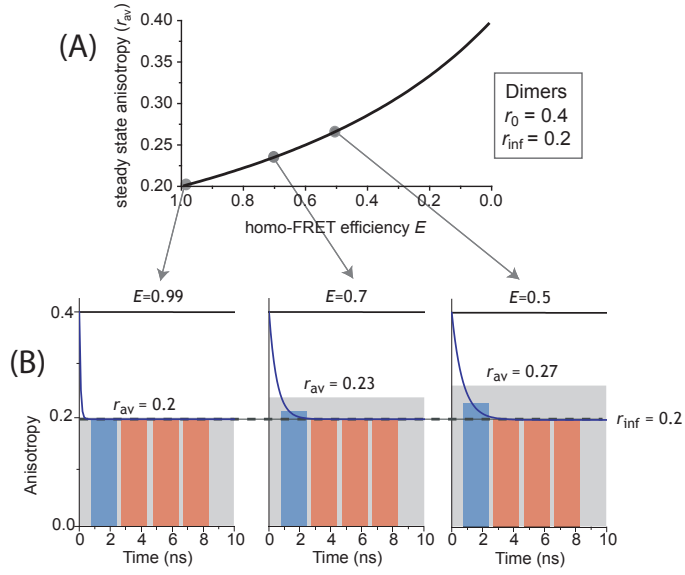

Fig. 2. (A) Graph of the steady state anisotropy of a dimer as a function of the homo-FRET efficiency (using Equation 6, r_{mono} = 0.4). (B) For three values of E, the time resolved anisotropy decays are plotted. The steady state anisotropy levels are indicated by the grey bar.

Time-gated fluorescence anisotropy imaging set-up

A modified confocal scanning laser microscope (CSLM, Nikon PCM 2000) was employed. The excitation polarization direction was defined by a linear polarizer (Meadowlark, Frederick, CO, USA) and a broadband polarizing beam splitter cube (PBS, OptoSigma, Santa Ana, CA,

USA) was used to split the emission in a parallel and a perpendicular channel with respect to the excitation light. The excitation light was provided by a frequency doubled picosecond pulsed Ti:Sa laser (Tsunami, Spectra Physics) tuned to 460 nm; a pulse picker was used to reduce the repetition rate to 8.2 MHz. The excitation pulses were transferred to the confocal microscope using a single-mode optical fiber. For imaging, a NA=1.20 / 40x water immersion objective (Plan Apo, Nikon) was used. Such high NA objectives yield lower value of r_0 due to the effect of the high acceptance angle on the anisotropy measurement (Axelrod, 1989; Gautier et al., 2001; Lidke et al., 2003; Sharma et al., 2004; Squire et al., 2004). Here, a value of r_0 = 0.33 was found instead of 0.40. Each of the two emission channels ("parallel" and "perpendicular") was equipped with its own detection system consisting of a high quantum efficiency fiber-coupled PMT (Hamamatsu H7422P-40), a pre-amplifier and a fluorescence lifetime imaging module (LiMo, Nikon Instruments BV, Badhoevedorp, The Netherlands)(de Grauw and Gerritsen, 2001). The LiMo captures four images using four consecutive time gates of approximately 2 ns width. By employing two such modules, one for each polarization direction, a four channel time-resolved anisotropy decay can be acquired for each pixel.

Determination of the time-resolved anisotropy using the two separate detection channels requires careful synchronization in time and correction for their difference in sensitivity. The former was achieved by using a aqueous solution of Rose Bengal (τ_F = 70 ps) as a reference. The time offset of the first gate with respect to the excitation pulse was adjusted in such a way that the first gate opened after 90% of the Rose Bengal fluorescence was emitted. The correction factor for the difference in transmission (c_{tr}) between both channels was determined by recording an anisotropy image of an aqueous solution of fluorescein. In this case, fast rotation of the fluorophore will result in emission that is completely depolarized before the second gate opens. Consequently, the anisotropy in the last three gates will be zero, and $I_{par} = c_{tr} I_{per}$. Finally, a correction was applied to correct for small difference in gate width between the parallel and perpendicular channel. These differences were determined using a sample containing 10 μM GFP monomers in 50/50 glycerol/buffer. In this solution, rotation of the fluorophore is much slower than the fluorescence lifetime ($\Phi >> \tau$). Consequently, the anisotropy will remain constant at the r_0 level. For every gate, a correction factor was determined that ensures that the anisotropy in this gate is identical to the steady state anisotropy. The absence of concentration dependent homo-FRET in the GFP solution was checked by lowering the concentration; no increase in anisotropy was observed.

To record high time resolution fluorescence anisotropy decays, the two LiMo's were replaced by two time-correlated single photon counting boards (TimeHarp, Picoquant, Germany). Again, an aqueous solution of fluorescein was used to calculate the difference in transmission of the two polarization channels, and a solution of Rose Bengal was used for temporal synchronization of the channels.

Data handling

Cluster size images were obtained by extracting r_{inf}-values from the time-gated fluorescence anisotropy images. The anisotropy values in the last gates are, in good approximation, equal to r_{inf}, provided that E is high enough. Based on Fig. 2(a) this condition is met for the three last gates provided that E > 0.5. Four-gate anisotropy decays were created by binning the intensities I_{par} and I_{per} per gate in regions of interest. In the anisotropy imaging experiments a threshold of $I_{par,inf} + 2.I_{per,\ inf} > 300$ counts was applied to all images. In theory, this number of counts corresponds to a standard deviation in the anisotropy of 0.05 (Lidke et al., 2005).

Simulation of photo-bleaching

The effect of photo-bleaching on the anisotropy of *N*-mers was simulated using MS Excel. First order chemical kinetics, equal photo-bleaching probabilities for every GFP and inter fluorophore distances smaller than the Förster distance R_0 were assumed (Sharma et al., 2004). Three model distributions of N-mers were generated. For each initial distribution of N-mers, the distribution after photo-bleaching a certain fraction of molecules was calculated. This can be conceived as follows. Bleaching of a population of N-mers will result in a distribution of N-mers, (N-1)-mers, (N-2)-mers, etc. For example, bleaching a fraction x of the GFP trimers will result in the following distribution: $(1-x)^3$ trimers, $3.x.(1-x)^2$ dimers, $3.x^2.(1-x)$ monomers and x^3 fully bleached GFP. The final distributions of N-mers from each initial N-mer were summed per final N-mer. Next, the fraction of the total signal for each final N-mer was calculated. This was repeated for a range of bleaching percentages, thus creating a simulated bleaching curve.

The three models of N-mer distributions were adjusted to match the initial experimental cluster size. Model 1 assumes only monomer and dimers; the fraction of the latter was tuned. Model 2 is based on a Gaussian distribution of N-mers that is centered at N = 0; tuning was achieved by varying the width of this distribution. Finally, model 3 involves monomers and a varying fraction of large clusters. Here, a Gaussian distribution with a mean cluster size of 5 was assumed. The amplitude of the distribution was adjusted to match the initial cluster size. These models are depicted in Fig. 7(c).

Results and discussion

Evaluation of the set-up

The rotational mobility of fluorescein in solutions of varying glycerol content was used to evaluate the time-resolved fluorescence anisotropy imaging setup. Anisotropy decays were recorded using both time-gated imaging and time-correlated single photon counting (TCSPC). The resulting decays are shown in Fig. 3. The black lines correspond to the anisotropy decays recorded using TCSPC (in non-imaging mode) and the bars correspond to the average time-gating based anisotropy decays over the 160*160 pixels of the image. The anisotropy decay slows down in a more viscous environment. Importantly, the decays recorded using the time-gating match the ones recorded using TCSPC. For fluorescein in 75/25 glycerol/water, fitting with a simple mono-exponential decay yielded Φ = 6.4 ± 0.15 ns (TCSPC) and Φ = 6.6 ± 0.6 ns (time-gating).

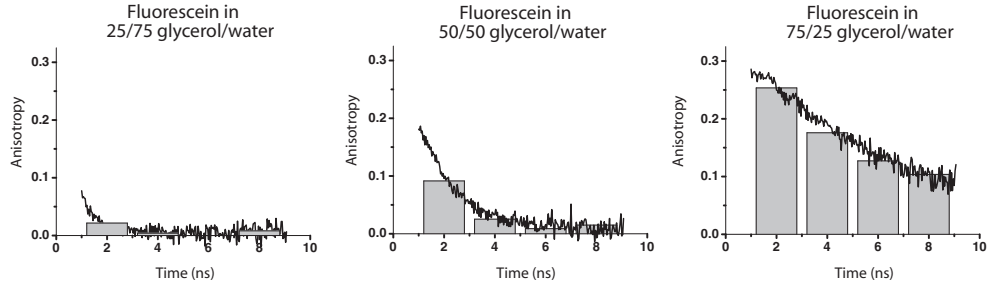

Fig. 3. Time-resolved anisotropy decays of fluorescein in glycerol/water (v/v) solutions. The black lines represent the decays obtained using time-correlated single photon counting; the bars are the result of time gated anisotropy imaging, averaged over 160x160 pixels.

Cluster size imaging in cells

To evaluate the potential of the approach in cellular imaging, clustering of GPI-anchored GFP was analysed. In Fig. 4, an image of a NIH 3T3 fibroblast stably expressing GPI-GFP is shown. In the intensity image of this cell, clear labeling of the plasma membrane can be observed and plasma membrane ruffles are visible (Fig. 4(a)). Also in the cytoplasm some structures can be distinguished; the relatively high intensity region is the Golgi apparatus. The anisotropy image reveals clear heterogeneities in anisotropy (Fig. 4(b)). Particularly large differences in anisotropy are observed between the Golgi (blue bordered region of interest (RoI)) and the ruffles (e.g. green bordered RoI). In the absence of homo-FRET the anisotropy in a monomeric solution of GFP (in 50/50 glycerol/buffer) was found to be 0.33. This serves as a reference value for the anisotropy level of monomers, i.e. in absence of homo-FRET. The lower anisotropy in the plasma membrane and ruffles can be attributed to homo-FRET in GPI-

GFP clusters.

The average time-gated anisotropy decays of ruffles and Golgi are shown in green and blue respectively (Fig. 4(d)). The decay of the monomeric reference solution of GFP (in 50/50 glycerol/buffer) is shown in yellow. The constant level of the anisotropy of the GFP monomers gives the initial anisotropy in the decays of GPI-GFP in the cell, i.e., $r_{mono} = r_0 = 0.33$. In these decays, the occurrence of homo-FRET can be readily observed. The anisotropy decays much faster than can be expected from GFP rotation alone. This indicates homo-FRET takes place in clusters of GPI-GFP. The anisotropy in the last gates is to a good approximation equal to r_{inf} (a direct measure of the cluster size, see Eq. 7). Here, r_{inf} was estimated from the average anisotropy in the last three gates. A slow decay can still be observed in these gates, probably due to inefficient homo-FRET or minor rotation of GFP. However, the determination of the cluster size is hardly affected by such a slow decay and the averaging strongly improves

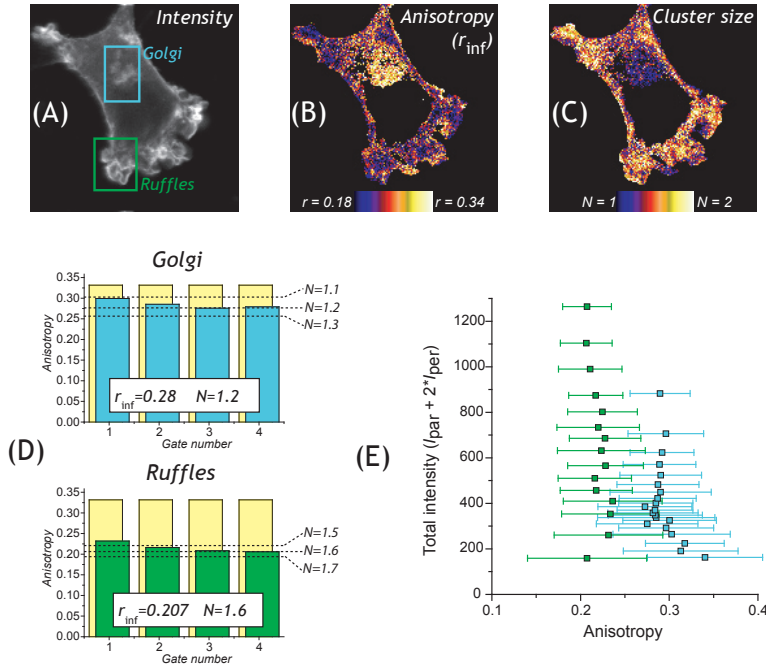

Fig. 4. (A, B, C) Intensity, anisotropy (r_{inf}) and cluster size image of a NIH 3T3 cell expressing GPI-GFP. (D) Time-gated anisotropy decays of the ruffle region and the Golgi apparatus (yellow bars are the decay of GFP monomers in 50/50 glycerol/buffer). The dashed lines indicate the r_{inf} levels for the given cluster sizes. (E) Plots of the average anisotropy (over 50 pixels of similar intensity) vs total counts ($I_{par} + 2*I_{per}$) of the ruffle region and the Golgi apparatus. The error bars indicate the standard deviation of anisotropy values per intensity range.

the signal-to-noise ratio of the r_{inf} determination. The dashed lines in Fig. 4(d) indicate the r_{inf} levels for various cluster sizes. This shows that the effect of the slow decay on the cluster size determination is much less than 0.1. In the ruffle RoI r_{inf} = 0.207, whereas in the Golgi RoI r_{inf}

= 0.280. The corresponding cluster sizes are 1.6 and 1.2, respectively. The values of r_{inf} in Fig. 4(b) are also calculated from the intensities in the last three gates. The corresponding GPI-GFP cluster size image was calculated using these r_{inf} values (Fig. 4(c)).

To exclude the possibility of concentration induced homo-FRET, scatter plots of intensity versus anisotropy were made (Varma and Mayor, 1998) (Fig. 4(e)). The blue dots in this figure correspond to the Golgi RoI, while the green dots correspond to the ruffle RoI in the plasma membrane. In case of concentration induced homo-FRET a correlation between intensity and anisotropy is expected. Fig. 4(e) shows that in ruffles there is no significant correlation between anisotropy and intensity. This indicates that in ruffles small nanoscale clusters are present and that intensity is only a measure of the number of clusters, not their size. In the Golgi RoI below an intensity of 400 counts a concentration-dependence might be present. It should, however, be noted that in the Golgi GPI-GFP is still "under construction" (the attachment of the GPI anchor to the GFP takes place in the Golgi), a situation not representative for the properties of GPI-GFP in membranes.

To explore cell dependent variations in GPI-GFP clustering intensity and cluster size images were recorded of four different cells (Fig. 5). Clear local differences in both the intensity and cluster sizes can be observed. In general, the cluster size in the Golgi is low and in the membrane regions significant clustering can be observed. Strong ruffling of the plasma membrane seems to be accompanied by high GPI-GFP clustering (Fig. 5(b)). In the absence of ruffling, some cells exhibit less clustering in the plasma membrane (Fig. 5(c) and (d)). To further explore the local heterogeneities in N, a 3D-stack of images of a GPI-GFP expressing cell was recorded (Fig. 6). It is clear that in the plasma membrane the cluster size is larger than in the interior of the cell.

An important advantage of the confocal approach to image cluster sizes is the improved contrast and suppression of out-of-focus signals. This is particularly important for cluster size imaging in plasma membrane systems. Discriminating out-of-focus contributions from the signal improves the accuracy of the cluster size determination.

Effects of photo-bleaching on the cluster size

Besides quantification of the average cluster size per pixel, also information on the distribution of N-mers can be obtained from a controlled photo-bleaching series of cluster size images. The effect of photo-bleaching on homo-FRET was initially exploited by Sharma *et al* (Sharma et al., 2004). Their modeled data was compared to the experimentally observed decrease in anisotropy after photo-bleaching. The analysis, however, involved an assumption of the values of r_N (N = 2, 3, 4). In the current methodology these values are readily available. Moreover, it is not necessary to incorporate the anisotropy in the modeling; the effect of photo-bleaching on the cluster size can be directly compared to a bleaching series of cluster size images.

To obtain more detailed information on cluster size distributions photo-bleaching curves of a NIH 3T3 cell expressing GPI-GFP were recorded. The decrease in cluster size

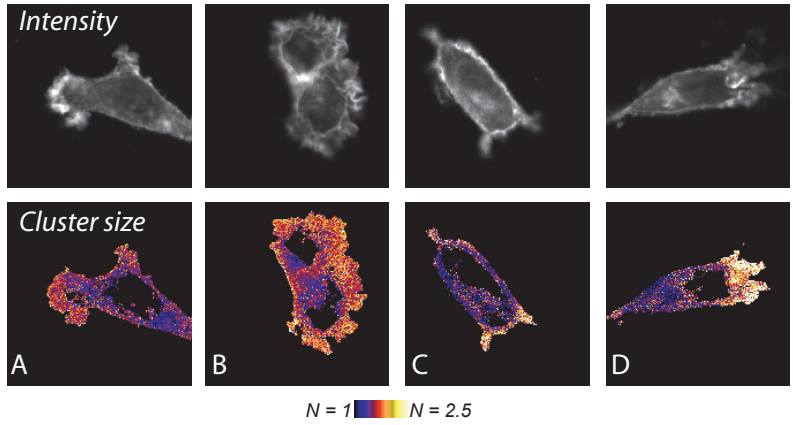

Fig. 5. Intensity and cluster size image of a NIH 3T3 cell expressing GPI-GFP.

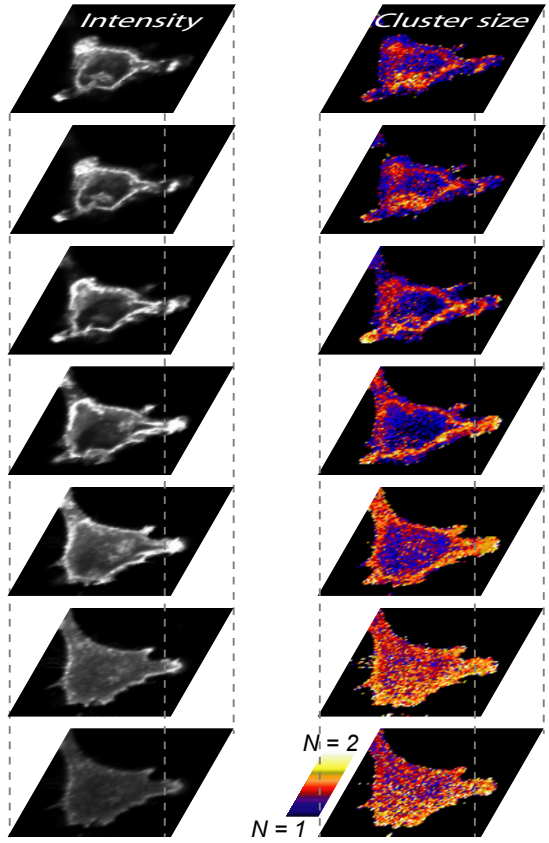

Fig. 6. 3D confocal intensity and cluster size images of NIH 3T3 cells expressing GPI-GFP. Each image is 33 μm^2 (80 by 80 pixels); the step size in the Z-direction is 1 μm

after photo-bleaching is plotted (red dots in Fig. 7(b)) for two RoI in the cell (see Fig. 7(a)). These results are compared to three models of N-mer distributions, (1) monomers and a variable fraction of dimers, (2) Gaussian distributions of variable width centered at $N = 0$, and (3) monomers and a Gaussian distribution of variable width centered at $N_{av} = 5$ (see Fig. 7(c)). For these three models, the theoretical photo-bleaching curves are plotted as well (dark blue, light blue and green lines for model 1, 2 and 3, respectively in Fig. 7(b)). The experimental data is reasonably well described by model 2 for both RoI. This suggests that both in the 'normal' plasma membrane and in ruffles GPI-GFP is present in small clusters. Clusters of size larger than two must be present to account for the measurements. However, the measurements can not be explained by a mix of monomers and large clusters. When assuming that model 2 is correct, the fraction of GFP in monomers, dimers and oligomers ($N \geq 3$) amounts to 0.35, 0.37 and 0.28 respectively in ruffles and 0.40, 0.38 and 0.21 respectively in the membrane.

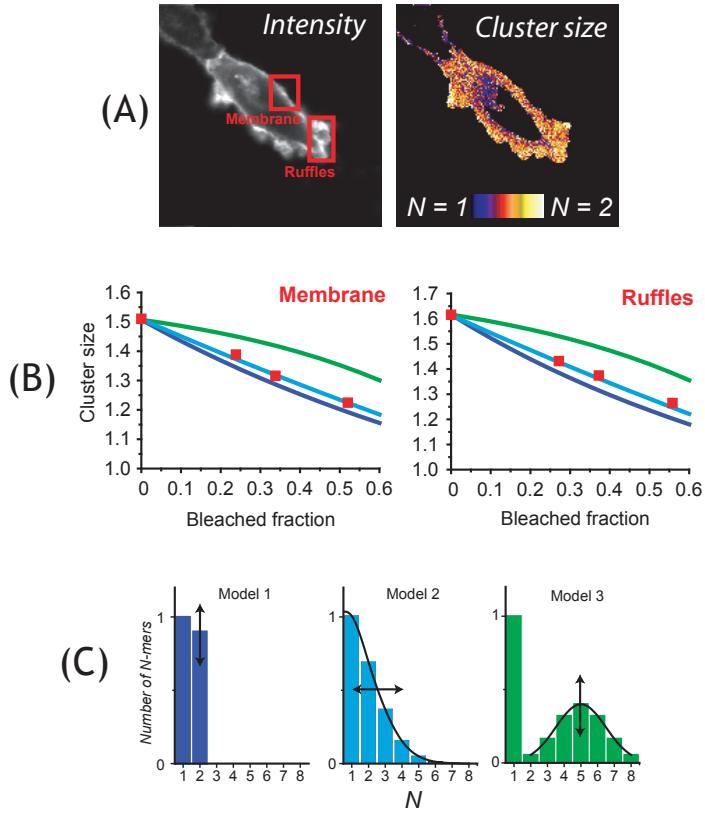

Fig. 7. (A) Intensity and cluster size image of a 3T3 cell expressing GPI-GFP. For the two regions of interest (membrane and ruffles, highlighted in red), the decrease in cluster size was plotted versus the fraction of the GFPs that is bleached (B, red dots). For three models distributions (C), the theoretical bleaching curves are plotted in (B) as well. The arrows in (C) indicate how these models are tuned to match the initial experimental cluster size for the two regions of interest.

Conclusions

The results presented here demonstrate the potential of confocal time-gated fluorescence anisotropy imaging for the study of homo-FRET in cells. The time-resolved anisotropy decays reveal the occurrence of homo-FRET. Importantly, the r_{inf} derived from the anisotropy images can be readily transferred to cluster size images without information about the energy transfer efficiency. The method is expected to be more accurate than approaches based on steady state anisotropy. The high sensitivity of the method afforded for the first time to record cluster size maps of single cells. Moreover, the implementation in a confocal microscope afforded the recording of 3-D cluster size images. The cluster size images showed that the interior of cells can have significantly different cluster sizes than the plasma membrane. Finally, it was demonstrated that photo-bleaching can be exploited to obtain additional information about the distribution of N-mers in clusters.

Acknowledgement

This work is financially supported by the NWO/ALW MtC program.

References

Anderson, R. G. and Jacobson, K. (2002). A role for lipid shells in targeting proteins to caveolae, rafts, and other lipid domains. *Science* **296**, 1821-5.

Arganovich, V. M. and Galanin, M. D. (1982). Electronic excitation energy transfer in condensed matter. Amsterdam: North-Holland Publishing.

Axelrod, D. (1989). Fluorescence polarization microscopy. *Methods Cell Biol* **30**, 333-52.

Bader, A. N., Hofman, E. G., Henegouwen, P. v. B. e. and Gerritsen, H. C. (2007). Confocal time-resolved fluorescence anisotropy imaging. In *Imaging, Manipulation, and Analysis of Biomolecules, Cells, and Tissues V,* vol. 6441, pp. 64410C. San Jose, CA, USA: SPIE.

Bancroft, J. D. and Stevens, A. (1982). Theory and practice of histological techniques: Churchill Livingstone.

Brown, D. A. and London, E. (1998). Functions of lipid rafts in biological membranes. *Annu Rev Cell Dev Biol* **14**, 111-36.

Centonze, V. E., Sun, M., Masuda, A., Gerritsen, H. and Herman, B. (2003). Fluorescence resonance energy transfer imaging microscopy. *Methods Enzymol* **360**, 542-60.

Clayton, A. H., Hanley, Q. S., Arndt-Jovin, D. J., Subramaniam, V. and Jovin, T. M. (2002). Dynamic fluorescence anisotropy imaging microscopy in the frequency domain (rFLIM). *Biophys J* **83**, 1631-49.

de Grauw, C. J. and Gerritsen, H. C. (2001). Multiple Time-Gate Module for Fluorescence Lifetime Imaging. *Appl. Spectrosc.* **55**, 670.

Esposito, A., Gerritsen, H. C. and Wouters, F. S. (2005). Fluorescence lifetime heterogeneity resolution in the frequency domain by lifetime moments analysis. *Biophys J* **89**, 4286-99.

Gautier, I., Tramier, M., Durieux, C., Coppey, J., Pansu, R. B., Nicolas, J. C., Kemnitz, K. and Coppey-Moisan, M. (2001). Homo-FRET microscopy in living cells to measure monomer-dimer transition of GFP-tagged proteins. *Biophys J* **80**, 3000-8.

Jares-Erijman, E. A. and Jovin, T. M. (2003). FRET imaging. *Nat Biotechnol* **21**, 1387-95.

Krauss, G. (2001). Biochemistry of Signal Transduction and Regulation. Weinheim: Wiley-VCH.

Lidke, D. S., Nagy, P., Barisas, B. G., Heintzmann, R., Post, J. N., Lidke, K. A., Clayton, A. H., Arndt-Jovin, D. J. and Jovin, T. M. (2003). Imaging molecular interactions in cells by dynamic and static fluorescence anisotropy (rFLIM and emFRET). *Biochem Soc Trans* **31**, 1020-7.

Lidke, K. A., Rieger, B., Lidke, D. S. and Jovin, T. M. (2005). The role of photon statistics in fluorescence anisotropy imaging. *IEEE Trans Image Process* **14**, 1237-45.

Periasamy, A. (2001). Methods in Cellular Imaging. Oxford: Oxford University Press.

Runnels, L. W. and Scarlata, S. F. (1995). Theory and application of fluorescence homotransfer to melittin oligomerization. *Biophys J* **69**, 1569-83.

Sharma, P., Varma, R., Sarasij, R. C., Ira, Gousset, K., Krishnamoorthy, G., Rao, M. and Mayor, S. (2004). Nanoscale organization of multiple GPI-anchored proteins in living cell membranes. *Cell* **116**, 577-89.

Siegel, J., Suhling, K., Leveque-Fort, S., Webb, S. E. D., Davis, D. M., Phillips, D., Sabharwal, Y. and French, P. M. W. (2003). Wide-field time-resolved fluorescence anisotropy imaging (TR-FAIM): Imaging the rotational mobility of a fluorophore. *Review of Scientific Instruments* **74**, 182.

Squire, A., Verveer, P. J., Rocks, O. and Bastiaens, P. I. (2004). Red-edge anisotropy microscopy enables dynamic imaging of homo-FRET between green fluorescent proteins in cells. *J Struct Biol* **147**, 62-9.

Suhling, K., Siegel, J., Lanigan, P. M., Leveque-Fort, S., Webb, S. E., Phillips, D., Davis, D. M. and French, P. M. (2004). Time-resolved fluorescence anisotropy imaging applied to live

cells. *Opt Lett* **29**, 584-6.

Sytsma, Vroom, de, G. and Gerritsen. (1998). Time-gated fluorescence lifetime imaging and microvolume spectroscopy using two-photon excitation. *Journal of Microscopy* **191**, 39-51.

Tanaka, F. and Mataga, N. (1979). Theory of time-dependent photo-selection in interacting fixed systems. *Photochemistry and Photobiology* **29**, 1091-1097.

Valeur, B. (2002). Molecular Fluorescence. Principles and Applications. Weinheim: Wiley-VCH.

Varma, R. and Mayor, S. (1998). GPI-anchored proteins are organized in submicron domains at the cell surface. *Nature* **394**, 798-801.

Chapter 4

Direct quantification of the degree of clustering of biomolecules by time-resolved and/or two-photon fluorescence anisotropy imaging

Arjen N. Bader[a], Erik G. Hofman[b], Jarno Voortman[b], Paul M. P. van Bergen en Henegouwen[b], Hans C. Gerritsen[a]

[a] Molecular Biophysics, Utrecht University, Utrecht

[b] Cellular Architecture and Dynamics, Utrecht University, Utrecht

Submitted

Abstract

Fluorescence anisotropy based homo-FRET imaging methods are well suited to study clustering of identical proteins in cells. However, the direct relation between the measured anisotropy and the degree of clustering is difficult to implement. Here, we have investigated the depolarization due to controlled dimerization and oligomerization by utilizing green fluorescent protein constructs that contain the FK506-binding protein (FKBP12). This is performed for various experimental approaches and the benefits of utilizing two-photon excitation and/or time-resolved detection are investigated. Optimal dynamic range in anisotropy values was observed with two-photon excitation. No direct relation between cluster size and anisotropy was observed which is probably due to a non-random orientation of the fluorophores. The commonly used assumption that one energy transfer step can completely depolarize the fluorescence emission is therefore not valid. However, by determining the relation between anisotropy and protein cluster size we show that the average cluster size or fraction of clusters can be imaged in a quantitative way. Using this approach, it is shown that in the plasma membrane GPI-anchored proteins can form clusters that are on average composed of more than two subunits. In addition, we provide evidence that ~40% of the unstimulated epidermal growth factor receptors (EGFR) is present in the plasma membrane as pre-dimer.

Introduction

Binding events between proteins are essential in the broad range of cellular processes. Especially in the field of signal transduction (Krauss, 2001), transmission of the signal is governed by multiple interactions between proteins from the signal transduction chain. Initiation of the signaling cascade is often mediated by the binding of identical proteins to each other, i.e., dimerization or oligomerization. Also, the clustering of identical lipids is supposed play an important role in signaling. Clustering of proteins is usually investigated by co-immunoprecipitation or chemical crosslinking (Yu et al., 2002; Zhu et al., 2003). Both techniques are prone to artifacts since the experimental conditions may induce clustering of proteins. More recently, spectroscopical methods like Homo-FRET imaging has been developed to study these clustering processes (Bader et al., 2007b; Sharma et al., 2004; Yeow and Clayton, 2007). Similar to regular FRET, homo-FRET (Bader et al., 2007b; Blackman et al., 1998; Gautier et al., 2001; Jares-Erijman and Jovin, 2003; Lidke et al., 2003; Runnels and Scarlata, 1995; Sharma et al., 2004; Squire et al., 2004; Valeur, 2002; Varma and Mayor, 1998; Yeow and Clayton, 2007) involves the transfer of excited state energy between fluorophores that are located within 10 nm of each other. Unlike regular FRET, homo-FRET concerns energy transfer between identical fluorophores, without affecting the emission spectrum or fluorescence lifetime of the probes. With homo-FRET, the occurrence of protein clustering is accompanied by a decrease of the fluorescence anisotropy of the probe. The combination of anisotropy detection and microscopy affords the imaging of molecular scale clustering of identical (bio)molecules in cells.

In addition to cluster size determination, homo-FRET can be used for other applications. For instance, from the time-resolved anisotropy the rate of the homo transfer can be derived, which can be used to determine the distance between the fluorophores(Gautier et al., 2001; Jares-Erijman and Jovin, 2003; Sharma et al., 2004). In addition, it has been shown that anisotropy can be used to determine the relative orientation of the fluorophores(Gautier et al., 2001). Finally, the anisotropy can be related to the number of fluorophores per cluster (Bader et al., 2007b; Sharma et al., 2004; Yeow and Clayton, 2007), which is the subject of this study. So far, cluster sizes of a few proteins have been determined by homo-FRET and include human erythrocyte band 3, GPI-anchored proteins and the EGFR. However, this property has been exploited mainly in an indirect way, i.e., either by controlled photobleaching (Sharma et al., 2004) or fractional labeling studies (Blackman et al., 1998; Yeow and Clayton, 2007). In the current work, we have investigated the direct quantification of protein clustering in cells by fluorescence anisotropy based on homo-FRET imaging. A major advantage of such an approach is that subcellular cluster size heterogeneities can be determined and changes in cluster size can be followed.

The theoretical framework that relates fluorescence anisotropy to the cluster size have been provided by Runnels and Scarlata (Runnels and Scarlata, 1995). Critical factors that

frustrate the practical application of anisotropy based cluster size determination are that both the efficiency of the energy transfer and the relative orientation of the fluorophores should be known (Bader et al., 2007b; Runnels and Scarlata, 1995). Previously, we have demonstrated that time-gated fluorescence anisotropy imaging can be used to circumvent the former issue(Bader et al., 2007b). Here, we have experimentally investigated the relation between anisotropy and cluster size by using the green fluorescent protein (GFP) that can undergo either controlled dimerization or oligomerization. Regulated dimerization or oligomerization was achieved by the fusion of monomeric GFP (mGFP) with the FK506-binding protein (FKBP12) that can be dimerization by binding of its ligand AP. Using this approach, we have addressed the following issues: (1) what is the degree of depolarization due to homo-FRET in dimers and oligomers of GFP, (2) what are the advantages of utilizing time-resolved detection and/or two-photon excitation, and (3) how is the observed depolarization related to the average number of fluorophores per cluster? We show that (semi-) quantitative images can be made of the average number of fluorophores per cluster per pixel or of the average fraction of clusters per pixel.

This homo-FRET technology was subsequently used to study the clustering of two raft-localized proteins in the plasma membrane: an mGFP isoform linked to glycosyl-phosphatidylinositol (GPI) and the receptor for the epidermal growth factor (EGFR) C-terminally fused to mGFP. GPI-linked receptors have been described to partition into specific lipid domains, resulting in nanoscale clustering of GPI-anchored proteins (Sharma et al., 2004). Similarly, the EGFR has been found to partition into lipid rafts. A wealth of information exists about the presence of the EGFR as dimers or even oligomers in the plasma membrane of resting cells. By using both time-resolved and two-photon fluorescence anisotropy imaging we demonstrate that both GPI-anchored GFP as well as EGFR fused to GFP can form small nanoscale clusters in the plasma membrane of the resting cell.

Materials and methods

Recombinant DNA constructs

Monomeric GFP was mutated at position 206 by site directed mutagenesis on pEGFP-N3 (Clontech, Mountain View, CA) with the Quick-Change method using the following primers: forward 5'-cagtcc**aag**ctgagcaaagaccccaacgagaagcgcgatcac-3' and reverse 5'-gtgatcgcgcttc tcgttggggtctttgctcag**ctt**ggactg-3' (mutagenic codon in bold), in accordance to Zacharias et al (Zacharias et al., 2002). GFP and mGFP was amplified from pEGFP-N3 by PCR with flanking primers (forward 5'-atatactagtatggtgagcaagggcgaggagctgttc-3'and reverse-5' ttacttgtacagctcgt ccatgccgagag-3') using the high-fidelity DNA polymerase Phusion (Finnzymes, Espoo, Finland), and inserted into the SpeI and BamHI sites of the pC4-Fv1E vector (Ariad Pharmaceuticals, Cambridge, MA) to produce pC4-Fv1-mGFP. pC4-Fv2-mGFP was constructed by exchanging

the XbaI-SpeI fragment of pC4-Fv1-mGFP for a XbaI-SpeI fragment from pC4M-Fv2E (Ariad). Introduction of a flexible linker encoding 4 glycine and one serine residues (G4S), was performed by insertion of primers forward 5'-ctagtggtggcgggggatcca-3' and reverse 5'-ctagtggatcccccgccacca-3' at the SpeI site. All constructs were multiplied in *E.coli* and isolated with an endotoxin-free plasmid isolation kit (Machery-Nagel, Dueren, Germany), and verified by DNA sequencing.

Cell culture and sample preparation

NIH 3T3 cells were cultured in Dulbecco's modified Eagle's medium (Invitrogen, Breda, the Netherlands) supplemented with 7.5% foetal bovine serum (v/v) and 2 mM L-glutamine at 37°C in the presence of 5% CO_2 under a humidified atmosphere. Prior to transfections, cells were trypsinized and seeded in 6-well plates at 70% confluency. After 4 h, transfections were performed according to the manufacturer's protocol, using 4 µg of DNA and 10 µl of Lipofectamine 2000 (Invitrogen). Cells transfected with pC4-Fv-mGFP or pC4-Fv2-mGFP are named FKBP-mGFP or 2xFKBP-mGFP, respectively. 12 h post-transfection cells were trypsinized and allowed to grow on 18 mm coverslips (microscopy) or in 12-well plates (Blue-native PAGE). After 24 h, cells were either incubated for 1-2 h with 1 µM AP20187 (Ariad) or MOCK-treated with 0.1% ethanol. For microscopy, cells grown to 20-30 % confluency were washed with PBS, fixed with freshly prepared 4% formaldehyde at 37°C for 20 minutes, and quenched by 100 mM glycine for 10 min. Coverslips were mounted with Mowiol and stored at -20°C until further use. These preparations are not expected to influence the observed degree of clustering (Bancroft and Stevens, 1982).

Blue-native Gel electrophoresis

Cells expressing FKBP-GFP or 2xFKBP-GFP grown to 80% confluency, either treated with AP20187 or Mock-treated as described, washed with PBS and lysed in 60 µl Native PAGE sample buffer (Invitrogen) supplemented with 1% n-dodecyl-β-D-maltoside (DDM) and Complete protease inhibitors cocktail (Roche, Indianapolis, IN). After centrifugation of the lysates for 30 min at 13.000 x g, 25 µl of the supernatant was taken and supplemented with NativePAGE™ G-250 sample additive (Invitrogen) to a final concentration of 0.25%. The lysates were loaded on a pre-cast 3-12% NativePAGE™ gel (Invitrogen) and allowed to size-separate for 100 min at 150 V. Proteins were transferred to PVDF membranes by semi-dry blotting, detected with a monoclonal anti-GFP IgG (Roche, Indianapolis, IN) in combination with donkey-anti-mouse IgG, followed by visualization with an enhanced chemiluminescence reagent.

Fluorescence anisotropy imaging set-up

Fluorescence anisotropy imaging was carried out on a modified confocal scanning laser microscope (CSLM, C1, Nikon Instruments Europe, Badhoevedorp, The Netherlands). For the

one-photon excitation (OPE) experiments, the excitation was provided by a 473 nm pulsed diode laser (Becker & Hickl BDL-473, Berlin, Germany) operating at 50 MHz. For two-photon excitation (TPE) experiments, a Ti:Sapphire laser (Chameleon Ultra II, Coherent, Santa Clara, CA, USA) running at 82 MHz and tuned to 860 nm was used. The excitation pulses were coupled directly into the modified C1 scan head. The excitation light is normally fiber coupled into the scan head. This, however, would both cause excessive broadening of the femto second laser pulse and complicate polarization dependent measurements. Therefore the fiber coupler and first lens in the excitation path of the scan head were removed and the laser was directly coupled into the scan head. A linear polarizer (Meadowlark, Frederick, CO, USA) was positioned in the laser beam to define the excitation polarization direction.

In the OPE experiments, a 60x, NA=1.20 water immersion objective (Plan Apo, Nikon) was used. The excitation beam did not fill the whole back aperture of the objective. The effective excitation NA amounted to approximately 0.5. This resulted in only a minor decrease in the value of r_0 due to the NA of the objective(Axelrod, 1989); for GFP a value of r_0 = 0.38 was found in stead of the theoretical value of 0.4. As a consequence of the reduced excitation NA, the resolution of the microscope is somewhat reduced.

In the TPE experiments, a 20x, NA=0.75 multi immersion objective was used (Plan Fluor, Nikon; using water immersion). A beam expander was used to expand the diameter of the excitation beam and completely fill the back aperture of the objective. The high NA of the objective resulted in moderate depolarization; for GFP a value of r_0 = 0.51 was found in stead of the theoretical value of 0.57.

A broadband polarizing beam splitter cube (PBS, OptoSigma, Santa Ana, CA, USA) was used to split the emission in a parallel and a perpendicular channel with respect to the excitation light. The two emission channels were both fiber coupled to detection systems consisting of a fluorescence lifetime imaging module (LIMO, Nikon Instruments BV, Badhoevedorp, The Netherlands)(de Grauw and Gerritsen, 2001) equipped with an internal photon counting photomultiplier tube. For each pixel in the image, the LIMO's collect photons in four 2 ns wide consecutive time gates. By employing two synchronized LIMOs, one for each polarization direction, a four channel time-resolved anisotropy decay can be acquired for each pixel. An acquisition time of 3ms per pixel was applied. A threshold of 300 counts was applied (maximum number of counts was approximately 4500). All images contain 160x160 pixels and cover an area of 50x50 μm. The steady state anisotropy images were obtained by summation of the intensities in all four gates. The procedures of data analysis, synchronization and correction for sensitivity differences between the two channels were based on using reference dyes. This procedure was described in detail previously(Bader et al., 2007a; Bader et al., 2007b).

Theoretical background

Steady state fluorescence anisotropy imaging

The relation between homo-FRET and fluorescence anisotropy has been extensively described in literature (Bader et al., 2007b; Gautier et al., 2001; Jares-Erijman and Jovin, 2003; Lidke et al., 2003; Runnels and Scarlata, 1995; Yeow and Clayton, 2007). Briefly, the fluorescence anisotropy r is defined as the intensity corrected difference between the emission parallel (I_{par}) and perpendicular (I_{per}) to the excitation polarization direction (Valeur, 2002):

$$r(t) = \frac{I_{par} - I_{per}}{I_{par} + 2I_{per}} \quad [1]$$

The most common source of depolarization (i.e., reduction of the anisotropy) is by rotation of the fluorophores. For fluorophores that are large and fixed or surrounded by a high viscosity medium, rotation takes place on a timescale similar to or longer than fluorescence and consequently the emission will be polarized. In such cases, additional depolarization due to homo-FRET in clusters of fluorophores can be easily observed. In these clusters, two types of fluorophores can be distinguished: fluorophores that are directly excited by the polarized light or indirectly excited by homo-FRET. The former are photo selected and therefore their anisotropy will be identical to monomers ($r = r_{mono}$). This is not the case for the indirectly excited fluorophores; they will have a broader distribution of orientations and hence their anisotropy will be lower ($r = r_{et}$). The measured anisotropy contains contributions of both directly and indirectly excited molecules and depends on the number of fluorophores per cluster. Runnels and Scarlata (Runnels and Scarlata, 1995) related the steady state anisotropy (r_{ss}) to the cluster size N (i.e., the average number of fluorophores per cluster) and homo-FRET efficiency E. The latter is included as the product of homo-FRET rate ω and fluorescence lifetime τ ($\omega\tau = E / (E\text{-}1)$):

$$r_{ss} = r_{mono}\frac{1+\omega.\tau}{1+N.\omega.\tau} + r_{et}\frac{(N-1).\omega.\tau}{1+N.\omega.\tau} \quad [2]$$

Utilization of Equation 2 in fluorescence microscopy is complex and not practical due to the low signal levels. Both the homo-FRET rate ω and the anisotropy r_{et} need to be known to obtain quantitative information about the cluster size N. The rate ω can be derived from the time-resolved anisotropy decay. In steady-state fluorescence anisotropy imaging, however, ω is either estimated or assumed to be much faster than the rate of fluorescence, and consequently $\omega\tau \rightarrow \infty$ (under these conditions homo-FRET efficiency E=1). Now, equation 2 simplifies to:

$$r_{ss}(E=1) = r_{\text{mono}}\frac{1}{N} + r_{et}\frac{N-1}{N} \quad [3]$$

For randomly oriented fluorophores, r_{et} is approximately zero (the theoretical value is 0.016 (Arganovich and Galanin, 1982; Runnels and Scarlata, 1995)), but for non-random orientations r_{et} will obviously be higher. The assumption of randomly orientated fluorophores simplifies Equation 2 even further; the steady state anisotropy can be approximated by:

$$r_{ss}(E=1, r_{et}=0) = \frac{r_{\text{mono}}}{N} \quad [4]$$

Time-resolved and two-photon excitation fluorescence anisotropy imaging

Time-resolved anisotropy decays provide more detailed information about homo-FRET than steady state data. In absence of rotation, the decay due to homo-FRET is described by (Gautier et al., 2001; Tanaka and Mataga, 1979):

$$r_{\text{homo-FRET}}(t) = (r_{\text{mono}} - r_{\text{inf}})e^{-2\omega t} + r_{\text{inf}} \quad [5]$$

Fitting the measured anisotropy decay using Equation 4 yields the value of the homo-FRET rate. However, it should be realized that the number of photons that are typically collected per pixel is in practice not sufficient for a reasonable estimation of ω.

Within nanoseconds, the anisotropy levels off at the limiting anisotropy r_{inf}; a situation where homo-FRET has occurred multiple times and all fluorophores have equal probability of emitting a photon. When homo-FRET is very efficient, this situation is reached rapidly and $r_{ss} = r_{inf}$. The limiting anisotropy is therefore a direct measure for the cluster size N that is independent of the rate / efficiency of homo-FRET and (Bader et al., 2007b):

$$r_{\text{inf}} = \frac{r_{\text{mono}}}{N}\left(+r_{et}\frac{N-1}{N}\right) \quad [6]$$

The value of r_{inf} is always lower than the steady state anisotropy r_{ss} and the reduction in r_{inf} due to clustering is more pronounced than the reduction in r_{ss}. Consequently, variations in the degree of clustering can be more accurately determined by measuring r_{inf}. The extent of this improvement depends on the rate / efficiency of homo-FRET (see Fig. 1).

For one-photon excitation (OPE) of fluorophores with parallel excitation and emission transition dipole moments, the theoretical value of r_0 is 0.4. Using two-photon excitation (TPE), this anisotropy increases to a theoretical maximum value of 0.57 (Volkmer et al., 2000). Whereas the anisotropy of directly excited fluorophores increases (r_{mono} = 0.57), the anisotropy of the fluorophores indirectly excited after homo-FRET (r_{et}) is difficult to predict. Only a minor increase is expected since the distribution of orientation of the directly excited fluorophores is

more confined and the energy transfer to fluorophores oriented perpendicular to the excitation light will be less efficient. Therefore, similar to time-resolved detection, two-photon excitation increases the dynamic range of depolarization due to homo-FRET.

Results

Controlled dimerization and oligomerization of GFP

To control either dimerization or oligomerization of a fluorescent protein, GFP was fused with one or two FK506-binding protein (FKBP) domains (Fooksman et al., 2006). Binding of one ligand (AP20187) to two FKBP domain results in their dimerization. Since AP20187 can easily pass the plasma membrane dimerization of the GFP-FKBP fusion proteins can be induced by adding this ligand to cells expressing these constructs. Proteins that contain one FKBP domain will dimerize, whereas the constructs that contain two FKBP domains will oligomerize in a

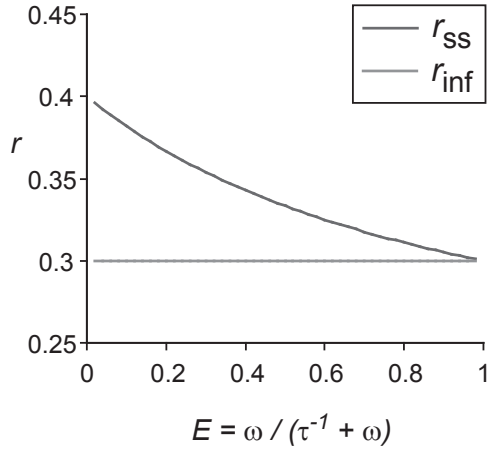

Fig. 1. Comparison of the effect of the homo-FRET efficiency on the steady state (r_{ss}) and limiting time resolved (r_{inf}) anisotropy. The value of r_{inf} depends on the degree of clustering; r_{ss} is also dependent on E.

broad distribution of cluster sizes. The constructs used here are composed of monomeric GFP (mGFP) directly attached to one or two FKBP domains. mGFP has been made by mutating alanine residue at position 206 into lysine. Here, we refer to the dimerizing and oligomerizing constructs as FKBP-mGFP and 2xFKBP-mGFP, respectively.

To validate the dimerization and oligomerization properties of the constructs, we employed native polyacrylamide-gel electrophoresis (PAGE) of lysed NIH 3T3 cells. Blue-native PAGE preserves the proteins in their native conformation (Wittig et al., 2006). Here, cells were lysed in a buffer containing the relatively mild detergent n-dodecyl-β-D-maltoside

(DDM), which does not disturbs the binding of the ligand AP20187 to the FKBP domains. The lysate is size-separated on a native-PAGE gel, and after transfer of the proteins from the PAGE-gel to a PVDF membrane, the mGFP tag is detected with a monoclonal antibody directed against GFP. In the absence of AP20187, FKBP-mGFP is found predominantly in the monomeric form (Fig. 2), while only a small fraction of FKBP-mGFP is visible as dimers. Treatment of the cells with AP20187 resulted in the formation of mainly dimeric FKBP-mGFP. Also the 2xFKBP-mGFP control without AP20187 showed mainly monomers. Addition of AP20187 to the 2xFKBP-mGFP constructs resulted in a broad distribution of oligomers of the mGFP construct, the majority of the protein existing in dimeric, trimeric or tetrameric form (Fig. 2).

Steady state confocal fluorescence anisotropy imaging of GFP clustering

Images of NIH 3T3 cells transfected with the two FKBP-mGFP constructs were made using the confocal fluorescence anisotropy imaging microscope operated in the steady state mode. The constructs were present in both the cytoplasm and the nucleus of the cell and no significant variations in subcellular anisotropy values were observed (Fig. 3A). Interestingly, the ratio of nucleus/cytoplasm localization of mGFP changed after the addition of the ligand. This may be due to the nuclear impermeability of proteins larger than ~50 kDa. The intensities of all significant pixels were summed for both the parallel and perpendicular channel and the average anisotropy values for five different cells were determined (Fig. 3B). In our experimental setup, we observe an initial anisotropy value (r_{mono}) for GFP in solution of 0.38. Compared to GFP in solution, the cytoplasmic FKBP-mGFP showed already a slight but significant drop in anisotropy of about 0.019. For 2xFKBP-mGFP, the decrease in anisotropy was even larger (Δr = 0.031). This decrease cannot be explained by an increase in rotational mobility of the

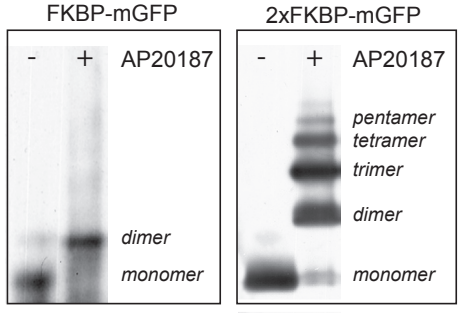

Fig. 2. Native PAGE analysis of dimerization constructs. Cells expressing FKBP-mGFP or 2xFKBP-mGFP, either incubated with AP20187 or mock-treated, were lysed under non-reducing and non-denaturing conditions. After size-separation on a Native PAGE gel and blotting to PVDF membrane, proteins were detected with anti-GFP antibodies.

fluorophore and is therefore attributed to homo-FRET. Apparently, already in absence of the dimerization inducing ligand AP20187 some clustering occurs, which is in agreement with the PAGE experiments (Fig. 2). The fact that a lower anisotropy value was observed for the double FKBP construct than for single FKBP, suggests that the FKBP domain is (partly) responsible for this clustering. A strong decrease of the anisotropy was observed for FKBP-mGFP (Δr = 0.055) after incubation of the cells with 1 µM AP20187 for 2 hrs at 37°C (Fig. 3B). For the 2xFKBP-mGFP, an even larger decrease was observed (Δr = 0.084). These data clearly demonstrate that steady-state fluorescence anisotropy imaging can discriminate between monomers, dimers and oligomers. However, despite the fact that the effect on the anisotropy of both dimerization and oligomerization is significant, the dynamic range of anisotropy reduction is limited.

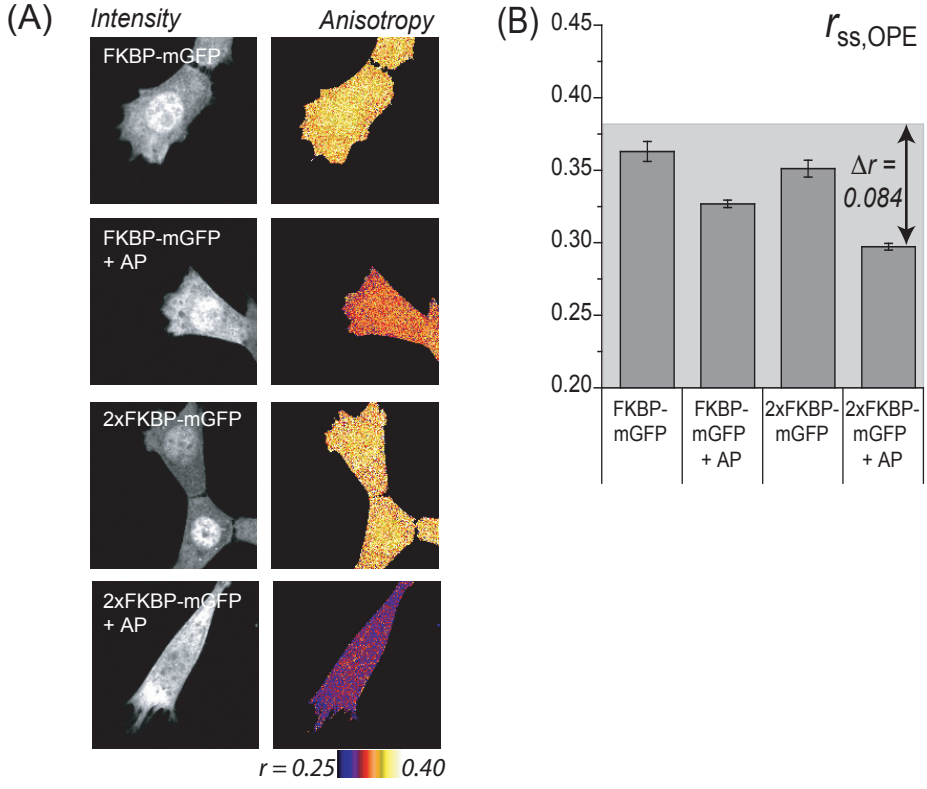

Fig. 3. (A) Confocal steady-state intensity and fluorescence anisotropy images of cells expressing GFP-FKBP and GFP-2xFKBP, both in presence and absence of AP20187 (AP). (B) Histograms of the average anisotropy of the samples in (A). Per sample 5 cells were imaged. The intensity values of all significant pixels were summed and the overall anisotropy per cell was calculated. The error bars give the standard deviation between the cells. r_{mono} = 0.382.

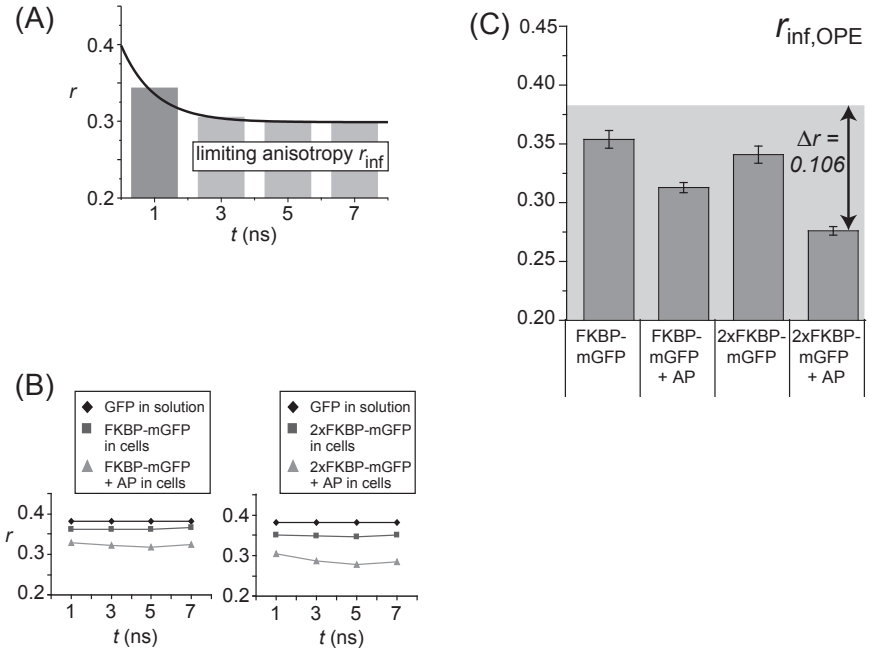

Fig. 4. Confocal time-gated fluorescence anisotropy imaging. (A) A schematic of a typical r-decay due to homo-FRET. The limiting anisotropy (r_{inf}) is independent on the homo-FRET efficiency for E>0.5. (B) Time resolved anisotropy decays of cells expressing FKBP-mGFP and 2xFKBP-mGFP, both in presence and absence of AP20187 (AP). For all images per sample, the intensities per gate in the significant pixels were summed to create the average r-decays. (C) The average anisotropy for each sample is plotted in a histogram. The dynamic range (Δr) is larger than for r_{ss} (compare Fig. 3B). r_{mono} = 0.382.

Time-resolved confocal fluorescence anisotropy imaging of GFP clustering

There are major advantages of using time-resolved detection in fluorescence anisotropy imaging. Firstly, the average time-resolved anisotropy decay can be obtained by averaging over all significant pixels in (part of) the cell. In a typical time-resolved anisotropy decay, homo-FRET results in a rapid exponential decay that levels off (Fig. 4A). The rate of the decay (~2ω) is often much faster than the rotational correlation time of fluorophores such as GFP. Since the decays due to rotation and homo-FRET can be easily distinguished, the occurrence of homo-FRET can be verified. Secondly, r_{inf} can be obtained from the time-resolved anisotropy decay, which is a homo-FRET efficiency independent measure for the degree of clustering (Eq. 6).

Time-resolved anisotropy imaging requires more complex experimental approaches than steady state anisotropy imaging (Bader et al., 2007a; Bader et al., 2007b; Clayton et al., 2002; Siegel et al., 2003). Fortunately, comparatively low time resolution is sufficient to obtain information about the occurrence of homo-FRET. In the current work, time-resolved anisotropy imaging was realized using time-gated detection systems equipped with four 2 ns wide gates.

To obtain the anisotropy decay, the intensities per gate and per channel were summed for all significant pixels. A schematic presentation of a typical homo-FRET decay, both at high resolution and time-gated is shown in figure 4A. This figure shows that a low time resolution is sufficient to establish r_{inf} and to detect the presence of homo-FRET.

Following this approach, the time-gated anisotropy decay of GFP in solution was recorded. Only a minor decrease of the anisotropy of GFP was observed in time (Fig. 4B). This is in agreement with the long rotational correlation times (>15 ns) for GFP found earlier (Gautier et al., 2001; Sharma et al., 2004). Also for NIH 3T3 cells expressing either the dimerization or oligomerization construct the time gated anisotropy decays were determined (Fig. 4B). The relatively low anisotropy in the first time gated indicates that rapid depolarization occurs. Since this initial fast decay cannot be explained by rotational motion of the GFP fluorophore, we conclude that this decay is representing homo-FRET. For FRET efficiencies of E > 0.5, the anisotropy remained approximately constant in the last three gates. Therefore, we summed the intensities in these gates and the obtained anisotropy value was used for r_{inf} (Fig. 4A). For both the dimerization and oligomerization constructs, the average values of r_{inf} were compared (Fig. 4C). Similar to the steady state results, little depolarization was observed in the absence of AP20187. Addition of the clustering ligand induced a decrease in anisotropy, and again oligomerization caused more depolarization than dimerization. The main difference between steady state and the limiting anisotropy r_{inf} is that an increase in the dynamic range is observed. For 2xFKBP-mGFP with AP20187, the decrease in r_{inf} was Δr = 0.0106, which corresponds to an increase of ~25% as compared to the steady state results.

Two-photon excitation fluorescence anisotropy imaging of GFP clustering

To enhance the depolarization due to homo-FRET in clusters, we decided to implement two-photon excitation in the fluorescence anisotropy microscope. An increase in anisotropy reduction due to homo-FRET is expected as the theoretical value of r_0 for two-photon excitation (TPE) increases to 0.57 (Volkmer et al., 2000). Two-photon excitation measurements of cells expressing either FKBP-mGFP or 2xFKBP-mGFP were performed for both steady state and time-resolved detection. The average anisotropy decays have a profile similar to the one-photon excitation results (Fig. 5). The value of r_{mono} increased to 0.51. As a result, the depolarization due to oligomerization (2xFKBP + AP20187) increased to Δr = 0.127 and Δr = 0.154 for steady state and time-resolved detection, respectively. Using two-photon excitation, the amount of depolarization due homo-FRET is enlarged by 45-50% compared to one-photon excitation.

Direct relation between anisotropy and cluster size

As shown by Equation 2, relating the steady state anisotropy to the cluster size requires knowledge of (1) the efficiency / rate of homo-FRET and (2) the relative orientation of the

fluorophores and consequently r_{et}. From the difference between r_{ss} and r_{inf} it can be concluded that the homo-FRET efficiency E is not 1, but approximately 0.7 (for both one and two photon excitation). Therefore, r_{inf} is used to determine the degree of clustering.

Although induced clustering resulted in a clear and significant decrease in r_{inf}, the observed depolarization was less than expected. Dimerization resulted in a r_{inf}-reduction of only ~20% whereas for oligomerization a reduction of ~30% was observed (for both one- and two-photon excitation). A commonly used assumption is that the orientation of the indirectly excited fluorophores is random (and consequently r_{et} = 0). The anisotropy then equals r_{mono}/N

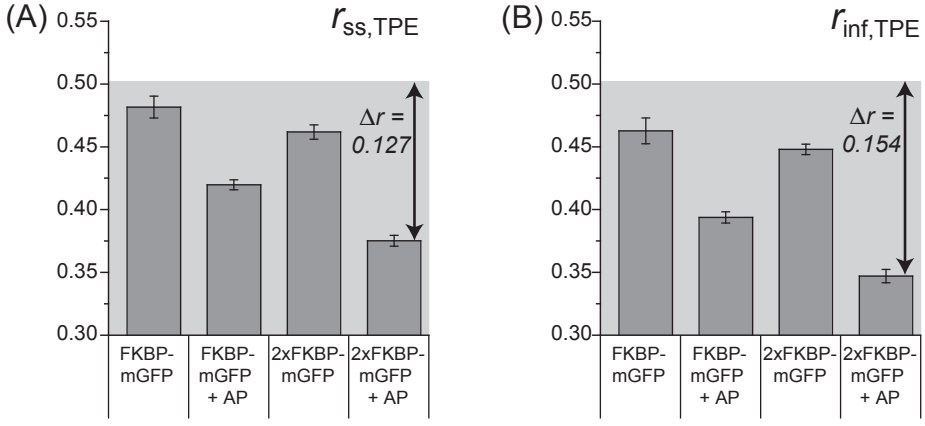

Fig. 5. Two-photon excitation fluorescence anisotropy imaging. Analogous to Figures 3B and 4C, the average anisotropy per sample was measured using two-photon excitation. For both steady state (A) and time-gated detection (B) the dynamic range (Δr) increases compared to one-photon excitation. r_{mono} = 0.505.

and dimerization is expected to yield an anisotropy reduction of about 50%. Oligomerization is expected to reduce the anisotropy even more. From the limited reduction in anisotropy observed here can thus be concluded that this orientation is not random. This apparently fixed orientation can be either forced by the binding of the FKBP domains to AP20187, or by binding to (semi-)specific dimerization sites on the fluorophores themselves. To reduce the former effect, an FKBP-mGFP construct was made with a flexible linker between FKBP and mGFP (FKBP-g4s-mGFP). The presence of this linker did not increase the reduction of r_{inf} (Fig. 6A).

It is thus assumed that also for monomeric GFP semi-specific dimerization sites are present that fix the relative orientation of the fluorophores. The observed efficiency of the transfer (E=0.7) corresponds to an inter fluorophore distance of ~4 nm (Förster radius for GFP dimers is 4.65)(Sharma et al., 2004). This is comparable to the size of GFP. From its crystal structure (Yang et al., 1996), it is known that GFP is a fluorophore located in the center of a barrel that is 2.5 nm in diameter and 4 nm high. Compared to these dimension, the inter fluorophore distance in dimerized FKBP-mGFP allows chemical interactions.

No difference in anisotropy was observed when GFP was used that still contained a

functional dimerization domain (Fig. 6A). This is consistent with crystal structure data from GFP that shows that GFP dimerization results in an anti-parallel orientation of the two fluorescent proteins (Yang et al., 1996). Sterical effects do probably not allow such dimerization when GFP is attached to dimerized FKBP, even in the presence of the flexible linker. Our results suggest the presence of chemical interactions between two parallel GFPs that are not related to the main dimerization site. Even when the strength of these interactions is weak, they still occur since the local concentration of the fluorophores in clusters is high. A schematic of this model is depicted in Figure 6B.

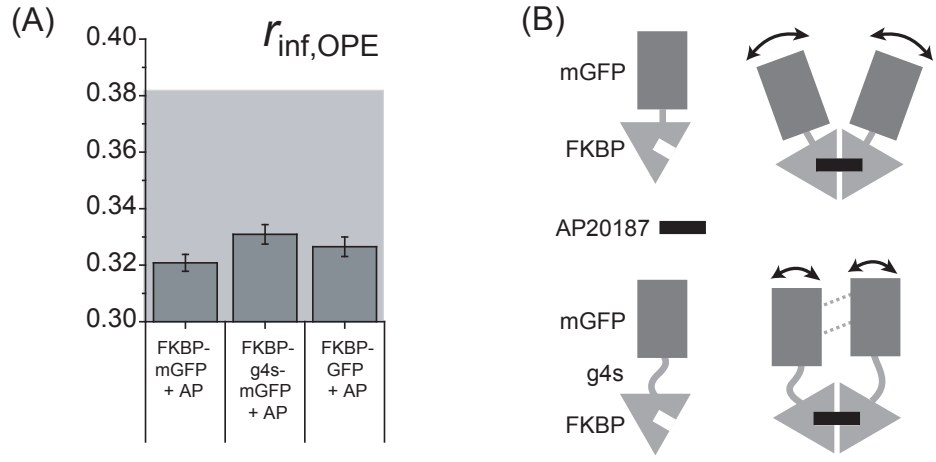

Fig. 6. (A) Anisotropy reduction due to homo-FRET is not altered due to the presence/absence of a flexible linker or dimerization domain in the fluorophore. (B) Schematic of the possible relative orientations of the GFP fluorophores in FKBP induced dimers. r_{mono} = 0.382.

Also, we note that incomplete maturation of GFP can have an affect on the observed anisotropy. Single molecule studies on the clustering of DsRed revealed that a significant fraction of this protein is still present as a immature green species (Garcia-Parajo et al., 2001). More recently, also for GFP incomplete maturation was observed. Approximately 20% of the fluorophores was found to be present in a biologically active non fluorescent conformation (Ulbrich and Isacoff, 2007). The immature species (Niwa et al., 1996) is expected to be non-absorbing in the wavelength range of GFP's emission and can therefore not function as a FRET acceptor. As a consequence, one can consider the FKBP subunits to be fractionally labeled (Yeow and Clayton, 2007). Based on the work of Yeow and Clayton(Yeow and Clayton, 2007) and Equation 5, the dimer anisotropy as a function of the labeled fraction f is:

$$r_{\mathrm{inf},N=2} = (1-\tfrac{f}{2})r_{\mathrm{mono}} + \tfrac{f}{2}r_{et} \qquad [7]$$

When f is assumed to be 0.8, the anisotropy after homo-FRET (r_{et}) is 0.21. Consequently, the anisotropy of dimers should be 0.29 in stead of the value of 0.31 measured here.

In conclusion, the non-random orientation of clustered GFP fluorophores and incomplete maturation of GFP complicates the theoretical prediction of the anisotropy for given numbers of cluster sizes. However, the presented results provide general reference values of the anisotropy for dimers and oligomers. As mentioned, when the inter-fluorophore distance is less than 4 nm there are chemical interactions between the (m)GFP barrels that fix their relative orientation. It is assumed that these orientations are independent on the biomolecules GFP is fused to. This means for most GFP fusions the degree of clustering can be determined. Under the restriction that homo-FRET is fast, the resulting anisotropy reduction can be compared to the reference values determined using (2x)-FKBP-mGFP.

The current work provides the reference values of the reduction of the anisotropy due to clustering. To be independent on variations in r_{mono}, relative values of the depolarization are given here, i.e., r_{inf}/r_{mono}. For dimerization r_{inf}/r_{mono} is 0.81, whereas for oligomerization 0.72 is determined (Fig. 7). This information can be used for two types of clustering studies. First, based on the degree of depolarization, the average oligomerization state is determined: r_{inf}/r_{mono} values from 1 to 0.87 correspond to N_{av} = 1, 0.87 to 0.77 corresponds to N_{av} = 2 and 0.77 to 0 correspond to $N_{av} \geq 3$ (Fig. 7). This way, anisotropy images can be converted to semi-quantitative cluster size images. Second, the anisotropy can be used to determine the ratio between monomers and oligomers (N=2,3,4,…). With the knowledge that the r_{inf}/r_{mono} of oligomers is 0.72, the fraction of oligomers $F_{clusters}$ is defined by:

$$\frac{r_{\mathrm{inf}}}{r_{\mathrm{mono}}} = (1 - 0.28F_{\mathrm{cluster}}) \qquad [8]$$

Images of r_{inf} can therefore also be converted to images of $F_{cluster}$. The practical application of both types of clustering studies is demonstrated below.

Nanoscale clustering of GPI-GFP

This technology was subsequently used to determine the cluster size in resting cells of a model for GPI-anchored proteins: a mGFP fused with a GPI-anchor. The construct encoding for mGPI-GFP was stably expressed in NIH-3T3 and protein cluster sizes were determined using confocal time-gated anisotropy imaging experiments. Cells expressing this protein display GFP fluorescence on distinct locations in the cells, although the Golgi apparatus and plasma membrane are the most prominent sites (Fig. 8B). Due to the absence of rotational effects, the average time-resolved anisotropy decay found in these cells can be attributed to homo-FRET (Fig. 8A). The fast initial decay in anisotropy points to an efficient energy transfer (E > 0.7), meaning that the inter fluorophore distance is small enough to allow a chemical interaction

between the GFP barrels. This suggests that the interactions of the fluorophores in GPI-GFP are similar to in FKBP constructs. Therefore, the r_{inf} image (Fig. 8C) can be transferred to a cluster size image (Fig. 8D). As expected, the anisotropy and cluster size images demonstrate differential clustering behavior of GPI-GFP, dependent of the subcellular localization. The majority of GPI-GFP is located at the plasma membrane where it forms nanometer scale clusters. The size of these clusters is, on average, larger than two. In contrast, the Golgi located GPI-GFP is predominantly present as monomers, suggesting that factors regulating cluster formation are only present in the plasma membrane.

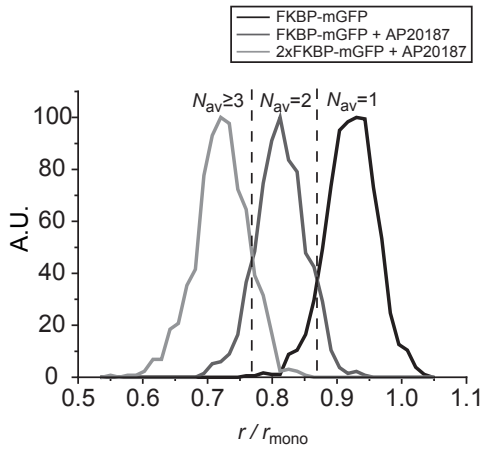

Fig. 7. Histograms of the r_{inf} values in cells expressing FKBP-mGFP (in presence/absence of AP20187) or 2xFKBP-mGFP (in presence of AP20187). In 80x80 pixel images, a threshold of 1200 counts was applied (maximum 4500 counts were observed). For the significant pixels the degree of depolarization (r/r_{mono}, r_{mono} = 0.382) was determined and plotted in the histogram. The dashed lines give the borders of the anisotropy ranges for average cluster sizes N_{av}=1, 2 and >3.

Nanoscale clustering of EGFR

To study the aggregation state of the EGFR in resting cells, NIH 3T3 cells were stably transfected with a construct encoding the human EGFR fused with mGFP. Comparative flow cytometry indicates that the cell line used is expressing the EGFR-GFP fusion proteins at an average level of ~50,000 receptors/cell. Moreover, control exeriments show that activation kinetics and activation levels of EGFR or EGFR-GFP are indistinguishable, which is also in agreement with other studies (data not shown). To determine the degree of EGFR-mGFP pre-clustering in non-stimulated cells time-resolved anisotropy images were recorded (Fig. 9). The time-resolved anisotropy decay of all the significant pixels in the cells shows that fast homo-FRET results in depolarization of the emission (Fig. 9A). Averaged over five cells, a depolarization r_{inf}/r_{mono} of 0.89 was observed, which, according to Equation 8, corresponds to the presence ~60% of EGFR as monomers and ~40% of all EGFR are present as dimers or even higher order oligomers. In conclusion, both GPI-GFP and EGFR-GFP are found in small nanoscale clusters in the plasma membrane of the NIH 3T3 cells, with a signifant larger cluster formation for GPI-GFP when compared to EGFR.

Discussion

In the presented work, we demonstrate that in fluorescence microscopy the anisotropy can be used to directly determine the degree of clustering of proteins and lipids in cells. Dimerization and oligomerization was induced in cells expressing mGFP fused with the dimerization domain FKBP. A stepwise decrease in the anisotropy was observed upon dimerization and oligomerization. Independent of the anisotropy imaging method used (e.g., steady state or time-resolved detection, confocal or two photon excitation), the FKBP fusions of GFP provide reference values for the anisotropy of monomers, dimers and oligomers. When homo-FRET is fast, these reference values for dimerization and oligomerization can be used for other GFP fusions as well. Consequently, images of the average cluster size per pixel or the average fraction of cluster per pixel can be obtained.

The advantages of using time-resolved detection are large. The average anisotropy decay of multiple pixels can be used to verify that homo-FRET occurs and whether it is fast. Also, the limiting anisotropy r_{inf} is derived from the decays, which is related to the cluster size N independent on the rate / efficiency of the transfer. Both time-resolved detection and two photon excitation improve the dynamic range over which homo-FRET decreases the anisotropy. However, significantly more photobleaching is observed when TPE was used and consequently the count rate is often reduced. On a pixel level, where in the order of 10^3 counts are collected, the accuracy of the anisotropy is strongly reduced (Lidke et al., 2005). The benefits of the improved dynamic range can thereby be lost.

To demonstrate the application of this imaging technology in the determination of the fraction of oligomers, we studied the clustering of a model molecule for GPI-anchored proteins, mGPI-GFP. We previously investigated this issue using steady state anisotropy similar as to the work of Sharma et al. (Sharma et al., 2004). With time resolved anisotropy detection significant larger clusters of GPI-GFP were found, again emphasizing the larger dynamic range of our novel approach. Specifically in the plasma membrane a large number of pixels was found with cluster sizes of 3 or more suggesting the presence of signifantly larger clusters than previously anticipated. The absence of any GPI-GFP cluster in the Golgi system suggest the presence of a factor that stimulate cluster formation of GPI-GFP in the plasma membrane. As GPI-anchored protein are found to partition into lipid rafts, their presence in these lipid domains may be responsible for the clustering process. This implies that GPI-GFP is only present in lipid rafts in the plasma membrane meaning that lipid rafts are either absent in the Golgi or other regulatory factors are involved.

In addition to GPI-GFP, the cluster behavior of EGFR was studied using time-resolved anisotropy. The EGF receptor is the most studied member of the family of receptor protein tyrosine kinases. The classical model of EGFR activation predicts that EGF is inducing receptor dimerization followed by an allosteric activation of the EGFR tyrosine kinase. However, there is a growing body of evidence that the EGFR is already present on the plasma membrane as receptor dimers. This has been studied by co-immunoprecipitation and chemical

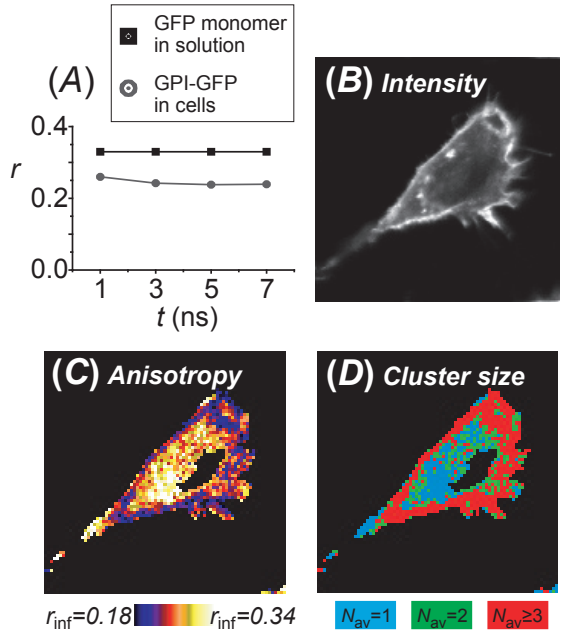

Fig. 8: Confocal time-gated anisotropy imaging shows nanoscale clustering of GPI-GFP in the plasma membrane. (A) Time resolved anisotropy decay, obtained by summing the intensities per gate in the significant pixels. (B) Intensity, (C) limiting anisotropy and (D) cluster size images of cells expressing GPI-GFP. The latter two images are binned to 80x80 pixels. r_{mono} = 0.330.

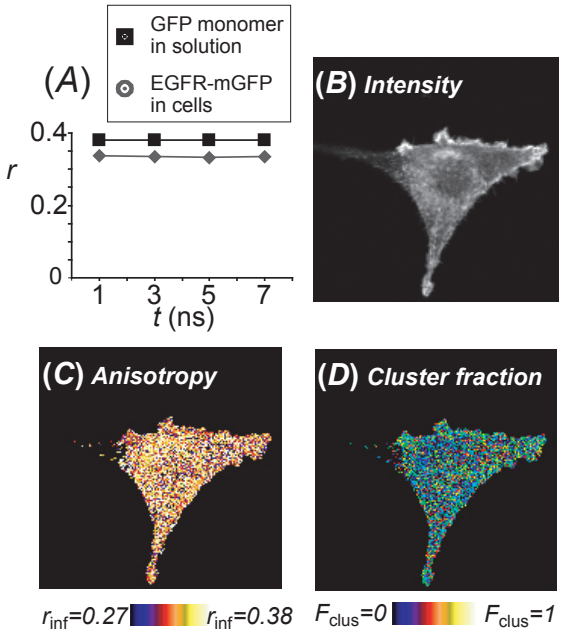

Fig. 9. Confocal time-gated anisotropy imaging shows 40% clustering of EGFR-mGFP in the plasma membrane. (A) Time resolved anisotropy decay, obtained by summing the intensities per gate in the significant pixels. (B) Intensity, (C) limiting anisotropy and (D) fraction of clusters in a cell expressing EGFR-mGFP. The images are binned to 80x80 pixels. r_{mono} = 0.381.

crosslinking studies. However, since these methods might induce receptor aggregation other microscopical methods have been applied. First of all, the oligomeric state of` the EGFR has been studied using fracture labeling electron microscopy demonstrating the presence of 55% monomers, 40% dimers and 5% oligomers (van Belzen et al., 1988). With image correlation microscopy the presence of 2.2 receptors per cluster was observed, and more recently by using FCS and fluorescent brightness analysis, a distribution of 70% monomers, 20% dimers and 10% oligomers was found (Clayton et al., 2005; Saffarian et al., 2007). These results are in nice agreement with our data where we found evidence for the presence of ~40% in the predimerized or even oligomerizaed state. It would be interesting to see the effect of EGF on this distribution which will be subject of our future research.

An important question that remains is which factor(s) is(are) regulating the predimer formation of the EGFR. As described by Teramura et al. (2006), signaling via EGFR predimers might occur with two orders of magnitude faster than signaling via monomers, simply because the dimer can directly be activated rather than first finding a potential dimerization partner (Teramura et al., 2006). As such, this factor might regulate the sensitivity of the cell for EGFR signaling. Similar as to the situation for GPI-GFP, predimer formation of the EGFR might be induced by their presence in lipid rafts. In a previous paper we have shown that the EGFR colocalizes with the raft lipid GM1, in a manner independent of cholesterol (chapter 2 of this thesis). Extraction of Cholesterol by cyclodextrin was found to enhance receptor clustering whereas cholesterol loading decreased receptor clustering. These findings suggest that receptor aggregation is sensitive to the lipid composition of the plasma membrane and furthemore that the sphingolipid GM1 is not involved in this process.

In conclusion, we provide evidence that anisotropy based imaging methods are very well suited to determine the clustering of proteins in cells. Confocal and two-photon microscopy based cluster size imaging methods are both suited for this purpose; time-resolved detection is preferred. Both GPI-GFP and EGFR-GFP we found to be clusterd in the plasma membrane already before the stimulation of signaling. Factors that regulate the aggregation state of these types of receptor is subject of our future experiments.

References

Arganovich, V. M. and Galanin, M. D. (1982). Electronic excitation energy transfer in condensed matter. Amsterdam: North-Holland Publishing.

Axelrod, D. (1989). Fluorescence polarization microscopy. *Methods Cell Biol* **30**, 333-52.

Bader, A. N., Hofman, E. G., van Bergen en Henegouwen, P. M. and Gerritsen, H. C. (2007a). Confocal time-resolved fluorescence anisotropy imaging. In *Imaging, Manipulation, and Analysis of Biomolecules, Cells, and Tissues V*, vol. 6441, pp. 64410C. San Jose, CA, USA: SPIE.

Bader, A. N., Hofman, E. G., van Bergen en Henegouwen, P. M. P. and Gerritsen, H. C. (2007b). Imaging of protein cluster sizes by means of confocal time-gated fluorescence anisotropy microscopy. *Opt. Express* **15**, 6934.

Bancroft, J. D. and Stevens, A. (1982). Theory and practice of histological techniques: Churchill Livingstone.

Blackman, S. M., Piston, D. W. and Beth, A. H. (1998). Oligomeric State of Human Erythrocyte Band 3 Measured by Fluorescence Resonance Energy Homotransfer. *Biophys. J.* **75**, 1117-1130.

Clayton, A. H., Hanley, Q. S., Arndt-Jovin, D. J., Subramaniam, V. and Jovin, T. M. (2002). Dynamic fluorescence anisotropy imaging microscopy in the frequency domain (rFLIM). *Biophys J* **83**, 1631-49.

Clayton, A. H., Walker, F., Orchard, S. G., Henderson, C., Fuchs, D., Rothacker, J., Nice, E. C. and Burgess, A. W. (2005). Ligand-induced dimer-tetramer transition during the activation of the cell surface epidermal growth factor receptor-A multidimensional microscopy analysis. *J Biol Chem* **280**, 30392-9.

de Grauw, C. J. and Gerritsen, H. C. (2001). Multiple Time-Gate Module for Fluorescence Lifetime Imaging. *Appl. Spectrosc.* **55**, 670.

Fooksman, D. R., Gronvall, G. K., Tang, Q. and Edidin, M. (2006). Clustering Class I MHC Modulates Sensitivity of T Cell Recognition. *J Immunol* **176**, 6673-6680.

Garcia-Parajo, M. F., Koopman, M., van Dijk, E. M. H. P., Subramaniam, V. and van Hulst, N. F. (2001). The nature of fluorescence emission in the red fluorescent protein DsRed, revealed by single-molecule detection. *Proceedings of the National Academy of Sciences* **98**, 14392-14397.

Gautier, I., Tramier, M., Durieux, C., Coppey, J., Pansu, R. B., Nicolas, J. C., Kemnitz, K. and Coppey-Moisan, M. (2001). Homo-FRET microscopy in living cells to measure monomer-dimer transition of GFP-tagged proteins. *Biophys J* **80**, 3000-8.

Jares-Erijman, E. A. and Jovin, T. M. (2003). FRET imaging. *Nat Biotechnol* **21**, 1387-95.

Krauss, G. (2001). Biochemistry of Signal Transduction and Regulation. Weinheim: Wiley-VCH.

Lidke, D. S., Nagy, P., Barisas, B. G., Heintzmann, R., Post, J. N., Lidke, K. A., Clayton, A. H., Arndt-Jovin, D. J. and Jovin, T. M. (2003). Imaging molecular interactions in cells by dynamic and static fluorescence anisotropy (rFLIM and emFRET). *Biochem Soc Trans* **31**, 1020-7.

Lidke, K. A., Rieger, B., Lidke, D. S. and Jovin, T. M. (2005). The role of photon statistics in fluorescence anisotropy imaging. *IEEE Trans Image Process* **14**, 1237-45.

Niwa, H., Inouye, S., Hirano, T., Matsuno, T., Kojima, S., Kubota, M., Ohashi, M. and Tsuji, F. I. (1996). Chemical nature of the light emitter of the Aequorea green fluorescent protein. *Proceedings of the National Academy of Sciences* **93**, 13617-13622.

Runnels, L. W. and Scarlata, S. F. (1995). Theory and application of fluorescence homotransfer to melittin oligomerization. *Biophys J* **69**, 1569-83.

Saffarian, S., Li, Y., Elson, E. L. and Pike, L. J. (2007). Oligomerization of the EGF receptor investigated by live cell fluorescence intensity distribution analysis. *Biophys J* **93**, 1021-31.

Sharma, P., Varma, R., Sarasij, R. C., Ira, Gousset, K., Krishnamoorthy, G., Rao, M. and Mayor, S. (2004). Nanoscale organization of multiple GPI-anchored proteins in living cell membranes. *Cell* **116**, 577-89.

Siegel, J., Suhling, K., Leveque-Fort, S., Webb, S. E. D., Davis, D. M., Phillips, D., Sabharwal, Y. and French, P. M. W. (2003). Wide-field time-resolved fluorescence anisotropy imaging (TR-FAIM): Imaging the rotational mobility of a fluorophore. *Review of Scientific Instruments* **74**, 182.

Squire, A., Verveer, P. J., Rocks, O. and Bastiaens, P. I. (2004). Red-edge anisotropy microscopy enables dynamic imaging of homo-FRET between green fluorescent proteins in cells. *J Struct Biol* **147**, 62-9.

Tanaka, F. and Mataga, N. (1979). Theory of time-dependent photo-selection in interacting fixed systems. *Photochemistry and Photobiology* **29**, 1091-1097.

Teramura, Y., Ichinose, J., Takagi, H., Nishida, K., Yanagida, T. and Sako, Y. (2006). Single-molecule analysis of epidermal growth factor binding on the surface of living cells. *Embo J* **25**, 4215-22.

Ulbrich, M. H. and Isacoff, E. Y. (2007). Subunit counting in membrane-bound proteins. *Nat Meth* **4**, 319.

Valeur, B. (2002). Molecular Fluorescence. Principles and Applications. Weinheim: Wiley-VCH.

van Belzen, N., Rijken, P. J., Hage, W. J., de Laat, S. W., Verkleij, A. J. and Boonstra, J. (1988). Direct visualization and quantitative analysis of epidermal growth factor-induced receptor clustering. *J Cell Physiol* **134**, 413-20.

Varma, R. and Mayor, S. (1998). GPI-anchored proteins are organized in submicron domains at the cell surface. *Nature* **394**, 798-801.

Volkmer, A., Subramaniam, V., Birch, D. J. S. and Jovin, T. M. (2000). One- and Two-Photon Excited Fluorescence Lifetimes and Anisotropy Decays of Green Fluorescent Proteins. *Biophys. J.* **78**, 1589-1598.

Wittig, I., Braun, H.-P. and Schagger, H. (2006). Blue native PAGE. *Nat. Protocols* **1**, 418.

Yang, F., Moss, L. G. and Phillips, G. N. (1996). The molecular structure of green fluorescent protein. *Nat Biotech* **14**, 1246.

Yeow, E. K. L. and Clayton, A. H. A. (2007). Enumeration of Oligomerization States of Membrane Proteins in Living Cells by Homo-FRET Spectroscopy and Microscopy: Theory and Application. *Biophys. J.* **92**, 3098-3104.

Yu, X., Sharma, K. D., Takahashi, T., Iwamoto, R. and Mekada, E. (2002). Ligand-independent Dimer Formation of Epidermal Growth Factor Receptor (EGFR) Is a Step Separable from Ligand-induced EGFR Signaling. *Mol. Biol. Cell* **13**, 2547-2557.

Zacharias, D. A., Violin, J. D., Newton, A. C. and Tsien, R. Y. (2002). Partitioning of lipid-modified monomeric GFPs into membrane microdomains of live cells. *Science* **296**, 913-6.

Zhu, H.-J., Iaria, J., Orchard, S., Walker, F. and Burgess, A. W. (2003). Epidermal Growth Factor Receptor: Association of Extracellular Domain Negatively Regulates Intracellular Kinase Activation in the Absence of Ligand. *Growth Factors* **21**, 15 - 30.

Chapter 5

Ligand-induced EGF receptor oligomerization is kinase-dependent and promotes internalization

Erik G. Hofman[a], Arjen N. Bader[b], Dave van den Heuvel[b], Jarno Voortman[a], Arie J. Verkleij[a], Hans C. Gerritsen[b], and Paul M.P. van Bergen en Henegouwen[a]

[a] Cellular Architecture and Dynamics, Science Faculty, Utrecht University, Utrecht, the Netherlands

[b] Molecular Biophysics, Science Faculty, Utrecht University, Utrecht, the Netherlands

Submitted

Abstract

The activation model of the EGFR predicts that binding of EGF induces the dimerization of the EGFR leading to allosteric activation of the intracellular tyrosine kinase. Subsequently, the EGFR is shown to oligomerize without known function. In this study, we have used confocal time-resolved fluorescence anisotropy imaging microscopy (CTRFAIM) to investigate the oligomerization of the EGFR. Our data show that in the absence of ligand, ~40% of the EGFR population is dimerized. EGF stimulation induces the oligomerization of the EGFR. This ligand-induced oligomerization was not observed for EGFRs lacking either tyrosine kinase activity or nine different tyrosine kinase substrate residues. Mimicking receptor oligomerization using EGFRs fused with the dimerization domain FKBP resulted in a drastically increased receptor internalization. Our data demonstrate, that EGF-induced receptor oligomerization is the result of EGFR signaling and promotes receptor internalization.

Introduction

The epidermal growth factor receptor (EGFR or ErbB1) is implicated in growth and differentiation of a range of cell types. Like other members of the ErbB receptor tyrosine kinase family i.e. ErbB2, 3 and 4, it is composed of a ligand binding extracellular domain (ectodomain), a transmembrane stretch and an intracellular domain containing the intrinsic tyrosine kinase and a C-terminal tail containing several tyrosine residues (Ullrich et al., 1984). The first step in the signal transduction cascade is the binding of ligands such as EGF or TGF-α to the ectodomain, resulting in receptor dimerization and subsequent phosphorylation of tyrosine residues in the intercellular tail. Ligand binding results in allosteric activation of the tyrosine kinase allowing phosphorylation of the substrate domain by their mutual tyrosine kinases (Zhang et al., 2006). Dimerization with other non-phosphorylated receptors is subsequently responsible for amplification of the signal (Ichinose et al., 2004; Verveer et al., 2000). The phosphotyrosines serve as docking sites for adaptor proteins and kinases such as Grb2 and Shc, containing phosphotyrosine-specific SH2 or PTB domains. Eventually, the receptor is internalized via both clathrin-dependent and independent pathways (Sigismund et al., 2005).

Although EGF-binding and dimerization seem to be strictly connected, biochemical studies have demonstrated that in resting cells the receptor is already found on the cell surface as non-activated dimers, the so-called predimers. This phenomenon was initially demonstrated using electron microscopy and immunogold labeling of the EGFR (van Belzen et al., 1988). In the resting cell ~35% of the total receptor population was identified as dimers. These observations were confirmed using protein chemical crosslinking and co-immunoprecipitation with differentially tagged EGFRs (Moriki et al., 2001; Yu et al., 2002; Zhu et al., 2003). More recently, light microscopical methods have also been used to address this question. In the absence of ligands EGFR pre-dimerization has now been demonstrated using fluorescence correlation microscopy, steady-state fluorescence anisotropy, Förster resonance energy transfer and single molecule imaging (Gadella and Jovin, 1995; Lidke et al., 2003; Saffarian et al., 2007; Sako et al., 2000; Teramura et al., 2006; van Belzen et al., 1988). Clayton and coworkers have used image correlation microscopy to show that in the absence of ligand EGFR aggregates into clusters of 2.2 receptors per cluster increasing to 3.7 receptors per cluster in the presence of ligand. However, factors controling EGFR oligomerization or the function for receptor oligomerization are poorly understood.

In this paper we have used confocal time-resolved fluorescence anisotropy imaging microscopy (CTRFAIM) to investigate a possible function of the intracellular domain in the regulation of EGFR oligomerization. This method is based upon Förster resonance energy transfer between identical fluorophores (homo-FRET), and can detect nanometer proximity between identical reporter fluorophores such as GFP with high sensitivity. Application of this novel method has shown that in the resting cell ~40% of the total EGFR population is already present as predimers (chapter 4 of this thesis). A large increase in receptor oligomerization

is seen after ligand binding, corresponding to clustersizes larger than 3 receptors per cluster or more. This EGF-induced receptor clustering requires both kinase activity and the substrate tyrosine residues. Inducing oligomerization using the FKBP dimerization domains demonstrates that this receptor clustering is found to enhance EGFR internalization after ligand-induced receptor stimulation.

Materials and methods

Materials

Mouse anti-EGFR antibody was purchased from Santa Cruz Biotechnology (Santa Cruz, CA), mouse anti-Tyr1068 phospho EGFR antibody was from Cell Signaling Technologies (Danvers, MA), mouse anti-phosphotyrosine (clone PY20) antibody was from BD Biosciences (Alphen aan de Rijn, the Netherlands) and mouse anti-GFP antibody (mixture of two monoclonals) was from Roche (Mannheim, Germany). BSA (fraction V) and protein A Sepharose were from Sigma (Zwijndrecht, the Netherlands). Lipofectamine 2000 and Zeocin were from Invitrogen (Carlsbad, CA). Human EGF was from Oxford Biotechnology (Oxfordshire, UK). The ARGENT regulated homodimerization kit including plasmids pC4-Fv1E and pC4-Fv2M and ligand AP20187 was from Ariad (Cambridge, MA). Carrier free Na-^{125}I was obtained from Perkin-Elmer (Waltham, MA). CellBind plates were from Corning (Lowell, MA). DMEM was from Invitrogen and Hepes/DMEM was from PAA (Pasching, Austria).

Plasmid construction

The starting plasmid, pEGFP-N1, was PCR amplified using primers 5'-atat<u>actagt</u>atggtgagcaa gggcgaggagctgttc-3' and 5'-atat<u>ggatcc</u>ttacttgtacagctcgtccatgccgagagt-3', introducing flanking restriction sites SpeI and BamHI (underlined). The eGFP PCR product was inserted into the corresponding sites of pC4-Fv1E to produce pC4-Fv1E-GFP. A monomeric variant of eGFP (mGFP) was constructed by sited directed mutagenesis using primers 5'-cagtcc**aag**ctgagcaaa gaccccaacgagaagcgcgatcac -3' and 5'-gtgatcgcgcttctcgttggggtctttgctcag**ctt**ggactg-3' (mutated codon in bold) as described previously by (Zacharias et al., 2002).

Plasmids encoding wildtype EGFR (pCDNA3.1-EGFR), K721A EGFR or 9YF mutations (kindly provided by S. Sigismund, Milan, Italy) were used as templates for PCR amplification. EGFR constructs were PCR amplified with primers 5'-atatat<u>caattg</u>atgcgaccctccgggacggccg-3' and 5'-atatatt<u>ctaga</u>tgctccaataaattcactgctttgtgg-3' introducing flanking MunI and XbaI sites (underlined), and inserted into pC4-Fv1E-mGFP. To construct EGFR-mGFP and EGFR K721A-mGFP, the FKBP domain was removed by digestion with XbaI and SpeI and self-ligation. For cells stably expressing the gene products, the EGFR constructs were subcloned into pCDNA3.1-zeo (Invitrogen, Carlsbad, CA). Final constructs were amplified in *E.coli*, purified using an endotoxin-free plasmid isolation kit and confirmed by sequencing.

Cell culture

NIH 3T3 2.2 cells lacking detectable expression of EGFR, Her14 and A431 cells stably expressing human EGFR were grown in DMEM supplemented with 2 mM L-glutamine and 7.5% foetal calf serum, at 37°C in 5% CO_2 under humidified conditions. Transient transfection with all constructs was performed with Lipofectamine 2000 according to the manufacturer's protocol. Cells stably expressing EGFR-FKBP-mGFP or its mutants were produced by

growing them under selective conditions (500 µM Zeocine) for 2 months, and FACS-sorting for GFP expression. As a control, untransfected cells were grown under similar conditions, which resulted in complete cell death within two weeks. For microscopy, cells were grown on coverslips for 2 days to 50% confluency. For ^{125}I-EGF internalization cells were grown on 24-wells CellBind plates.

EGF-iodination

^{125}I-EGF was prepared by the chloramine T method as described previously (Berkers et al., 1991). Briefly, 1 µg of EGF dissolved in 0.5 M K-phosphate buffer pH 7.5 was allowed to react with 1 mCi of ^{125}I and 75 µg/ml chloramine T for 10 minutes. The reaction was stopped with Na-bisulfite. ^{125}I-EGF was separated from free label on a AG1-X8 ion-exchange column (Bio-Rad, Hercules, CA), and eluted in 3 fractions of 0.5 ml. The second fraction contained the majority of ^{125}I-EGF. BCA precipitation showed that 98% of ^{125}I was precipitable, and the specific activity of ^{125}I-EGF was >400,000 cpm/ng.

^{125}I-EGF internalization

Cells grown to 80% confluency in 12-well plates were serumstarved in DMEM supplemented with 0.5% FCS for 16 hrs. One hour prior to EGF stimulation, cells were placed on ice and incubated for 1 hour with binding medium (DMEM, 20 mM HEPES, pH 7.4, 0.1 % BSA) supplemented with either 1 µM AP20187, or 0.1% ethanol (mock). Then, cells were placed for 5 min. at 37°C to recover. Then, 1 ng/ml ^{125}I-EGF was added in a total volume of 0.5 ml, for 3, 6, 9 and 12 min. at 37ºC. Cells were put on ice to stop further internalization and washed twice with ice-cold PBS to remove unbound ligand. Subsequently, cells were incubated for 5 min. with ice-cold acid wash buffer (25 mM NaOH/CH_3COOH, pH 3.8, 150 mM NaCl), followed by one wash step with ice-cold acid wash buffer. Samples were collected and, after one PBS wash, cells were lysed in 1M NaOH. Acid wash samples (representing the surface bound fractions) and cell lysates (representing the internalized fractions) were counted in a γ-counter (Perkin-Elmer). The experiment contained triplicate samples. The ratio of internalized and surface radioactivity was plotted against time. The linear regression coefficient of the dependence of this ratio on time represents the specific rate constant for internalization.

EGFR phosphorylation assays

NIH 3T3 2.2 cells were grown to subconfluency in 12-well plates, and Lipofectamine 2000-transfected with pEGFR-FKBP-GFP, pEGFR-FKBP-mGFP, pEGFR-K721A-FKBP-mGFP or pEGFR-FKBP-9YF-mGFP. After 16 hrs, the cells were transferred to fresh 12-well plates and grown for 24 hrs. Overnight, the culture medium was replaced with low-serum DMEM (0.5% FCS). Cells were incubated with 1 µM AP20187 for 1 hr or with 8nM EGF for 10 min., or a combination of both. After washing twice with PBS, the cells were lysed in lysis buffer

(1% Triton X-100, 100 mM NaCl, 2 mM EDTA, 50 mM Tris-HCl, pH 7.4, Complete™ mixture of protease inhibitors). The EGFR-FKBP-mGFP constructs were immunoprecipitated with protein A-sepharose beads and anti-GFP, and size-separated with SDS-PAGE, followed by immunoblotting with anti-phosphotyrosine or anti-GFP.

Confocal time-resolved fluorescence anisotropy imaging microscopy

Fluorescence anisotropy microscopy was essentially performed as described previously (Bader et al., 2007b). A 473 nm pulsed diode laser (Becker and Hickel BDL-473; Berlin, Germany) operating at 50 MHz was directly coupled into the modified confocal scan head (C1, Nikon Instruments Europe, Badhoevedorp, The Netherlands). No optical fibers were used in excitation since this would complicate polarization dependent measurements. A linear polarizer (Meadowlark, Frederick, CO, USA) was positioned in the laser beam to define the excitation polarization direction. The microscope was equipped with a 60x, NA=1.20 water immersion objective (Plan Apo, Nikon). The excitation beam did not fill the whole back aperture of the objective. The effective excitation NA amounted to approximately 0.5. For GFP a value of r_0 = 0.38 was found instead of the theoretical value of 0.4.

The emission light was split into a parallel and perpendicular channel with a broadband polarizing beam splitter cube (PBS, OptoSigma, Santa Ana, CA, USA). The two emission channels were both fiber coupled to detection systems consisting of a fluorescence lifetime imaging module (LIMO, Nikon Instruments BV, Badhoevedorp, The Netherlands)(de Grauw and Gerritsen, 2001) equipped with an internal photon counting photomultiplier tube. For each pixel in the image, the LIMO's collect photons in four 2 ns wide consecutive time gates. By employing two synchronized LIMOs, one for each polarization direction, a four channel time-resolved anisotropy decay can be acquired for each pixel. An acquisition time of 3ms per pixel was applied. A threshold of 200 counts was applied (maximum number of counts was approximately 4500). All images were recorded in a 160x160 pixel mode, covering an area of 50x50 µm. The procedures of data analysis, synchronization and correction for sensitivity differences between the two channels were based on using reference dyes. This procedure was described in detail previously (Bader et al., 2007a; Bader et al., 2007b).

Results

EGFR forms predimers on the plasma membrane

To study the clustering of the EGFR in the plasma membrane we have developed a novel method, which we have indicated as confocal time-resolved fluorescence anisotropy imaging (CTRFAIM). This time-resolved approach based on homo-FRET allows the direct quantification of the number of fluorophores in a nanometer scale cluster. This is determined from the limiting anisotropy (r_{inf}) in the time-resolved anisotropy decay. Unlike the steady-state anisotropy, this measure is not frustrated by fluctuations in the efficiency of the energy transfer. For monomers

the value of $r_{inf} = r_{mono} \approx 0.4$ (the anisotropy of monomers), and r_{inf} decreases to zero with increasing degree of clustering. The results are presented as the degree of depolarization (r_{inf}/r_{mono}). For each set of experiments, the anisotropy of a strictly monomeric reference sample, in our case a solution of 10 µM GFP in 50/50 glycerol/buffer, is measured to determine r_{mono}. Per condition five cells were analysed; the average value of r_{inf} per cell was used for statistic analysis.

To determine the oligomerization state of the EGFR we fused the coding sequence of EGFR with a GFP variant mutated at position 206 (A206K), which reduces their dimerization binding affinity to >74 mM (Fig. 1A) (Zacharias et al., 2002). Mouse fibroblasts, which are devoid of endogenous EGFR (NIH 3T3 clone 2.2), were stably transfected with a vector encoding EGFR-mGFP. Comparison of expression levels using FACS indicated that the EGFR-mGFP cells express ~50,000 receptors/cell. Control experiments demonstrated that

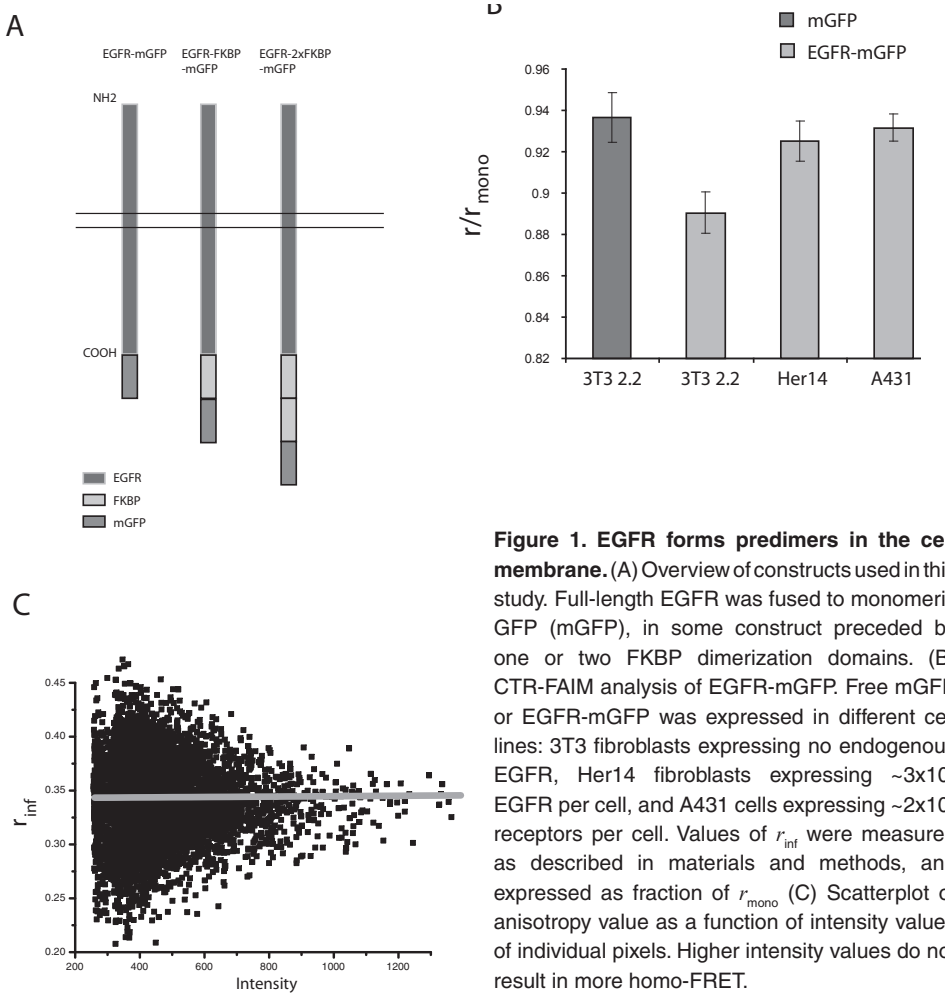

Figure 1. EGFR forms predimers in the cell membrane. (A) Overview of constructs used in this study. Full-length EGFR was fused to monomeric GFP (mGFP), in some construct preceded by one or two FKBP dimerization domains. (B) CTR-FAIM analysis of EGFR-mGFP. Free mGFP or EGFR-mGFP was expressed in different cell lines: 3T3 fibroblasts expressing no endogenous EGFR, Her14 fibroblasts expressing ~3x10^5 EGFR per cell, and A431 cells expressing ~2x10^6 receptors per cell. Values of r_{inf} were measured as described in materials and methods, and expressed as fraction of r_{mono} (C) Scatterplot of anisotropy value as a function of intensity values of individual pixels. Higher intensity values do not result in more homo-FRET.

activation of this EGFR-mGFP construct is indistinguishable from the wildtype EGFR (data not shown), which is in agreement with other publications (Carter and Sorkin, 1998; Clayton et al., 2005). As a cellular reference for a monomeric protein we used mGFP. Cells expressing the mGFP proteins were fixed and analyzed by CTRFAIM. EGFR-mGFP has a significant higher loss of anisotropy as compared to cytoplasmic mGFP (Fig 1B). The anisotropy loss indicates that ~40% of the EGFR is present on the cell membrane as pre-existing dimers. To further proof that the anisotropy loss is due to receptor predimer formation, we co-expressed EGFR-mGFP in cells with a high level of endogenous EGFRs ($3x10^5$ and $2x10^6$ receptors/cell for HER14 and A431 cells respectively). This is based upon the idea that heterodimerization of EGFR-mGFP with endogenous EGFR does not result in homo-FRET, resulting in anisotropy values similar as the mGFP control values (Lidke et al., 2003). Anisotropy analysis indicates that this is indeed the case: the anisotropy of EGFR-mGFP in these cells was increased in HER14 as well as A431 cells to the situation for mGFP (Fig. 1B). We subsequently analysed whether this predimer formation was dependent upon the EGFR concentration. The intensity values of individual pixels, representing a large population of pixels with different EGFR expressions levels, were plotted against their anisotropy value. No differences in anisotropy values were apparent in pixels with higher intensities indicating that EGFR predimer formation is concentration independent (Fig. 1C). In conclusion, by using CTRFAIM we provide evidence that ~40% of the total EGFR-mGFP population exists as predimers on the plasma membrane of NIH 3T3 cells.

Ligand-induced receptor oligomerization

We next investigated the effect of EGF on the oligomerization state of its receptor using CTRFAIM. The effect of EGF stimulation on the clustering of EGFR was determined with mGFP fusion constructs, expressed in 3T3 2.2 fibroblasts. Cells were treated for 10 min. at 37° C with 8 nM EGF and fixed using 4% formaldehyde. Confocal microscopy reveals the presence of the EGFR-mGFP constructs in the plasma membrane with more intense staining in membrane ruffles (Fig. 2A). In EGF-stimulated cells EGFR-mGFP is present on intracellular vesicles reflecting the EGF-induced internalization of the active EGFR (Fig. 2A). This can be seen as an intrinsic control for receptor activation. Anisotropy experiments were subsequently performed, and effects on anisotropy r are indicated in false colors (Fig. 2A). A clear effect of EGF on the anisotropy is observed. The anisotropy values of two representative cells from both conditions show a comparable Gaussian distribution, showing a true shift in the mean value of r (Fig. 2B). The almost instant drop of r as shown in the time-gated decay, shows that a high homo-FRET efficiency was present (Fig. 2C). The average anisotropy was found to be significantly lower in the EGF-stimulated cells (Fig. 2D). Subsequently, based on earlier described correlations between anisotropy and clustersize, the average clustersize per pixel was determined and divided into three groups: monomers, dimers and a group of oligomers with ≥ 3 receptors (chapter 4 of this thesis). The EGF-induced oligomerization of the receptor

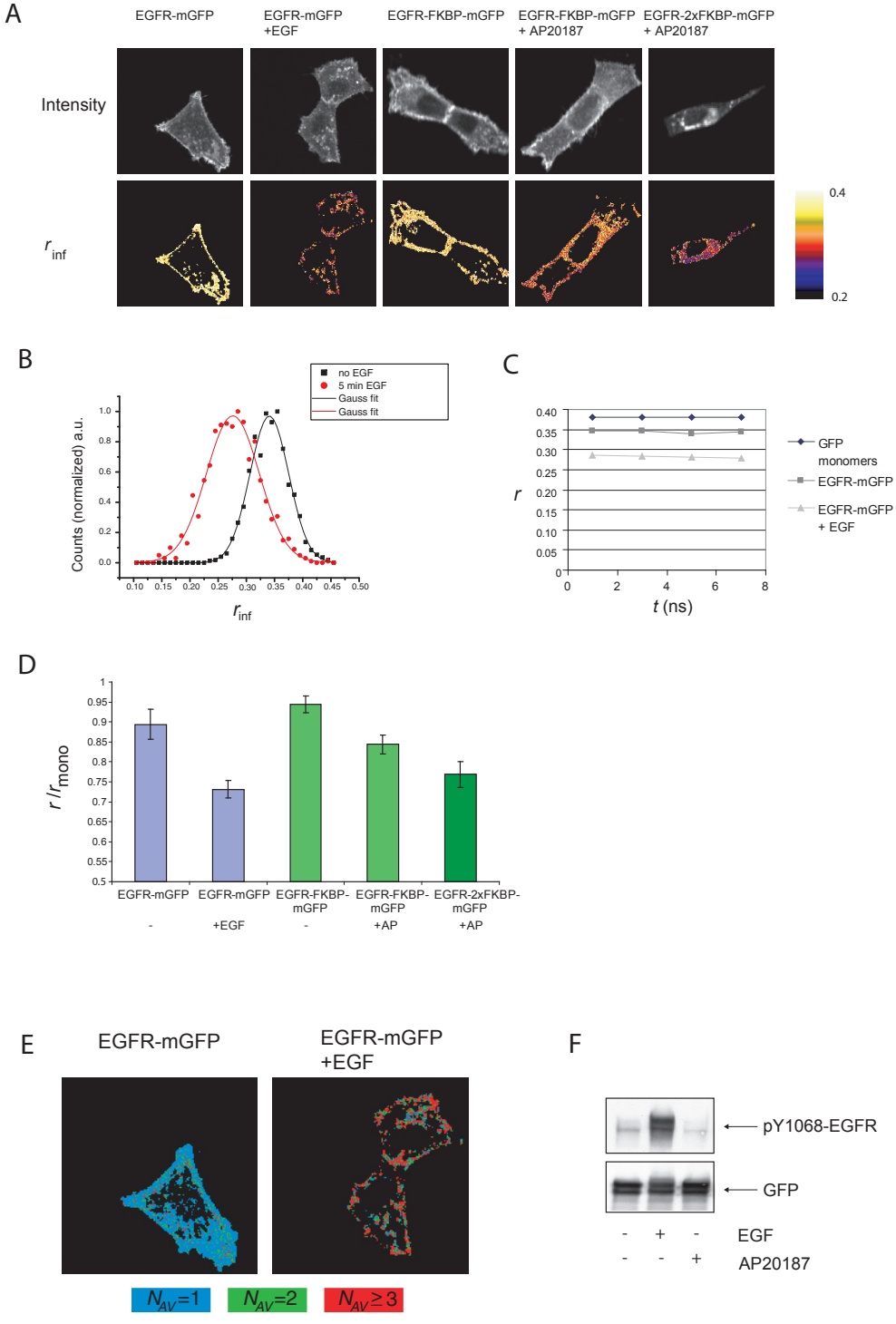
A
EGFR-mGFP
EGFR-mGFP +EGF
EGFR-FKBP-mGFP
EGFR-FKBP-mGFP + AP20187
EGFR-2xFKBP-mGFP + AP20187
Intensity
r_{inf}
0.4
0.2
B
no EGF
5 min EGF
Gauss fit
Gauss fit
Counts (normalized) a.u.
r_{inf}
C
r
t (ns)
GFP monomers
EGFR-mGFP
EGFR-mGFP + EGF
D
r / r_{mono}
EGFR-mGFP -
EGFR-mGFP +EGF
EGFR-FKBP-mGFP -
EGFR-FKBP-mGFP +AP
EGFR-2xFKBP-mGFP +AP
E
EGFR-mGFP
EGFR-mGFP +EGF
N_{AV}=1
N_{AV}=2
$N_{AV}\geq 3$
F
pY1068-EGFR
GFP
EGF
AP20187

Figure 2. EGFR-mGFP is oligomerized after EGF stimulation. (A) Cellular distribution of GFP intensities and anisotropy values. NIH 3T3 2.2 cells expressing EGFR-mGFP were stimulated with 8 nM EGF for 10 minutes, or left untreated. Cells expressing EGFR-FKBP-mGFP or EGFR-2xFKBP-mGFP were incubated for 2 hours with 1 μM AP20187, or left untreated. Values of r_{inf} were measured as described in materials and methods (B) Distribution of anisotropy values from EGF-stimulated or untreated cells expressing EGFR-mGFP (C) Time-gated anisotropy decay of representative cells. A solution of 10 μM GFP in 50% glycerol was used a monomeric reference (D) Average anisotropy values of constructs. The limiting anisotropy value r_{inf} is expressed as fraction of r_{mono}. (E) Representation of clustersize values of EGFR-mGFP before and after EGF stimulation. Anisotropy values of cells shown in (B) were classified according to equation 8 from chapter 4 (F) AP20187-induced EGFR predimer formation does not affect EGFR activation. 3T3 2.2 cells expressing EGFR-FKBP-GFP were incubated with 1 μM AP20187 for 2 hours or 8 nM EGF for 10 minutes, or a combination of both. Cell lysates were analysed by immunoblotting using antibodies against the activated EGF receptor (pY1068) or against GFP to detect the total EGFR-FKBP-GFP population.

is very clear from these data (Fig. 2E). The majority of EGF receptors were found in nanoscale clusters of 3 or more receptors per cluster.

To further proof the existence of the EGFR oligomers with CTRFAIM, we also used reference proteins. These reference proteins contain one copy of the monomeric form of GFP (mGFP) and one or two copies of the dimerization domain from the peptidyl-prolyl isomerase FKBP12 (Fig. 1A). Addition of the ligand for the FKBP domain (AP20187) induces the dimerization of the FKBP-mGFP construct and oligomerization for the 2xFKBP-mGFP construct (chapter 4, Bader et al). First of all, we analyzed the effect of AP20187-induced EGFR dimerization or oligomerization on the activity state of the receptor. In contrast to previously published data, our constructs were not activated by the addition of AP20187 (Fig. 2F)(Wang et al., 2007). As judged from the confocal images, the addition of AP20187 to the cells induced the internalization of the EGFR-FKBP-mGFP constructs, with a much stronger internalization for the 2xFKBP contruct. The AP20187-induced internalization of such EGFR constructs is in agreement with studies from Wang et al., and can be seen as an internal control for the functionality of the FKBP ligand (Wang et al., 2007). Anisotropy analysis of cells expressing the EGFR-FKBP-mGFP constructs show a clear reduction in anisotropy after incubation with AP20187, and this reduction was clearly stronger for the EGFR-2xFKBP-mGFP construct (Fig 2A+D). This indicates that the anisotropy detection can distinguish between dimerization and oligomerization. By comparing these values with the value from the EGFR-mGFP constructs we can conclude that the EGFR-mGFP receptor becomes oligomerized upon stimulation with EGF.

Receptor oligomerization is kinase-dependent

Structural data of the ectodomain suggest that ligand-induced receptor dimerization is orchestrated by conformational changes in the ectodomain. Crystal studies have suggested that the EGFR ectodomain might have both head-to-head and back-to-back interactions suggesting that the ectodomain might be sufficient for oligomerization as well (Garrett et al., 2002). We anticipated, however, that the affinity between the head-to-head dimer may be not

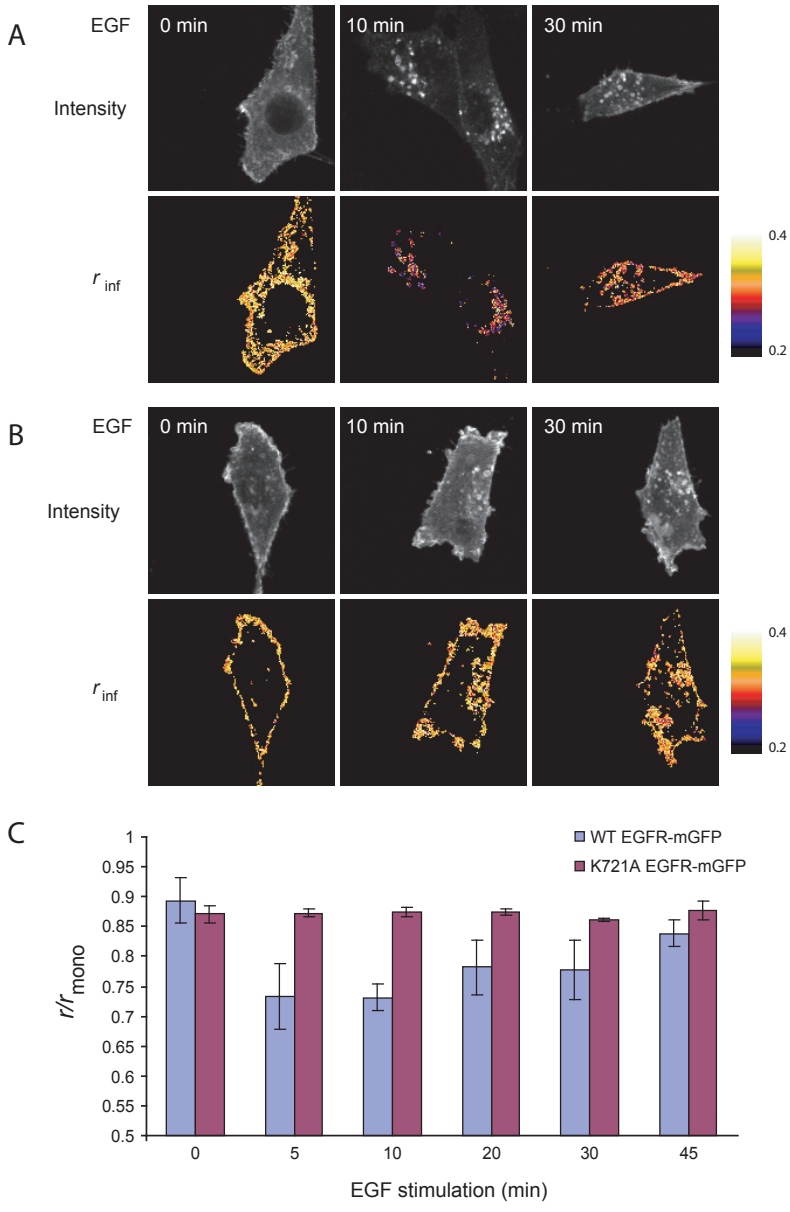

Fig 3. EGFR kinase activity is essential for EGF-induced oligomerization.
(A) Cellular distribution of GFP intensities and anisotropy values of 3T3 2.2 cells expressing EGFR-mGFP, followed in time during stimulation with 50 ng/ml EGF. The limiting anisotropy value is determined as described in materials and methods (B) Cellular distribution of GFP intensities and anisotropy values of 3T3 2.2 cells expressing EGFR K721A-mGFP, followed in time during stimulation with 50 ng/ml EGF. The limiting anisotropy value is determined as described in materials and methods (C) Average anisotropy data of wildtype EGFR-mGFP and kinase dead K721A EGFR-mGFP, followed in time during stimulation with 50 ng/ml EGF. The limiting anisotropy r_{inf} is expressed as fraction of r_{mono}.

be sufficient to stabilize the oligomer. We therefore searched for molecular determinants within the intracellular domain of the EGF receptor that are critical for receptor oligomerization.

To find out whether tyrosine kinase activity is involved in the oligomerization of the EGFR we used a kinase dead (K721A) EGFR construct fused with mGFP. Cells expressing EGFR-mGFP or EGFR K721A-mGFP were incubated for different time periods with 8 nM EGF, fixed and analyzed with CTRFAIM. For EGFR K721A-mGFP a distribution pattern was found that was similar to the wildtype receptor (Fig 3A+B). The mutant receptor was found predominantly in the membrane ruffles and after EGF-stimulation the receptor was internalized, although at a lower speed, as judged from the appearance of vesicles after 10-20 minutes (Fig. 3B), which is in agreement with previous studies (Stoorvogel et al., 2004; Wang et al., 2005). In the absence of ligand, the K721A receptor and wildtype receptors displays similar anisotropy values (Fig. 3C). For the wildtype receptors, the anisotropy values decreased within 5 minutes to values that correspond to oligomers (Fig. 3C). Ligand-induced EGFR oligomerization is maintained for at least 20 minutes after stimulation. These results are in agreement with electron microscopy studies previously performed by van Belzen et al (van Belzen et al., 1988). A gradual increase in anisotropy is seen from 10 to 45 minutes after activation. This decrease in homo-FRET may be the result of receptor dissociation or due to lysosomal degradation of the receptor oligomers. The oligomerization of the kinase dead mutant was analyzed for the same period of time. Remarkably, this mutant did not display a change in anisotropy for the entire observation period of 45 minutes. Based on these results we conclude that the ligand-induced EGF receptor oligomerization is a kinase-dependent process.

EGFR oligomerization requires receptor tyrosine phosphorylation

The primary substrate of the EGFR kinase domain is formed by a number of tyrosine residues within the intracellular tail. In addition, the kinase can interact with other kinases such as the non-receptor tyrosine kinase Src that can phosphorylate other tyrosines. This will eventually lead to tyrosine phosphorylation of EGFR. Since the activity of the kinase domain was found to be essential for EGFR oligomerization, we wanted to see whether preventing tyrosine phosphorylation had similar effects on receptor oligomerization as kinase deficiency. To investigate the role of the kinase-induced tyrosine phosphorylation in receptor clustering, we used an EGFR mutant in which nine known tyrosine residues were mutated into phenylalanines (EGFR-9YF). A fusion protein with FKBP was made as an internal control for the anisotropy system. In parallel, similar constructs with the wildtype and with the kinase-dead EGFR were produced.

We first performed control experiments regarding the tyrosine kinase activity and tyrosine phosphorylation of these constructs. Cells expressing these proteins were incubated with 8 nM EGF for 10 min., 1 μM AP20187 for 2 hrs, or a combination of both. After lysing the cells and immunoprecipitation with anti-GFP, the phosphorylation was determined by

immunoblotting with an anti-phosphotyrosine antibody (Fig. 4A). The wildtype EGFR-FKBP-mGFP protein is phosphorylated by EGF, both in the presence and in the absence of AP20187. In contrast, the K721A and 9YF mutants do not show tyrosine phosphorylation after incubation with EGF and/or AP20187.

We then investigated the effect of these mutations on the anisotropy. NIH 3T3 cells, stably expressing these contructs were, when indicated, preincubated with AP20187 for 1 hr, stimulated with 8 nM EGF for 10 min and fixed. In the absence of ligand, the anisotropy of the wildtype receptor, K721A and 9YF mutants is the same (Fig. 4B). A decrease in anisotropy values was observed for all contructs after AP20187 treatment, indicating that all three constructs are readily dimerizible. As expected, the wildtype receptor shows a decrease in anisotropy after EGF stimulation, as well as in the presence of AP20187, reflecting an increase

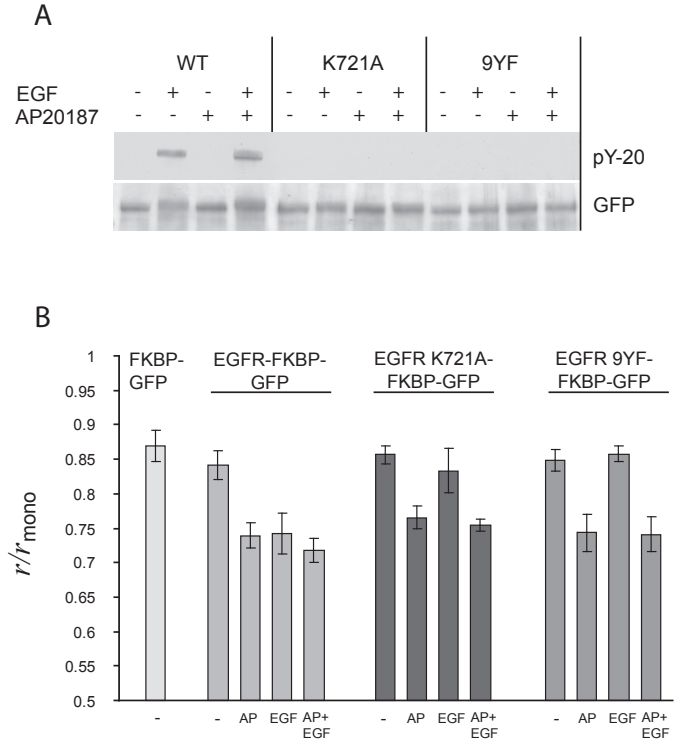

Fig 4. Tyrosine phosphorylation is required for EGF-induced oligomerization.
(A) Immunoblots from 3T3 2.2 cells expressing wildtype, K721A or 9YF EGFR-FKBP-GFP constructs. Cells were incubated with either 1 μM AP20187 for 2 hours, 8 nM EGF for 10 minutes, or a combination of both. After cell lysis fusion proteins were immunoprecipitated with an anti-GFP antibody, and immunoblotted with anti-phosphotyrosine or anti-GFP antibody. (B) Average anisotropy data of the cells expressing dimerization constructs in the absence or presence of AP20187, 8 nM EGF or both. The limiting anisotropy value r_{inf} is expressed as fraction of r_{mono}.

in homo-FRET and consequently oligomerization. Treatment of the cells expressing the K721A or 9YF mutants did not result in a change in anisotropy as compared to untreated cells. This observation demonstrates that the kinase dependent EGFR oligomerization is mediated by the phosphorylation of tyrosine residues in the intracellular domain of the EGFR.

EGFR clustering enhances receptor internalization

An important question is the possible function for the kinase-induced EGFR oligomerization. Modelling of EGFR activation via monomers and predimers shows that activation via the predimers would result in a 100x faster activation or phosphorylation of the receptor (Teramura et al., 2006). An important role for receptor oligomerization has been found in amplification and lateral propagation of the signal (Ichinose et al., 2004; Verveer et al., 2000). Consequently, the predimerization or even preoligomerization would result in a faster signaling and higher sensitivity of the cell for EGF. To test the possible role of predimer formation on EGFR activation, we expressed EGFR fused with one copy of FKBP (Fig. 1A). Cells were either pretreated with 1 μM AP20187 for 1 hr to induce predimer formation, or left untreated, followed by an incubation with 8 nM EGF for 10 min.at 37°C. Anisotropy analysis already showed that incubation of the cells expressing this construct leads to reduction in anisotropy reflecting the increase in EGFR predimers (Fig. 2B). However, combined treatment with AP20187 and EGF did not, at least under the conditions used, enhance receptor activation when compared to EGF alone indicating that no function for receptor predimerization in the EGFR activation process can be discerned (Fig 4A).

We next investigated a possible role for the kinase-induced EGFR oligomerization in the internalization process. For this purpose, cell lines stably expressing FKBP fusion protein of EGFR wildtype or EGFR K721A were incubated for a short period of time (< 12 min) with 8 nM EGF and/or 1 μM AP20187 for confocal microscopy and 1 ng/ml ^{125}I-EGF for the determination of the internalization rate constant. While the non-treated EGFR-mGFP is expressed in the plasma membrane, the EGF- and AP-treated cells show internalized EGFR as judged from the presence of intracellular endocytotic vesicles (Fig. 5A). The doubly treated cells, with both AP and EGF, show the most prominent internalization of the EGFR. Subsequently, the internalization speed was determined by measuring the ratio between surface and internalized ^{125}I-EGF, as described previously (Fallon et al., 2006). Plotting this ratio as a function of EGF-incubation time yields the internalization rate constant k_e. In the wildtype EGFR-FKBP-GFP construct this rate constant equals 0.0221 min^{-1}, which is clearly increased for ~30% to 0.0285 min^{-1} by a preincubation of the cells with AP20187, indicating that predimerization of the EGFR results in an enhancement of receptor internalization (Fig. 5B). Likewise, the internalization rate constant of the K721A construct was doubled from 0.0098 min^{-1} in the absence to 0.0202 min^{-1} in the presence of AP20187. We conclude that predimerization of the EGFR increases the internalization speed of the EGFR, independent of kinase activity. Kinase-dependent phosphorylation increases the internalization speed further.

Discussion

In order to get a better insight into the oligomerization before and during EGFR activation, we applied a novel non-invasive technique in which the oligomerization state of the total receptor population can be imaged: CTRFAIM. Time-resolved anisotropy decays give rise to more accurate determinations of protein clustering than steady-state measurements, as evaluated previously (chapter 4 of this thesis). In addition, reference EGFR constructs were used that

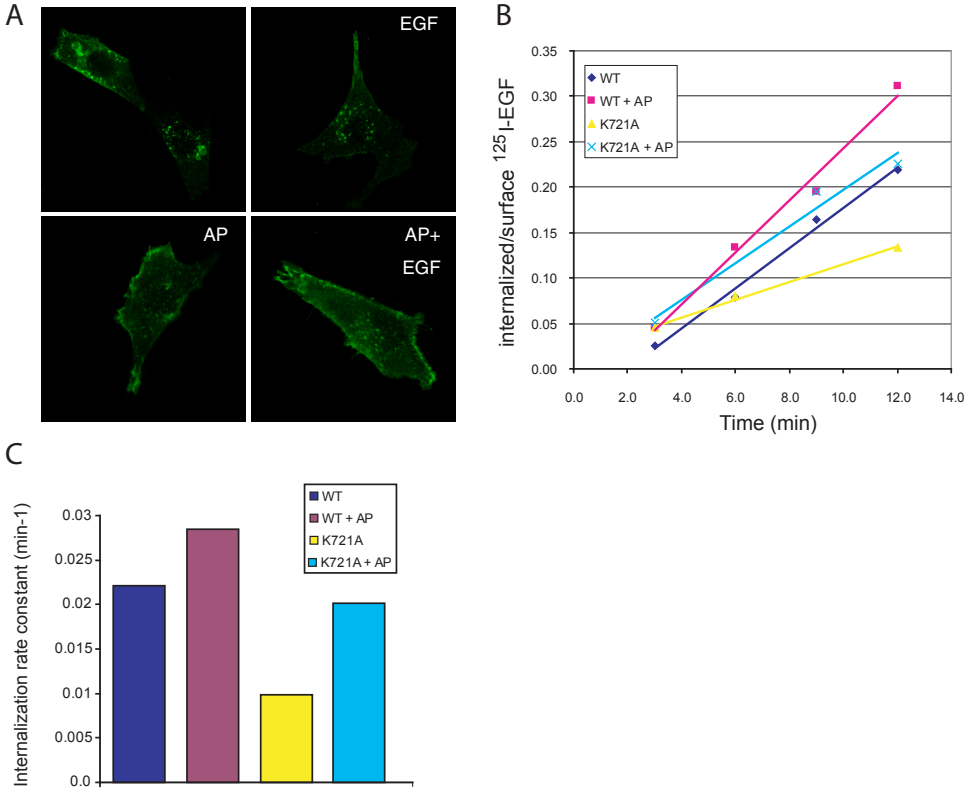

Fig 5. Oligomerization increases the internalization speed. (A) EGF and AP-mediated internalization. 3T3 2.2 cells expressing EGFR-FKBP-GFP were incubated at 37°C with either 8 nM EGF for 10 minutes, 1 μM AP20187 for 2 hours or a combination of both. (B) 3T3 2.2 cells expressing FKBP-constructs of either wildtype EGFR or K721A EGFR were incubated for 2 hours with 1 μM AP20187. Then, 1 ng/ml ^{125}I-EGF was added for different time periods (3, 6, 9, 12 minutes). After washing, the ratio of internalized versus surface ^{125}I-EGF was determined. (C) The internalization rate constant as determined from the slopes of the lines in fig 5B.

allow us to control dimerization or oligomerization by induced crosslinking. The reporter protein that we have used in this study is the monomeric mutant of enhanced GFP-A206K, or mGFP. This mutant was found to have a highly reduced association constant compared to wildtype,

and was therefore considered to be strictly monomeric (Zacharias et al., 2002).

Our CTRFAIM data clearly show that in resting cells the anisotropy of EGFR-mGFP is reduced when compared to cytosolic mGFP. Important for this study is the choice for mGFP as a reference molecule. A major difference between mGFP and the EGFR-mGFP fusion protein is the fact that mGFP can move freely in a three dimensional space, whereas the EGF receptor can only diffuse in the plane of the membrane. As association of proteins might be affected by the diffusion rate of the proteins, it would have been more appropriate to use a membrane-anchored mGFP as a reference protein. However, the organization of the plasma membrane into different compartments or domains is very likely to promote the clustering of membrane-inserted molecules. Moreover, the lack of rotational mobility in both mGFP and EGFR-mGFP, as deducted from the slope of the anisotropy decay, indicates that free mobility is equally restricted. Thus, mGFP is selected as an appropriate reference protein for this study.

Alternatively, EGFR predimer formation was demonstrated by diluting GFP-tagged EGFR with untagged EGFR in EGFR expressing cells. Assuming that EGFR-mGFP associates with equal preference to EGFR and EGFR-mGFP, the formation of hetero- or homodimers is proportional to the relative expression levels of both receptor types. The A431 and HER14 cell lines used in this study express approximately $2x10^6$ and $3x10^5$ receptors, respectively, whereas 3T3 2.2 cells are completely devoid of endogenous EGFR. As the amount of non-fluorescent receptor increased, a decrease in clustersize was found, which approximated the level of cytosolic monomeric GFP. Similar data were provided by Lidke et al, who used CHO cells instead of 3T3 fibroblasts (Lidke et al., 2003), indicating that predimerization is an intrinsic property of EGFR. The presence of EGFR predimers has now been demonstrated by a great variety of techniques. Our results using CTRFAIM are in high agreement with the original electronmicroscopical data obtained from A431 cell (van Belzen et al., 1988). By investigating EGFR clustering with gold-conjugated anti-EGFR monoclonal antibodies, it was found that 55% of the EGFR is monomeric, 35% dimeric and 10% oligomeric (clusters >3).

An interesting question is the mechanism that controls EGFR predimer formation. First of all, predimerization is not the result of basal receptor activity in the absence of EGF. For the kinase-dead EGFR, no significant differences in anisotropy values were obtained in the unstimulated state, suggesting that the formation of predimers is independent of kinase activity. Predimers may be formed between two opposite domains II in a back-to-back fashion, a dimer comparable to the dimer formed in the presence of EGF. The intramolecular tether between domains II and IV is suggested to be rather weak, and suggest an equilibrium of ~10% of the EGFR in the predimer configuration (Ferguson, 2004). However, the existence of stable EGFR back-to-back predimers is not very probable, since FRET studies using A431 cells have shown the occurrence of a conformational change in the ectodomain of predimers after EGF stimulation (Martin-Fernandez et al., 2002). Moreover, recent studies have shown that predimers are specifically recognized by the MoAb 806 suggesting another conformation

for the monomers or EGF-induced dimers (Gan et al., 2007). As shown by immunoprecipitation studies, both the extra- and the intracellular domains of the receptor contain elements that show interaction with each other, suggesting that these elements may cooperate in a low affinity binding of both domains for each other in the non-activated EGFR state resulting in predimer formation (Yu et al., 2002; Zhu et al., 2003). Indeed, deletion of an intracellular domain of EGFR was found to be required for predimer formation. Finally, cholesterol levels were found to regulate the number of predimers (Saffarian et al., 2007). As we previously demonstrated that the EGFR colocalizes with the lipid raft marker GM1 (chapter 2 of this thesis), we hypothese that the partitioning of EGFR in lipid raft domains might play a role in EGFR predimer formation.

The functional importance of EGFR predimerization is another issue that we have addressed in this study. The induction of predimers by means of artificial crosslinking has been done previously by introducing a Cys-residue just outside the cells (Sorokin et al., 1994). This resulted in an activation of the receptor kinase. This has alternatively been investigated by using the FKBP dimerization domain. Remarkably, our construct was not activated by the FKBP-dimerization, which is in constrast to previous studies (Wang et al., 2007). The fact that our FKBP fusion construct is not activated by AP20187 incubation is possibly the result of differences in the orientation of the dimerization domains in our constructs. In this respect, the relative geometry of the monomers seems to be critical for activation (Moriki et al., 2001). Our data clearly show that our FKBP-mediated dimerization of the receptor did not result in tyrosine phosphorylation. Thus, our FKBP-mediated predimerization system generates functional, non-active EGFR predimers.

EGFR activation modelling studies have shown that signaling via the predimer might occur two orders of magnitude faster than via the monomeric receptor simply because the time to find a binding partner is not required (Teramura et al., 2006). Enhancing the amount of EGFR predimers did not affect EGF-mediated signaling. This might be due to the fact that to find a role for predimers in signaling the amount of predimers should be lowered rather than increased. Moreover, a more precise analysis of concentration- and time-dependent effects are required to find an effect of predimer formation on signaling.

Our CTRFAIM data clearly show that EGF-stimulation causes an increase in the average clustersize of the EGFR. As deducted from the clustersize pictures (Fig. 2D), the majority of the ligand-stimulated EGF receptors on the plasma membrane is found in nanoscale clusters larger than 3 receptors. Furthermore, the EGF-induced oligomerization of EGFR-mGFP corresponds to the oligomerization obtained with the EGFR-2xFKBP-mGFP construct. This is in agreement with electronmicroscopical studies of A431 cells, which showed that after activation of the EGF receptors on the plasma membrane, 40% oligomers of 4 or more receptors were formed (van Belzen et al., 1988). In addition, Clayton et al showed by image correlation microscopy that EGF induced the formation of EGFR clusters with 3.7 receptors per clusters, which points to the formation of tetramers (Clayton et al., 2005). Although our

technical set up does not allow for clustersize determination in such detail, our observations using CTRFAIM are is full agreement with these data.

In contrast to other studies, we followed clustersize formation of EGFR also at the subcellular level as it trafficked from the cell surface to endosomes and probably lysosomes. Since this process includes recruitment and uptake into vesicles, one might argue that the observed increase in clustersize is the result of tight packing in these endosomes. Therefore it was surprising to see that the kinase-dead mutant of EGFR did not show an increase in clustersize after EGF stimulation, although it was internalized via vesicles. This observation shows that our clustersize data are not attributable to concentration of the receptor in endosomes, but describe merely a process of receptor oligomerization at nanoscale levels.

Similar as for the EGFR predimer we used the FKBP system to analyze for a possible function for the EGF-induced oligomerization. Induction of the predimerized state of the receptor resulted in a clear enhancement of receptor internalization. This was observed for both the kinase dead and the kinase active EGFR, although the effect on the kinase dead version was much more pronounced. The AP20187-induced dimerization appears to compensate for the lack of EGF-induced clustering, thereby increasing the internalization of kinase dead EGFR. Probably, the predimers are already associated to the preexisting internalization machinery as coated vesicles. This might be mediated by the double leucine motif present in the EGFR, as this motif was particularly found to mediate receptor internalization of kinase dead receptors (Wang et al., 2007). Even more dramatic effects may be expected for the EGFR-2xFKBP constructs, since microscopy recordings learned that this protein was highly internalized after incubation with AP20187 (Fig. 2A).

The most important observation of our study is that EGFR oligomerization is the result of receptor tyrosine kinase activity rather than provoking it. Similar results were obtained with the 9YF mutant, suggesting that the kinase-induced oligomerization is excerted via phosphotyrosines. The question remains which specific tyrosine residues are responsible for the EGF-induced oligomerization. As receptor clustering is clearly important for receptor internalization, the candidate residues may be found in those residues that have been found involved in the internalization process, which include 1045, 1068, and 1086. Tyrosine 1068 and 1086 form docking sites for Grb2, which serves as an adaptor protein for the E3 ligase Cbl, which is on his turn binding to residue Y1045. The RING domain of c-Cbl has been shown to be involved in the internalization process while also the Cbl-induced ubiquitination of the EGFR is involved in this process (Holler and Dikic, 2004; Jiang and Sorkin, 2003).

Alternatively, a role for the actin cytoskeleton might play a role in the oligomerization process. The EGF receptor is an actin-binding protein by itself, interacting directly with F-actin by residues 989-994 (den Hartigh et al., 1992; Stoorvogel et al., 2004) and in addition, via a second actin-binding domain that includes tyrosine 1148 (Song et al., 2008). Moreover, Grb2 is also connected to the actin cytoskeleton, and can recruit and activate the Wilcott-Aldrich Syndrome protein (WASp), which serve as a docking site for the actin related protein (Arp)2/3

complex (She et al., 1997). Finally, also residues 1148 and 1173 connect the EGF receptor to actin filaments as they form the binding sites for the adaptor protein Shc, which was found to have F-actin binding capacities (Thomas et al., 1995). The generation of more precise EGFR mutants will be required to understand this process completely.

Based upon our data the following sequence of events during the process of EGFR activation is proposed (Fig. 6). The receptor is present both as monomers and as predimers or even oligomers on the plasma membrane. Factors involved in the regulation of this system may involve the lipid composition of the membrane. Ligand binding induces a conformational change of the ectodomains leading to the formation of back-to-back dimers. Consequently, the intracellular kinase domains are rearranged, resulting in an activated asymmetric kinase dimer. Activated receptors oligomerize with non-activated receptors resulting in signal amplification and lateral propagation of the signal (Ichinose et al., 2004; Verveer et al., 2000). Subsequently, the phosphorylated tysosine residues induce recruitment of proteins that stabilize the receptor oligomers, and may include proteins from the endocytic machinery. This entrapment of active EGFR into clusters may finally lead to the endocytosis of the oligomerized receptors.

Acknowledgements

We want to thank Ger Arkesteijn for support with the FACS sorter, and Ariad Inc. for supplying the ARGENT regulated homodimerization kit.

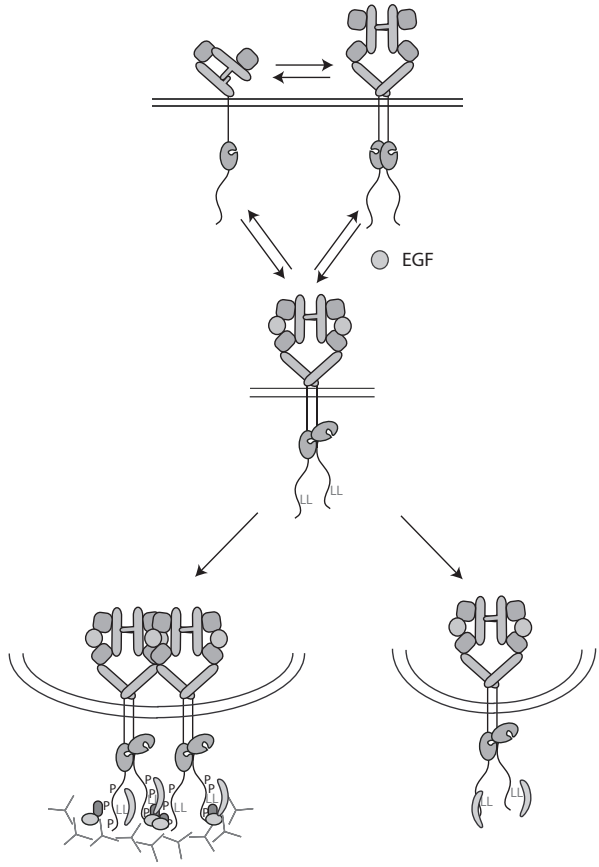

Fig 6. Summarizing model. Kinase activity and phosphorylation tyrosine are responsible for both ligand induced dimerization and oligomerization. The recruitment of phosphotyrosine binding proteins results in clathrin-mediated endocytosis. By blocking kinase activity and autophosphorylation, receptor clustering is prevented. In that scenario, internalization will take place mainly by the dileucine motif (LL). The factors involved in this pathway need further identification.

References

Bader, A. N., Hofman, E. G., van Bergen en Henegouwen, P. M. and Gerritsen, H. C. (2007a). Confocal time-resolved fluorescence anisotropy imaging. In *Imaging, Manipulation, and Analysis of Biomolecules, Cells, and Tissues V*, vol. 6441, pp. 64410C. San Jose, CA, USA: SPIE.

Bader, A. N., Hofman, E. G., van Bergen en Henegouwen, P. M. P. and Gerritsen, H. C. (2007b). Imaging of protein cluster sizes by means of confocal time-gated fluorescence anisotropy microscopy. *Opt. Express* **15**, 6934.

Berkers, J. A., van Bergen en Henegouwen, P. M. and Boonstra, J. (1991). Three classes of epidermal growth factor receptors on HeLa cells. *J Biol Chem* **266**, 922-7.

Carter, R. E. and Sorkin, A. (1998). Endocytosis of Functional Epidermal Growth Factor Receptor-Green Fluorescent Protein Chimera. *J. Biol. Chem.* **273**, 35000-35007.

Clayton, A. H., Walker, F., Orchard, S. G., Henderson, C., Fuchs, D., Rothacker, J., Nice, E. C. and Burgess, A. W. (2005). Ligand-induced dimer-tetramer transition during the activation of the cell surface epidermal growth factor receptor-A multidimensional microscopy analysis. *J Biol Chem* **280**, 30392-9.

de Grauw, C. J. and Gerritsen, H. C. (2001). Multiple Time-Gate Module for Fluorescence Lifetime Imaging. *Appl. Spectrosc.* **55**, 670.

den Hartigh, J. C., van Bergen en Henegouwen, P. M., Verkleij, A. J. and Boonstra, J. (1992). The EGF receptor is an actin-binding protein. *J Cell Biol* **119**, 349-55.

Fallon, L., Belanger, C. M., Corera, A. T., Kontogiannea, M., Regan-Klapisz, E., Moreau, F., Voortman, J., Haber, M., Rouleau, G., Thorarinsdottir, T. et al. (2006). A regulated interaction with the UIM protein Eps15 implicates parkin in EGF receptor trafficking and PI(3)K-Akt signalling. *Nat Cell Biol* **8**, 834-42.

Ferguson, K. M. (2004). Active and inactive conformations of the epidermal growth factor receptor. *Biochem Soc Trans* **32**, 742-5.

Gadella, T. W., Jr. and Jovin, T. M. (1995). Oligomerization of epidermal growth factor receptors on A431 cells studied by time-resolved fluorescence imaging microscopy. A stereochemical model for tyrosine kinase receptor activation. *J Cell Biol* **129**, 1543-58.

Gan, H. K., Walker, F., Burgess, A. W., Rigopoulos, A., Scott, A. M. and Johns, T. G. (2007). The epidermal growth factor receptor (EGFR) tyrosine kinase inhibitor AG1478 increases the formation of inactive untethered EGFR dimers. Implications for combination therapy with monoclonal antibody 806. *J Biol Chem* **282**, 2840-50.

Garrett, T. P., McKern, N. M., Lou, M., Elleman, T. C., Adams, T. E., Lovrecz, G. O., Zhu, H. J., Walker, F., Frenkel, M. J., Hoyne, P. A. et al. (2002). Crystal structure of a truncated epidermal growth factor receptor extracellular domain bound to transforming growth factor alpha. *Cell* **110**, 763-73.

Holler, D. and Dikic, I. (2004). Receptor endocytosis via ubiquitin-dependent and -independent pathways. *Biochem Pharmacol* **67**, 1013-7.

Ichinose, J., Murata, M., Yanagida, T. and Sako, Y. (2004). EGF signalling amplification induced by dynamic clustering of EGFR. *Biochem Biophys Res Commun* **324**, 1143-9.

Jiang, X. and Sorkin, A. (2003). Epidermal growth factor receptor internalization through clathrin-coated pits requires Cbl RING finger and proline-rich domains but not receptor polyubiquitylation. *Traffic* **4**, 529-43.

Lidke, D. S., Nagy, P., Barisas, B. G., Heintzmann, R., Post, J. N., Lidke, K. A., Clayton, A. H., Arndt-Jovin, D. J. and Jovin, T. M. (2003). Imaging molecular interactions in cells by dynamic and static fluorescence anisotropy (rFLIM and emFRET). *Biochem Soc Trans* **31**, 1020-7.

Martin-Fernandez, M., Clarke, D. T., Tobin, M. J., Jones, S. V. and Jones, G. R. (2002). Preformed oligomeric epidermal growth factor receptors undergo an ectodomain structure

change during signaling. *Biophys J* **82**, 2415-27.
Moriki, T., Maruyama, H. and Maruyama, I. N. (2001). Activation of preformed EGF receptor dimers by ligand-induced rotation of the transmembrane domain. *J Mol Biol* **311**, 1011-26.
Saffarian, S., Li, Y., Elson, E. L. and Pike, L. J. (2007). Oligomerization of the EGF receptor investigated by live cell fluorescence intensity distribution analysis. *Biophys J* **93**, 1021-31.
Sako, Y., Minoghchi, S. and Yanagida, T. (2000). Single-molecule imaging of EGFR signalling on the surface of living cells. *Nat Cell Biol* **2**, 168-72.
She, H. Y., Rockow, S., Tang, J., Nishimura, R., Skolnik, E. Y., Chen, M., Margolis, B. and Li, W. (1997). Wiskott-Aldrich syndrome protein is associated with the adapter protein Grb2 and the epidermal growth factor receptor in living cells. *Mol Biol Cell* **8**, 1709-21.
Sigismund, S., Woelk, T., Puri, C., Maspero, E., Tacchetti, C., Transidico, P., Di Fiore, P. P. and Polo, S. (2005). Clathrin-independent endocytosis of ubiquitinated cargos. *Proc Natl Acad Sci U S A* **102**, 2760-5.
Song, W., Wu, J., Ge, G. and Lin, Q. (2008). Two domains of the epidermal growth factor receptor are involved in cytoskeletal interactions. *Biochem Biophys Res Commun* **370**, 589-93.
Sorokin, A., Lemmon, M. A., Ullrich, A. and Schlessinger, J. (1994). Stabilization of an active dimeric form of the epidermal growth factor receptor by introduction of an inter-receptor disulfide bond. *J Biol Chem* **269**, 9752-9.
Stoorvogel, W., Kerstens, S., Fritzsche, I., den Hartigh, J. C., Oud, R., van der Heyden, M. A., Voortman, J. and van Bergen en Henegouwen, P. M. (2004). Sorting of ligand-activated epidermal growth factor receptor to lysosomes requires its actin-binding domain. *J Biol Chem* **279**, 11562-9.
Teramura, Y., Ichinose, J., Takagi, H., Nishida, K., Yanagida, T. and Sako, Y. (2006). Single-molecule analysis of epidermal growth factor binding on the surface of living cells. *Embo J* **25**, 4215-22.
Thomas, D., Patterson, S. D. and Bradshaw, R. A. (1995). Src Homologous and Collagen (Shc) Protein Binds to F-actin and Translocates to the Cytoskeleton upon Nerve Growth Factor Stimulation in PC12 Cells. *J. Biol. Chem.* **270**, 28924-28931.
Ullrich, A., Coussens, L., Hayflick, J. S., Dull, T. J., Gray, A., Tam, A. W., Lee, J., Yarden, Y., Libermann, T. A., Schlessinger, J. et al. (1984). Human epidermal growth factor receptor cDNA sequence and aberrant expression of the amplified gene in A431 epidermoid carcinoma cells. *Nature* **309**, 418-25.
van Belzen, N., Rijken, P. J., Hage, W. J., de Laat, S. W., Verkleij, A. J. and Boonstra, J. (1988). Direct visualization and quantitative analysis of epidermal growth factor-induced receptor clustering. *J Cell Physiol* **134**, 413-20.
Verveer, P. J., Wouters, F. S., Reynolds, A. R. and Bastiaens, P. I. (2000). Quantitative imaging of lateral ErbB1 receptor signal propagation in the plasma membrane. *Science* **290**, 1567-70.
Wang, Q., Villeneuve, G. and Wang, Z. (2005). Control of epidermal growth factor receptor endocytosis by receptor dimerization, rather than receptor kinase activation. *EMBO Rep* **6**, 942-8.
Wang, Q., Zhu, F. and Wang, Z. (2007). Identification of EGF receptor C-terminal sequences 1005-1017 and di-leucine motif 1010LL1011 as essential in EGF receptor endocytosis. *Exp Cell Res* **313**, 3349-63.
Yu, X., Sharma, K. D., Takahashi, T., Iwamoto, R. and Mekada, E. (2002). Ligand-independent Dimer Formation of Epidermal Growth Factor Receptor (EGFR) Is a Step Separable from Ligand-induced EGFR Signaling. *Mol. Biol. Cell* **13**, 2547-2557.
Zacharias, D. A., Violin, J. D., Newton, A. C. and Tsien, R. Y. (2002). Partitioning of lipid-modified monomeric GFPs into membrane microdomains of live cells. *Science* **296**, 913-6.
Zhang, X., Gureasko, J., Shen, K., Cole, P. A. and Kuriyan, J. (2006). An Allosteric Mechanism

for Activation of the Kinase Domain of Epidermal Growth Factor Receptor. *Cell* **125**, 1137.
Zhu, H.-J., Iaria, J., Orchard, S., Walker, F. and Burgess, A. W. (2003). Epidermal Growth Factor Receptor: Association of Extracellular Domain Negatively Regulates Intracellular Kinase Activation in the Absence of Ligand. *Growth Factors* **21**, 15 - 30.

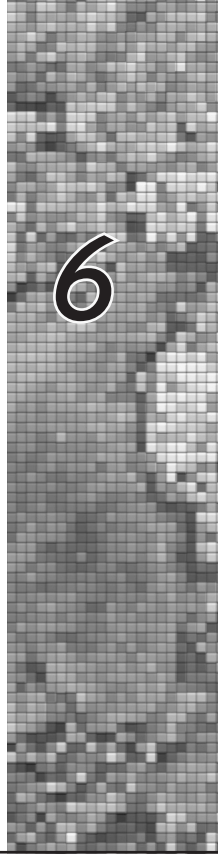

Chapter 6

Summarizing discussion

Membrane organization: an interplay between lipids and proteins

The plasma membrane is one of the most dynamic structures of the cell. As the final barrier separating the cells interior from the extracellular environment, it serves as the medium through which all transport and communication processes have to take place. The organization of the plasma membrane has been subject of investigation for decades. Throughout the years, ideas about its composition and structure have gone through diverse models. The ideas are highly divergent, ranging from protein domains such as tight junctions to coated structures, or phase-separated lipid domains and the cytoskeleton based picket-and-fence model. The concept of the plasma membrane as a non-ideal lipid mixture of molecules with variable degrees of mutual miscibilities has now gained general acceptance (Kusumi et al., 2004). In particular, lipids such as gangliosides and cholesterol as well as GPI-anchored proteins tend to form separate clusters in the plasma membrane. The question remains, however, how this behavior of membrane molecules relates to their function. In order to investigate the function and dynamics of lipid domains, a clear definition of these structures is a first prerequisite. Since the forces responsible for non-homogenous distribution of membrane molecules can generate domains as small as a few molecules, the definition of membrane domains may include clusters of three molecules, of which at least one molecule is cholesterol or a saturated lipid.

Model membranes of two or three different lipids show that they can generate phase-separated domains. However, the organization of the plasma membrane is not static, but dynamic as a result of temperature, diffusion and metabolic processes. Despite this dynamic behavior, the molecules comprising the plasma membrane do not act in a disordered fashion. Organizing processes can change the composition of the membrane, on short-range or longe-range scales. The two major classes of membrane constituents, lipids and proteins, are highly interconnected. Plasma membrane proteins can be either embedded by one or more transmembrane stretches, or connected to the perifery of the bilayer by means of lipid anchors. In addition, specialized protein domains bind to specific lipids, such as the PH-domain, which mediates its binding to phosphatidylinositol lipids. Changes in protein interactions can therefore affect the organization of the other membrane constituents. This is clearly exemplified in signal transduction processes, such as the hydrolysis of $PtdInsP_2$ into $InsP_3$ and DAG during activation of a number of receptors. On the contrary, lipid interactions may also be responsible for the regulation of protein:protein interactions, by enhancing or preventing the distance between them and consequently regulate the probability of their interaction. For example the T-cell receptor, expressed on the cell surface of T-cells, can be activated by crosslinking the receptor, but also by patching the GM1 gangliosides which surround the receptor (Janes et al., 1999). Thus, the organization of the plasma membrane and signal transduction seem to be highly interconnected.

Another transmembrane protein, the EGF receptor (EGFR), is involved in growth and differentiation of several cell types. From biochemical studies it was concluded that EGFR can be found in areas of the plasma membrane that are resistant to extraction by Triton X-

100, called detergent-resistant membrane domains (DRMs). These domains, isolated as light buoyant fractions on a density gradient, are thought to represent clusters of lipids carrying saturated fatty acids, and cholesterol. In model membranes, the saturation of the fatty acids allows tight packing with cholesterol, which drives phase separation of these liquid ordered (L_O) domains from the remaining liquid disordered (L_D) bilayer. Partitioning of certain protein and lipids into these "lipid rafts" can therefore enable their mutual interaction. Especially in the case of growth factor receptors, these may generate signaling platforms consisting of several interaction partners. However, the biochemical analysis of these lipid rafts suffers from a number of limitations that frustrate reliable interpretations. Results from detergent extraction suffer from the risk of artificial clustering of membrane components, do not give spatial information on the distribution of domains, and do not discriminate between different domains in a heterogeneous population. Moreover, the sensitivity of proteins for extraction varies with the type of detergent used (TX-100, Brij-98 or 96, Tween 20, octylglucoside), suggesting that the discrimination between L_O and L_D is more complex (Delaunay et al., 2008; Pike et al., 2005). Alternative methods with a less invasive character are therefore needed to study the localization of these growth factor receptors in lipids domains in the cellular context.

Nanoscale interactions between EGFR, gangliosides and GPI-anchored proteins

This thesis describes the investigation of the way how EGFR signaling changes its local environment in the plasma membrane, in particular raft lipids and other EGF receptors. By studying intact cells in a microscope, the spatial distribution is conserved. Technical advancements are prerequisite to study the membrane-associated processes in great detail. Both temporal and spatial resolution need to be high in order to study the dynamics of single molecules or clusters. The putative submicron scale of membrane domains could not be directly visualized in the light microscope, because of the optical resolution limit. Microscale colocalization of cellular components, as provided by light microscopy, is unsufficient to study objects as small as a few tens of nanometers. The nanoscale colocalization of the EGFR and components of lipid rafts was therefore investigated indirectly, by detecting the proximity of these molecules. Förster resonance energy transfer (FRET), a process in which fluorescent molecules transfer energy from one to the other, can detect this proximity since it requires a minimal distance in the order of 5-10 nm. The extent to which FRET takes place is measured by means of fluorescent lifetime imaging microscopy (FLIM). In the presence of an appropriate acceptor fluorophore, the fluorescent lifetime of the donor probe is reduced. A microscopic set-up with specialized hardware allows detection of this fluorescent lifetime on a nanosecond scale. This thesis describes the application of FRET-FLIM to study the relationship between EGFR and raft lipids. In addition, it describes the development of a novel methodology to investigate the function of this interaction, and offers opportunities for similar questions.

The experiments described in this thesis have been performed with two generally

used raft markers, GPI-anchored green fluorescent protein (GPI-GFP) and cholera toxin B-subunit (CTB). The latter probe binds specifically to ganglioside GM1 and can be supplied to cells ectopically, whereas GPI-GFP is a non-functional protein expressed in cells of interest. As a result, in a fluorescence microscope GPI-GFP can be seen at multiple sites throughout the entire cell, ranging from the Golgi complex to plasma membrane, whereas fluorescent CTB is found exclusively on the plasma membrane (Fig.1). Therefore, the cell surface is the only location where the two probes may colocalize. **Chapter 2** describes the FRET-FLIM based method to study the nanoscale interaction of the two raft markers, and confirms that these probes are in close proximity. To confirm that this colocalization is mediated by raft-like behavior, the cholesterol dependence of the interaction was determined. Nystatin, a compound that is known to sequester cholesterol, was supplied to the cells, resulting in a disappearance of colocalization. To study the presence of the EGF receptor in these lipid domains required the development of novel probes, which combined several properties required for this method. Ideal probes in studies on lipid rafts are specific, monovalent, small and non-agonistic. The so-called nanobodies were chosen as ideal candidates for this purpose. These single domain antibody fragments were selected from an immune library, selected for specificity and antagonism and purified. Three different anti-EGFR nanobodies were characterized by functional analysis. This showed that the nanobodies are highly specific for EGFR, do not activate the receptor, and have differential abilities to block ligand binding. Compared to other available probes to label EGFR, these nanobodies are superior for our application. After labeling with fluorescent markers the nanobodies were used as highly specific probes against the EGFR in FRET-FLIM assays. Careful FRET-FLIM analysis confirmed the hypothesis that EGFR colocalizes with GM1, but in a remarkably cholesterol-independent fashion. On the other hand no colocalization was found between EGFR and the second raft marker, GPI-GFP. This suggests that GPI-GFP and EGFR are localized in different structures on the plasma membrane. After stimulation of EGFR the GPI-GFP was redistributed on the plasma membrane, so that it colocalized with the receptor. This indicates that after EGFR activation the different microdomains fused into a novel structure, for which cholesterol is not essential. The existence of different scales of membrane domains has recently been suggested by Ken Jacobson (Jacobson et al., 2007). Signaling processes are thought to be responsible for the transition of small, unstable domains into larger and more stable platforms. The fusion of GPI-GFP containing domains with EGFR-GM1 domains is in line with this hypothesis.

The lipid raft marker GPI-GFP used in our studies lacks any functionality. It is composed of GFP, linked to a GPI-anchor during biogenesis by the presence of an anchoring signal. Therefore, any effect seen on the behavior of this probe is probably the result of its lipid anchor. The question remains whether this probe represents an existing protein, interacting with EGFR *in vivo*. The GPI-linked placental alkalic phosphotase PLAP was found previously to colocalize with EGFR in electromicroscopy (Ringerike et al., 2002). Future investigations with FRET-FLIM may elucidate the dependance of PLAP localization on ligand-stimulation.

The ganglioside environment in the cell membrane is an important factor for proper functioning of the EGFR. Gangliosides are characterized by their glycan moiety including minimally one sialic acid residue. The synthesis of these lipid starts with the generation of lactosylceramide, from which diverse synthesis paths diverge. The next enzyme in the synthesis of the majority of ganglioside species is GM3 synthase. Knock-out of this enzyme generates a major depletion in ganglioside content. Recently, primary fibroblasts were isolated from patients suffering from an autosomal recessive mutation in GM3 synthase, leading to a 93% reduction of cellular ganglioside levels (Liu et al., 2008). In addition, these cells display a highly reduced EGF binding although EGFR levels were unaffected. Also EGF-induced proliferation

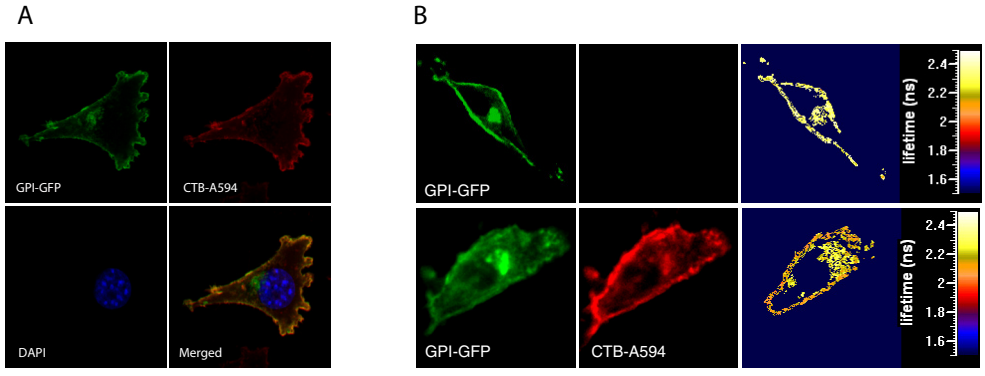

Fig 1. Microscale and nanoscale colocalization of GPI-GFP and CTB. (A) Her14 cells, stably expressing GPI-GFP, were incubated with CTB-Alexa594 for 1 hour, fixed and counterstained with DAPI. The fluorescent images were made under wide-field conditions on an Olympus AX70 microscope equipped with a Nikon CCD camera (DXM1200) (60x, oil immersion, NA=1.25/PlanFl). (B) Her14 cells, expressing GPI-GFP, incubated with CTB-Alexa-594 for 1 hour (lower half) or left untreated (upper) and fixed, were analysed with FRET-FLIM. Left and middle panel show distribution of the two raft marker, whereas the right panel shows the lifetime distribution of the GPI-GFP donor probe by FLIM analysis. The plasma membrane, where both probes are found, is characterized by a lifetime reduction whereas the lifetime is unaffected in intracellular compartments. Figure B adopted from chapter 2.

and migration were reduced, which correlated with reduced EGFR phosphorylation and Rho/Rac1 activation. In contrast, elevated levels of gangliosides are overexpressed and actively shed in the environment in a number of cancers (Kaucic et al., 2001; Sawada et al., 2002; Tokuyama et al., 1997). Moreover, depleting melanoma cells from gangliosides by inhibiting the synthesis of glucosylceramide greatly impaired cell growth (Weiss et al., 2003).

How gangliosides exert their influence on the EGFR is far from clear. It has been suggested that the glycan headgroups can differentially affect the conformation of the ectodomain, preventing or enhancing favorable conformations for signaling. This view is supported by the ability of EGFR to directly bind the ganglioside glycans, depending on glycosylation of the receptor (Miljan et al., 2002). The mode of interaction between EGFR and GM1 suggests that the receptor is surrounded by a lipid shell. After stimulation of the receptor

this interaction was retained throughout the formation of larger platforms, which suggests that the EGFR-GM1 interaction is very stable. This suggests that the interaction of EGFR with raft lipids is fundamentally different from the interaction between other components of the raft. The latter appears to depend on the presence of cholesterol for its stability, whereas the former is based on direct interactions, for example mediated by sugar moieties. The mechanism behind the lack of cholesterol in the perimeter of the receptor may be multiple. Firstly, highly specific and direct interactions of the receptor with gangliosides have been reported, which may spatially exclude the cholesterol in this shell (Miljan et al., 2002). Secondly, cholesterol is excluded from the boundary region of transmembrane proteins. This immiscibility has been attributed to the roughness of the transmembrane domain, which is incompatible with the rigid, bulky sterol ring of the cholesterol (Kusumi et al., 2004). In fact, cholesterol even appears to inhibit EGFR functioning. Cholesterol depletion increases the EGFR affinity for ligand, the predimerization and causes hyperphosphorylation (Pike and Casey, 2002; Ringerike et al., 2002; Roepstorff et al., 2002). This may be explained by the release of gangliosides from cholesterol-dependent rafts, such as the domains containing both GM1 and GPI-anchored proteins described in **chapter 2**. This would suggest that GM1 is equilibrated over cholesterol-dependent and -independent domains, and that its availability for EGFR can be regulated by the concentration of cholesterol.

The heterogeneity in the membrane domains reported in **chapter 2** is restricted to two different populations. Presumably, the full spectrum of micro- and nanodomains is much larger, which emphasizes the need for additional markers of these domains. In fact, several studies provide evidence for the presence of a heterogenous population of rafts. Thy-1 and and the GPI-linked prion protein do not co-immunoprecipitate, although both proteins are GPI-anchored (Madore et al., 1999). Immunofluorescence microscopy showed that the the raft lipids GM1 and GM3 and raft proteins CD44 and the urokinase plasminogen activator receptor distribute into two different domains on the plasma membrane, although they are found in the same DRM fraction. In one domain, CD44 and GM1 are found, whereas in the other the plasminogen activator receptor and GM3 can be found (Gomez-Mouton et al., 2001). The study described in chapter 2 can therefore be extended to markers of specific subsets of membrane domains. Selection of nanobodies against specific sphingolipids will, due to their monovalent nature, lead to highly superior probes for microdomains and could generate very usefull data on the organization of lipids into domains.

Clustering of GPI-anchored proteins and EGFR

Membrane domains are thought to produce a local concentration of proteins with comparable preferences for the (lipid) environment. **Chapter 3** describes the development of a method, confocal time-resolved fluorescence anisotropy imaging microscopy (CTRFAIM), to measure the clustering of fluorescent proteins. Comparable to hetero-FRET (between two chemically

different probes) described in chapter 2, homo-FRET is based on the transfer of energy from a donor to an acceptor fluorophore. However, since the two probes are identical, the FLIM measurements are not feasible for homo-FRET. The detection method in homo-FRET is based on the depolarization of highly polarized excitation light. The degree of polarization is expressed as anisotropy (r), which is the intensity corrected difference between the intensity in the direction parallel and perpendicular to the original direction. This method had been used before in other studies, but could be improved to gather more reliable detection of protein clustering (Sharma et al., 2004). In contrast to the generally used steady-state mode of excitation, which uses a constant illumination and detection, this method uses a pulsed laser as excitation source, and detects the emission in a time-gated fashion. The new methodology circumvents the need to calculate the FRET-efficiency, which affects the steady-state anisotropy but not the limiting anisotropy (r_{inf}). The latter is the anisotropy level that appears after FRET processes have reached equilibrium, where anisotropy is only determined by molecular rotation.

To investigate if the raft component GPI-GFP is clustered as predicted, it was expressed in fibroblasts and analysed by CTRFAIM. **Chapter 3** describes the differential clustering of GPI-GFP, which was calculated to appear in average clusters of 1.2 in the Golgi apparatus, whereas in ruffles on the plasma membrane it forms clusters of 1.6 on average. It was also shown that the homo-FRET was not a side-effect resulting from high concentration, since the anisotropy was independent of the intensity of GFP. This suggests that factors on the plasma membrane increase the clustering of GPI-anchored proteins. CTRFAIM measurements in combination with controlled photobleaching were performed to get indications on the clustersize distributions of GPI-GFP. From these experiments, it was shown that the majority of GPI-GFP in ruffles is clustered, as 37% is present as dimers whereas 22% forms clusters larger than 3 GPI-GFPs, which is in line with earlier reports (Sharma et al., 2004).

In **chapter 4** the CTRFAIM method is further evaluated by the use of inducible dimers and oligomers of GFP. Fusion of a monomeric variant of GFP (mGFP) to one or two FKBP domains should give rise to a protein that can be dimerized or oligomerized by the addition of AP20187. To test this, the proteins were ectopically expressed in cells, in the absence or presence of AP20187. The formation of dimers and oligomers was shown by polyacrylamide gel electrophoresis under non-denaturing and non-reducing conditions. When analysed by CTRFAIM, the anisotropy reduction was shown to be larger in the case of oligomers. However, when the clustersize was calculated from this anisotropy loss, a clear underestimation was observed. Although the source of this discrepancy is subject to speculation, rough estimations on clustersize can be made when a correction factor is applied. By applying this modification in the calculations, one can distinguish monomers, dimers and larger oligomers of three or more molecules. To evaluate the possibility that the dynamic range of CTRFAIM can be improved, different detection and excitation modes are compared in **chapter 4**. In comparison to steady-state anisotropy measurements, time-resolved detection gives rise to larger decreases in anisotropy, increasing the dynamic range of the measurements. In addition a two-photon

excitation set-up was used, which is a popular way to reduce the optical plane of illumination. Moreover, in theory it should result in a higher initial anisotropy value accompanied by larger decreases in case of homo-FRET. Indeed, the dynamic range of the anisotropy was found to increase, in both steady-state and time-resolved measurements, allowing more precise determinations of clustersize. However, due to increased photobleaching the accuracy of the measurement were reduced, and the advantage of two-photon imaging was lost. In conclusion, the CTRFAIM approach was found to provide reliable protein clustersizes, in a direct manner which is superior to steady-state homo-FRET approaches.

Then, the anisotropy decay of GPI-GFP and EGFR was determined in order to estimate their degree of clustering. In line with chapter 3, the GPI-GFP was found to form clusters on the plasma membrane. Applying the novel methodology learned that GPI-GFP clustersizes on the plasma membrane are heterogeneous, depending on the subcellular localization. These clusters are on average larger than two. In the cytosolic compartments, GPI-GFP is mainly monomeric. Compared to GPI-GFP, the EGF receptor has a lower degree of clustering. However, it is not strictly monomeric, but instead 40% of the receptor is found to be clustered, either dimeric or oligomeric. Remarkably, this oligomerization was found in the absence of ligand. Although this confirms earlier findings in electronmicroscopy, fluorescence correlation spectroscopy and single molecule imaging, it shows that our method can produce reliable estimations of protein clustering in non-invasive manner and offers future opportunities for live-cell imaging (Clayton et al., 2005; Sako et al., 2000; van Belzen et al., 1988). The existence of pre-existing oligomers was further illustrated in **chapter 5** by varying the ratio of wildtype EGFR to EGFR-mGFP, thereby changing the fraction of fluorescent monomers and dimers. Similar results with an EGFR mutant lacking kinase activity (K721A) indicate that this pre-oligomerization is independent of receptor signaling. Artificial dimerization of the receptor further illustrated that oligomerization and kinase activity are two separate processes, since the dimerization alone was not sufficient for receptor activation. The predimerized EGFR was readily activated with EGF, which shows that EGF binding induces additional conformational changes in the ectodomain, that presumably reorient the intracellular kinase domains. The function of pre-dimers or pre-oligimers is still unclear. However, modeling indicated that the formation of signaling dimers is much faster when the receptor is predimerized (Teramura et al., 2006). This suggests that predimers increase the chance of signaling after ligand-binding. Future experimental data should provide evidence for this theory.

EGFR activation induces kinase-dependent clustering and internalization

In **chapter 5** the clustering of EGFR was studied by CTR-FAIM, in particular during receptor activation. Activation of the receptor with EGF resulted in a large increase in homo-FRET. Comparison with an induced EGFR oligomer indicated that the receptor was oligomerized to clusters of more than 3 receptors (fig. 2). The oligomerization was sustained for at least

20 minutes during the internalization process. Similar measurements on the K721A mutant showed that ligand-induced clustering of EGFR is dependent of kinase activity and tyrosine phosphorylation. The anisotropy of this kinase-dead mutant did not change after ligand binding. This implicates that the signaling complex recruited to its C-terminal phosphotyrosines is involved in the oligomerization of EGFR. To confirm this, an EGFR mutant was investigated in which 9 tyrosine residues were changed to phenyalanines. Anisotropy imaging showed that also this mutant is non-responsive to EGF. Thus, kinase-dependent phosphorylation of EGFR tyrosine residues is directly related to its EGF-induced clustering.

A number of reports describe the activation of EGFR as a process that involves lateral propagation of the signal. Focal stimulation of transfected MCF7 cells resulted in a quick activation of receptors throughout the cell (Verveer et al., 2000). Also single-molecule techniques suggest that activated receptors can activate inactive receptors by lateral signal amplification (Ichinose et al., 2004). Recently, EGF-binding isotherms were fitted in a novel model in which negative cooperation was allowed. Remarkably, the binding of the second ligand to a dimer was found to decrease the association constant for the receptors in a dimer, suggesting that the signaling dimer was dissociated upon full ligand occupation (Macdonald and Pike, 2008). Subsequently, secondary dimers of active and non-active receptor may be formed, resulting in lateral propagation of the signal. Lack of kinase activity in the K721A mutant may therefore prevent dissociation of EGFR dimers after full ligand binding, which explains the absence of ligand-induced clustering in this mutant.

Oligimerization of the EGF receptor may result in a higher local activity. Since the activation of the receptor is antagonized by cytosolic factors such as phosphatases, the local concentration of active receptors may overcome a certain threshold for signal propagation upon ligand binding. Secondly, the clustering of the receptor appeared to be directly associated with its internalization. Induced clustering of the receptor enhanced its internalization rate in response to EGF, both for the wild-type as for the K721A mutant. The ligand-induced clustering of EGFR and its internalization are likely to result from the same machinery. Receptor activation has been studied extensively and has resulted in the identification of dozens of interactions with cytosolic proteins. Strinkingly, kinase activity does not account for all internalization processes, as the kinase-dead mutant is also internalized. Clustering of this receptor even increased the internalization in response to EGF. This indicates that apart from the kinase-dependent internalization pathway a second route of endocytosis is present on these cells. Earlier reports support our observations that EGFR kinase activity is not required for internalization. Instead, dimerization has been suggested as the essential mechanism for endocytosis (Wang et al., 2005).Our observations have shown that the kinase-dead receptor behaves like the wildtype receptor in terms of predimerization. In addition, the two affinities as found in wildtype EGFR have been reported in the kinase-dead mutant as well (Honegger et al., 1990; van Belzen et al., 1990).

The proteins involved in the clustering of EGFR have not been identified. However,

since this process is found to be connected to EGFR internalization, studies on the latter can guide the identification of these factors. Main candidate for involved proteins is actin, which is intimately involved in receptor internalization and associates with the receptor after activation, although high-affinity receptors show this association prior to activation (van Belzen et al., 1990). A transient burst in actin polymerization accompanies the last steps of clathrin mediated internalization. Treatment of Swiss 3T3 cells with latrunculin A to depolymerize the

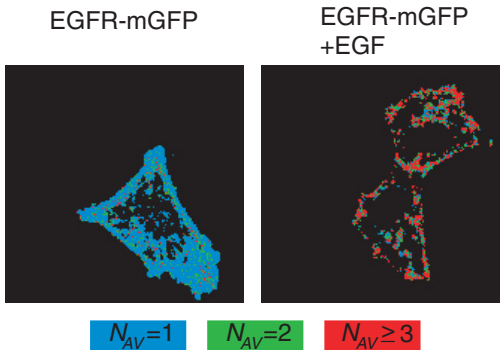

Fig 2. CTRFAIM analysis of EGFR-mGFP clustering in response to EGF stimulation. The anisotropy value per pixel was categorized into three classes, as described in chapter 4. Activation of the receptor induced an increase in average clustersize, mainly generating clusters of 3 or more receptors. Picture taken from chapter 5.

cortical actin cytoskeleton resulted in a dramatic decrease of EGF-induced endocytosis (Lunn et al., 2000). Isolation of cytoskeleton from A431 cells learned that before activation 5% of the receptors are associated to actin, mainly of the high-affinity class. EGF induced a dramatic increase in the number of EGF receptors associated to the cytoskeleton, which were mainly from the low-affinity class (van Bergen en Henegouwen et al., 1989).

A proteomic study investigated the temporal dynamics of protein activation after EGF-stimulation (Blagoev et al., 2004). Interestingly, proteins involved in actin remodeling displayed a very distinctive temporal pattern, involving a rapid drop within 1 minute after activation, followed by a recovery to initial levels after 5 minutes. One of these proteins, gelsolin, is known to be inhibited by binding to $PtdInsP_2$, which is suggested to be released from the juxtamembrane domain of EGFR after activation (McLaughlin et al., 2005). These data suggest that the EGF receptor is released from its cytoskeletal restraints during the first few minutes after activation. This would allow the receptor to diffuse to other receptors, resulting in dimerization or oligomerization. This interaction does not neccesarily imply stable association between receptors, but may rather act in a kiss-and-run fashion, allowing rapid progression of the signal in the plane of the cell (Verveer et al., 2000). After this initial cytoskeletal release, the actin is rearranged in order to allow clustering and efficient internalization of the activated receptors.

Combined model for EGF-induced plasma membrane organization

As shown in chapter 2, activation of the EGF receptor induces a reorganization of the plasma membrane, resulting in the formation of a larger signaling platform including GPI-anchored

proteins. In addition, this activation also leads to the formation of EGFR oligomers in a kinase-dependent fashion as shown in chapter 5. How the clustering of EGFR relates to its localization in lipid domains is not clear. In this respect, the association with the cytoskeleton may again provide suggestions to this issue. Interestingly, treatment of cells expressing EGFR with sphingomyelinase induces the association with the cytoskeleton (van Belzen et al., 1990). This suggests that sphingolipids prevent the clustering of EGFR in their unstimulated state, whereas reduction of the sphingolipid content results in EGFR concentration, probably by their increased partitioning in the bulk membrane. An alternative mechanism may be that the lipid shell prevents hop-diffusion of EGFR to neighbouring transient confinement zones, and by release from the shell receptors are free to form clusters and associate with the cytoskeleton. This does not exclude the possibility that collision of shell-surrounded proteins is prevented in the absence of stimulation. Instead, these small structures may fuse in steady-state conditions, but are largely unstable structures due to the lack of stabilizing factors.

Another important question that remains is whether all EGF receptors are surrounded by GM1 shells. **Chapter 5** has shown that both monomers and pre-associated receptors exist on the cell membrane. Consequently, affinity for raft components may also differ between monomeric and pre-oligomerized receptor forms. Morever, GPI-GFP was only detected in the vicinity of EGFR after activation and receptor oligomerization. The FKBP-constructs used in chapter 5 offer new opportunities to gather information on the relation between EGFR oligomerization and raft localization. The preference of molecules for a certain membrane environment is expressed as the partitioning coefficient K_p. In a situation comprising two phases, a value of 1 corresponds to equal partitioning, whereas values smaller or greater than 1 indicate preferential residence in one or the other environment. In case a particular protein has a weak preference for a particular phase (e.g. K_p=3), the chance that it will be in that phase will be 3 times higher than its partitioning in the other phase. However, still a significant part of the protein is present in the latter phase. Crosslinking the protein will enhance the partitioning in the preferred phase, since the resultant K_p is the product of the individual values (Simons and Vaz, 2004). For example, the protein described above will have a K_p of 9 when dimerized, 27 when trimerized, etc.). Thus, clustering may change molecules with a weak preference for raft domains into strong raft-resident molecules. Clustering of membrane components such as EGFR may therefore provide a driving force for the generation of stable signaling platforms.

One aspect of membrane domains is their sidedness, as lipids are embedded in one leaflet of the bilayer. Nevertheless, signaling platforms are considered to protrude through the bilayer, thereby connecting the two leaflets. Lipid rafts, in particular the larger domains, are considered to be transmembrane structures with similar raft-like behavior of intracellular lipids. Therefore, it is intriguing how simply clustering GPI-anchored proteins on the cell surface induces clusters of H-Ras in the inner leaflet, whereas the distribution of K-Ras was unchanged (Eisenberg et al., 2006). Since these two Ras isoforms only differ in their lipid anchor, these data suggest that this clustering is mediated by a lipid specific partitioning.

Interdigitation of the fatty acids from both leaflets has been proposed to form the connection between the inner and outer plane of the platform. In model studies using solid supported asymmetric bilayers, it was found that clusters of lipids in one leaflet coincided with equal-sized clusters of lipids in the other leaflet (Kiessling et al., 2006). Alternatively, connection of components from both sides with a transmembrane protein may have similar effects. As shown in chapter 2, GPI-anchored proteins do not necessarily colocalize with other constituents of lipid rafts such as EGFR. The activation of the receptor is necessary for recruitment of GPI-GFP.

In addition to the direct interaction between EGFR and gangliosides in the outer leaflet, comparable binding can take place on the inner leaflet. The intracellular juxtamembrane domain contains a stretch of basic residues that can bind and probably sequester the negatively charged $PtdInsP_2$ lipids. This phospholipid is an important factor in EGFR signaling. Thus, the EGF receptor may form the transmembrane connection between the outer leaflet ganglioside domain, and an inner leaflet $PtdInsP_2$-rich zone. Upon signaling this interaction is disturbed by the binding of Ca^{2+}/CaM to the basic stretch, releasing the $PtdInsP_2$ from the protein (McLaughlin et al., 2005). Modulation of $PtdInsP_2$ exposure has dramatic effects on the membrane-cytoskeletal interaction (Kwik et al., 2003). In view of the cytoskeletal rearrangements occuring during EGFR signaling, this release of $PtdInsP_2$ may be an important regulatory step. The availability of $PtdInsP_2$ is important for interaction with the cortical actin network, and enhances their adhesion (Anderson and Marchesi, 1985; Raucher et al., 2000). Sequestering of $PtdInsP_2$ with PH-domains reduces the interaction between the membrane and the actin cytoskeleton. Thus, the interaction of EGFR with gangliosides in the outer leaflet, and phospholipids such as $PtdInsP_2$ on the inner leaflet, may offer the basis for the formation of a signaling platform after receptor stimulation. In addition, the recruitment of small G-proteins such as Ras or Src with specific lipid anchors changes the local inner leaflet lipid environment of EGFR. This also contributes to the formation of a transmembrane signaling platform.

Based on the data from chapters 2 and 5, and from literature data as described above, the following sequence of events during EGFR stimulation is proposed (Fig. 3). In the resting cell EGFR is present as monomers and predimers. The positive effect of GM1 on EGFR signaling suggests that primarily the predimers are surrounded by a lipid shell consisting of GM1. Other membrane domains, such as GPI-GFP and GM1 containing rafts, are present on the plasma membrane independent of the EGFR-containing domains. Ligand-binding induces a conformational change in the ectodomain, which in turn reorients the kinase domains resulting in auto-phosphorylation of the receptor. From this point, a number of parallel events contribute to the formation of signaling platforms. The active dimer dissociates and forms secondary dimers, resulting in lateral propagation of the signal. At the same time, cytosolic factors binding to the cytosolic EGFR domains induce the clustering of the receptor, thereby stimulating the fusion of multiple shells surrounding EGFR. This promotes the fusion with other domains, including the GPI-GFP containing rafts. The inner leaflet is reorganized

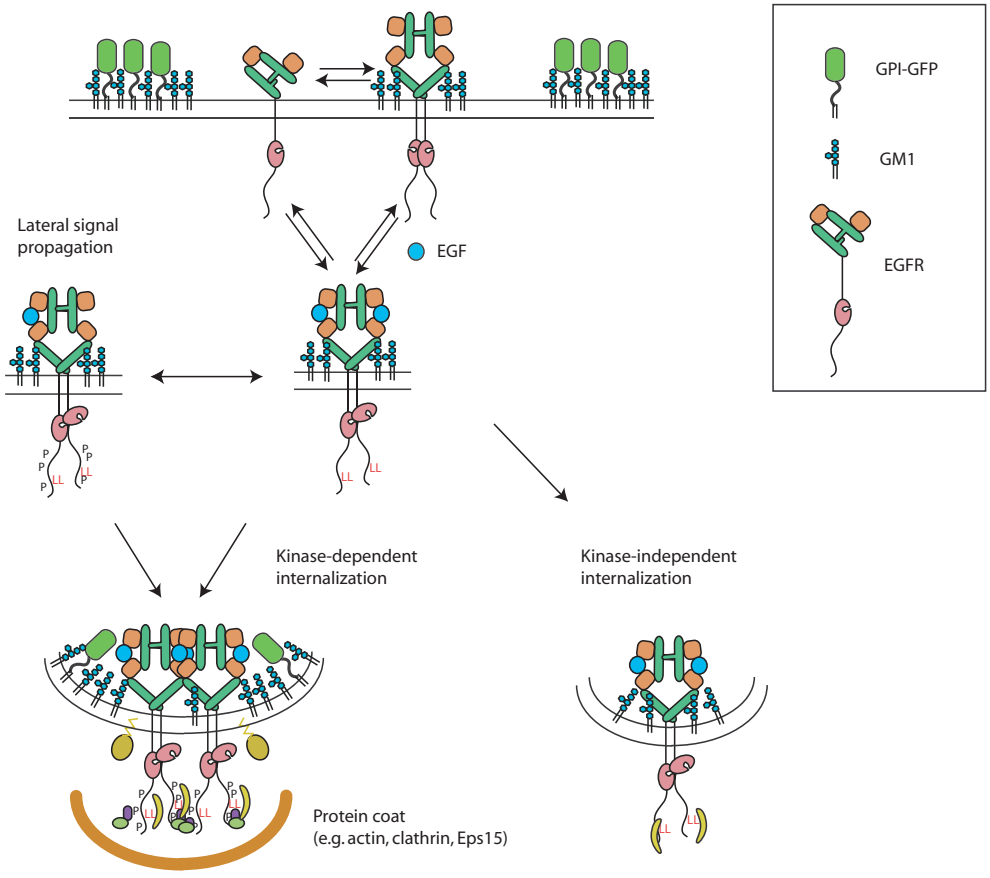

Fig 3. Summarizing model for EGFR-mediated organization of lipid and protein organization. The EGFR is localized in GM1 enriched domains in the outer leaflet. This colocalization of EGFR with GM1 is mainly found for pre-existing dimers. Other membrane domains containing GPI-GFP and GM1 are also found (upper part of illustration). Stimulation of EGFR with ligand results in lateral signal propagation by the formation of secondary dimers (middle part). Recruitment of adaptor proteins, membrane-anchored kinases, and a protein coat, which may involve proteins such as clathrin, actin or Eps15, eventually leads to the oligomerization of the receptor, and the coalescence of different membrane domains, resulting in the formation of a signaling platform that involves both membrane leaflets (see text for details).

by a number of simultaneous events, including $PtdInsP_2$ release and the recruitment of lipid-anchored Ras and Src proteins. In addition, the fusion with GPI-GFP domains containing cholesterol may drive the formation of a signaling platform consisting of both leaflets. Receptor clusters can now dock to clathrin or alternative actin-mediated endocytic coats, resulting in the formation of clathrin-dependent and –independent pits.

In contrast, the absence of kinase activity prevents lateral signal amplification, formation of a signaling platform, receptor clustering and clathrin-mediated endocytosis. However, the kinase-dead receptor is endocytosed via a di-leucine motif, and this process

can be enhanced by receptor clustering (Wang et al., 2007). This is probably due to the local concentration of di-leucine motifs, but may also contribute to the clathrin-independent endocytosis.

Concluding remarks

The research described in this thesis resulted in the following methodological novelties:

1. Nanobodies against EGFR form superior probes for highly specific, monovalent, non-stimulating and non-antagonistic fluorescent labeling, and can be used for FRET-based assays;
2. CTRFAIM is a powerful method to determine nanoscale clustering of (membrane) proteins, and is superior to steady-state anisotropy.

The research described in this thesis led to the following important biological conclusions:

1. the EGF receptor is surrounded by GM1;
2. other proteins, such as GPI-GFP are found in other GM1 environments;
3. after receptor activation, GPI-GFP and EGFR are found in the same membrane domain;
4. EGFR activation results in oligomerization of the receptor, which is dependent on kinase activity and tyrosine phosphorylation;
5. the internalization of EGFR is enhanced by clustering.

References

Anderson, R. A. and Marchesi, V. T. (1985). Regulation of the association of membrane skeletal protein 4.1 with glycophorin by a polyphosphoinositide. *Nature* **318**, 295-8.

Blagoev, B., Ong, S. E., Kratchmarova, I. and Mann, M. (2004). Temporal analysis of phosphotyrosine-dependent signaling networks by quantitative proteomics. *Nat Biotechnol* **22**, 1139-45.

Clayton, A. H., Walker, F., Orchard, S. G., Henderson, C., Fuchs, D., Rothacker, J., Nice, E. C. and Burgess, A. W. (2005). Ligand-induced dimer-tetramer transition during the activation of the cell surface epidermal growth factor receptor-A multidimensional microscopy analysis. *J Biol Chem* **280**, 30392-9.

Delaunay, J.-L., Breton, M., Trugnan, G. and Maurice, M. (2008). Differential solubilization of inner plasma membrane leaflet components by Lubrol WX and Triton X-100. *Biochimica et Biophysica Acta (BBA) - Biomembranes* **1778**, 105.

Eisenberg, S., Shvartsman, D. E., Ehrlich, M. and Henis, Y. I. (2006). Clustering of raft-associated proteins in the external membrane leaflet modulates internal leaflet H-ras diffusion and signaling. *Mol Cell Biol* **26**, 7190-200.

Gomez-Mouton, C., Abad, J. L., Mira, E., Lacalle, R. A., Gallardo, E., Jimenez-Baranda, S., Illa, I., Bernad, A., Manes, S. and Martinez, A. C. (2001). Segregation of leading-edge and uropod components into specific lipid rafts during T cell polarization. *Proc Natl Acad Sci U S A* **98**, 9642-7.

Honegger, A. M., Schmidt, A., Ullrich, A. and Schlessinger, J. (1990). Separate endocytic pathways of kinase-defective and -active EGF receptor mutants expressed in same cells. *J Cell Biol* **110**, 1541-8.

Ichinose, J., Murata, M., Yanagida, T. and Sako, Y. (2004). EGF signalling amplification induced by dynamic clustering of EGFR. *Biochem Biophys Res Commun* **324**, 1143-9.

Jacobson, K., Mouritsen, O. G. and Anderson, R. G. (2007). Lipid rafts: at a crossroad between cell biology and physics. *Nat Cell Biol* **9**, 7-14.

Janes, P. W., Ley, S. C. and Magee, A. I. (1999). Aggregation of lipid rafts accompanies signaling via the T cell antigen receptor. *J Cell Biol* **147**, 447-61.

Kaucic, K., Etue, N., LaFleur, B., Woods, W. and Ladisch, S. (2001). Neuroblastomas of infancy exhibit a characteristic ganglioside pattern. *Cancer* **91**, 785-93.

Kiessling, V., Crane, J. M. and Tamm, L. K. (2006). Transbilayer effects of raft-like lipid domains in asymmetric planar bilayers measured by single molecule tracking. *Biophys J* **91**, 3313-26.

Kusumi, A., Koyama-Honda, I. and Suzuki, K. (2004). Molecular dynamics and interactions for creation of stimulation-induced stabilized rafts from small unstable steady-state rafts. *Traffic* **5**, 213-30.

Kwik, J., Boyle, S., Fooksman, D., Margolis, L., Sheetz, M. P. and Edidin, M. (2003). Membrane cholesterol, lateral mobility, and the phosphatidylinositol 4,5-bisphosphate-dependent organization of cell actin. *Proc Natl Acad Sci U S A* **100**, 13964-9.

Liu, Y., Su, Y., Shevchuk, N. A., Wiznitzer, M., Epifano, O. and Ladisch, S. (2008). Ganglioside depletion and EGF Responses of Human GM3 Synthase Deficient Fibroblasts. *Glycobiology*, cwn039.

Lunn, J. A., Wong, H., Rozengurt, E. and Walsh, J. H. (2000). Requirement of cortical actin organization for bombesin, endothelin, and EGF receptor internalization. *Am J Physiol Cell Physiol* **279**, C2019-2027.

Macdonald, J. L. and Pike, L. J. (2008). Heterogeneity in EGF-binding affinities arises from negative cooperativity in an aggregating system. *Proc Natl Acad Sci U S A* **105**, 112-7.

Madore, N., Smith, K. L., Graham, C. H., Jen, A., Brady, K., Hall, S. and Morris, R. (1999).

Functionally different GPI proteins are organized in different domains on the neuronal surface. *Embo J* **18**, 6917-26.

McLaughlin, S., Smith, S. O., Hayman, M. J. and Murray, D. (2005). An electrostatic engine model for autoinhibition and activation of the epidermal growth factor receptor (EGFR/ErbB) family. *J Gen Physiol* **126**, 41-53.

Miljan, E. A., Meuillet, E. J., Mania-Farnell, B., George, D., Yamamoto, H., Simon, H. G. and Bremer, E. G. (2002). Interaction of the extracellular domain of the epidermal growth factor receptor with gangliosides. *J Biol Chem* **277**, 10108-13.

Pike, L. J. and Casey, L. (2002). Cholesterol levels modulate EGF receptor-mediated signaling by altering receptor function and trafficking. *Biochemistry* **41**, 10315-22.

Pike, L. J., Han, X. and Gross, R. W. (2005). Epidermal growth factor receptors are localized to lipid rafts that contain a balance of inner and outer leaflet lipids: a shotgun lipidomics study. *J Biol Chem* **280**, 26796-804.

Raucher, D., Stauffer, T., Chen, W., Shen, K., Guo, S., York, J. D., Sheetz, M. P. and Meyer, T. (2000). Phosphatidylinositol 4,5-bisphosphate functions as a second messenger that regulates cytoskeleton-plasma membrane adhesion. *Cell* **100**, 221-8.

Ringerike, T., Blystad, F. D., Levy, F. O., Madshus, I. H. and Stang, E. (2002). Cholesterol is important in control of EGF receptor kinase activity but EGF receptors are not concentrated in caveolae. *J Cell Sci* **115**, 1331-40.

Roepstorff, K., Thomsen, P., Sandvig, K. and van Deurs, B. (2002). Sequestration of epidermal growth factor receptors in non-caveolar lipid rafts inhibits ligand binding. *J Biol Chem* **277**, 18954-60.

Sako, Y., Minoghchi, S. and Yanagida, T. (2000). Single-molecule imaging of EGFR signalling on the surface of living cells. *Nat Cell Biol* **2**, 168-72.

Sawada, M., Moriya, S., Saito, S., Shineha, R., Satomi, S., Yamori, T., Tsuruo, T., Kannagi, R. and Miyagi, T. (2002). Reduced sialidase expression in highly metastatic variants of mouse colon adenocarcinoma 26 and retardation of their metastatic ability by sialidase overexpression. *Int J Cancer* **97**, 180-5.

Sharma, P., Varma, R., Sarasij, R. C., Ira, Gousset, K., Krishnamoorthy, G., Rao, M. and Mayor, S. (2004). Nanoscale organization of multiple GPI-anchored proteins in living cell membranes. *Cell* **116**, 577-89.

Simons, K. and Vaz, W. L. (2004). Model systems, lipid rafts, and cell membranes. *Annu Rev Biophys Biomol Struct* **33**, 269-95.

Teramura, Y., Ichinose, J., Takagi, H., Nishida, K., Yanagida, T. and Sako, Y. (2006). Single-molecule analysis of epidermal growth factor binding on the surface of living cells. *Embo J* **25**, 4215-22.

Tokuyama, S., Moriya, S., Taniguchi, S., Yasui, A., Miyazaki, J., Orikasa, S. and Miyagi, T. (1997). Suppression of pulmonary metastasis in murine B16 melanoma cells by transfection of a sialidase cDNA. *Int J Cancer* **73**, 410-5.

van Belzen, N., Rijken, P. J., Hage, W. J., de Laat, S. W., Verkleij, A. J. and Boonstra, J. (1988). Direct visualization and quantitative analysis of epidermal growth factor-induced receptor clustering. *J Cell Physiol* **134**, 413-20.

van Belzen, N., Spaargaren, M., Verkleij, A. J. and Boonstra, J. (1990). Interaction of epidermal growth factor receptors with the cytoskeleton is related to receptor clustering. *J Cell Physiol* **145**, 365-75.

van Bergen en Henegouwen, P. M., Defize, L. H., de Kroon, J., van Damme, H., Verkleij, A. J. and Boonstra, J. (1989). Ligand-induced association of epidermal growth factor receptor to the cytoskeleton of A431 cells. *J Cell Biochem* **39**, 455-65.

Verveer, P. J., Wouters, F. S., Reynolds, A. R. and Bastiaens, P. I. (2000). Quantitative imaging of lateral ErbB1 receptor signal propagation in the plasma membrane. *Science* **290**,

1567-70.
Wang, Q., Villeneuve, G. and Wang, Z. (2005). Control of epidermal growth factor receptor endocytosis by receptor dimerization, rather than receptor kinase activation. *EMBO Rep* **6**, 942-8.
Wang, Q., Zhu, F. and Wang, Z. (2007). Identification of EGF receptor C-terminal sequences 1005-1017 and di-leucine motif 1010LL1011 as essential in EGF receptor endocytosis. *Exp Cell Res* **313**, 3349-63.
Weiss, M., Hettmer, S., Smith, P. and Ladisch, S. (2003). Inhibition of melanoma tumor growth by a novel inhibitor of glucosylceramide synthase. *Cancer Res* **63**, 3654-8.

Nederlandse samenvatting

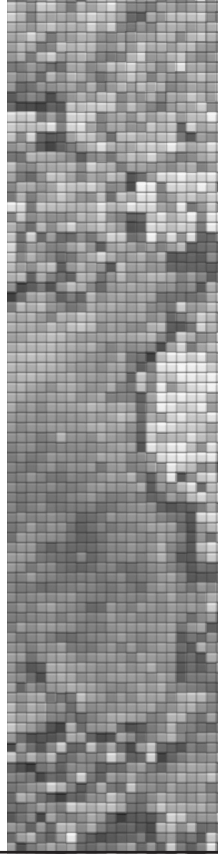

Een volwassen lichaam groeit niet. Toch vindt er in uw lichaam voortdurend een proces van celdeling plaats. Dit is nodig om de afbraak van andere cellen te compenseren. Dit doen cellen vaak niet op eigen initiatief, maar wordt van hogerhand aangestuurd. Deze aansturing vindt onder andere plaats door groeifactoren, die in de omgeving van de cel terecht komen. Bepaalde celtypen zijn uitgerust met bepaalde receptoren voor deze groeifactoren, waardoor de vermenigvuldiging en differentiatie van deze cellen specifiek kan worden gereguleerd.

Een van deze receptoren is de epidermale groeifactor receptor, kortweg EGFR. Deze receptor kan de epidermale groeifactor (EGF) binden, waardoor de receptor geactiveerd wordt. Tussen activatie van de receptor en bijv. celdeling zit een complex systeem van biochemische reacties. Een aantal moleculaire aspecten hiervan zijn inmiddels uitgebreid onderzocht. Zo is bekend dat de receptor moet binden aan een andere EGFR (dimerisatie) voordat activatie kan plaatsvinden, en dat tijdens dat proces een structuurverandering in de receptor optreedt. Ook is bekend dat er regulatie mechanismen in de cel aanwezig zijn die ongecontroleerde groei voorkomen. Bij een aantal typen kanker is deze regulatie van de EGFR verstoord, waardoor een continue stimulatie van celdeling optreedt. De opheldering van het moleculaire mechanisme waardoor de EGFR geactiveerd en gereguleerd wordt is daarom van groot belang voor toekomstige therapieën tegen deze vormen van kanker.

De receptor is door middel van een transmembraan domein verankerd in de plasmamembraan van de cel. In de plasmamembraan zijn tientallen verschillende lipiden te vinden, en bestaat daarnaast voor een groot gedeelte uit eiwitten die ofwel de membraan doorkruisen, ofwel de membraan zijdelings kunnen binden. Bovendien is de samenstelling van de plasmamembraan niet constant, maar onderhevig aan dynamische processen zoals productie, afbraak en transport van de diverse componenten. Het laatste decennium is geopperd dat de lipiden in de plasmamembraan niet homogeen verdeeld zijn over het oppervlak. Bepaalde soorten lipiden, in het bijzonder degenen die verzadigde vetzuurstaarten bezitten, hebben een voorkeur om in elkaars omgeving te zitten. Hierdoor clusteren deze lipiden, hetgeen leidt tot de vorming van “eilandjes”, zogenaamde lipid rafts, omringd door de overige lipiden. Dit gedrag van lipiden is aangetoond in simpele modelsystemen bestaande uit enkele goed gedefinieerde lipiden. Via biochemische methoden, waarbij onderdelen van de cel worden gescheiden op dichtheid, is aangetoond dat bepaalde eiwitten, waaronder EGFR, verrijkt zijn in zulke lipid rafts. Daarnaast blijken bepaalde lipiden die in rafts gevonden worden een sterk invloed te hebben op de werking van de receptor. Dit roept de vraag op of EGFR in de intacte cel in lipid rafts kan worden gevonden. Het visualiseren van zowel EGFR als lipid rafts is een belangrijke stap om deze vraag te beantwoorden.

Om dit in detail te kunnen bestuderen moet de gebruikte methode voldoende resolutie hebben, dat wil zeggen dat de mate waarin details kunnen worden waargenomen zodanig moet zijn dat de lipid rafts als afzonderlijke onderdelen kunnen worden gezien. Daarnaast geniet het de voorkeur een techniek te gebruiken die ook toepasbaar is op levende cellen, zodat de fysiologische omstandigheden van de cel het best benaderd kunnen worden. Fluorescentie microscopie is een veelgebruikte techniek om cellulaire componenten te visualiseren en te localiseren. Door de moleculen van interesse met geschikte probes aan te kleuren, is het mogelijk om te bepalen of deze componenten op dezelfde plek in de cel gelocaliseerd zijn. De resolutie van deze techniek (200 nanometer) is echter beperkt, en waarschijnlijk niet toereikend voor de bestudering van de lipid rafts. Op een indirecte manier is desondanks wel te bepalen of twee fluorescente probes in elkaars nabijheid verkeren. Deze methode is gebaseerd op de overdracht van fluorescentie energie van de ene probe (donor) naar de ander (acceptor). Het gevolg van deze energie-overdracht (FRET) is dat de tijdsduur van fluorescentie van de donorprobe afneemt. Aangezien dit proces sterk afhankelijk is van de afstand tussen de moleculen, is het aan de hand van de fluorescentie levensduur (lifetime, of τ) te bepalen of twee probes op een afstand van enkele nanometers van elkaar verwijderd zijn. Door middel van Fluorescence Lifetime Imaging Microscopy (FLIM) kan die levensduur

voor elk punt (pixel) in een afbeelding van de cel bepaald worden. Hiermee wordt zichtbaar waar in de cel moleculen dichtbij elkaar zitten.

In dit proefschrift wordt beschreven hoe deze techniek werd toegepast om te bepalen of de EGF receptor gelocaliseerd is in lipid rafts. Om dit te kunnen bepalen was het noodzakelijk om over probes te beschikken die ofwel de lipid raft danwel de EGFR aankleuren. Hoofdstuk 2 beschrijft hoe allereerst een aantal geschikte probes werden ontwikkeld om de receptor te kunnen visualiseren. Hiervoor werd gebruik gemaakt van lama-antilichaam technologie, die het mogelijk maakte om antilichaam fragmenten te ontwikkelen die geen effect hebben op de activiteit van de receptor, maar anderzijds deze activatie niet kunnen remmen. De koppeling van de zogenaamde nanobodies aan fluorescente moleculen maakt ze tot unieke probes voor de visualisatie van in dit geval de EGFR. Met behulp van FRET/FLIM werd gevonden dat de EGFR in de nabijheid van lipid raft marker Cholera Toxin B-subunit (CTB) zit, maar niet in de omgeving van GPI-GFP, een andere lipid raft marker bestaande uit een GPI lipide gekoppeld aan een groen fluorescerend eiwit (GFP). Blijkbaar is er op de celmembraan een verzameling lipid rafts aanwezig die van elkaar verschillen in samenstelling. Een opvallende observatie is dat na activatie van de EGFR een verschuiving van de raft markers optreedt, zodat EGFR zowel in de directe omgeving van GM1 als van GPI-GFP zit. Dit duidt op een fusie van de twee soorten lipid rafts als gevolg van de activatie van EGFR. Blijkbaar vindt er na de activatie van EGFR een reorganisatie van de membraan plaats, die kan leiden tot de vorming van een zogenaamd signaleringsplatform. Deze structuur leidt dan tot de recrutering van allerlei eiwitten die belangrijk zijn bij de ketting van reacties die volgen op de activering van de receptor.

De voorkeur van EGFR voor localisatie in lipid rafts zou kunnen leiden tot een verhoging van de locale concentratie van de receptor, d.w.z dat de receptor clusters vormt. Om die reden is het belangrijk over een methode te beschikken waarmee de clustering van eiwitten in de plasmamembraan gemeten kan worden. Hiervoor werd gebruik gemaakt van het FRET-principe zoals beschreven in hoofdstuk 2. Dit proces is ook toe te passen op identieke fluorescente probes, en wordt dan homo-FRET genoemd. Om dit te kunnen meten is een andere benadering nodig, die gebaseerd is op het meten van de polarisatierichting van de fluorescentie, ookwel fluorescentie anisotropie genoemd. Als meer moleculen zich in elkaars nabijheid bevinden, dan zal er meer homo-FRET plaatsvinden. Elke keer dat homo-FRET plaatsvindt, zal de anisotropie iets lager worden. Hoe groter de clustering van fluorescerende moleculen is, hoe lager de fluorescentie anisotropie dus wordt. Op deze manier is vast te stellen in welke mate fluorescente moleculen geclusterd zijn.

In hoofdstuk 3 en 4 wordt een nieuwe fluorescentie microscopie methode beschreven waarmee de fluorescentie anisotropie direct gerelateerd wordt aan het aantal fluorescerende moleculen in een cluster. Voor elk punt in een afbeelding van de cel wordt een tijdsopgelost anisotropie verval gemeten. Daaruit wordt de gemiddelde grootte van de clusters van moleculen in dat deel van de cel gehaald. Door de populatie fluoroforen te bleken en vervolgens de anisotropie waarden uit te zetten tegen de blekingsgraad, valt bovendien af te leiden wat de verhouding tussen de verschillende clustergrootten is. Hoofdstuk 3 beschrijft de toepassing van deze methoden op cellen die de lipid raft marker GPI-GFP tot expressie brengen. De conclusie is dat GPI-GFP op de plasmamembraan kleine clusters vormt van 1-5 moleculen per cluster.

In hoofdstuk 4 werd een evaluatie uitgevoerd van de verschillende anisotropie benaderingen. De tijdsopgeloste anisotropie werd vergeleken met de steady-state anisotropie en een-foton excitatie met twee-foton excitatie. Om de metingen te kunnen relateren aan de bekende clustergrootte, werd een systeem ontwikkeld om de dimerisatie danwel oligomerisatie van GFP te kunnen reguleren. Fusie van GFP met een of twee FKBP domeinen leidt tot een eiwit wat respectievelijk gedimeriseerd danwel geoligomeriseerd kan worden. Biochemische analyse met een natieve eiwit polyacrylamide gelelectroforese bevestigde de werking van

dit systeem. Deze evaluatie bleek erg belangrijk te zijn aangezien de gemeten waarden van de clustergrootte consequent lager uitvallen dan verwacht mag worden aan de hand van de theoretische en biochemische gegevens. De oorzaak van deze afwijking werd vastgesteld, er kan op eenvoudige wijze voor gecorrigeerd worden. De clustering van de EGFR werd op deze manier bepaald aan de hand van een GFP-gefuseerde analoog van de receptor. In een niet-gestimuleerde cel werd gevonden dat reeds 40% van de receptoren gedimeriseerd is, wat duidt op het bestaan van zogenaamde pre-dimeren.

Vervolgens werd bestudeerd welke invloed stimulatie met EGF heeft op de clustergrootte van EGFR (hoofdstuk 5). Binnen 5 minuten leidt dit tot een vergroting van de gemiddelde clustering, waarbij clusters van meer dan 3 receptoren worden gevormd. De anisotropie waarde van de gestimuleerde receptor lag op een niveau wat vergelijkbaar was met een artificiëel gevormde EGFR-GFP oligomeer. Deze oligomerizatie bleek afhankelijk te zijn van de kinase-activiteit van de receptor, aangezien geen verandering in clustergrootte optrad bij receptoren met een defect kinase-domein. Mutatie van 9 tyrosine residuen in de C-terminus van de receptor, die fungeren als directe fosforylatie plaatsen van het kinase-domein, bleken hetzelfde negatieve effect teweeg te brengen. Dit duidt erop dat de kinase-geinduceerde fosforylatie van de tyrosine residuen direct betrokken is bij de oligomerisatie van de EGF receptor.

Aangezien EGFR activatie, oligomerizatie en internalizatie vrijwel gelijktijdige processen zijn, werd onderzocht of er een direct verband was tussen clustering van de receptor en diens internalizatie. Hiervoor werd gebruik gemaakt van de induceerbare EGFR-FKBP-GFP constructen. Dimerizatie van dit construct leidde niet tot activatie van de receptor. Wel leidde dit tot een versnelling van de internalisatie na stimulatie met EGF. Op vergelijkbare wijze wordt ook de internalisatie van de kinase-dode receptor versneld met een dergelijke clustering, alhoewel bij deze mutant de snelheid lager ligt dan die van de wildtype receptor. Samenvattend blijkt uit deze gegevens dat EGF binding aan de EGF receptor leidt tot de kinase-gemediëerde clustering van de receptor, hetgeen resulteert in een versnelde internalisatie. Toekomstig onderzoek zal moeten uitwijzen of dit direct gerelateerd is aan de aanwezigheid van lipid rafts en de vorming van signaleringsplatforms, wat wellicht een nieuwe mogelijkheid biedt om de werking van EGFR te beïnvloeden.

Dankwoord

Nadat u het hele boekje minutieus hebt doorgelezen, wil ik hierbij het woord richten aan degenen die - op welke wijze dan ook - betrokken waren bij dit alles. Het is misschien een cliché om te vermelden, maar de totstandkoming van dit proefschrift was niet mogelijk zonder de hulp van een grote groep mensen. Aangezien het vrijwel onvermijdelijk is dat dit dankwoord onvolledig is iedereen die de afgelopen jaren direct danwel zijdelings betrokken is geweest bij dit onderzoek, bedankt voor alle hulp. Toch wil ik een aantal personen in het bijzonder vermelden.

Allereerst mijn co-promotor Paul, je titel “leader-slash-inspirator” is niets teveel gezegd. Dank je voor je enthousiasme, eindeloze geduld, oneindige stroom ideeën en dagelijkse portie wijsheid (“promoveren is net als een berg beklimmen”).
Mijn promotor Arie, bedankt voor het van een afstand bewaken van dit project. Je kritische blik hield ons scherp, en ik hoop dat je nu net zo enthousiast bent over deze technologie als ik.
Mika, you created the fundament for this research years ago, thank you for all your effort you put into the set-up of the system. Johannes, dank je voor je feedback en het delen van je EGFR expertise tijdens de werkbesprekingen.

En dan natuurlijk mijn kamergenoten van N505. Vier jaar lang deelden we dezelfde ruimte, en voorlopig zijn we nog niet van elkaar af. Jarno, partner in crime, je hebt me vanaf de eerste dag wegwijs gemaakt in alle ins-and-outs van het lab en de diverse technieken. Bedankt voor alles, en misschien kun je me nog eens uitleggen hoe je al die biersoorten (twee) uit elkaar houdt? Rob, the king of cloning, bedankt voor al je input en hulp. Zonder jouw expertise (o.a. balletje-balletje) had dit proefschrift er heel anders uitgezien. Jord, je nam altijd de tijd om me van advies te voorzien, dank je wel daarvoor. Geoordeeld naar de grote stapels papier op onze bureaus heb ik ook in organisatorisch opzicht veel van je opgestoken.

Mijn (oud-)labgenoten van N529, Edward, Renée, Irina, bedankt voor al jullie medewerking de afgelopen jaren. Onder het mom “wetenschap moet vooral leuk zijn” bleven we niet gespaard van practical jokes en bijdragen aan de Wall Of Shame. En wat een geluk dat we precies dezelfde muzieksmaak bleken te hebben (FM 107.7)! Daarnaast grote hulde aan Fons, dankzij jou hadden we altijd verse PBS en paraformaldehyde.
Mijn studenten Robin, David, Els en Annette, ik wil jullie bedanken voor de bijdrage die jullie geleverd hebben aan dit onderzoek. Het materiaal bleek vaak een stuk weerbarstiger dan was voorzien, maar jullie hebben zeker een substantiële bijdrage geleverd aan de totstandkoming van dit boekje.

Veel dank ook voor rest van de vakgroep die ik vaak aantrof aan de koffietafel, de gezelligste hangplek van het Kruytgebouw. Helaas werd het uitwisselingsproject met de kussens en letters niet door iedereen op waarde geschat, maar leuk was het wel. Het wordt teveel om iedereen uit onze grote vakgroep bij naam te noemen dus: iedereen van MCB, EMSA danwel CA&D, bedankt voor jullie gezelligheid, hulp en interesse.

En dan natuurlijk de plek waar het allemaal gebeurde: het Ornstein-lab. Regelmatig liep ik met een bak vol verse FRET-preparaten (“celletjes”) richting Moleculaire Biofysica om de rest

van de dag in het donker door te brengen. Een andere wereld, met verfrissende denkwijzen en andere wetten, zo leek het soms. Hans, dank je voor al je inbreng tijdens de diverse bijeenkomsten van MtC, werkbesprekingen en soms ook tijdens het meten zelf. Arjen en Dave, het was telkens een klein feestje om in de kelders (The Cave) van het gebouw te mogen meten. Natuurlijk heeft de Afrikaanse-didgeridoo-funk-en-soul-muziek daar zeker aan bijgedragen, maar vooral de behendigheid waarmee - naar mijn idee willekeurig - allerlei draden en kabels met knipperende kastjes werden verbonden was onnavolgbaar. Bovendien was er tijdens de metingen ook voldoende tijd om de andere zaken in het leven te bespreken. Bedankt voor al jullie inzet en hulp, deskundigheid en broodnodige humor als de metingen een tijd niet meezaten.

Met de vakgroep Membraan Enzymologie ontstond in de loop der jaren een levendige ruilhandel in cellen, plasmiden, remmers en antilichamen. Op zich niet zo vreemd, want we hadden een gezamenlijk project. Gerrit, bedankt voor je enthousiasme en input voor dit project. Tijdens de MtC bijeenkomsten wist je als geen ander de brug te slaan tussen de fysici en de biologen ("Paul bedoelt dus...."). Hein, bedankt voor het delen van je kennis en hulp met de celfractionering en electroporaties. Sandra, bedankt voor alle hulp, en voor het delen van onze promotie-frustraties. Succes met de afronding! Ook Sylvia, Selene, Fikadu, Patricia, Joost, Joep en iedereen die ik niet genoemd heb, bedankt voor jullie hulp en het "bruiklenen" van chemicaliën en levend materiaal.

De andere (oud-)AIO's van het IB, in het bijzonder Sigrid, Masja, Catheleyne, Nicoline, Thijs en Maaike: bedankt voor alle gezelligheid! De jaarlijkse retraite (met bonte avond en Twister) was een welkome afwisseling temidden van het pipetteergeweld.

Ondanks dat een promotieonderzoek niet direct bevorderlijk schijnt te zijn voor je sociale leven en vakverdwazing vaak op de loer ligt, wil ik toch even stilstaan bij alle steun die ik heb gehad uit mijn prive-omgeving Alle vrienden en familie die geinteresseerd waren in mijn vorderingen in het onderzoek, bedankt voor jullie interesse door de jaren heen, en hopelijk heb ik nu weer iets meer tijd om jullie te zien.
Pa en Karin, voor jullie was het soms lastig te volgen wat ik daar in Utrecht nu precies uitvoerde ("iets met een microscoop"). Hetzelfde geldt ook voor mijn schoonfamilie, die met veel verbazing dachten dat ik een paar keer per week mijn cellen moest "omdraaien". Bedankt voor jullie interesse en steun de afgelopen jaren.

Maaike, het begin van mijn promotietraject en het begin van onze relatie vallen vrijwel samen. En ik ga ervanuit dat alleen de promotietijd nu ten einde komt! Misschien was het voor jou nog wel lastiger om langs de zijlijn van mijn promotie te moeten staan dan zelf in het veld te staan. Dank je voor je onophoudelijke optimisme, geduld en de nodige afleiding. De rollen worden nu omgedraaid, veel succes!

Curriculum vitae

Erik Gerben Hofman werd geboren op 25 juni 1977 in Joure. Na het behalen van zijn VWO diploma aan de Alexander Hegius Scholengemeenschap in Deventer, begon hij in 1995 aan een studie Biologie aan de Radboud Universiteit Nijmegen. Tijdens zijn specialisatie medische biologie liep hij stage aan de afdeling Cellulaire Dierfysiologie onder begeleiding van prof. Eric Roubos en drs. Sharon Kolk aan dezelfde universiteit, waarbij hij onderzoek deed naar de distributie van dopamine in de nucleus accumbens bij Apo-sus en -unsus ratten. Vervolgens liep hij stage bij de afdeling Celfysiologie van UMC St. Radboud, onder leiding van dr. Peter Deen en drs . Bas van Balkom. Hier verrichte hij onderzoek aan de regulatie van het transport van het waterkanaal Aquaporin-2. In januari 2004 begon hij aan zijn promotieonderzoek aan de afdeling Moleculaire Celbiologie (thans bekend als Cellular Architecture and Dynamics) aan de Universiteit Utrecht, onder supervisie van prof. Arie Verkleij en dr. Paul van Bergen en Henegouwen, hetgeen leidde tot dit proefschrift. Sinds juli 2008 werkt hij als post-doc aan deze afdeling, waar hij onderzoek doet naar de regulatie van de productie van reactieve zuurstofradicalen.

List of publications

van Balkom, B. W., Graat, M. P., van Raak, M., Hofman, E., van der Sluijs, P. and Deen, P. M. (2004). Role of cytoplasmic termini in sorting and shuttling of the aquaporin-2 water channel. *Am J Physiol Cell Physiol* **286**, C372-9.

van Balkom, B. W., Savelkoul, P. J., Markovich, D., Hofman, E., Nielsen, S., van der Sluijs, P. and Deen, P. M. (2002). The role of putative phosphorylation sites in the targeting and shuttling of the aquaporin-2 water channel. *J Biol Chem* **277**, 41473-9.

Bader, A. N., Hofman, E. G., van Bergen en Henegouwen, P. M. P. and Gerritsen, H. C. (2007). Imaging of protein cluster sizes by means of confocal time-gated fluorescence anisotropy microscopy. *Opt. Express* **15**, 6934.

Hofman, E. G., Ruonala, M. O., Bader, A. N., van den Heuvel, D., Voortman, J., Roovers, R. C., Verkleij, A. J., Gerritsen, H. C. and van Bergen En Henegouwen, P. M. (2008). EGF induces coalescence of different lipid rafts. *J Cell Sci* **121**, 2519-28.